

University of Hamburg

Faculty of Mathematics, Informatics and Natural Sciences  
Center for Earth System Research and Sustainability

**Observed and modelled onshore-offshore variability of  
oxygen and plankton on a high resolution North Sea  
transect: estimations of nutrient concentrations within a  
selected offshore area of the transect**

Master Thesis

Darko Salaj

Hamburg, 24 May 2018

## Versicherung an Eides statt

Ich versichere, dass ich die Arbeit selbständig verfasst und keine anderen als die angegebenen Hilfsmittel benutzt habe. Insbesondere habe ich keine im Quellenverzeichnis nicht benannten Internet-Quellen verwendet. Die Arbeit habe ich vorher nicht in einem anderen Prüfungsverfahren eingereicht. Die eingereichte schriftliche Fassung entspricht genau der auf dem elektronischen Speichermedium. Einer Veröffentlichung dieser Arbeit stimme ich zu.

Hamburg, den

.....

## Abstract

This master thesis considers the following main subjects: (1) An investigation of onshore-offshore variability of the model ECOHAM (ECOLOGical model HAMBurg) and observed data for physical (salinity, temperature and oxygen) and biological (phytoplankton, microzooplankton and mesozooplankton) parameters in a transect across the North Sea. (2) Develop a concept to estimate nitrate and ammonium concentrations in a specified offshore area in the transect.

A cruise (HE428) was performed by the Institute for Hydrobiology and Fisheries Sciences (IHF) of University of Hamburg between the 9-14 July 2014. Their subjects were to map biodiversity hot spots and gradients during the summer transect across the North Sea. For the present work the expedition's transect is divided into two tracks: Helgoland - Stonehaven and Stonehaven - Helgoland, respectively.

A one-to-one comparison with the physical and biological parameters between the observed and simulated transects has been carried out and analysed for both tracks in space and in short time as well as in long time. In comparison to the observed transects, the temperature and salinity transects as well as the northern part of the transects for the phytoplankton were reproduced well ECOHAM. In contrary, no considerable similarities across the transects have been detected between the observed and modelled transects for the microzooplankton and mesozooplankton as well as the southern part of the transects for phytoplankton.

A statistical method with two cost functions has been implemented in order to interpret the expedition transects in space and time. Generally, both cost functions revealed an increase of values towards NE for both salinity and temperature. In contrary, oxygen values decreased towards NE for both cost functions. Regarding the biological parameters, values increased by displacing the transects in both directions for both cost functions. With respect to the short time series, the values changed slightly for the parameters phytoplankton and mesozooplankton in both cost functions for both tracks. Only for one cost function a decrease of values in the parameter microzooplankton for both transects was observed. Generally, no trend in the cost functions could be identified for all parameters in long time series for both transects. Additionally, both cost functions have been used to examine the threshold of size class between microzooplankton and mesozooplankton with the observed and the simulated data. The best threshold exhibited at a size class  $258 \mu m$ .

The representativeness of the model ECOHAM in space and time has been investigated by comparing the simulated expedition transects in space and time. Regarding the short time, the simulated expedition transects revealed in the deeper part a considerably high representativeness for the physical parameters, whereas only partially for the biological parameters. In contrary, no parameter can be considered as representative at broad spatial and long term coverage.

As no nutrients were measured during the expedition, a concept has been developed to estimate nitrate and ammonium concentrations in a specified area for both transects. The concept was derived from observational oxygen data of the expedition as well as from observational data of a long term series from 1960 to 2014 and supported by ECOHAM. The obtained concentrations can be regarded as *in situ* measurements of the expedition. Estimations of the nutrient concentrations in the specified area revealed two different behaviours. (1) Towards the Dogger Bank, the estimation of nitrate and ammonium becomes more accurate with concentrations of about  $2 - 3 \text{ mmol}/m^3$  for ammonium and  $5 - 8 \text{ mmol}/m^3$  for nitrate which is in agreement with the observation. (2) In contrary, towards the deeper part of the central North Sea both nutrient concentrations tend to be overestimated.

# Contents

<b>1</b>	<b>Introduction</b>	<b>1</b>
1.1	North Sea . . . . .	1
1.2	General dynamic of the North Sea . . . . .	2
1.3	Salinity of water masses in the North Sea . . . . .	3
1.4	Seasonal stratification in the North Sea . . . . .	4
1.5	Seasonal variability of salinity and temperature in the North Sea . . . . .	4
1.6	Plankton and nutrient in the North Sea . . . . .	5
1.6.1	Winter . . . . .	6
1.6.2	Spring . . . . .	6
1.6.3	Stratified North Sea during summer . . . . .	6
1.6.4	Mixed coastal zone during summer . . . . .	7
1.6.5	Autumn . . . . .	7
1.7	Oxygen in the North Sea . . . . .	7
1.8	Objective of the Thesis . . . . .	8
<b>2</b>	<b>Material and Methods</b>	<b>8</b>
	<b>First part</b>	<b>8</b>
2.1	Physical model HAMSOM . . . . .	8
2.2	Biogeochemical model ECOHAM . . . . .	9
2.2.1	Oxygen cycle . . . . .	9
2.2.2	Nitrogen cycle . . . . .	10
2.2.3	Model setup . . . . .	10
2.3	Expedition of HE428 in the North Sea . . . . .	11
2.4	Measurement devices from the expedition of HE428 . . . . .	11
2.5	Technical tools . . . . .	12
2.6	Observed dataset . . . . .	12
2.6.1	CDT from the LOPC device . . . . .	13
2.6.2	Chlorophyll-a scaling factor . . . . .	13
2.7	ECOHAM dataset . . . . .	14
2.8	Visualisation of the observed and simulated data . . . . .	15
2.8.1	Observed transect . . . . .	15
2.8.2	ECOHAM transect . . . . .	16
2.9	Comparison between the observed and simulated expedition transects . . . . .	17
2.9.1	Cost function A . . . . .	18
2.9.2	Cost function B . . . . .	18
2.10	Biomass size spectra . . . . .	19
2.10.1	Threshold between microzooplankton and mesozooplankton . . . . .	19
2.10.2	Technical measurement of plankton . . . . .	20
2.11	Spatial displacement of the transects . . . . .	21
2.12	Representativeness of the simulated expedition transects . . . . .	23
2.13	Statistical analysis of the transects in space and time . . . . .	24
	<b>Second part</b>	<b>24</b>
2.14	Estimation of nutrient concentrations within a selected area for the observed transect	25
2.14.1	Estimation of the nutrient concentration concept . . . . .	25
2.14.2	Basic principle of the estimation of nutrients . . . . .	27
2.14.3	Preformed component . . . . .	27
2.14.4	Physical component . . . . .	28
2.14.5	Apparent Oxygen Utilisation . . . . .	28
2.14.6	Regenerated component . . . . .	29
2.14.7	Range of the regenerated component . . . . .	31
2.14.8	The m factor . . . . .	33
2.14.9	Estimation of nutrient concentrations in the selected area . . . . .	33

<b>3 Results</b>	<b>34</b>
<b>First part</b>	<b>34</b>
3.1 Threshold between microzooplankton and mesozooplankton . . . . .	34
3.2 Comparison between the observed and simulated expedition transects . . . . .	35
3.2.1 Temperature . . . . .	35
3.2.2 Salinity . . . . .	36
3.2.3 Oxygen . . . . .	37
3.2.4 Phytoplankton . . . . .	39
3.2.5 Microzooplankton . . . . .	40
3.2.6 Mesozooplankton . . . . .	41
3.3 Representativeness of the simulated expedition transects . . . . .	42
3.3.1 Temperature . . . . .	43
3.3.2 Salinity . . . . .	44
3.3.3 Oxygen . . . . .	45
3.3.4 Phytoplankton . . . . .	46
3.3.5 Microzooplankton . . . . .	47
3.3.6 Mesozooplankton . . . . .	48
3.4 Statistic analysis of the transects in space and time . . . . .	49
3.4.1 Cost functions of physical parameters . . . . .	49
3.4.2 Cost functions biological parameters . . . . .	50
3.4.3 Correlation coefficient and significance levels of the transects in space and time	52
<b>Second part</b>	<b>55</b>
3.5 Mixed layer depth in the selected water columns . . . . .	55
3.6 Regenerated component . . . . .	55
3.6.1 Remineralisation and nitrification using the AOU in a selected cell . . . . .	55
3.6.2 Range of remineralisation and nitrification over the AOU in the selected cells .	57
3.7 Physical component . . . . .	58
3.8 Estimation of nitrate and ammonium concentrations in the specified area . . . . .	59
<b>4 Discussion</b>	<b>59</b>
<b>First part</b>	<b>59</b>
4.1 Spatial displacement of the transects towards SW and NE . . . . .	59
4.2 Determined threshold between microzooplankton and mesozooplankton . . . . .	60
4.3 Southern Dogger Bank and Oyster Grounds . . . . .	60
4.4 Simulated oxygen data from 2010 and 2005 . . . . .	60
<b>Second part</b>	<b>60</b>
4.5 Temperature criterion for the mixed layer depth . . . . .	60
4.6 Regenerated component . . . . .	61
4.6.1 Remineralisation value $R_0$ . . . . .	61
4.6.2 Factor m for each cell of the selected area . . . . .	61
4.6.3 Simulation of oxygen mass budget . . . . .	62
4.6.4 True Oxygen Utilisation . . . . .	62
4.6.5 Not considered processes . . . . .	63
<b>5 Outlook</b>	<b>63</b>
5.1 Threshold between microzooplankton and mesozooplankton . . . . .	63
5.2 Estimations of nitrate and ammonium concentrations . . . . .	63
<b>6 Appendix</b>	<b>64</b>

<b>A</b>	<b>Observed transect</b>	<b>64</b>
A.1	TRIAXUS samples . . . . .	64
A.2	Amount of measurements from the expedition of HE428 . . . . .	64
A.3	Difference of salinity and temperature between LOPC device and TRIAXUS . . . . .	64
A.4	Original depth measurements . . . . .	65
A.4.1	TRIAXUS . . . . .	65
A.4.2	LOPC device . . . . .	66
A.5	Original chlorophyll-a measurements of the TRIAXUS . . . . .	66
A.6	Potential density anomalies . . . . .	66
A.7	Linear regression of chlorophyll-a of reference samples and TRIAXUS samples . . . . .	67
A.8	Oxygen saturation concentration . . . . .	69
A.9	Oxygen saturation in percentage . . . . .	69
A.10	Expedition transect through ECOHAM-grid . . . . .	69
A.11	Apparent Oxygen Utilisation . . . . .	72
A.11.1	Values of the AOU of the selected area in the transects . . . . .	72
A.11.2	AOU concentrations in the observed transects . . . . .	73
A.12	Range of remineralisation and nitrification over the AOU in the selected cells . . . . .	73
A.12.1	Remineralisation value: $R_0 = 151.5$ . . . . .	73
A.12.2	Remineralisation value: $R_0 = 140$ . . . . .	74
A.12.3	Remineralisation value: $R_0 = 138$ . . . . .	75
A.13	Conversion from particle into concentration units . . . . .	75
A.14	Confidence interval for Pearson's Correlation . . . . .	76
A.15	Statistic of the transects in space and time . . . . .	78
A.16	Microzooplankton and Mesozooplankton of other size classes . . . . .	82
A.16.1	Expedition transects . . . . .	82
A.16.2	Statistic in space and time . . . . .	84
<b>B</b>	<b>ECOHAM transect</b>	<b>90</b>
B.1	Topography . . . . .	90
B.1.1	Original . . . . .	90
B.1.2	Shifted . . . . .	90
B.2	Transect shifting towards NE and SW . . . . .	91
B.3	Ammonium and nitrate concentration . . . . .	93
B.4	Potential density anomalies . . . . .	93
B.5	Fast and slow sinking detritus concentration . . . . .	94
B.6	Apparent Oxygen Utilisation . . . . .	94
B.7	Representativeness of the modelled expedition transects . . . . .	95
B.8	Short time series . . . . .	95
B.9	Mixed layer depth of ECOHAM water columns from the selected area . . . . .	96
B.10	State variables of the reduced ECOHAM dataset . . . . .	97
B.11	Simulated oxygen expedition transect 2005 and 2010 from Helgoland - Stonehaven . . . . .	97
B.12	Simulated mass budgets of the selected cells . . . . .	98
B.13	The factor $m$ . . . . .	99
B.14	Estimation of nitrate and ammonium concentrations . . . . .	100
<b>C</b>	<b>ND130 data: box number 123 - 125</b>	<b>102</b>

# 1 Introduction

## 1.1 North Sea

The North Sea is a shallow marginal sea and is part of the Northwest European Continental Shelf. In its north, it has a large opening towards the Atlantic Ocean and a smaller opening in the English Channel in the southwest. In the east, it is connected to the Baltic Sea across the Skagerrak and Kattegat. The North Sea encompasses a surface area of approximately 575000 km<sup>2</sup> within its borders at 50.8°N, 0.7°E - 50.6°N, 1.1°E in southwest, 57.7°N, 9.6°E - 57.9°N, 9.9°E in northeast, 62.2°N, 0.1°W - 62.2°N, 5.4°E in north and 58.7°N, 3.1°W - 62.2°N, 0.1°W) in northwest (Otto et al., 1990; Pätsch and Kühn, 2008; van Beusekom and Diel-Christiansen, 2009; Quante et al., 2016).

A bathymetry from the North Sea is shown in Figure 1.1. Special geographical characteristics are the Dogger Bank (~54.5°N, 2°E) in the central North Sea with a depth of approximately 25 m, the Norwegian Trench (NT) with depths >700 m located in the Skagerrak (~58°N, 10°E), the Fladen Ground (~58.5°N, 0.5°E) in the northern part of the North Sea with an average depth of 110 m and the Oyster Grounds (OG) in the southern part of the North Sea with a depth of approximately 50 m located at ~54.5°N, 4.5°E (Weston et al., 2008).

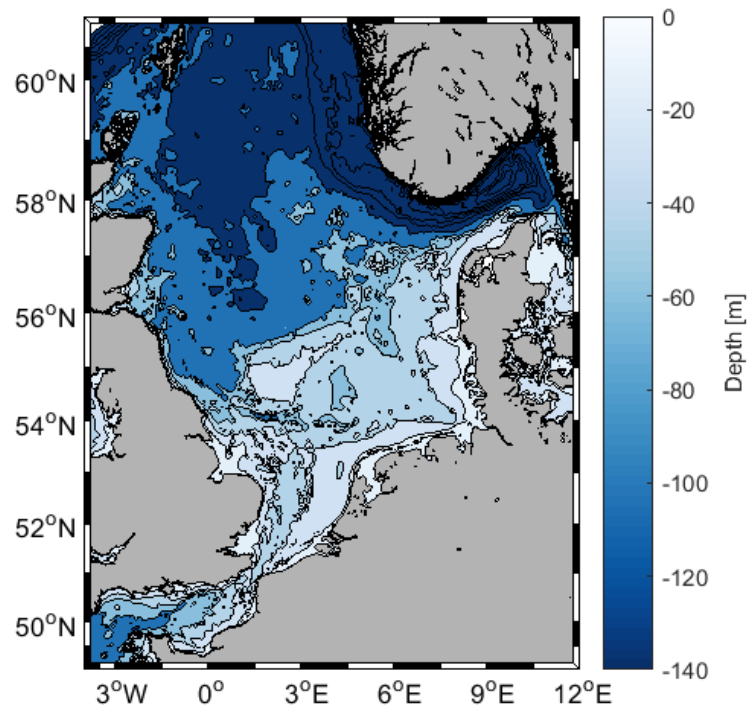


**Figure 1.1** – Bathymetry of the North Sea (map produced by using M Map v1.4i). North Sea borders: southwest ([50.8°N, 0.7°E], [50.6°N, 1.1°E]), northeast ([57.7°N, 9.6°E], [57.9°N, 9.9°E]), north ([62.2°N, 0.1°W], [62.2°N, 5.4°E]) and northwest ([58.7°N, 3.1°W], [62.2°N, 0.1°W]). Geographic characteristics: Dogger Bank (~54.5°N, 2°E), Fladen Ground (~58.5°N, 0.5°E), Oyster Grounds (~54.5°N, 4.5°E) and Norwegian Trench with its maximum depth in the Skagerrak (~58°N, 10°E).

Along the northern Dutch, German and southern Danish coast stretches the Wadden Sea. This region includes a coastline (to over 500 km) reaching from Den Helder (~52.9°N, 4.75°E) in Netherlands to the Skallingen peninsula (~55.5°N, 8.25°E) in Denmark. The Wadden Sea is a band of tidal flats, sandbanks and barrier islands. This band is on average 10 km wide, but in some areas it exceeds over 30 km. Tidal forces, wind and water turbulence have a high impact and, over time, have caused the formation of the Wadden Sea. Westwards and northwards of the Wadden Sea, the tidal range is about 1.5 m and increases to around 3 m in the central part near the estuaries of the rivers Weser and Elbe. The remineralisation in the Wadden Sea is higher than the primary production due to accumulation of particles and organic matter from the open North Sea (S. Brasse and A. Reimer and R. Seifert and W. Michaelis., 1999; van Beusekom, J. E. E. and Brockmann, U. H. and Hesse, K. -J. and Hickel, W. and Poremba, K. and Tillmann, U., 1999; van Beusekom and Diel-Christiansen, 2009).

## 1.2 General dynamic of the North Sea

Wind, tidal currents and stratification are the essential dynamic features of the North Sea (Otto et al., 1990; van Beusekom and Diel-Christiansen, 2009; Sündermann and Pohlmann, 2011). The tides propagate cyclonic (anti-clockwise) in the North Sea (see Figure 1.2). In general, the sea water in the North Sea has a residence time of 4 months to 1 year (Otto et al., 1990).

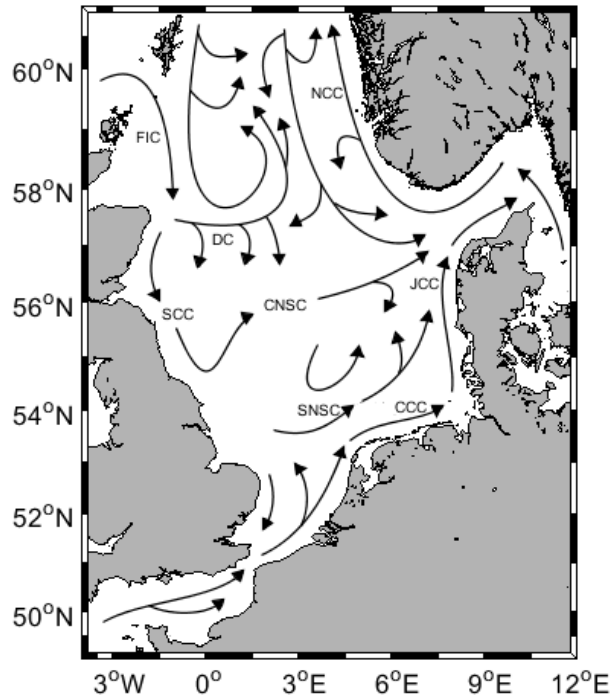


**Figure 1.2** – General current circulation in the North Sea (adapted from Turrell (1992); Jakobsen (2000); Hill et al. (2008); Queste et al. (2013)). FIC: Faire Isle Current. NCC: Norwegian Coastal Current. DC: Dooley Current. SCC: Scottish Coastal Current. CNSC: Central North Sea Current. SNSC: Southern North Sea Current. CCC: Continental Coastal Current. JCC: Jutland Coastal Current.

The Dogger Bank (DB) plays a relevant role in the North Sea. It separates the North Sea into two different parts with different physical, biological and chemical properties (Otto et al., 1990). The northern part is predominately influenced by the Atlantic water inflow from the north and the southern part is affected by the Atlantic water inflow via the channel in the southwest. Only a minor portion of the northern inflows reaches the region southerly of the DB (Thomas et al., 2005).

The northerly deeper part exhibits depths of approximately 150 m on the shelf, increases towards the Norwegian channel to 400 m and exceeds a depth of 700 m on the Skagerrak. During winter this area is vertically well-mixed. From spring to autumn most of this region is permanently stratified and is interrupted only by physical processes such as turbulent mixing and upwelling (Brockmann et al., 1988). Terrestrial influences are marginal. Riverine inputs from the Scandinavian peninsula and Baltic Sea admix with the North Atlantic water only in a narrow band (Norwegian Coastal Current) along the Norwegian coast (NCC) (Thomas et al., 2005).

In contrast, the shallow southern part of the North Sea shows water depths of usually less than 50 m and near the coast it decreases to less than 20 m. The majority of the water columns in this area are mixed by tides and winds throughout the year. Exceptions are the regions on OG and German Bight. Here, long stratification periods may occur during the summer (Greenwood et al., 2010; Queste et al., 2013; Große et al., 2016). Additionally, the shallow southern part receives vast fresh water input and is strongly affected by terrestrial and anthropogenic nutrient inputs (organic as well as inorganic). These inputs perform a significant control of the biogeochemical cycles (van Beusekom and Diel-Christiansen, 2009; Thomas et al., 2005).

Hydrographically, the northern part of the North Sea (see Figure 1.2) is strongly affected by water masses from the North Atlantic which enters via the Fair Isle Passage ( $\sim 59.5^\circ\text{N}$ ,  $1^\circ\text{W}$ ), via the region

east of the Shetland Islands ( $\sim 60^\circ\text{N}$ ,  $0.5^\circ\text{E}$ ) and via the western side of the Norwegian Trench only at depth ( $\sim 60^\circ\text{N}$ ,  $3^\circ\text{E}$ ). A major part of the inflow via the Fair Isle Passage (Fair Isle Current) and via east of the Shetland Islands flows eastward ( $\sim 57.5^\circ\text{N}$ ). Meanwhile a major part of the inflow, which intrudes via the western side of the Norwegian Trench (NT), turns back ( $\sim 57^\circ - 58^\circ\text{N}$ ) to join the northerly outflow (Norwegian Coastal Current) along the Norwegian coast (Dooley, 1974; Svendsen et al., 1991; Turrell et al., 1992; Turrell, 1992).

At the turning point of the Fair Isle Current (FIC) (see Figure 1.2) one branch propagates along the Scottish and northern English coast as the Scottish Coastal Current (SCC), while the second branch circulates further eastwards as the Dooley Current (DC). During the eastward circulation of the DC, a fraction of the water masses from the DC propagates across the central North Sea and reaches the north of the DB. An admixing with the water masses from the Central North Sea Current (CNSC) are conceivable (see Figure 1.2).

The water masses from the SCC turn to east ( $\sim 55^\circ\text{N}$ ) and flow along the north of the DB as the CNSC (see Figure 1.2). It splits into two branches. (1) One rejoins the southern water masses from the Southern North Sea Current (SNSC) before leaving the North Sea through the Norwegian Trench. (2) The other one propagates into the OG from the eastern part of the DB ( $\sim 55.5^\circ\text{N}$ ,  $4.5^\circ\text{E}$ ) (Thomas et al., 2005; Hill et al., 2008; Weston et al., 2008; Queste et al., 2013).

The southern part of the North Sea is affected by the Atlantic water which enters via the English Channel ( $\sim 50.5^\circ\text{N}$ ,  $1.5^\circ\text{E}$ ) (see Figure 1.2) and, in contrast to the northern part, it is highly influenced by the river discharge from the southern English coast (Humber and Thames) and continental coast (Scheldt, Meuse, Rhine, Ems, Weser and Elbe).

Due to the wind, density driven residual flow and the anti-clockwise residual currents from the tidal motion (Sündermann and Pohlmann, 2011), that strongly influence the shallow southern part and all coasts of the North Sea, and the Atlantic water inflow via the English Channel (EC), the continental run-off (Continental Coastal Current) spreading is limited to a narrow zone along the continental coast (Weston et al., 2008; van Beusekom and Diel-Christiansen, 2009). The water masses of the Continental Coastal Current (CCC) propagates eastwards alongside the Dutch coast and German Bight, continues as the Jutland Coastal Current (JCC) along the Denmark coast into the Skagerrak and finally leaves the North Sea via the NT (Jakobsen, 2000; Queste et al., 2013).

Atlantic water that is not admixed with the water masses from the continental run-off propagates south of the OG as SNSC towards the German Bight (GB) and rejoins later as the northern water masses from CNSC ( $\sim 56^\circ\text{N}$ ,  $7^\circ\text{E}$ ) (see Figure 1.2).

### 1.3 Salinity of water masses in the North Sea

In the North Sea, the water masses can be identified by their different salinities. The Atlantic water which enters from the northern boundary into the North Sea is recognised by salinity ranging from 35 - 35.3, also reaching the central North Sea. But an interannual discrepancy in the amount of Atlantic water masses which enter from the northern boundary into the North Sea can be observed (Turrell et al., 1992; Turrell, 1992; Turrell et al., 1996).

The intruding of Atlantic water via the EC can be characterised by the salinity  $>34.75$  (van Beusekom and Diel-Christiansen, 2009). Along the Scottish, English and Continental coast, the water masses contain lower salinity due to the admix of fresh water run-off with the Atlantic water. Alongside the Scottish and the northern part of the English coast salinities are typically between 34 and 35 (van Beusekom and Diel-Christiansen, 2009). Whereas in the middle and southern part of the English coast salinities are usually between 33 and 34. It is primarily because of the riverine input of the Thames, Wash and Humber (Weston et al., 2008). Alongside the continental coast, the salinity reaches as low as 29 - 30 (van Beusekom and Diel-Christiansen, 2009).

The Baltic Sea outflow ( $\sim 57.5^\circ\text{N}$ ,  $9^\circ\text{E}$ ) enters the North Sea via the Skagerrak and Kattegat between Denmark and Norway and plays an important role in the North Sea's hydrologic balance. The outflow mainly occurs in the upper layers and has a salinity of approximately 24 - 30 throughout the year (Brockmann et al., 1990; Thomas et al., 2005; van Beusekom and Diel-Christiansen, 2009). Meanwhile in the lower layers, the Atlantic water, which has its origin in the inflows between the east of the Shetland Islands and the western side of the Norwegian Trench, intrudes towards the Skagerrak and Kattegat. A persistent haline stratification in this area occurs (Gowen et al., 2012). In some situations, haline stratification can be found in the GB which is caused by river discharges. Yet, tides

and winds rapidly break the stratification down. During summer, the Baltic Sea outflow may intrude further more into the central North Sea due to persistent northerly winds during this season (Otto et al., 1990).

#### 1.4 Seasonal stratification in the North Sea

During winter, the irradiation is at its minimum at high latitude. The air above the North Sea is warmer than over the continent, as the water mass releases heat to the atmosphere due to absorption of solar radiation and heat capacity of sea water (Quante et al., 2016). Strong winds, convection and tidal generated turbulence mix the water columns in the deeper part as well as in the shallower regions of the North Sea (Otto et al., 1990). Hence, the temperature remains relatively homogeneous from the surface to the bottom. A thermal stratification is therefore prevented.

During spring-summer, the solar radiation increases continuously due to increasing daylight and decreases of inclination. Now, the situation is reversed, as the North Sea absorbs heat from the atmosphere. Hence, the heat exchange with the atmosphere becomes a predominate factor. As a result of the heat exchange into deeper layers, a seasonal thermal stratification builds up in large areas in the North Sea. The onset of persistent stratification occurs usually during mid-April and remains until autumn. In this period, the pycnocline, which is a result of temperature change, splits the water column into upper surface mixed layer (SML) and a lower layer which comprises the bottom mixed layer (BML). During summer, the SML and the bottom water reaches its maximum temperatures.

Below the pycnocline, an extensive pool of cold dense bottom water is trapped from the previous winter. Its temperature is established by the onset of persistent stratification by surface heat exchange during winter and early spring. After, the isolation temperature rises very slowly. In addition, in the deeper areas of the central, northern and northeastern North Sea, the sea water below the seasonal stratification is more saline due to the penetration of the saltier Atlantic water (Hill et al., 2008).

The central and northern North Sea are stratified in summer. The thermocline depth in this area is approximately 30 - 40 m (Quante et al., 2016). In the southern part, some regions are stratified with water depth deeper than 30 m (Pingree et al., 1978; Brockmann et al., 1988). Non-stratified regions can be observed in the shallower southwestern area and mostly at the continental coast. Strong tidal motions prevent the onset of persistent stratification and stir the entire water columns.

During autumn, the irradiation decreases continuously and the air over the North Sea is again warmer than over the continent. Especially the northern part of the North Sea is affected of the decreasing irradiation. The occurrence of stronger wind breaks down the stratification in this season and mixes the water columns consistently with deeper cold waters. As the stratification is ruptured, cold bottom water intrude into the upper layer, but the heat exchange through the air-sea interface cannot compensate the vertical heat loss in the water column beneath and therefore the reestablishment of stratification is prevented.

#### 1.5 Seasonal variability of salinity and temperature in the North Sea

Generally, the distribution of salinity concentration at the surface and the bottom alters marginally during the entire year in the North Sea (Hinrichs et al., 2017). Seasonal variability is not extensive in most regions. In the central, northwestern and southern part, the sea surface salinity (SSS) reveals low variability (0.1) and is elevated towards the coasts and in the northern part (0.25 - 0.5). High seasonal variability can be observed in the northeastern area with a concentration of 1 - 2 (Quante et al., 2016). This higher variability is caused by the Baltic Sea outflow.

Completely different behaviour is found for the temperature in the North Sea. There exists a dominant seasonal cycle which is mainly determined by the air-sea heat flux and the vertical exchange of heat within the water columns beneath (Otto et al., 1990). Particularly winter and summer seasons are distinctive.

During winter, when the water column is stirred from the surface to the bottom, a spatial temperature gradient from the southern to the northern North Sea can be observed. The southern part exhibits temperatures less than 7°C, whereas in the northern part temperatures of 7 - 10°C can be found. Augmented temperatures in the northern part are the result of the inflow of the warmer Atlantic water. Furthermore, a spatial gradient can be found in the North Sea. It runs from northeast to southwest and is more distinctive in the southern as in the northern part (Hinrichs et al., 2017).

This gradient is induced by the declining influence of the warm North Atlantic Current towards the central North Sea, the advection of air masses over the North Sea towards the east and increasing influence of cold continental air masses (Quante et al., 2016).

In summer, the situation is reversed. High sea surface temperature (SST) can be found in the southern part of the North Sea (16 - 19°C). In the northern part a decrease can be observed from the central to the northern part of the North Sea. Whereas the central North Sea exhibits SST of approximately 14 - 16°C, the northern part has varying SST around 10 - 14°C (Hinrichs et al., 2017). The inverted situation leads to a change in the isotherm's orientation due to the faster and stronger warming of the air over land than over the sea towards the summer (Quante et al., 2016).

During stratification period, a strong temperature gradient can be observed at the bottom of the North Sea. Non-stratified areas exhibit equal temperatures from surface to bottom. Lower temperatures (10 - 15°C) can be found in stratified areas in the southern North Sea, transitional regions and on the DB. The central and northern part of the North Sea, which are dominated by stratification, exhibit temperatures between 6 - 10°C (Hinrichs et al., 2017).

The seasonal variability of SST shows a spatial gradient from southeast to northwest in the North Sea. The southern part exhibits the largest variability with 6 - 7°C. Whereas the central part exhibits approximately 5°C, the northern part shows the lowest variability with 3 - 4°C (Quante et al., 2016).

## 1.6 Plankton and nutrient in the North Sea

Due to its geographical location, the North Sea is a temperate sea with a clear seasonal cycle in solar irradiation and temperature. Inasmuch the phytoplankton growth primarily depends on light and temperature, it follows also a clear seasonal cycle.

Two main routes of energy transfer exist in pelagic systems. (1) The classical type of food web prevails during nutrient-rich periods: microphytoplankton (diatom) production is immediately transferred into secondary (herbivore) and higher trophic levels. (2) Picophytoplankton and nanophytoplankton (flagellates) dominate during nutrient-poor periods typically in summer. Its production is mainly canalised through microzooplankton (heterotrophic flagellates and ciliates) as primary grazers via mesozooplankton (copepods) to the higher trophic levels (van Beusekom and Diel-Christiansen, 2009) or is attained to higher trophic levels via bacterial production (microbial loop, Azam et al. (1983); Fenchel (2008)).

A large amount of phytoplankton biomass across the North Sea arise during bloom period inshore in the coastal areas of southern England, along the continental coast, within tidal fronts, and at the OG and the DB. The biomass of zooplankton is controlled by its growth rate as well as food quality and hydrodynamical and chemical conditions (Quante et al., 2016).

Nutrient availability plays as a limiting factor an important role in marine ecosystems. Especially during summer at high latitudes, when the phytoplankton growth is not limited by solar radiation and temperature, it mainly depends on the rate of nutrient regeneration and the input of regenerated nutrients into the photic zone (Brockmann et al., 1988). In sea water, nutrients are predominantly available in inorganic forms of phosphorus, silica (disposable as compound of silicate) and nitrogen, which typically is disposable in compounds of ammonium, nitrite and nitrate. Ammonium is an important nutrient for the phytoplankton growth. It is predominantly generated by the remineralisation of organic matter (OM). A quantity of the produced ammonium by remineralisation is further oxidised to nitrite and nitrate by nitrifying bacteria.

Nutrients in the North Sea originate from several sources: the Atlantic ocean, the atmosphere, the river run-off, the diffusion, direct discharges from the ships, platforms and dredged materials and biogeochemical conversion processes such as remineralisation and nitrification (Brockmann et al., 1990; Brockmann and Kattner, 1997). Sinks for nutrients in the North Sea are mainly the outflow and the recirculation at the northern boundary and denitrification. In the long term, the reduction of nutrients in the water column mainly takes place through burial of sedimented material and through exchange with the atmosphere in gaseous form, but only in consideration of nitrogen (Brockmann et al., 1988, 1990).

### 1.6.1 Winter

Biological activity is low during the winter season. The limiting factors for zooplankton are temperature and food, whereas the phytoplankton is primarily limited by light. The occurrence of early diatom bloom in winter is only possible under sporadic favourable weather conditions and may appear in the shallow and low-turbidity waters such as on DB and off the Dutch west coast (van Beusekom and Diel-Christiansen, 2009). The early primary production bloom on the DB is the basis for the supply of the zooplankton production observed in the southeastern North Sea during winter (Nielsen et al., 1993).

The distribution of nutrients in the North Sea is related to the different hydrographical regimes and is explored best in the winter when the biological processes, especially the primary production is at its minimum, and only the remineralisation process is low (Brockmann and Kattner, 1997).

Generally, during winter the surface concentrations are similar to the bottom concentrations in the entire North Sea due to vertical mixing by wind, tidal motion and surface cooling (Pätsch and Kühn, 2008).

### 1.6.2 Spring

After the winter months the net phytoplankton growth increases with increasing daylight. When light disposability traverses a critical level, phytoplankton growth enters an exponential phase: known as spring bloom (van Beusekom and Diel-Christiansen, 2009). First, phytoplankton bloom reaches the southern North Sea in March, then the open North Sea during April, and finally the most turbid zones in May. The rapid growth of phytoplankton outcomes in consumption of all the required nutrients (N, P, Si) (Brockmann et al., 1988). However, a coastal gradient of phytoplankton concentration can be observed which reaches its maximum in April. The surface concentration from the southern North Sea towards onshore increases, whereas towards offshore it decreases.

Immediately after the beginning of the phytoplankton bloom, the zooplankton starts to graze. But the blooming occurs days or weeks after the peak of phytoplankton. The phytoplankton production is not controlled by herbivores in spring and autumn. Only during the summer months zooplankton grazing matches temporally the primary production in coastal and open sea areas. Roughly 1/3 of the grazed biomass will be partly mineralised by the zooplankton and excreted as nutrients ammonium or phosphate and urea. These nutrients are then provided to the phytoplankton growth within minutes that a short-cycled nitrogen and phosphorus flux will be established (Brockmann et al., 1988).

A relatively large fraction of the primary production and zooplankton is lost to the environment in form of particulate organic matter (POM) and sinks from the euphotic zone to the bottom. In the shallower southern part of the North Sea, most of these particles are channelled directly into the benthic system (Brockmann et al., 1988; van Beusekom and Diel-Christiansen, 2009). In contrary, the POM which sinks in the region of the deeper central and northern part of the North Sea is remineralised through the water column by bacteria. Only a small portion reaches the sediments (Pätsch and Kühn, 2008).

### 1.6.3 Stratified North Sea during summer

Seasonal stratification has a strong impact on biological components. During spring, water temperature continuously increases due to an increasing irradiation at high latitudes. As a result, in deeper parts of the North Sea a thermal stratification forms the water column. A stratification is prevented in the shallower parts of the North Sea due to tide-induced turbulence (Otto et al., 1990). These two different hydrographic conditions segregate the plankton community into low-turbulent, nutrient-poor central and northern North Sea and nutrient-rich turbulent coastal zones (van Beusekom and Diel-Christiansen, 2009). Hence, a rapid depletion of nutrients after the onset of stratification in upper layer is due to the uptake of the phytoplankton which might be dominated by autotrophic nano- and picophytoplankton during summer (Quante et al., 2016).

Owing to the low concentration in nutrients, a phytoplankton bloom occurs closely to or in the pycnocline after its formation in the subsurface. This deep chlorophyll maxima (DCM) is supplied by the input of regenerated nutrients from the nutrient-rich bottom layer to the pycnocline and was recorded since Lorenzen (1966) developed a technique of continuous chlorophyll concentration measurement by using a fluorometry. In the North Sea, DCM has been identified in a transect between

Flamborough Head to the DB by Richardson and Pedersen (1998). DCM also appear in the north (Weston et al., 2005; Fernand et al., 2013) as well as in the south of the DB (Nielsen et al., 1993; Richardson et al., 2000) and from the central North Sea to the Danish coast (Richardson et al., 1998; Fernand et al., 2013). The supplement of nutrients across the thermocline for DCM can be aided by tidal mixing and aggrandised by spring-neap tidal cycles. Particularly internal waves are a potential source of mixing around the DB (van Haren et al., 1999). In frontal regions (transition zones between different water masses), the DCM is also intensified (Sharples et al., 2007; Fernand et al., 2013).

Regarding the nutrients, the concentrations in the upper layers are more or less homogeneous and low due to steady mixing and rapid depleting of the earlier phytoplankton bloom, whereas the sub layer exhibits higher concentrations caused by remineralisation and nitrification processes. Additionally, the stratification instantly hinder the remineralised nutrients from reentering into the mixed layer. Strong winds during summer may break the stratification down and nutrient-rich bottom water can intrude up to the surface before the stratification is restabilised. Sources of regenerated nutrients from the lower layer into the surface layer can also be supplied by turbulent diffusion or by breaking internal waves. Upwelling is another possible process that brings nutrient-rich bottom water up to the surface. It is often located in areas where fronts separate the stratified and unstratified water along the coasts and on the banks (Brockmann et al., 1990; Pedersen, 1994; Richardson and Pedersen, 1998). These processes initialise a new phytoplankton bloom in the subsurface closely to the thermocline during the stratified season.

Two parameters may influence the phytoplankton - mesozooplankton abundance: (1) the dimension of phyto - zooplankton interaction during the spring bloom and (2) the amount of nutrient injection into the euphotic zone by physical processes (see above) (Riegman et al., 1990; van Beusekom and Diel-Christiansen, 2009).

#### **1.6.4 Mixed coastal zone during summer**

In contrary to the deeper part of the North Sea, the coastal area is subdued by the continuous nutrient input. Main sources are rivers and remineralised organic matter. The biomass in the coastal zone is controlled by the interaction between nutrient levels, nutrient ratios, phytoplankton species composition and zooplankton grazing during summer (van Beusekom and Diel-Christiansen, 2009).

#### **1.6.5 Autumn**

Identically to the annual debut, the end of phytoplankton growth is determined by light disposability. The surface layer of the open North Sea starts to cool and the thermocline becomes continuously weaker. Autumn storms break down the stratification and an autumn bloom occurs in some regions by an injection into the nutrient-rich bottom layer (Brockmann et al., 1988; van Beusekom and Diel-Christiansen, 2009).

### **1.7 Oxygen in the North Sea**

Dissolved oxygen (DO) is an essential biochemical component and it is utilised as a key supporting component in defining the ecological status of marine environments (Greenwood et al., 2010). In sea water, DO originates by photosynthesising organisms in the euphotic zone. Advection distributes the DO in diverse areas or is transported by vertical mixing in the interior of the water column (Peña et al., 2010; Queste et al., 2016). In the interior, the DO concentration decreases towards the bottom layer due to biological consumption. Benthic processes stand for the main oxygen consumers in the bottom layer which account for more than 50% of the overall consumption (Große et al., 2016) and may affect the DO concentration in upper layers of the water column. Air-sea gas-exchange of  $O_2$  at the sea surface is a further important source of DO in sea water. Chemical processes rapidly transform the gaseous  $O_2$  into DO.

According to Große et al. (2016), the North Sea oxygen dynamics can be divided into three different areas: (a) an elevated productive, non-stratified coastal area, (b) a productive, seasonally stratified area with a slight sub-thermocline volume, and (c) a productive, seasonally stratified area with a huge sub-thermocline volume. The vertical extension of the sub-thermocline volume is considered as the depth between thermocline and bottom mixed layer (BML). Large sub-thermocline volume controls the oxygen dynamics in the most parts of the central and northern North Sea. In contrary, a small

sub-thermocline volume dominates around the north of the DB and partially in the southern part of the North Sea (e.g. Oyster Grounds and German Bight). Other parts of the southern North Sea are affected by strong tidal mixing which inhibits a seasonal stratification.

Generally, the seasonal cycle of DO concentration follows the seasonal cycle of phytoplankton in the North Sea. During summer, a spatial gradient of DO concentration can be observed. The gradient increases from south to north. Higher temperatures accompanied by tidal mixing and higher biological activities tend to lower surface concentration in the southern part. In the stratified northern part, the higher surface concentration can be the result of lower surface temperature which absorbs more DO concentration due to a change of oxygen solubility and a low production rate of DO by primary production. In contrary, below the thermocline lower concentration occurs due to consumption and a lack of generating DO by primary production. Continuous consumption within the water column can lead to oxygen deficiency at the bottom in some regions such as the north of the DB and southeastern of the North Sea (Große et al., 2016).

In situations where the rate of consumption for relevant duration is higher than the rate of oxygen supply hypoxia take place. Hypoxia is defined as the oxygen concentration below  $125 - 190 \text{ mmol/m}^3$  ( $4 - 5 \text{ mg/dm}^3$ ) by the Oslo and Paris Commission (OSPAR) in the Ecological Quality Objective (EcoQO) for the North Sea and is classified as "problem area" in terms of eutrophication (Queste et al., 2013; Große et al., 2016). In this work the definition of "oxygen deficiency" will be utilised rather than the term hypoxia used in the context by OSPAR. An outline of the impact of hypoxia on coastal marine organisms is described in Vaquer-Sunyer and Duarte (2008).

## 1.8 Objective of the Thesis

The aim of the present thesis is (1) to investigate the onshore-offshore variability of physical (salinity, temperature and oxygen) and biological (phytoplankton, microzooplankton and mesozooplankton) parameters in a transect across the North Sea and (2) to develop a concept to estimate nitrate and ammonium concentrations in a specified area offshore of the transect without measured *in situ* nutrients of nitrate and ammonium.

The specific objectives are the following:

- To identify the threshold of sizes classes between microzooplankton and mesozooplankton in ECOHAM by the observed data recorded during the expedition carried out in summer 2014.
- To analyse the simulated physical and biological parameters within the transects in comparison with the observed parameters from the expedition and to interpret these in space and time.
- To examine the representativeness of all simulated parameters of the expedition's transects in space and time.
- To estimate nitrate and ammonium concentration in the specified area of the expedition transect by using the apparent oxygen utilisation with support by ECOHAM and a compiled climatological observation data from 1960 - 2014.

## 2 Material and Methods

### First part

#### 2.1 Physical model HAMSOM

HAMSOM (HAMburg Shelf Ocean Model) is a non-linear three-dimensional (3D) hydrodynamical model, which simulates the advective flow field, the turbulent mixing, and the physical parameters temperature ( $T$ ) and salinity ( $S$ ) in the North Sea.

The development of HAMSOM dates back to the early eighties. Based on the Arakawa C-grid (Arakawa and Lamb, 1977), Backhaus and Maier-Reimer (1983) developed a 2D barotropic implicit numerical model with the primitive shallow water equations (see the equation (1) in Backhaus (1983)). Based on this previous model, a semi-implicit model was proposed by Backhaus (1983), and a few years later, Backhaus (1985) introduced a non-linear 3D baroclinic model to simulate the shelf sea

region of the North Sea. In the middle of the nineties, Pohlmann (1996b) enhanced the model and implemented additional equations (see the equations (4) and (5) in Pohlmann (1996b)) of a first order turbulent kinetic energy  $k$  and dissipation rate  $\varepsilon$ . These equations influence the physical as well as the biological processes (Pohlmann, 1996a).

HAMSOM employs the hydrostatic and the Boussinesq approximation and a free surface. The advective flow field ( $U, V, W$ ) is computed by Lax-Wendroff (details see in Rezzolla (2010) and Rezzolla and Zanotti (2013)) in the latest version of HAMSOM. As in the previous model version, the result is an improved resolution in stratification and ameliorates the coastal freshwater input (Pohlmann, 2006). A detailed description of the 3D hydrodynamical model HAMSOM is given in Backhaus and Hainbucher (1987), Pohlmann (1996a) and Pohlmann (1996b).

## 2.2 Biogeochemical model ECOHAM

ECOHAM (ECological model HAMBurg) is a biogeochemical model which simulates the cycles: carbon (C), nitrogen (N), oxygen ( $O_2$ ), phosphorus (P) and silicon (Si) in the North Sea and partially the deep North Atlantic (Pätsch and Kühn, 2008; Lorkowski et al., 2012). The 3D biogeochemical model is based on the 1D model by Kühn and Radach (1997), which is based on the model by Fasham et al. (1990). Afterwards, Pätsch et al. (2001) applied the model to the deep North Atlantic.

ECOHAM version 5 (latest model version) includes two phytoplankton groups (diatoms and flagellates), two zooplankton groups (microzooplankton and mesozooplankton), two fractions of detritus with different sinking velocity (slow and fast), bacteria, oxygen, 4 nutrients (nitrate, ammonium, phosphate and silicate), labile dissolved organic matter (LDOC, LDON, LDOP), semi-labile organic carbon, dissolved inorganic carbon (DIC), calcite ( $CaCO_3$ ), total alkalinity (TA) and the benthic variables calcite and particulate organic matter (POC, PON, POP, POSi).

Identical with HAMSOM, the horizontal resolution is  $1/3^\circ$  with 88 grid points in longitudinal direction and  $1/5^\circ$  with 82 grid points in latitudinal direction (see Figure A.9 in the appendix). This corresponds to approximately 20 km in both directions. The model covers a region of  $15.2^\circ W - 14.0^\circ E$  and  $47.5^\circ N - 63.9^\circ N$  (see Figure 2.6). In vertical dimension, the model exhibits a structure of 31 z-layers and a maximum depth of 4000 m. The surface layer is determined with a mean vertical extension of 10 m. It varies with time due to surface elevation. The underlying layers (10 - 50 m) are fixed by 5 m steps and increases up to 10 m with ensuing layers (50 - 100 m). Below 100 m, the thickness layer augment successively in depth.

The meteorological forcing of ECOHAM is provided by NCEP/NCAR reanalysis (Kalnay et al., 1996; Kistler et al., 2001) and consists of 6-hourly fields of air temperature, relative humidity, cloud coverage, wind speed, atmospheric pressure, irradiance (2h + 24h), wind stress in 2 dimensions, a forcing of respective boundary conditions of daily river loads (Lorkowski et al., 2012) and prescribed boundary conditions for all state variables. The biogeochemical equations and the fluxes between the different state variables and the model parameters are described in the appendix of Lorkowski et al. (2012).

### 2.2.1 Oxygen cycle

Gaseous exchange between atmosphere and ocean is a potential source of  $O_2$  in sea water. Chemical processes transforms the gaseous  $O_2$  into dissolved  $O_2$ . The air-sea flux of  $O_2$  at the sea surface is parametrised after Wanninkhof (1992) with ECOHAM. With respect to the biology, the  $O_2$  cycle is linked to the C, N and P cycle by phytoplankton, zooplankton respiration and bacterial remineralisation. Whereas photosynthesis is a source of dissolved  $O_2$ , the respiration of zooplankton as well as the remineralisation act as a sink. Nitrification is a further sink for dissolved  $O_2$  due to bacterial conversion processes of ammonium to nitrate. It only appears under aerobic conditions (dissolved  $O_2$  concentrations  $> 0 \text{ mmol/m}^3$ ). The nitrification process is more productive under weak light conditions due to its light-dependency and connects the  $O_2$  cycle only to the N cycle. Pelagic denitrification is also integrated in the model. But it is negligible as it only takes place under anaerobic conditions. Such conditions do not occur in the North Sea (Große et al., 2017).

The  $O_2$  cycle in ECOHAM is affected by benthic remineralisation in two ways. Firstly, the remineralisation in the sediment decreases the dissolved  $O_2$  concentration in the pelagic bottom layer above directly. Secondly, the released ammonium from the sediment can be nitrified within the water

column under dissolved  $O_2$  consumption. Benthic denitrification depends on the benthic dissolved  $O_2$  consumption in the model (Große et al., 2016).

### 2.2.2 Nitrogen cycle

Nitrogen is an important element for marine organisms and is closely coupled to the other cycles such as carbon, phosphorus and silicon. In sea water, nitrogen is predominantly available as reduced form of inorganic nitrogen like nitrite, nitrate and ammonium.

Figure 2.1 shows the interrelation of the nitrogen cycle as incorporated in ECOHAM. Steady state variables are signed as circles. Enumerated arrows point out to the involved flux.

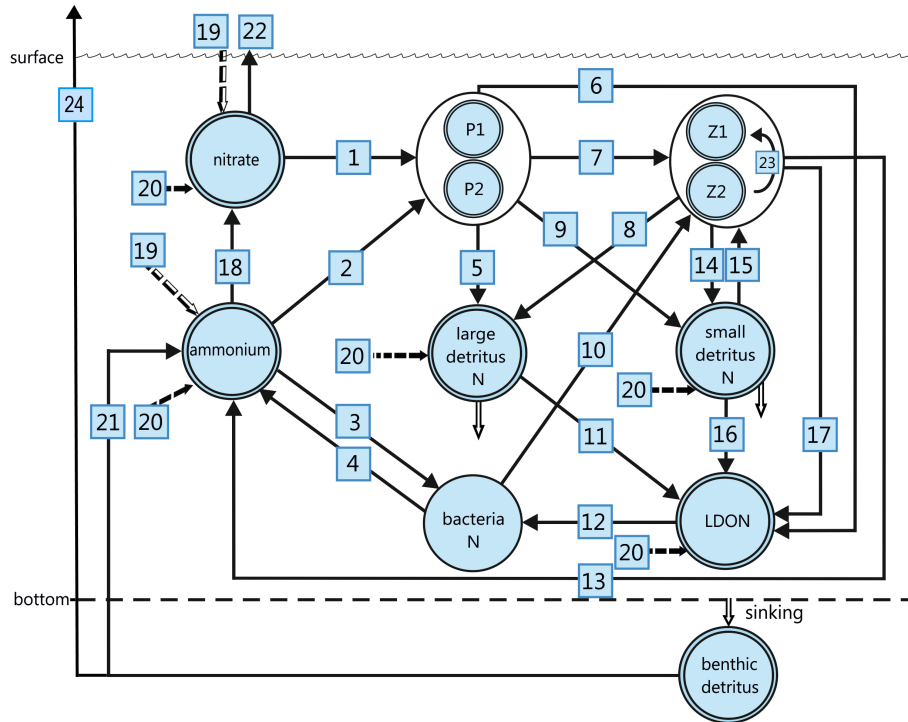


**Figure 2.1** – ECOHAM5 nitrogen cycle. P1: diatoms. P2: flagellates. Z1: mesozooplankton. Z2: microzooplankton. LDON: labile dissolved organic nitrogen. 1: uptake of nitrate. 2, 3: uptake of ammonium. 4, 13: excretion of ammonium. 5, 8: mortality. 6: exudation of LDON. 7, 10, 15, 23: grazing. 9, 14: fecal pellets. 11, 16: decay. 12: uptake of LDON. 17: excretion of LDON. 18: nitrification. 19: atmospheric input. 20: river input. 21: benthic remineralisation. 22: pelagic denitrification. 24: benthic denitrification.

The nutrients nitrate and nitrite are not regarded independently. These nutrients are added as steady state variable "nitrate". Ammonium and nitrate are defined together as the dissolved organic nitrogen (DIN). Phytoplankton utilise the DIN to generate its organic materials ( [ 1 ] and [ 2 ] ). Detritus of the particulate organic nitrogen (PON, [ 11 ] and [ 16 ] ), exudation ( [ 6 ] ) as well as excretion ( [ 17 ] ) of phytoplankton and zooplankton, respectively, produce labile dissolved organic nitrogen (LDON). Remineralisation by bacteria ( [ 4 ] ) and excretion from the zooplankton ( [ 13 ] ) release ammonium into the pelagic system. A fraction of the produced ammonium is nitrified by bacteria to nitrate ( [ 18 ] ). Another source of ammonium into the pelagic system originates from the buried benthic detritus which is remineralised by anaerobic bacteria ( [ 21 ] ). Meanwhile other anaerobic bacteria denitrify the nitrate to molecular nitrogen ( $N_2$ ) from the benthic and pelagic system. This produced  $N_2$  is released into the atmosphere in gaseous form ( [ 22 ] and [ 24 ] ) (Müller, 2008).

### 2.2.3 Model setup

The model setup of HAMSOM employs monthly, climatological distribution of  $S$  and  $T$  based on the World Ocean Atlas 2001 (details see in Conkright et al. (2002)) for the initialisation and open boundaries. According to the  $M_2$  tide, a fixed (Dirichlet) open boundary condition (OBC) is prescribed

at open boundaries and surface elevation (Große et al., 2016). A detailed description of OBC for  $S$  and  $T$  as well as advective flow is given in Chen et al. (2013). The meteorological forcing is derived from NCEP/NCAR reanalysis data which consists of 6-hourly information on air temperature, irradiation, relative humidity, cloud coverage and wind speed direction. The HAMSOM simulation was carried out with 10 minutes time step over the period 1977 - 2014. The calculated daily 3D-fields of  $S$ ,  $T$ , advective flow and vertical turbulent mixing coefficients were stored as output.

The simulation of ECOHAM was run off-line with a 30 minutes time step by using the daily average simulated physical forcing output from HAMSOM. Daily river run-off and nutrient load data for 24 rivers were provided by Lorkowski et al. (2012), meanwhile NCEP/NCAR reanalysis data supplied the meteorological forcing (see section 2.2). The C:N:P ratio is determined for both phytoplankton ( $C:N_p = 6.625$ ;  $N:P_p = 20$ ) and zooplankton ( $C:N_z = 5.5$ ;  $N:P_z = 20$ ) groups, respectively, and bacteria ( $C:N_b = 4.0$ ;  $N:P_b = 10$ ). Large detritus have a sinking velocity of 10 m/d and small detritus sinks with a velocity of 0.4 m/d (Lorkowski et al., 2012). The output of the biogeochemical simulation was saved as daily values for all state variables and fluxes.

### 2.3 Expedition of HE428 in the North Sea

The cruise HE428 was carried out between the 9-14 and 16 July 2014 by the Institute for Hydrobiology and Fisheries Science (IHF) of the University of Hamburg with the research vessel *FS Heincke* in the North Sea. Their subjects were monitoring of biodiversity hot spots and gradients at the summer transect across the North Sea.

*FS Heincke* started close to Helgoland (German Bight). This region ( $\sim 25 - 35$  m depth) is still influenced by the riverine freshwater input. Afterwards, the vessel crossed northerly of the Oyster Grounds ( $55.28^\circ\text{N}$ ,  $4.92^\circ\text{E}$ ) where water depths is  $\sim 35 - 40$  m. The water masses of this area are controlled by southern North Sea waters (Weston et al., 2008; van Beusekom and Diel-Christiansen, 2009; Burson et al., 2016). Subsequently, the vessel passed the southern adjacent of DB ( $55.44^\circ\text{N}$ ,  $4.58^\circ\text{E}$ ), travelled the relatively shallow area of DB ( $\sim 25$  m depth,  $55.48^\circ\text{N}$ ,  $4.25^\circ\text{E}$ ), crossed the northern adjacent of DB ( $55.68^\circ\text{N}$ ,  $3.92^\circ\text{E}$ ) before entering the deeper central part of the North Sea ( $>80$  m depth, see Figure 1.1). This part is strongly affected by the water masses from the North Atlantic Ocean. Later, *FS Heincke* cruised to the vicinity of Stonehaven (Scotland) before returning to Helgoland.

During the expedition of HE428, eleven different spatial and temporal samples (see Table A.1 in the appendix) of physical (salinity, temperature, oxygen, pressure and turbidity) and biological (chlorophyll-a, phycocyanin, phycoerethrin and plankton) parameters were conducted with the Remote Operated Towed Vehicle (ROTV) TRIAXUS, which was equipped with several devices (see section 2.4). The TRIAXUS was towed behind the survey vessel, undulated with a vertical speed of 0.3 m/s and covered an approximate depth range of 5 to 84 m during the cruise. The observed transect covers the region at  $54^\circ\text{N}$  to  $57^\circ\text{N}$  and  $2^\circ\text{W}$  to  $8^\circ\text{E}$  (see red line in Figure 2.4) and has a length of approximately 663 km.

Chronologically, there are two transects. First, the route from Helgoland - Stonehaven (9-12 July), second, the route from Stonehaven - Helgoland (12-14 July). On 16 July the research vessel tracked other locations in the North Sea which are not considered in this work. The observed transects are composed as follows: samples from 1 - 7 (fractional), combined, represent the transect from Helgoland - Stonehaven (H - S) and the other part of sample 7 together with the samples 8 - 11, merged, represent the transect from Stonehaven - Helgoland (S - H).

### 2.4 Measurement devices from the expedition of HE428

Several instruments were utilised to measure the biological and physical parameters during the cruise of HE428. The biological parameters such as phytoplankton (meted as fluorescence), phycocyanin and phycoerethrin concentrations as well the physical parameters turbidity, pressure and temperature were measured by a multi-sensor Turner C6 (Turner Designs Inc., USA) device. An Aanderaa Oxygen Optopode 4330F (Xylem Inc., USA) instrument was applied to measure the oxygen concentrations. Additionally, the physical parameters salinity, temperature and pressure were meted by the CTD device SBE 49 FastCAT CTD Sensor (Sea-Bird Scientific Inc., USA) (hereafter  $CDT_{TRIAXUS}$ ).

Particles in the sea water were detected with LOPC device ODIM BROOKE OCEAN (ODIM Inc.,

Canada), developed by Herman et al. (2004) which was supplemental mounted on the TRIAXUS. The technical measurements of particles are given in section 2.10.2. During the research, the LOPC device was defined to an observable particle size spectrum from  $15 \mu m$  -  $1920 \mu m$ . The bin size of the equivalent spherical diameter (ESD, see section 2.10.2) was determined with  $15 \mu m$  which gives 128 bins for each recorded sample. The sampling rate was calibrated at 1 Hz. In addition, the LOPC device was equipped with a CTD device SBE 49 FastCAT CTD (hereafter  $CDT_{LOPC}$ ) and meted simultaneously the salinity, temperature and pressure during the particles measurements. A video plankton recorder (VPR) which contained a Pulnix camera TM-1040 (detailed description see in Möller et al. (2012)) was applied to explore marine species and, additionally, to distinguish between living particles and detritus or marine snow.

## 2.5 Technical tools

Obtaining images of the measured and disposed simulated data or performing calculations, several technical tools are necessary: (1) MATLAB program version R2016a was utilised for the calculations and visualisations. The simulated data and the mass budgets (see section 2.14.4) were calculated in (2) FORTRAN program. (3) Climate Data Operators (CDO) version 1.7.2 was used for extracting the transects from the simulated data as well as generating new variables. Program CDO is available at: <http://www.mpimet.mpg.de/cdo>.

## 2.6 Observed dataset

The *in situ* data from the expedition of HE428 is saved in several file formats. The recorded data from the devices Turner C6, Aanderaa Oxygen Optopode 4330F,  $CDT_{TRIAXUS}$  and the depth as well as the coordinates from the TRIAXUS have been stored as txt-files. On the other hand, the recorded data from the LOPC device,  $CDT_{LOPC}$  and the depth as well as the coordinates from the LOPC device were applied in a hierarchical data format (HDF), such as a h5-file. Table A.2 in the appendix shows the amount of *in situ* measurements conducted with the LOPC device and the other devices (conducted by Turner C6, Aanderaa Oxygen Optopode 4330F and  $CDT_{TRIAXUS}$ ) during the cruise as chronologically single track (9-14 July) and as chronologically separated into two tracks from H - S and S - H, respectively (see section 2.3).

Following observed data were utilised: (1) data from Aanderaa Oxygen Optopode 4330F and Turner C6 with their corresponding depth and coordinates from the TRIAXUS for the parameters oxygen and phytoplankton, respectively, and (2) data from the LOPC device for the parameter zooplankton and  $CDT_{LOPC}$  for the parameters salinity and temperature. The parameter zooplankton is again separated into the parameters microzooplankton and mesozooplankton (see section 2.10).

Three remarks have to be emphasised here:

The first concerns the  $CDT_{TRIAXUS}$ . This device has not recorded data for the parameters salinity and temperature in the water columns from the transect S - H (see ECOHAM index 65 - 66 in the Figures A.1b and A.1d in the appendix). However, using salinity and temperature data from the  $CDT_{LOPC}$  the missing data can be circumvented (see section 2.6.1). Despite of utilising data from the  $CDT_{LOPC}$ , some data were not recorded during the research due to the missing registration of the depth 0 - 25 m for all observed parameters in the water column of ECOHAM index 41 (e.g. temperature in Figure 3.2b).

The second applies to the devices Aanderaa Oxygen Optopode 4330F and Turner C6. Due to an unit being out of service data are missing for the parameters oxygen and phytoplankton in the water columns of ECOHAM index 65 - 66 (see Figures 3.4b and 3.5b) from the transect S - H and, additionally, for the parameter oxygen from the transect H - S in the water columns of ECOHAM index 53 - 55 (see Figure 3.4a).

The third is related to the chlorophyll-a values of the parameter phytoplankton. Chlorophyll-a concentrations are approximately 10 fold higher as generally expected in July in the North Sea. The maximum mean value lies around  $84 mg \text{ Chl-a}/m^3$  in the transect of H - S (see ECOHAM index 63, depth layer 30 - 40 m, in Figure A.4a in the appendix), meanwhile a maximum mean value of approximately  $101 mg \text{ Chl-a}/m^3$  exhibits the transect of S - H (see ECOHAM index 62, depth layer 30 - 40 m, in Figure A.4b in the appendix). A previous work from Tiedje et al. (2010), which investigated a coastal offshore gradient from the German Bight to the Faroe Islands, revealed an  $1 mg \text{ Chl-a}/m^3$

offshore *in situ* mean chlorophyll-a value from July to September (1960 - 1994) and approximately 7 mg Chl-a/m<sup>3</sup> near the coast. Looking at satellite data, the median chlorophyll-a (April 2003) values show up to 60 mg Chl-a/m<sup>3</sup> along the Wadden Sea. These high values are probably caused by the bottom reflection and are not convenient for coastal water (Woerd and Pasterkamp, 2008; Tiedje et al., 2010). Consequently, the meted chlorophyll-a concentrations in both transects are exaggerated. In order to reach a settlement of range between the observed and simulated values, it has been suggested to add a scaling factor for the chlorophyll-a data (see section 2.6.2).

### 2.6.1 CDT from the LOPC device

Some data from the CDT<sub>TRIAXUS</sub> were missing for the parameters temperature and salinity. In contrary, the CDT<sub>LOPC</sub> have less missing data (see section 2.6). Identifying the derivations of salinity and temperature between both CTD devices, the difference has been calculated:

The salinity differences range is mostly between -0.02 to 0.06 from the transect H - S and -0.01 to 0.06 from the transect S - H (see Figures A.1a and A.1b in the appendix). Only some grid points show higher discrepancies on the transect of S - H.

The temperature differences range is mostly between -0.1 °C to 0.1 °C (see Figures A.1c and A.1d in the appendix) in both transects. Particularly in the water column of ECOHAM index 41 transect H - S, the surface layer transect S - H and at the thermocline in both transects exhibit larger variance of approximately ± 0.1 °C. These referred higher discrepancies are probably caused by diverse installed levels of the CTD devices on the TRIAXUS. The CDT<sub>LOPC</sub> was installed about 40 cm higher than the CDT<sub>TRIAXUS</sub>. However, the differences in salinity and temperature between both CTD devices usually revealed low distinctions in both tracks. Obtaining data from the CDT<sub>LOPC</sub> are legitimated.

### 2.6.2 Chlorophyll-a scaling factor

In section 2.6 it has been pointed out that a scaling factor for the observed chlorophyll-a data has to be evaluated due to exaggerated meted concentrations during the expedition of HE 428.

Water sampling was carried out before the beginning of the measurements with the TRIAXUS (see start time of sample 1 from Table A.1 in the appendix), between each end of the measurements from the previous sample and start of the ensuing sample of the TRIAXUS and after the end of the measurements with the TRIAXUS (see start time of sample 11 from Table A.1 in the appendix). A sketch is given in Figure 2.2.

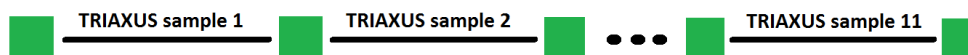


**Figure 2.2** – Temporal sketch of the water sample measurements during the expedition of HE428. Green square: water sampling.

Each water sample was filtered after their sampling and deep-frozen at -80°C. The water samples were examined for fluorescence by the Turner C6 device at the IHF. A method by Jeffrey and Humphrey (1975) has been applied to determine the chlorophyll-a concentration for the phytoplankton parameter (personal communication with Prof. Dr. Justus E. E. van Beusekom). The results of the analysed water samples are two reference samples A and B with their related 4D informations: latitude, longitude, depth and time (see Table A.3 in the appendix). These data are used to analyse the corresponding chlorophyll-a value from the TRIAXUS measurement (see steps below), enabling the evaluation a scaling factor.

Localising the proper corresponding TRIAXUS measurement of the chlorophyll-a concentration is all but impossible, due to the fact that the discrepancy of temporal and spatial values between the reference samples and TRIAXUS samples is not being meted at identical time and space during the cruise (compare the Tables A.1 and A.3 in the appendix). In order to localise the best possible corresponding measured value from the TRIAXUS a trade off has to be assumed.

The following steps have been applied to determine the corresponding TRIAXUS chlorophyll-a concentration for the parameter of phytoplankton:

In a first step, the time recorded by TRIAXUS should be as close as possible to the meted time of

the reference sample. The largest offset exhibits at the first day of the cruise (approximately between 2.5 h - 3 h). Otherwise it lies at about 20 minutes to around of 2 h.

In a second step, the depth recorded by TRIAXUS and of the reference samples should be identical. If an equivalent depth is not possible due to a huge time lag, then a reasonable upper or lower TRIAXUS depth value is applied. The largest deviation has a value of 6 m.

In a third step, linear regression among the values of the reference samples A and B and the suggested TRIAXUS values have been performed for the transects H - S and S - H; and as an individual transect (H - S and S - H merged). The best result revealed a linear regression between the values of the reference sample A and the transect of H - S. It shows a slope of around 11.14, an intercept of about 0.13 and a correlation coefficient of 0.8 (see Figure 2.3). Other performed linear regressions are illustrated in section A.7 in the appendix.

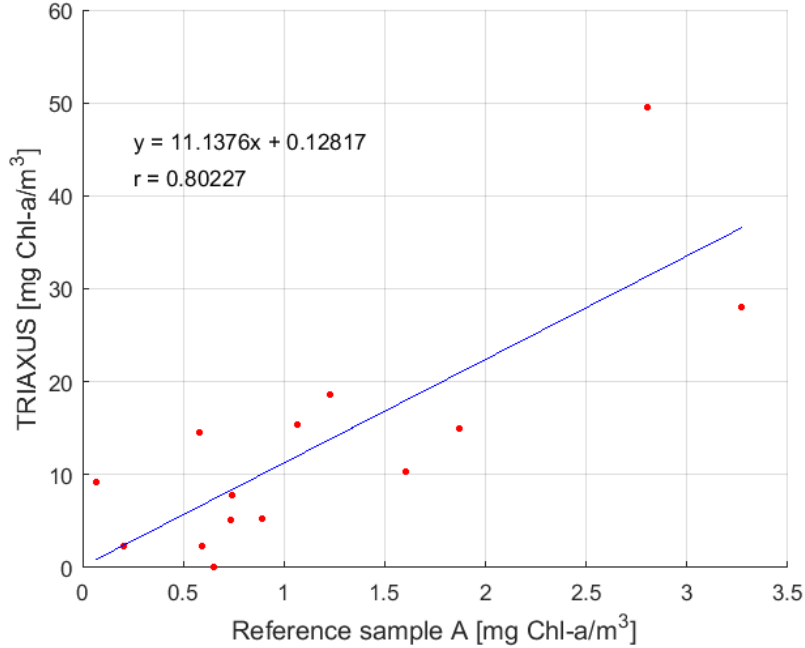


**Figure 2.3** – Linear regression of chlorophyll-a concentrations from the reference sample A and their suggested TRIAXUS chlorophyll-a concentrations from the transect Helgoland - Stonehaven.  $y$ : best-fit line.  $r$ : correlation coefficient.

Scaling the observed chlorophyll-a concentrations with the evaluated factor of 11.14 exhibit the values closer to the expected *in situ* concentrations of July in the North Sea. Additionally, the scaling factor is close to the factor of 10 which was applied to a previous expedition (HE427) in the North Sea to rescale their meted chlorophyll-a concentrations (personal communication with Prof. Dr. Justus E. E. van Beusekom). Despite this, two matters have to be accounted for: one is related to the intercept of the regression line that does not traverse the origin. Consequently, using the suggested scaling factor is normally not allowed. But, the difference between the origin and the intercept can be considered as relatively small and can be neglected. The other concerns the evaluated reference samples at the IHF which have to be accepted under reservation (personal communication with Prof. Dr. Justus E. E. van Beusekom).

## 2.7 ECOHAM dataset

In contrast to the differently saved file formats of the observational data, the dataset of ECOHAM is stored in a nc-file format. The dataset includes a time series of 2001 - 2014 with daily simulated mean values of all state variables in each cell of the model (state variables see in the appendix of Lorkowski et al. (2012)).

Due to the fact that not all state variables will be applied in this work, the dataset has been reduced. Table B.4 in the appendix shows the selected state variables from the reduced dataset. Each parameter is saved in a 4D matrix which contains information in space (longitude, latitude and depth) and time. Where the observed data only comprise one state variable for phytoplankton, the model

exhibits two varying simulated data of phytoplankton (diatom and flagellate). Therefore, a variable for both diatom and flagellate needs to be added to a one-state variable phytoplankton for this work (see third step in section 2.8.2).

The following parameters have to be used from the simulated data to compare with the observational parameters:

### Physical

- Temperature
- Salinity
- Oxygen

### Biological

- Phytoplankton
- Microzooplankton
- Mesozooplankton

## 2.8 Visualisation of the observed and simulated data

In order to have a reasonable comparison of the biological and physical parameters between the observed and simulated data, a p-color plot was compiled to illustrate the transects from H - S and S - H. The advantage of such a plot is the non-interpolated image, whereas an interpolation is performed in the common used contour plots which can lead to erroneous interpretations.

### 2.8.1 Observed transect

The following steps have been conducted to visualise the observed data as a transect:

In a first step, the axes have been determined. With respect to the determined depth layers of the model, the vertical axis is defined as depth (unit in meter) with 14 z-layers (0 - 10, 10 - 15, 15 - 20, 20 - 25, 25 - 30, 30 - 35, 35 - 40, 40 - 45, 45 - 50, 50 - 60, 60 - 70, 70 - 80, 80 - 90, 90 - 100). The horizontal axis represents the longitude. Numbers 41 - 69 corresponds to longitudinal ECOHAM index in the model resolution (see Figure A.9 in the appendix). Selecting a notation as index numbers is simpler to investigate areas in the transect than in coordinates because each index represents a water column. The corresponding index number can be obtained by calculation of the observed data through the ECOHAM-grid which revealed 29 index numbers (see second step). A detailed derivation through the ECOHAM-grid is given in section A.10 in the appendix. As a consequence of the splitting into the 29 water columns (x-axis) and 14 depth layers (z-axis), each grid cell in the observed transect contains a different amount of observed daily values, whereas the model includes only one daily mean value (see section 2.2).

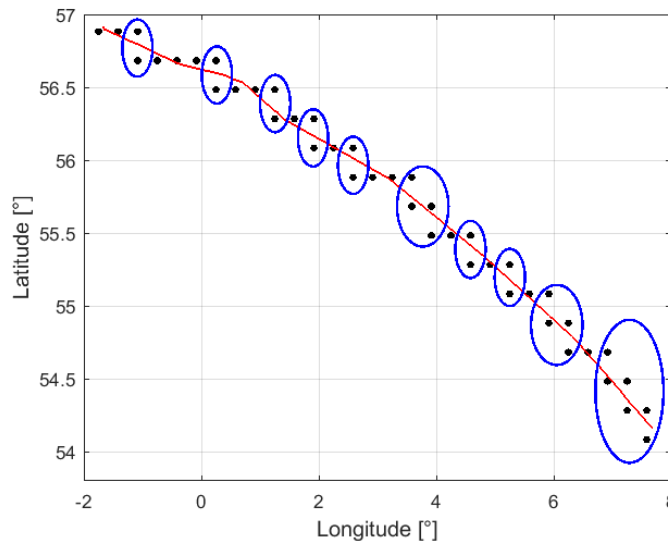


**Figure 2.4** – Observed transect through the ECOHAM-grid (derivation see section A.10 in the appendix) without weighted mean calculation. Black dots: ECOHAM-coordinates of the ECOHAM-cell. Blue circles: two ECOHAM-coordinates on identical longitudes. Red line: observed transect.

In a second step, a weighted mean has been calculated with the observational data through the

ECOHAM-grid for all parameters. After the proceeding, each grid-cell of the observed transect includes only one daily mean value. The aim of the second step is to find the ECOHAM-cells with their corresponding ECOHAM-coordinates in the model. These evaluated coordinates will be used to combine the model transects (see section 2.8.2) and to compute the wanted ECOHAM-coordinates of the displaced transects (see section 2.11). Due to the two affected ECOHAM-cells with their corresponding ECOHAM-coordinates on an identical longitude, finding the corresponding ECOHAM-coordinates is not distinctive without applying step two (see encircled black dots in Figure 2.4). The appearing of two ECOHAM-cells is caused by the ships route which crossed two neighbouring cells at equal longitudes in the model's resolution. However, the proceeding of the second step solves the problem: one of the concerned ECOHAM-cells is cancelled out and the corresponding ECOHAM-coordinates of the remaining ECOHAM-cell moves closer to the observed transect (compare for example the black dot number 43 in Figure 2.5b and the upper black dot from the first top left blue circle in Figure 2.4).

In a third step, all cells (gridded observations and modelled) between the depth measurements from the TRIAXUS, the LOPC device and the model topography have been removed. Additionally, cells are neglected when model topography is shallower than the observed depth. The objective of step three is to generate identical topography in the plots between the modelled and observed transects. The expedition topography (step three excluded) of the TRIAXUS and LOPC device from both transects is illustrated in the Figures A.2a and b, and Figures A.3a and b in the appendix, respectively.

The procedures above have been applied to additionally calculate the standard deviation for all observed parameters. Despite this, by using the suggested plot from MATLAB R2016a two remarks have to be pointed out here:

The first is related to the cell ECOHAM index 49, depth layer 80 - 90 m, for both transects. The observed mean value represents the whole cell between 80 - 90 m. But the maximum depth of the observed measurements during the expedition of HE428 lies approximately at 84 m. Consequently, the mean observed value represents the cell not completely.

The second concerns the cells thickness above the model bottom topography (see Figure B.1). The cell thickness can vary for each ECOHAM index (for example at the depth layer 70 - 80 m). Due to the fact that the suggested plot is only able to illustrate fixed depth layers within the transect, some thickness of the cells are probably not correctly illustrated above the modified bottom topography.

## 2.8.2 ECOHAM transect

According to the second step in section 2.8.1, the observed data revealed through the ECOHAM-grid 29 ECOHAM-cells with their corresponding ECOHAM-coordinates (see red filled cells in Figure 2.6). Based on these 29 ECOHAM-cells, the simulated transects will be compounded identically as the observed transects from H - S and S - H with (longitudinal) ECOHAM index 41 - 69 on the x-axis (see Figures 2.5a and b) and 14 depth layers on the z-axis. Identical treatment has also been applied on the displaced transects (see section 2.11) and on the transects of the short time series (see Table B.2 in the appendix) as well as on the long time series (2001 - 2014).

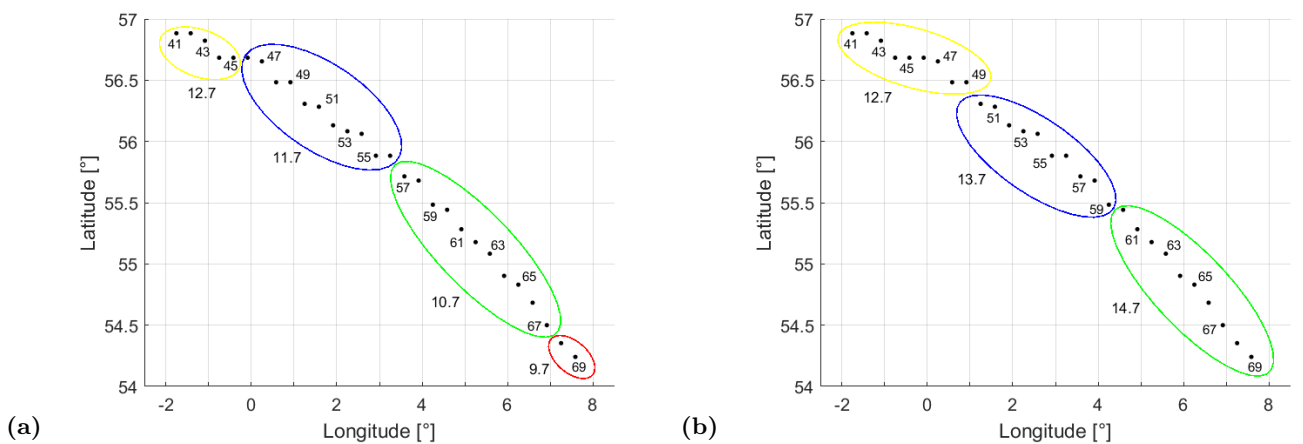


**Figure 2.5** – Daily sections of the modelled transect (circles). Numbers and dots represent (longitudinal) ECOHAM index and ECOHAM-coordinates, respectively. Note that only odd numbers are illustrated. (a) Transect from Helgoland - Stonehaven. (b) Transect from Stonehaven - Helgoland.

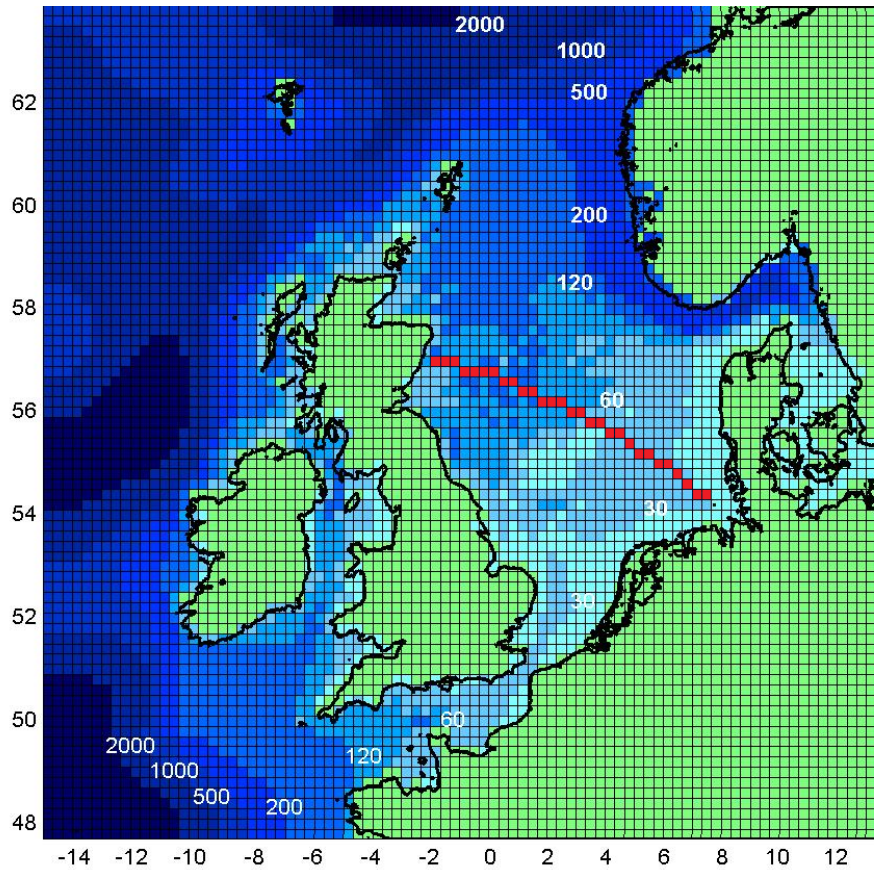


**Figure 2.6** – Horizontal grid and bottom topography of the HAMSOM-ECOHAM model domain. White values represent depth levels. Red filled cells: modelled expedition transect with their corresponding 29 grid cells.

The following steps have been applied to illustrate the simulated data as a transect:

In the first step, each day of the expedition has been considered as an own section of the entire transect. As a consequence, the track of H - S (9 to 12 July) is divided into 4 parts and the track of S - H (12 to 14 July) is split into 3 parts. Figures 2.5a and b show the daily sections (circles) of the modelled transects of H - S and S - H, respectively. Note that each section does not cover the equivalent amount of ECOHAM-cells in both tracks. When an ECOHAM-cell is affected on two days during the cruise (e.g. 10 and 11 July), this cell is considered as a part of the ensuing day.

In a second step, the state variables diatom and flagellate (see Table B.4 in the appendix) have been added as a new parameter phytoplankton, due to the fact that the observed phytoplankton does not distinct between species.

In a third step, the simulated data with the physical and biological parameters of each daily section has been combined as the transects of H - S and S - H.

In a fourth step, the bottom topography of the modelled transects has been equalised to the observed transects (see third step in section 2.8.1). The expedition topography from the simulated transect is illustrated in Figure B.1 in the appendix. Note that hereafter using the term "bottom" for the transects means the equalised bottom between the observed and modelled transect. Due to the fact that the modelled transects are composed in days, a standard deviation for all parameters is not possible as the model included in every cells only a daily mean value.

## 2.9 Comparison between the observed and simulated expedition transects

After the simulated and observed data were processed and visualised as transects, they can be compared among each other.

In a first step, a one-to-one comparison of the observed physical (temperature, salinity and oxygen) and biological (phytoplankton, microzooplankton and mesozooplankton) parameters, as well as the corresponding model results was carried out. For this, six simulated parameters have been extracted where the results match in time and space of the observational data and have to be compared with the observed parameters. The comparison of the six parameters have the intention to analyse the agree-

ment between the modelled and observed transects. A graphical comparison between the simulated and observed transects for all parameter is illustrated in section 3.2.

Additionally, the comparison of the observational and simulated data with all parameters were expanded. In order to understand a possible match, the corresponding data from the model has been extracted: (1) in space from the shifted tracks of 60 and 120 km northeast (NE) and southwest (SW), respectively (see section 2.11), (2) in time from 2001 - 2014 (long time series) as well as 1 - 2 weeks before and after the expedition. Table B.2 in the appendix shows the allocated days of the corresponding weeks for both transects.

Graphical comparison of both tracks with all six parameters in space and time is extensive. An improved method is the statistic approach. A typical method is the calculation of correlation coefficient between the simulated and observed data (see section 2.13).

A further common method is to measure the "distance" between the observational and simulated data by a so-called cost function. Two cost functions have been applied (see sections 2.9.1 and 2.9.2) for all six parameters as well for the threshold between microzooplankton and mesozooplankton (see section 2.10.1) for the transects H - S and S - H in space and time. Applying two cost functions can reduce misinterpretations and is useful for the comparison among each other. The results are illustrated in sections 3.4.1 for the physical parameters and 3.4.2 for the biological parameters.

### 2.9.1 Cost function A

The cost function A is described as follows:

$$C_{x,z} = \frac{Obs_{x,z} - Obs_{mean}}{SD_{Obs_{all,cells}}} - \frac{ECOHAM_{x,z} - ECOHAM_{mean}}{SD_{ECOHAM_{all,cells}}}, \quad (2.1)$$

$$D_A = \frac{1}{n} \sum_{i=1}^n |C_{x_i,z_i}|, \quad (2.2)$$

where  $Obs_{x,z}$  and  $ECOHAM_{x,z}$  are the observed and simulated values in a grid cell of the transect, respectively.  $Obs_{mean}$  and  $ECOHAM_{mean}$  are the mean of all grid cells in the transect. The standard deviation (SD) is defined as  $SD_{Obs_{all,cells}}$  for the observation and  $SD_{ECOHAM_{all,cells}}$  for the model. Note that the simulated and observed SD in the equation (2.1) have been calculated from the entire transect.

Whereas the first term on the right of equation (2.1) is the normalised observed anomaly of a grid cell, the second term of equation (2.1) is the normalised simulated anomaly of a grid cell. The term  $C_{x,z}$  on the left of the equation (2.1) represents the normalised difference of anomaly between observational data and simulated data in each grid cell of the transect.

The term  $D_A$  in equation (2.2) is the summation of each grid cell ( $C_{x,z}$ ) over the whole transect divided by the number of all counted grid cells in the transect. It describes the mean of the normalised difference of anomaly between the modelled and observed transects.

### 2.9.2 Cost function B

According to Villars (1996), the cost function B is defined as:

$$C_{x,z} = \frac{ECOHAM_{x,z} - Obs_{x,z}}{SD_{x,z}}, \quad (2.3)$$

$$D_B = \frac{1}{n} \sum_{i=1}^n |C_{x_i,z_i}|, \quad (2.4)$$

where  $ECOHAM_{x,z}$  is the simulated value and  $Obs_{x,z}$  is the observational value of each grid cell of the transect. The observational SD, given as  $SD_{x,z}$ , represents only one grid cell in the transect. Consequently, each grid cell in the observed transect has probably a different corresponding value for  $SD_{x,z}$ . Dividing each grid cell by the corresponding observed SD may exhibit a higher significance than by the mean value due to the fact that the SD contains higher and lesser values around the mean

value. On the other hand, a small evaluated SD value exhibits a large error in a grid cell due to the denominator in the equation (2.3).

The term  $C_{x,z}$  in equation (2.3) is the normalised deviation between the simulated and observed data and additionally, points out the "distance" of the relative error between the simulated and observational data at each point.

The term  $D_B$  in equation (2.4) is the summation of each grid cell ( $C_{x,z}$ ) over the whole transect divided by the number of all counted grid cells in the transect. It describes the mean relative error between the modelled and observed transects.

## 2.10 Biomass size spectra

Elton (1927) was one of the first that looked into the subject of the size spectrum of organisms. In the book chapter *THE ANIMAL COMMUNITY* in his book *Animal ecology*, he stated that smaller animals are much more abundant than larger ones. Additionally, he pointed out that a series of inter-connecting food chains from animal communities create a food web and concluded that the elemental food chains comprise a food web which are arranged in order of increasing organism size. The result is a general flow (energy transfer) through the community from the small organisms to large ones.

In the sixties, Sheldon and Parsons (1967) proposed a concept of the size spectrum. They demonstrated that measurements of particulate matter in the sea can be plotted as particle diameter on a logarithmic scale versus concentration of particles, expressed as biomass or volume. The slope of these so-called size spectra is uniform and approximately constant over the size range from bacteria to whales and covers all climate zone (Sheldon et al., 1972; Boudreau and Dickie, 1992). A linear negative relationship is reflected between the logarithm of size class, which is usually scaled in equivalent spherical meter (ESD), or body mass and logarithm of biomass or abundance.

### 2.10.1 Threshold between microzooplankton and mesozooplankton

As mentioned in section 2.2, the model ECOHAM includes two zooplankton groups: microzooplankton and mesozooplankton. But both groups do not contain the information about the size classes which can be used as the threshold to classify the meted particle size from the observed data into the microzooplankton and mesozooplankton. A comparison between simulated and observed data of both parameters is not feasible if the threshold has not yet been evaluated. Applying the suggested cost functions (see sections 2.9.1 and 2.9.2) with several specified size classes (see below) is an useful method to identify such a threshold.

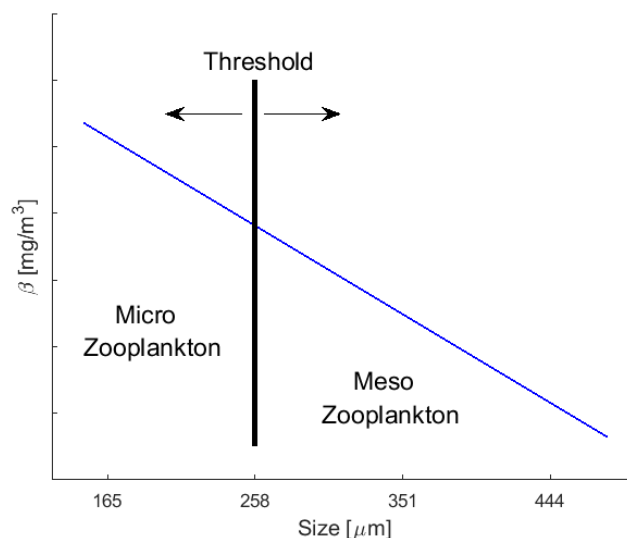


**Figure 2.7** – Sketch of biomass size spectrum theory. Blue line: slope of biomass. Black thick line: threshold between microzooplankton and mesozooplankton.

In order to identify the threshold between the microzooplankton and mesozooplankton following steps have been performed:

- Particle sizes of  $< 150 \mu m$  have been neglected due to the fact that such small particles include primarily phytoplankton species. As a consequence, the size spectra from the LOPC device decreases from  $5 \mu m - 1920 \mu m$  to  $150 \mu m - 1920 \mu m$ .
- The reduced size spectra has been divided into 20 size classes.
- 4 size classes have been defined to obtain the threshold:  $165 \mu m$ ,  $258 \mu m$ ,  $351 \mu m$  and  $444 \mu m$ . Each reasonable grouping will be tested. The result is the shifting of the threshold between microzooplankton and mesozooplankton (see Figure 2.7).
- The observed data has been separated into the parameters microzooplankton and mesozooplankton by the suggested size classes.
- The observed data has been separated into the parameters microzooplankton and mesozooplankton by the suggested size classes.
- The separated observed data has been converted into  $mmol C/m^3$  to allow comparison with the simulated data. The detailed derivation of the meted particle size into the carbon concentration unit is given in section A.13 in the appendix.
- The cost functions have been applied to each size class to obtain the threshold. The results of both transects are given in Figures 3.1a and b for the microzooplankton and in Figures 3.1c and b for the mesozooplankton, respectively.

When the threshold is identified by implementing the cost functions, the observed data is used to compare with the simulated microzooplankton and mesozooplankton parameters (see section 2.9). The results of the other size classes are given in section A.16.2 in the appendix.

### 2.10.2 Technical measurement of plankton

Whereas Lorenzen (1966) already introduced a continuous measurement technique for the estimation of chlorophyll concentration by an *in situ* fluorometry in the middle of the sixties, a standard for continuous measurement of zooplankton had not yet been established.

Hardy (1939) was the first to design an *in situ* continuous plankton recorder in the thirties, which was enhanced in the sixties by Longhurst et al. (1966). The technique was based on stripe gauzes to filter the plankton (Hardy, 1939; Longhurst et al., 1966, p. 11, p. 215).

A different technique to continuously measure the plankton *in situ* was introduced by Maddux and Kanwisher (1965). Their device, the electronic zooplankton counter, is based on the operating principle of the Coulter counter (Coulter, 1957) which uses differences in conductivity between the cell and the suspending fluid as the particles transit an electrode interspace. With this new technology, it was possible to count particles that pass an electrode gap and, additionally, to measure the size of these particles. Hence, *in situ* measurements with the electronic zooplankton counter would not only give instantaneous information about zooplankton abundances and spatial patterns but also allow the capture of physical dimensions of the organism. Finally, it is possible to identify some dominant species (Herman and Dauphinee, 1980).

In the end of the eighties, Herman (1988) developed a new generation of electronic particle counters: the optical plankton counter (OPC). His device was based on optics (LED), unlike an earlier version that was also based on conductivity (Herman and Dauphinee, 1980). The OPC was capable of counting and sizing particles within a range of  $550 \mu m - 2000 \mu m$  of equivalent spherical diameter (ESD). The method to calculate particles over the ESD goes back to the assumption that zooplankton is an oblate spheroid, with a semi-major and semi-minor axis (Herman, 1992). Note that the ESD analysis never correlates to the true particle dimension in the case of anisodiametric particles (Jennings and Parslow, 1988). Afterwards, a successor model of the OPC had been developed and was able to detect particles down to a size of  $250 \mu m$  (Herman, 1992).

The next and latest OPC generation is the laser optical plankton counter (LOPC). This device is now able to recognise particles on a size range from  $100 \mu m - 3500 \mu m$  of ESD (Herman et al., 2004). In addition, the new LOPC also reduced a well known coincidence count problem and was capable of generating shape profiles before calculating the size distribution (Herman et al., 2004). The

predecessor OPC as well as the LOPC have the same feebleness. They can not distinct between living particles and dead particles such as detritus or marine snow. This gap can be solved by using a video plankton recorder (VPR) device.

## 2.11 Spatial displacement of the transects

In most cases the points of coordinates are given and the distance is the wanted parameter. In the present case, the distances of the displaced tracks and the coordinates of the observed and the modelled transect are well-known. But the respective coordinates of the moved transects are unidentified. This problem can be solved by applying the great-circle distance.

The shortest distance between two points on the surface of a sphere is given by measuring the line along the great circle combining the two points, which is the curvature between the two points. According to Meeus (1998), the distance of two points on a sphere is defined as follows:

$$d = R \arccos [\sin(lat_1) \sin(lat_2) + \cos(lat_1) \cos(lat_2) \cos(lon_1 - lon_2)], \quad (2.5)$$

where  $d$  is the distance in km,  $R$  the earth radius with multiplication factor of  $\pi/180$  in km. The variables  $lat_1$  and  $lon_1$ , respectively,  $lat_2$  and  $lon_2$  are the coordinates of the points.

Shifting the transect exactly towards northeast (NE) and southwest (SW) for each coordinate of the expedition transect, the equation (2.5) simplifies itself (a detailed derivation is shown in appendix B.2) because the shift in NE and SW equates a slope of  $45^\circ$  between the well-know and wanted coordinates (see black arrows in Figure 2.8).

According to the Pythagorean theorem, the slope triangle has a value of one by using  $45^\circ$  and, consequently, the length of both cathetus are identical. The hypotenuse is the distance between each coordinates of the expedition transect and shifted transects (see e.g. ECOHAM index 49 from the red line and ECOHAM index 51 from the first blue line in NE and ECOHAM index 47 from the first blue line in SW, respectively, in Figure 2.8).

By displacing the transects only towards NE and SW it is possible to calculate the cathetus length by rearranging the Pythagorean theorem (see the equation (B.2) in the appendix). On the other hand, the evaluation of a slope triangle greater or lesser than  $45^\circ$  is more sophisticated. Such cases are not treated in this work. However, rearranging the equation (2.5) and using the restriction as mentioned before, the corresponding latitude coordinates can be obtained by

$$\begin{aligned} lat_2 &= lat_1 + \frac{l_{cath}}{R} \text{ for NE,} \\ lat_2 &= lat_1 - \frac{l_{cath}}{R} \text{ for SW,} \end{aligned} \quad (2.6)$$

and the corresponding longitude coordinates can be received by

$$\begin{aligned} lon_2 &= \arccos \left[ \frac{\cos \left( \frac{l_{cath}}{R} \right) - \sin^2(lat_1)}{\cos^2(lat_1)} \right] + lon_1 \text{ for NE,} \\ lon_2 &= lon_1 - \arccos \left[ \frac{\cos \left( \frac{l_{cath}}{R} \right) - \sin^2(lat_1)}{\cos^2(lat_1)} \right] \text{ for SW.} \end{aligned} \quad (2.7)$$

Where  $lat_2$  and  $lon_2$  are the new coordinates moved towards NE and SW, respectively, and  $l_{cath}$  is the cathetus length from the slope triangle which can be evaluated from the equation (B.2) in the appendix.

Due to the fact that the coordinates and the distance (60 and 120 km) of the observed transect are well-known, it is possible to identify the wanted coordinates of the displaced tracks over the equations (2.6) and (2.7). These tracks correspond in space to the observed expedition transect.

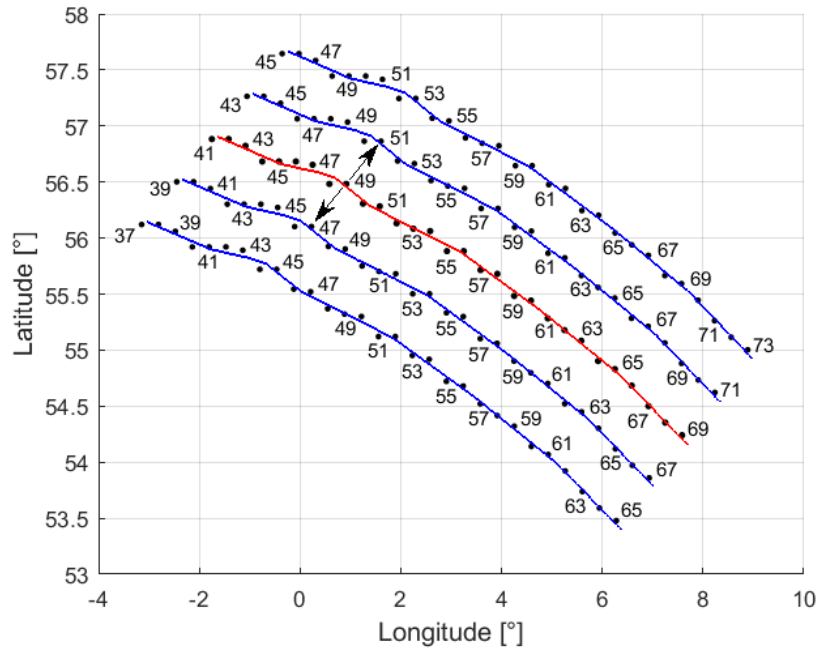


**Figure 2.8** – Displaced transects through ECOHAM-grid. Black dots: ECOHAM-coordinates. Numbers: ECOHAM index from the longitudinal direction (see Figure A.9 in the appendix). Note that only odd numbers of the ECOHAM indexes are illustrated. Red line: observed expedition transect. Blue lines: displaced transects 60 and 120 km towards NE and SW, respectively. Black arrows indicate the corresponding ECOHAM index of the displaced transects.

Afterwards, the new identified coordinates have to be recalculated into the ECOHAM-grid so that the corresponding ECOHAM-cells of the displaced transects can be evaluated by the model. Figure 2.8 illustrates the observed expedition track (red line) and the shifted tracks (blue lines) with their associated ECOHAM indexes. Note that only odd numbers of the ECOHAM indexes are shown.

As a result of the spatial displacement at  $45^\circ$ , the corresponding ECOHAM indexes of the expedition transect receives over the shifted transects a higher (towards NE) or a lower (towards SW) ECOHAM index number which equates to the smallest distance. But some parts are located on land mass (see green dots in Figure A.9 in the appendix). The Tables A.4 and B.1 in the appendix show the evaluated ECOHAM indexes with their corresponding indices and their corresponding coordinates for the expedition and displaced transects, respectively.

In order to guard against misunderstandings, all displaced transects are outfitted with a black thick line in the plots which indicate the beginning or the end of the expedition transect and the model bottom topography has been kept (see Figures B.1.2 (a) - (d) in the appendix). It should be kept in mind that equal ECOHAM indexes from the expedition and moved transects have the same coordinates in longitude but not in latitude (see for example ECOHAM index 49 in Figure 2.8). Note that for the displaced transects only the simulated data exist.

Some remarks have to be emphasised here by using the equations (2.6) and (2.7). The displaced transects exhibit in either directions a discrepancy of around 140 - 150 m (shifted 60 km) and of around 550 - 610 m (shifted 120 km) at lower latitudes towards higher latitudes (see Table B.1 in the appendix). Such discrepancies can be led back to two causes:

The first cause is referred to equation (2.5). According to Meeus (1998), equation (2.5) is only an approximation and may not work accurately with very small distances. Higher accuracy can be obtained by applying another method described in Meeus (1998).

The second cause is related to the mathematical space. In an Euclidean space the distance between two points is a straight line between them. Indeed, on the sphere no straight lines exists and the distance is substituted by geodesics which are the great circles on the sphere. The distance between two points is now an arc and not a straight line any more. Consequently, utilising longer distances in the equations (2.6) and (2.7) leads to higher deviations (see Table B.1 in the appendix). However, the deviation of the displaced transects by using the equations (2.6) and (2.7) and the calculated distances over the equation (2.5) lies in both directions from lower to higher latitudes of about 0.23 - 0.25% and 0.46 - 0.51% for 60 km and for 120 km, respectively (see Table B.1 in appendix). Due to the fact that

the model resolution exhibits 20 km in both directions, the determined shifted tracks are legitimated.

## 2.12 Representativeness of the simulated expedition transects

Two cost functions have been used statistically to compare the physical and biological parameters between the modelled and observed transects from H - S and S - H in space and time (see section 2.9). Such a reduction from the graphic to the statistic evaluation by the suggested cost functions is helpful but not sufficient, because the interpretation of the cost functions highlights only in one dimension. A representativeness of the modelled expedition transects in ECOHAM is not established in both space and time. Accordingly, another method has to be introduced to analyse the representativeness of the modelled expedition transect:

In a first step, three depth layers (0 - 10 m, 30 - 35 m and 60 - 70 m) have been selected to reduce the amount of data. These three depth layers represent the upper, middle and lower section of the model transect. It is assumed that all three depth layers together are adequate to represent the transect from the surface to the bottom of the previously selected plot (see section 2.8).

In a second step, model data of the minimum and maximum values in space and time have been extracted from the three depth layers from both tracks for the six parameters and additionally for the particulate organic carbon (state variables detritus fast and slow added, see Table B.4 in the appendix). The distance between the minimum and maximum allows to identify the variability. A low variability indicates an improved representativeness. In such cases, a relatively similar trend probably occurs through space and time in the transects. In contrary, a high variability trough the transects imply a low representativeness.

In a third step, a plot has been used to illustrate the variability. Each proposed 3 depth layers of both transects H - S and S - H are stated as ECOHAM index 41 - 69. For comparison with the distance, the modelled expedition transect (see expedition week in Table B.2 in the appendix) was implemented. Note that identical values of the modelled expedition transect and the extracted minimum or maximum values indicate a low representativeness in case of large variability. The results are shown in section 3.3.

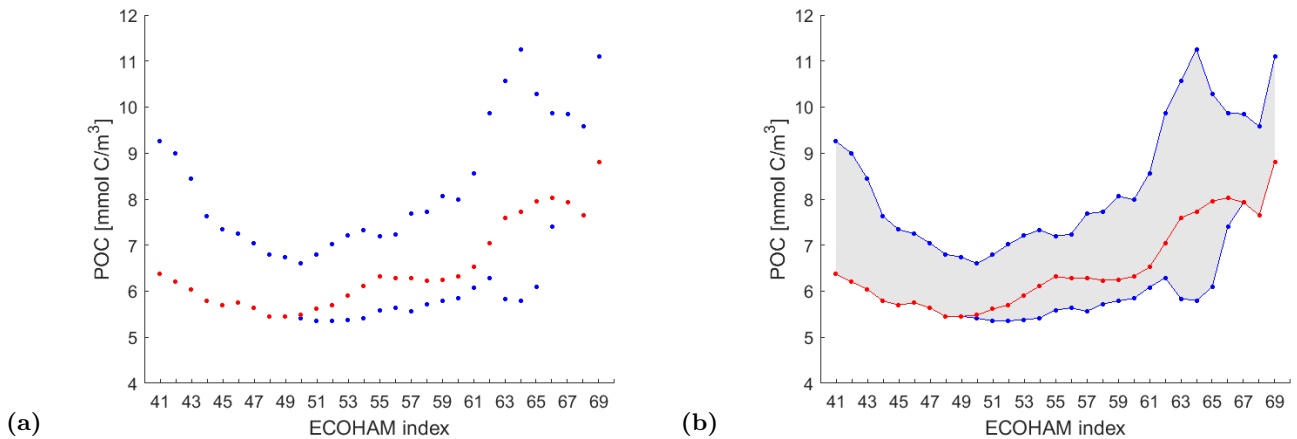


**Figure 2.9** – Simulated particulate organic carbon (POC) concentrations in depth layer 0 - 10 m from the transect Helgoland - Stonehaven of the long time series (2001 - 2014). (a) Transect as discrete function. (b) Transect as continuous function. Blue dots: minimum and maximum values. Red dots: modelled expedition transect. Gray shaded: distance from minimum to maximum values.

Two remarks concerning the plot have to be emphasised here:

The first concerns the extracted minimum and maximum values. Each minimum and maximum value in ECOHAM index 41 - 69 of the 3 depth layers are from different years of the long time series and different weeks of the short time series, respectively, and from different stated ECOHAM indexes of the shifted transects for all examined parameters.

The second is related to the visualisation. As the values from ECOHAM index 41 - 69 are discrete, the transect is only plotted as points (see Figure 2.9a). A graphical evaluation with such discrete values is arduous and can lead to erroneous interpretations. Therefore, two additional modifications have been performed into the plot which simplify the interpretation of the representativeness. Firstly, the

modelled expedition transect (red coloured) and the values of minimum and maximum (blue coloured) are plotted as a continuous function from ECOHAM index 41 - 69. Note that as a consequence of selecting the continuous function, the values between two neighbouring ECOHAM indexes are interpolated. Secondly, the distance between the minimum and maximum has been shaded grey to highlight the variability. Figure 2.9b shows the modifications for the parameter POC in the depth layer 0 - 10 m of the long time series for the transect H - S.

### 2.13 Statistical analysis of the transects in space and time

In section 2.9, a statistical method with two suggested cost functions has been implemented to compare the observed and simulated parameters in space and time. However, both cost functions do not exhibit the correlation between simulated and observed parameters. Utilising a simple linear regression and calculating the correlation coefficient is a common method of summarising the relationship between two state variables which is usually shown as a scatter plot with a single straight line. Additionally, the value of the correlation coefficient highlights the agreement between two variables or datasets (see section 2.9).

Simple linear regressions have been performed for all parameters between the simulated and observed data from the transects H - S and S - H in space and time. The results of the slopes and intercepts of the physical and biological parameters of the linear regression are shown in Tables A.9 and A.10 for both transects in the appendix.

Two correlation coefficients have been evaluated for each performed linear regression of both transects (see above):

One correlation coefficient is calculated only by the simulated data in space and time (stated as  $r_1$  in the Tables 3.1 and 3.2). The intention to calculate correlation coefficients only between the modelled transects is to highlight the statistical representativeness of the modelled expedition transects within the physical and biological parameters in space and time. It should be kept in mind that the representativeness of all parameters of  $r_1$  reflects the full transect, whereas the representativeness of the 3 suggested depth layers (0 - 10 m, 30 - 35 m and 60 - 70 m) in section 2.12 reflects only partially both transects for all parameters.

Other correlation coefficient is calculated between the simulated and observational data in space and time (stated as  $r_2$  in Tables 3.1 and 3.2). The correlation coefficient  $r_2$  quantifies the agreement of the model data in space and time. With respect to the 5 m thickness layer, the layers of 10 m thickness (depth layer: 0 - 10 m, 50 - 60 m, 60 - 70 m, 70 - 80 m and 80 - 90 m) have been weighted for the calculations of  $r_1$  and  $r_2$ .

In addition, a two sided confidence interval ( $r_U$  for upper limit and  $r_L$  for lower limit) of 95% and 99% and a two sided significance level  $\alpha$  of 5% and 1% have been computed for the physical and biological parameters in space and time for the transect H - S and S - H. Note that the two sided confidence intervals and the two sided significance levels are only evaluated from the correlation coefficient of  $r_2$ . The results of the confidence intervals for all six parameters are given in the Tables A.7 and A.8 in the appendix, whereas the Tables 3.1 and 3.2 show the results of the significance levels  $\alpha$  for all six parameters for both tracks. It should be mentioned that the check mark in significant level  $\alpha_{5\%}$  and  $\alpha_{1\%}$  in Tables 3.1 and 3.2 points out significance for the correlation coefficient  $r_2$ . In contrary, a blank significance level  $\alpha_{5\%}$  and  $\alpha_{1\%}$  points out no significance of the correlation coefficient  $r_2$ .

As the significance levels reveal only if the physical and biological parameters are statistically significant, a two sided p-value has been additionally evaluated. The p-value is applied as an alternative to provide the smallest level of significance at which the null hypothesis would be rejected (see more details in section A.14 in the appendix). The results are given in the Tables A.9 and A.10 in the appendix for the transect H - S and S - H. Note that p-values lower than 0.04% ( $z_0 > 3.5$  or  $z_0 < -3.5$ ,  $z_0$  values are from the standard normal distribution) have not been calculated. The derivation of the confidence interval and the significance level is illustrated in section A.14 in the appendix.

Additionally, the proceedings above have been implemented for the other size classes (165  $\mu m$ , 351  $\mu m$  and 444  $\mu m$ ) of the microzooplankton and mesozooplankton (see section 2.10.1). The results are illustrated as Tables in section A.16.2 in the appendix.

## Second part

### 2.14 Estimation of nutrient concentrations within a selected area for the observed transect

During the expedition of HE428 no nutrients were measured. Therefore, a concept has been developed to estimate the nutrient concentrations of ammonium and nitrate indirectly from the meted oxygen concentrations. The principal objects of this concept are:

- A comparison between the estimated and simulated nutrient concentrations to receive information about the accuracy of the model.
- A possible methodology aid to estimate nutrient concentrations which can be obtained indirectly by the observed oxygen concentrations if no nutrients have been measured on a cruise.

Plants as well as animals require nutrients for growth. In marine ecosystems nutrients are available in inorganic forms of nitrogen, phosphorus and silicon. During summer, a thermocline develops and splits the water columns into two layers in seawater at higher latitudes. As a result of forming a thermocline, the concentration of nutrients is low in the upper mixed layer due to rapid consumption, whereas it is high below the thermocline caused by the oxygen requirement processes remineralisation and nitrification, respectively.

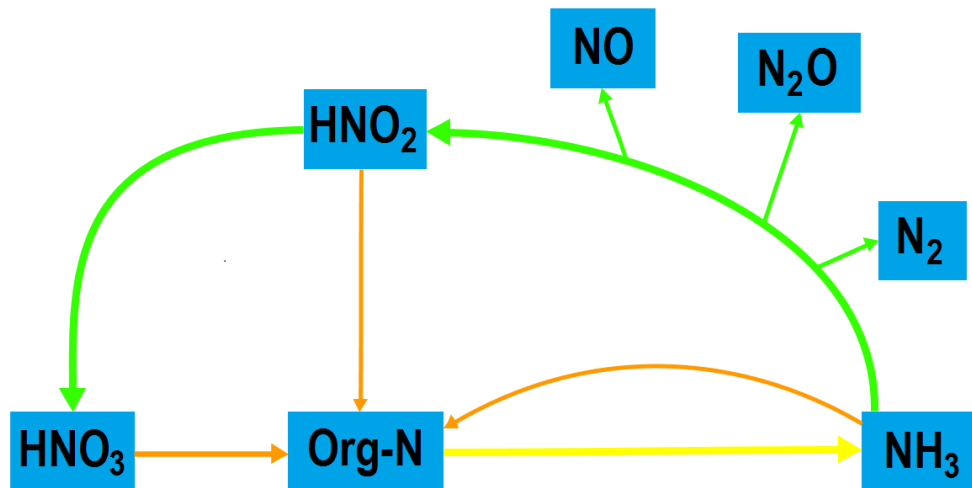


**Figure 2.10** – Simplified marine oxic nitrogen cycle (adapted from <https://www.mpi-bremen.de/Schleichwege-im-marinen-Stickstoffkreislauf.html>). Yellow: remineralisation. Green: nitrification. Orange: assimilation.  $HNO_3$ : nitrate.  $Org-N$ : organic matter.  $NH_3$ : ammonium.  $N_2$ : nitrogen.  $N_2O$ : nitrous oxide.  $NO$ : nitric oxide.  $HNO_2$ : nitrite.

The oxygen consumption is coupled to two main fluxes: the remineralisation of organic matter into inorganic matter and the nitrification of ammonium to nitrate. The remineralisation process (see yellow thick line in Figure 2.10) releases ammonium ( $NH_3$ ), whereas the nitrification process (see green thick line in Figure 2.10) releases nitrite ( $HNO_2$ ) in the first chemical reaction and in the second reaction nitrate ( $HNO_3$ ) is released. A simplified oxic marine nitrogen cycle is illustrated in Figure 2.10.

#### 2.14.1 Estimation of the nutrient concentration concept

Reliable estimation of nutrients is only feasible for a water parcel that is isolated (typically after the formation of a thermocline) from the atmosphere and its freshwater inputs. Hence, such conditions limit the possibility of estimation in the deeper parts of the North Sea, respectively in the interior of the oceans.

With respect to the transects H - S and S - H, the region is defined by the water columns of ECO-HAM index 47 - 54 below 40 m depth (see black thick line in Figures A.10a and b in the appendix).

These suggested water columns are always below the thermocline, hence not affected by the inputs of freshwater, and decoupled from the air-sea exchange. The horizontal dimension is approximately 160 km with a maximum vertical depth of about 90 m. It should be mentioned that the water columns of ECOHAM index 53 and 54 of transect H - S have been excluded due to the lack of observed oxygen data during the expedition.

Based on the model of Ito and Follows (2005), the estimation of nutrient concentration concept is determined with following components: the "preformed" and "regenerated" component and a new introduced "physics" component.

When a persistent stratification is developed, three different nutrient fractions can be distinguished in the water parcel: (1) The fraction of unused nutrient which was transported and subducted is referred as the "preformed" nutrient. Its concentration corresponds to the concentration of the previous day onset of a persistent stratification. (2) The fraction of nutrients that was regenerated by remineralisation and nitrification fluxes is referred as the "regenerated" nutrient. As the "regenerated" component represents the biological part, the biological activity can be derived by the apparent oxygen utilisation (AOU, see section 2.14.5). (3) The fraction of nutrient which was advected and vertically mixed is referred as the "physics" component. It should be kept in mind that the "physics" component is regarded as a non-isolated water parcel. In contrast, the "preformed" and "regenerated" components are considered as an isolated water parcel. Hence, the advection and mixing act as a sink or source in the "physics" component. As the "physics" component represents the physical part, the nutrient concentrations from the advection and mixing can be evaluated by the model output.

Some processes are neglected in the concept: assimilation processes of ammonium, nitrite and nitrate to organic matter, loss of ammonium concentrations during nitrification for nitric oxide ( $NO$ ), nitrous oxide ( $N_2O$ ) and nitrogen ( $N_2$ ) (see Figure 2.10), allochthonous respiration as well as regeneration of oxygen from the primary production in deeper layers. However, several proceedings are necessary that the estimated nutrient concentrations of ammonium and nitrate can be obtained in the defined area:

In a first step, the calculation of the persistent stratification ( $t_{stratification}$ ) is the basic principle to estimate the concentration of the "preformed" component. If the day of  $t_{stratification}$  is not identified then the estimation is not possible. In contrast to AOU values obtained by observational data,  $t_{stratification}$  can only be derived from the model output. A detailed description to determine the onset of persistent stratification for the selected water columns (ECOHAM index 47 - 54) in the specified region is given in section 2.14.3.

In a second step, the mass budgets of the physical and biological activities from the model has to be compiled from the time series of the previous day of the determined  $t_{stratification}$  until the day of the observed selected water columns of the expedition. The results are given in Tables B.5 and B.6 in the appendix for the transect H - S and S - H, respectively.

In a third step, the AOU has to be calculated. If no *in situ* data of the physical parameters oxygen, temperature and salinity is provided, an estimation is not feasible. Section 2.14.5 explains the method to calculate the AOU.

In a fourth step, the produced ammonium and nitrate have to be derived by the previously determined AOU. Accordingly, the amount of consumed oxygen (corresponds to the AOU) will be divided into two fractions: one part will be exhausted by the flux of remineralisation of organic matter to inorganic matter (generating of  $NH_3$ ) whereas the other part will be exhausted by the flux of nitrification from ammonium to nitrate (generating of  $HNO_3$ ). A schematic diagram of the AOU exhausting is given in Figure 2.11. Introducing a scaling factor  $m$  and  $(1 - m)$ , respectively, splits the quantity of AOU from both fluxes and can be written as follows:

$$AOU = m AOU_{remi} + (1 - m) AOU_{nitri}, m \in [0, 1], \quad (2.8)$$

where  $m AOU_{remi}$  is the amount of AOU exhausted by the remineralisation process and  $(1 - m) AOU_{nitri}$  is the amount of AOU used by the nitrification process.

In a fifth step, the introduced factors  $m$  and  $(1 - m)$  have to be determined. It should be mentioned that both factors are calculated only in the cells of ECOHAM index 47 - 54 from the top layer (40 - 45 m) in the specified area and are regarded as constant for all its deeper layers (see black thick line in Figures A.10a and b in the appendix). A detailed description is given in section 2.14.8.

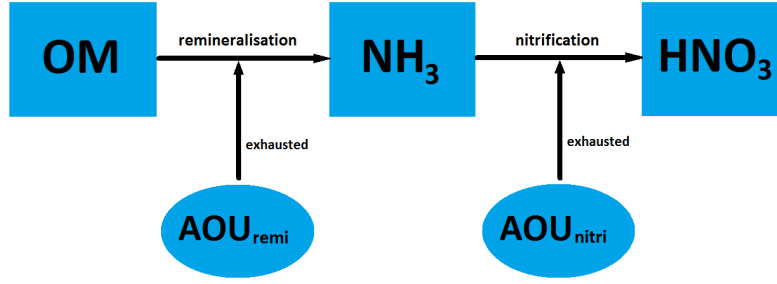


**Figure 2.11** – Schematic diagram of the AOU exhausting within the remineralisation and nitrification fluxes. OM: organic matter.  $\text{NH}_3$ : ammonium.  $\text{HNO}_3$ : nitrate. AOU: apparent oxygen utilisation. The amount of AOU is separated in two fractions:  $\text{AOU}_{\text{remi}}$  and  $\text{AOU}_{\text{nitri}}$ .

### 2.14.2 Basic principle of the estimation of nutrients

According to Ito and Follows (2005), the estimation of nutrient concentration is described as

$$\text{Nutrient}^* = \text{Nutrient}_{\text{preformed}} + \text{Nutrient}_{\text{regenerated}}, \quad (2.9)$$

where  $\text{Nutrient}^*$  is the estimated nutrient concentration, and  $\text{Nutrient}_{\text{preformed}}$  is the nutrient concentration from the previous day of the determined  $t_{\text{stratification}}$  and can be regarded as the initial concentration.  $\text{Nutrient}_{\text{regenerated}}$  is the nutrient concentration regenerated by biological activities.

As mentioned before, the "preformed" and "regenerated" components are considered as isolated water parcels. However, in the ocean an exchange also occurs among the neighbouring water parcels. Such water parcels are considered as non-isolated. Hence, involving an exchange among the neighbouring water parcels, equation (2.9) has been enhanced with an additional physical component:

$$\text{Nutrient}^* = \text{Nutrient}_{\text{preformed}} + \text{Nutrient}_{\text{regenerated}} + \text{Nutrient}_{\text{physics}}, \quad (2.10)$$

where the newly introduced term  $\text{Nutrient}_{\text{physics}}$  is the sum of the advected and vertically mixed nutrient concentration from the previous day of  $t_{\text{stratification}}$  to the day of the observational measurement from the expedition. Enhancing equation (2.9) from Ito and Follows (2005) with such a physical component has the effect that the estimation of the nutrients becomes more accurate.

### 2.14.3 Preformed component

As stated in section 2.14.1, the onset of persistent stratification ( $t_{\text{stratification}}$ ) remains until the observation time is deducible only from the simulated data. A method to determine the day of onset of persistent stratification is to calculate the mixed layer depth (MLD) in a water column throughout the year.

During summer the MLD is mostly restricted to the upper layer by stratification, whereas during winter the MLD reaches the bottom in shallow sea water or several hundreds of meters depth in deeper oceans (Große et al., 2015). Salinity, temperature and nutrient concentrations in the water columns of the MLD are relatively homogeneous due to steady mixing.

According to Große et al. (2015) a water column is regarded as a rectangular geometry with a depth of the mixed layer ( $D_{ML}$ ). Supposing that during the winter the maximum of  $D_{ML}$  is reached due to convection and is identical to the MLD, then the MLD determines the vertical extent of a water column. The  $D_{ML}$  is specified as the depth  $z$  between the surface to the maximum depth in a water column where the following temperature difference criterion is fulfilled:

$$\text{SST} - T(z) \leq 0.4 \text{ K}, \quad (2.11)$$

where SST is the sea surface temperature and  $T(z)$  the temperature in depth  $z$ . Note that the value of  $\Delta T = 0.4 \text{ K}$  is within the range of literature values of  $\Delta T = 0.1 \text{ K}$  to  $1.0 \text{ K}$  (Große et al., 2015; Kara et al., 2000). The term  $\Delta T$  will be discussed in section 4.5.

Applying the MLD criterion from equation (2.11) on the daily SST data from the model output and afterwards arranging each day from 1 January to 31 December (365 Days, without a leap year), the MLD can be obtained throughout the year for a water column (see dashed lines in Figures 3.16a

and b and in Figures B.8 (a) - (f) in the appendix). Note that the determined  $t_{stratification}$  for the water columns of ECOHAM index 47 - 54 have been applied in both transects with exception of the water columns ECOHAM index 53 - 54 in transect H - S due to lack of AOU data. A remark has to be emphasised here by using the contour plot in MATLAB R2016a to visualise the MLD throughout the year: The depth of the surface layer from the model can be identified by different values in the illustrated contour plot: 0 m, 5 m or 10 m. It has been defined as the minimum depth of the mixed layer to start at 8.75 m in the water column due to the fact the highest temperature gradient between upper and lower layer can be expected at this level. Hence, the 14 depth layer values of MLD in the transect (8.75 m, 15 m, 20 m, 25 m, 30 m, 35 m, 40 m, 45 m, 51.25 m, 60 m, 70 m, 80 m, 90 m, 102.5 m) are determined over the mean of the two middle values from the range of the upper and ensuing sub layer in the model (see z-axis values in section 2.8.1).

#### 2.14.4 Physical component

As mentioned in section 2.14.2, an additional physical component has been implemented in equation (2.10). It is the sum of changes in concentration caused by advection and mixing and can be evaluated for a compiled mass budget from the simulated data.

When the days of the onset of persistent stratification in all water columns (see section 2.14.3) are examined by the MLD criterion, the physical and biological mass budgets are compiled for the nutrients ammonium and nitrate of the cells of ECOHAM index 47 - 52, depth layer 40 - 45 m, for transect H - S and of the cells of ECOHAM index 47 - 54, depth layer 40 - 45 m, for transect S - H.

The time series of the mass budgets starts for each ECOHAM index at the previous day of  $t_{stratification}$  and ends with the corresponding ECOHAM index of the observational day. Tables B.5 and B.6 in the appendix show the mass budgets and time series of the selected cells in the determined area for both tracks. Note that the simulated biological and physical values from the top layer (40 - 45 m) of each ECOHAM index are regarded as constant for its deeper layers.

#### 2.14.5 Apparent Oxygen Utilisation

Primary production liberates oxygen through photosynthesis and increases the oxygen concentration in the ocean or freshwater systems, meanwhile processes of remineralisation as well as nitrification consume it and the oxygen concentration decreases. Such biological activities effect the dissolved concentration of oxygen in sea water.

Supposing that oxygen concentration in the water parcel was close to the saturation concentration at the surface, it can be estimated how much oxygen is consumed by the remineralisation and nitrification of organic molecules (Ito and Follows, 2005) in conditions that the water parcel is isolated from the atmosphere after the stratification and from its freshwater inputs. For other conditions an estimation is not reliable.

According to Ito et al. (2004) and Ito and Follows (2005), the AOU is the difference between the oxygen saturation concentration,  $O_{2,saturation}$ , and the observed oxygen concentration,  $O_{2,observed}$ , as defined in equation (2.12):

$$AOU = O_{2,saturation}(T, S) - O_{2,observed}, \quad (2.12)$$

where  $O_{2,saturation}$  is a function of temperature and salinity. A detailed description of the functions is depicted in Weiss (1970). Note that temperature and salinity have to be *in situ* measurements.

While AOU represents the sum of the biological consumption activity, their concentrations are low or negative in the layers above the thermocline. Negative values imply that the production of dissolved oxygen (DO) by primary production is higher than the amount of consumption. In contrary, high AOU concentrations are located below the thermocline and in the interior ocean due to a lack of generating DO by primary production. Generally, in such areas the DO is increasingly depleted as the water mass accumulates regenerated nutrients (Ito and Follows, 2005).

The values of  $O_{2,saturation}$  have been obtained by using a pre-assembled written MATLAB program from Christian Mertens, IfM Kiel, Revision: 1.0, Date: 01.05.1996. It has to be mentioned that the program is based on Weiss (1970). Figures A.10a and b in the appendix show the AOU for both observed transects. The black thick line determines the defined region where the nutrient concentrations has been estimated. The derived AOU values are given in Table A.5 in the appendix for both

transects. A deviation in percent has been evaluated from the top layer (40 - 45 m, regarded as the reference value) to the deepest layer of each water column (see Table A.6 in the appendix). The aim of the deviation is to highlight the variation of AOU within deeper layers in the selected area. Additionally, values of the oxygen saturation concentrations have been converted into percentage which simplify the interpretation. The Figures are illustrated for both tracks in section A.7 and A.8 in the appendix.

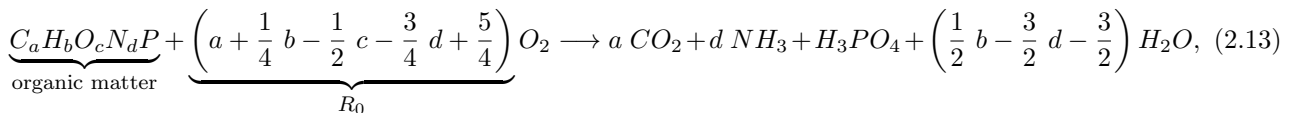
### 2.14.6 Regenerated component

In the open ocean, heterotrophic bacteria play a relevant role in the nutrient cycle: they use organic matter (OM) and transform it into inorganic form such as ammonium ( $NH_3$ ) and phosphate by remineralisation. Other heterotrophic bacteria species nitrify the produced  $NH_3$  into nitrate ( $HNO_3$ ). Both processes are aerobic and consume DO in sea water. A large fraction of the exported OM below the thermocline originates from primary production within the mixed layer and from the deep chlorophyll maximum (DCM). DCM can be considered as the main source of OM during summer.

Redfield (1934) pointed out that the amount of consumed oxygen is determined by the quantity of hydrogen, nitrogen, carbon, sulphur and phosphorus which oxidise in the decomposition of a given quantity of OM, and the relative changes in the amount of oxygen, phosphate, sulphate carbonate and nitrate depend precisely on the elementary composition of the plankton.

Based on his previous work (see above), Redfield developed a constant stoichiometric ratio of oxygen, carbon, nitrogen and phosphorus which are linked to biotic compounds and nutrient fluxes. The results revealed a ratio of  $-O_2:C:N:P = -138:106:16:1$  for plankton (Redfield, 1958) and is well-known as the Redfield ratio (hereafter stated as Redfield). In other words: organic matter that is remineralised by one mole of phosphorus generates 16 moles of nitrogen, 106 moles of carbon and requires 138 moles of dissolved oxygen. It should be mentioned that the composition of OM contains not only monosaccharides but also lipids, proteins and nucleic acids and as a consequence the stoichiometric Redfield can vary (Redfield et al., 1963; Richards, 1965; Anderson, 1995; Paulmier et al., 2009).

Aerobic remineralisation of OM requires DO and is a heterotrophic process that produces  $NH_3$ . According to Anderson (1995) and Paulmier et al. (2009) the aerobic remineralisation of OM can be described as follows:

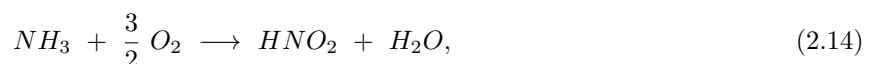


where a, b, c and d are the stoichiometric relations of OM in relation to one mole of phosphorus, and can potentially vary due to different composition of OM (see above), and include the Redfield 106:16:1 for C:N:P (see Table 2.1).

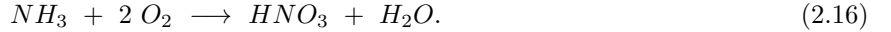
The required molar amount of DO by remineralisation is denoted as  $R_0$  in equation (2.13). Hence, the aerobic remineralisation  $R_0$  depends on the stoichiometric values of a, b, c and d and can be obtained from Table 2.1. Considering the maximum possible amount (for example: a = 108, b = 263, c = 23 and d = 16) of DO by the equation (2.13), the remineralisation value of  $R_0 = 151.5$  can be obtained. Proposing values of a = 106, b = 245, c = 30 and d = 18, a value of  $R_0 = 140$  is maintained, whereas for values a = 106, b = 251, c = 40 and d = 16 the Redfield ( $R_0 = 138$ ) can be received.

The maximum remineralisation ( $R_0 = 151.5$ ), the proposed remineralisation ( $R_0 = 140$ ), and Redfield ( $R_0 = 138$ ) are utilised to determine the production of  $NH_3$  by the remineralisation flux over AOU.

Nitrification is a two step process: first oxidation of ammonium to nitrite ( $HNO_2$ ) takes place, then oxidation of nitrite to nitrate ( $HNO_3$ ). Hence, one mole of  $NH_3$ , sustained by remineralisation of organic matter, is nitrified as follows:



and summarising equations (2.14) and (2.15) yields



It should be kept in mind that for example one mole of  $NH_3$  nitrified as in equation (2.16) demands double the amount of DO to produce one mole of  $HNO_3$ .

Regarding equation (2.8), the AOU is composed by two components:

$$AOU \left[ mmol O_2/m^3 \right] = x_{remi} \left[ mmol N/m^3 \right] \frac{R_0}{d} q + 2y_{nitri} \left[ mmol N/m^3 \right] q, \quad (2.17)$$

$$\text{with } q = \left[ \frac{mmol O_2/m^3}{mmol N/m^3} \right],$$

where  $x_{remi}$  is the quantity of produced  $NH_3$  and  $y_{nitri}$  is the quantity of produced  $HNO_3$ . The AOU value can be derived from equation (2.12).

With respect to equation (2.17), the AOU amount in the concerned cells from the selected area of the observed transects is separated into two parts: one fraction is exhausted over the remineralisation flux, the other part is exhausted over the nitrification flux (see Figure 2.11). The factors  $m$  and  $(1 - m)$  from equation (2.8) have been temporarily excluded in equation (2.17). Both factors are determined after the evaluated amount of  $x_{remi}$  and  $y_{nitri}$  from equation (2.17) (see section 2.14.8).

The following steps have been applied to obtain the produced amount of  $NH_3$  and  $HNO_3$  by using the AOU:

In a first step, the maximum possible production of  $NH_3$  and  $HNO_3$  has been evaluated. Setting the variables  $y_{nitri} = 0$  or  $x_{remi} = 0$  in equation (2.17), the maximum feasible production of  $NH_3$  or  $HNO_3$  respectively is obtained. These two values indicate the scope of the production from the remineralisation flux as well from the nitrification flux by using AOU. Connecting both maxima values of the produced  $NH_3$  and  $HNO_3$  with a line in the coordinate system (remineralisation on x-axis and nitrification on y-axis), the slope of the AOU between both fluxes can be derived (see the blue lines in Figures 3.17 (a) - (f) and in the other Figures in section A.12 in the appendix).

In a second step, the values of the simulated concentration from  $NH_3$  (see remineralisation in Table B.5 in the appendix) and from  $HNO_3$  (see nitrification in Table B.5 in the appendix) have been used to determine the modelled ratio of ammonium to nitrate production.

In a third step, the modelled ratio (see above) has been applied in equation (2.17) to obtain the produced value of  $NH_3$  and  $HNO_3$  by AOU with respect to the modelled ratio. As a consequence, a new variable ECOHAM<sup>•</sup> has been introduced to avoid disaccord between the simulated concentrations, the produced concentration over the AOU, and the ECOHAM indexes which are stated as water columns in the tables and plots in this work. An exemplary derivation for the cell of ECOHAM index 48, depth layer 40 - 45 m, for the transect H - S with the remineralisation  $R_0 = 151.5$  ( $R_0 = 140$  and  $R_0 = 138$  only the results) is given in section 3.6.1.

In a fourth step, the ECOHAM<sup>•</sup> value of each cell from the top layer (40 - 45 m) in the selected area of both transects has to be used to determine the factors  $m$  and  $(1 - m)$  for the equation (2.8) which has been temporarily excluded in equation (2.17).

The proceedings above have been implemented for each cell with the 3  $R_0$  in the top layer of the selected area for both transects with exception of the cells ECOHAM index 53 - 54 (40 - 45 m) of the transect H - S due to lack of AOU data. The black dots in Figures 3.17 (a) - (f) and in the other Figures in section A.12 in the appendix show the results of ECOHAM<sup>•</sup> graphically with respect to the modelled ratio over the slope of AOU.

Additionally, the amount of the simulated remineralisation and nitrification concentrations from the mass budgets (see Tables B.5 and B.6 in the appendix) have been inserted into the figures illustrated as crosses, diamonds and asterisks.

**Table 2.1** – Stoichiometric ratios of organic matter and its remineralisation. Data have been obtained from Paulmier et al. (2009).

Ratio	Name	Value
-------	------	-------

Organic matter composition		
$C_{org}/P_{org}$	a	$\approx 53 - 108$
$H_{org}/P_{org}$	b	$\approx 7 - 263$
$O_{org}/P_{org}$	c	$\approx 23 - 110$
$N_{org}/P_{org}$	d	$\approx 16 - 18$
Specific process		
Oxic: Remineralisation		
$-O_2/P_{org}$	$R_0$	$a + 1/4 b - 1/2 c - 3/4 d + 5/4$

### 2.14.7 Range of the regenerated component

As explained in the first step in section 2.14.6, the slope of the AOU between the remineralisation and nitrification fluxes can be graphically received for a cell of an ECOHAM index by connecting the maximum produced concentrations of  $NH_3$  and  $HNO_3$  from the equation (2.17) by using the AOU.

Introducing a range of minimum to maximum into the slopes of the AOU in the cells of the top layer (40 - 45 m) which is derived from observational data (see below), the scope can be obtained where the produced nutrients of both fluxes are feasible for the selected area from both transects. Additionally, the range indicates whether or not the parameter ECOHAM<sup>•</sup> is located inside the determined range.

The nutrient concentrations of minimum, mean and maximum of ammonium, nitrate and phosphate have been obtained from the grid configuration ND130, which were compiled in the technical reports from Radach et al. (1995a) and Radach et al. (1995b), that the range from minimum to maximum can be determined from the slope of AOU.

The observational dataset of the grid configuration ND130 is compiled as follows:

- composite dataset, a detailed description is given in section 4 in Radach et al. (1995a)
- North Sea is divided into 130 spatial boxes
- box resolution is mainly regular  $1^\circ \times 1^\circ$
- climatological monthly means and annual cycles within the boxes for the state variables:
  - phosphate
  - nitrate
  - ammonium
  - silicate
  - chlorophyll
- climatological ranges for the parameters (if compiled):
  - mean
  - median
  - standard deviation
  - minimum (Quantile: 16.6%)
  - maximum (Quantile: 83.3%)
- time series from 1960 - 1994

Whenever stratification occurred during summer in the North Sea, the boxes in ND130 were divided into upper and lower layer at a thermocline depth of 30 m (Radach et al., 1995a). Note that the selected water columns in the defined area begin on 40 m depth.

In the central North Sea a three-digit box number in ND130 represents the sub layer, whereas a two-digit box number represents the upper layer or not always stratified during the summer. Hence, only box numbers with three digits (123 - 125) can be considered for the selected region in the observed transects (see red framed boxes in Figure C.1 in the appendix). It should be mentioned that the boxes of ND130 is adapted to the HAMSOM model and each box of ND130 exhibits several HAMSOM grid

cells (see dots inside the ND130 boxes in Figure C.1 in the appendix). As a consequence of the lower resolution of ND130, data of the box numbers 123 - 125 were used multiple times for the same water column in the selected areas (see Table C.2 in the appendix).

Following data of April and July were extracted from the boxes 123 - 125 of ND130: mean, standard deviation (SD), maximum and minimum of the state variables ammonium, nitrate and additionally phosphate (see Table C.1 in the appendix). A simple linear interpolation was applied between other months in order to obtain concentration, if there was no data is compiled in April and July (see table header in Table C.1 in the appendix).

Two remarks have to be emphasised by using the observational data of April and July:

The first is related to the extracted data of April. Due to the fact that the evaluated onsets of stratification were always in April (see Tables B.5 and B.6 in the appendix), the data of April represents the "preformed" component from equation (2.10).

The second concerns the extracted data of July. July has to be regarded as *in situ* nutrient concentration from the expedition of HE428. Therefore, the data of July has not to be considered as the component of estimated nutrient concentration in equation (2.10), but rather as an aid to determine the range (minimum to maximum) on the slope of AOU for the "regenerated" component in equation (2.10).

As the data for July in boxes 124 and 125 from ND130 shows a lack of ammonium, additional data from Hinrichs et al. (2017) has been used to obtain observed ammonium concentrations for July. For that matter, a couple of remarks should be emphasised here by employing the additional data with respect to the compiled dataset of ND130:

- values have been determined graphically for the 50 m level
- images were interpolated
- only climatological monthly mean values exist
- the month of August has been used
- the range of minimum to maximum concentration has been selected from the scaled concentration colorbar in the examined pictures
- time series from 1960 - 2014

Note that hereafter using the term ND130 for the observational data of the grid configuration ND130 means also includes additional data obtained from Hinrichs et al. (2017). However, rearranging the equation (2.10) and applying the ND130 parameters mean, minimum and maximum, the observed range for the "regenerated" component can be obtained as follows:

$$\begin{aligned}
 Nutrient_{regenerated,mean} &= Nutrient_{July,mean} - Nutrient_{April,mean} - Nutrient_{physics}, \\
 Nutrient_{regenerated,min} &= Nutrient_{July,min} - Nutrient_{April,max} - Nutrient_{physics}, \\
 Nutrient_{regenerated,max} &= Nutrient_{July,max} - Nutrient_{April,min} - Nutrient_{physics},
 \end{aligned} \tag{2.18}$$

where the first term on the right of equation (2.18) is the considered *in situ* nutrient concentrations of July. Whereas the middle term on the right of equation (2.18) are the nutrient concentrations of the "preformed" components of April, the third term on the right of the equation (2.18) is the nutrient concentrations from the "physics" components.

Nutrient concentrations of April and July are well-known from the collected data from ND130 in Table C.1 in the appendix and the nutrient concentrations of the "physics" components can be obtained from the compiled mass budgets in Tables B.5 and B.6 in the appendix.

The range has been implemented graphically into the slopes of AOU for the remineralisation  $R_0 = 151.5$ ,  $R_0 = 140$  and  $R_0 = 138$  and is stated as follows: maximum is green dotted, mean is yellow dotted and minimum is red dotted. The results are shown in Figures 3.17 (a) - (f) for the cells of ECOHAM index 47 - 49, layer 40 - 45 m, for the transect H - S and for the cells of ECOHAM index 53 - 54, layer 40 - 45 m, from the transect S - H in section 3.6.2, whereas Figures from the other ECOHAM cells, layer 40 - 45 m, are shown in section A.12 in the appendix. Note that the range of

the cells for the ECOHAM index 53 - 54 for the transect H - S have not been computed due to absence of AOU data.

However, evaluations with ammonium concentrations from ND130 for the "regenerated" ammonium concentrations revealed consistently negative values in equation (2.18), whereas for the "regenerated" nitrate concentrations only the minimum value of the cell ECOHAM index 53 exhibited a negative value. Therefore, the obtained range from the "regenerated" nitrate concentrations are implemented in the slopes of the AOU.

### 2.14.8 The m factor

Following the equation (2.17), the factor  $m$  and the factor  $(1 - m)$  can be obtained by computing

$$m = \frac{x_{remi}}{x_{max,remi}} \text{ respectively } (1 - m) = \frac{y_{nitri}}{y_{max,nitri}}, \quad (2.19)$$

where  $x_{remi}$  is the produced amount of  $NH_3$  and  $x_{max,remi}$  the maximal possible produced quantity of  $NH_3$  over AOU, respectively. The  $y_{nitri}$  is the produced amount of  $HNO_3$  and  $y_{max,remi}$  is the maximal possible produced quantity of  $HNO_3$  over AOU, respectively.

Whereas the value of  $x_{max,remi}$  has to be evaluated by setting the nitrification flux to zero in equation (2.17), the values of  $x_{remi}$  can be derived by the parameter ECOHAM<sup>•</sup> and by the ND130 parameters minimum, maximum and mean of the range which have been derived in section 2.14.6 and 2.14.7.

Reciprocal, the value of  $y_{max,nitri}$  has to be evaluated by setting the remineralisation flux to zero in equation (2.17) and the values of  $y_{nitri}$  can be obtained by the implemented parameters of ECOHAM<sup>•</sup>, minimum, maximum and mean on the slope of the AOU.

Implementing these factors into equation (2.8), the factor  $m$  defines the exhausted amount of AOU by the remineralisation flux and the factor  $(1 - m)$  fixes the exhausted quantity of AOU by the nitrification flux (see Figure 2.11).

The factors  $m$  and  $(1 - m)$  have been determined for the parameter ECOHAM<sup>•</sup>, and for the parameters of the range of ND130 (minimum, maximum and mean) in the slope of AOU by applying the remineralisation values  $R_0 = 151.1$ ,  $R_0 = 140$  and  $R_0 = 138$  in each cell from the top layer (40 - 45 m) in the selected area. The cells ECOHAM index 53 - 54 of track H - S have been excluded due to lack of AOU values. Tables B.7 and B.8 in the appendix show the results for both transects. Note that values for the ND130 parameter minimum in the cell of ECOHAM index 53 do not exist due to the negative result of the "regenerated" component over equation (2.18) and have been neglected (see Figures 3.17f, 3.17c and 3.17e). The determined factor  $m$  and  $(1 - m)$  from each cell of the ECOHAM index in the top layer will be regarded as constant for its deeper layers.

### 2.14.9 Estimation of nutrient concentrations in the selected area

Regarding equation (2.10) and using the introduced parameter ECOHAM<sup>•</sup> as well as the range from equation (2.18) with the ND130 parameters minimum, maximum and mean, the nutrient concentration of ammonium and nitrate can be estimated as follows:

$$\begin{aligned} Nutrient_{mean}^* &= Nutrient_{April,mean} + Nutrient_{regenerated,mean} + Nutrient_{physics}, \\ Nutrient_{minimum}^* &= Nutrient_{April,mean} + Nutrient_{regenerated,minimum} + Nutrient_{physics}, \\ Nutrient_{maximum}^* &= Nutrient_{April,mean} + Nutrient_{regenerated,maximum} + Nutrient_{physics}, \\ Nutrient_{ECOHAM}^* &= Nutrient_{April,mean} + Nutrient_{regenerated,ECOHAM^{\bullet}} + Nutrient_{physics}, \end{aligned} \quad (2.20)$$

where the terms  $Nutrient^*$  are the estimated concentrations. The terms  $Nutrient_{April,mean}$  in equation (2.20) are the nutrient concentrations of the "preformed" components and can be obtained from Table C.1 in the appendix. Whereas the terms  $Nutrient_{regenerated}$  in equation (2.20) represent the nutrient concentrations of the "regenerated" components. The third terms  $Nutrient_{physics}$  from the equation (2.20) are the nutrient concentrations of the "physics" components. The amount of nutrient

concentration of "regenerated" components can be derived over the slope of the AOU between the remineralisation and nitrification fluxes which is pointed out in section 2.14.6 for the model and for the observational data (minimum, maximum and mean) in section 2.14.7. The quantity of the nutrient concentrations from the "physics" components can be obtained from Tables B.5 and B.6 in the appendix.

Due to the fact that AOU values strongly vary at some water columns in the selected area (see Tables A.5 and A.6 in the appendix), the estimated nutrient concentrations would also strongly vary. As a consequence of the variation, the estimated concentration of the minimum and maximum values of remineralisation  $R_0 = 151.5$ ,  $R_0 = 140$  and  $R_0 = 138$  have been extracted for each water column. The results are given in Tables B.9 and B.10 in the appendix for track H - S and in Tables B.11 and B.12 in the appendix for track S - H, respectively.

### 3 Results

#### First part

##### 3.1 Threshold between microzooplankton and mesozooplankton

Two cost functions have been applied to identify the threshold between the microzooplankton and mesozooplankton. Both cost functions show the calculated "distance" between the simulated and observational data. Smaller distances of the expedition transect in space and time reveal a better agreement between the simulated and observed data. The cost function A describes the mean normalised difference of anomaly between the modelled and observed data. The cost function B describes the mean relative error between the modelled and observed data.

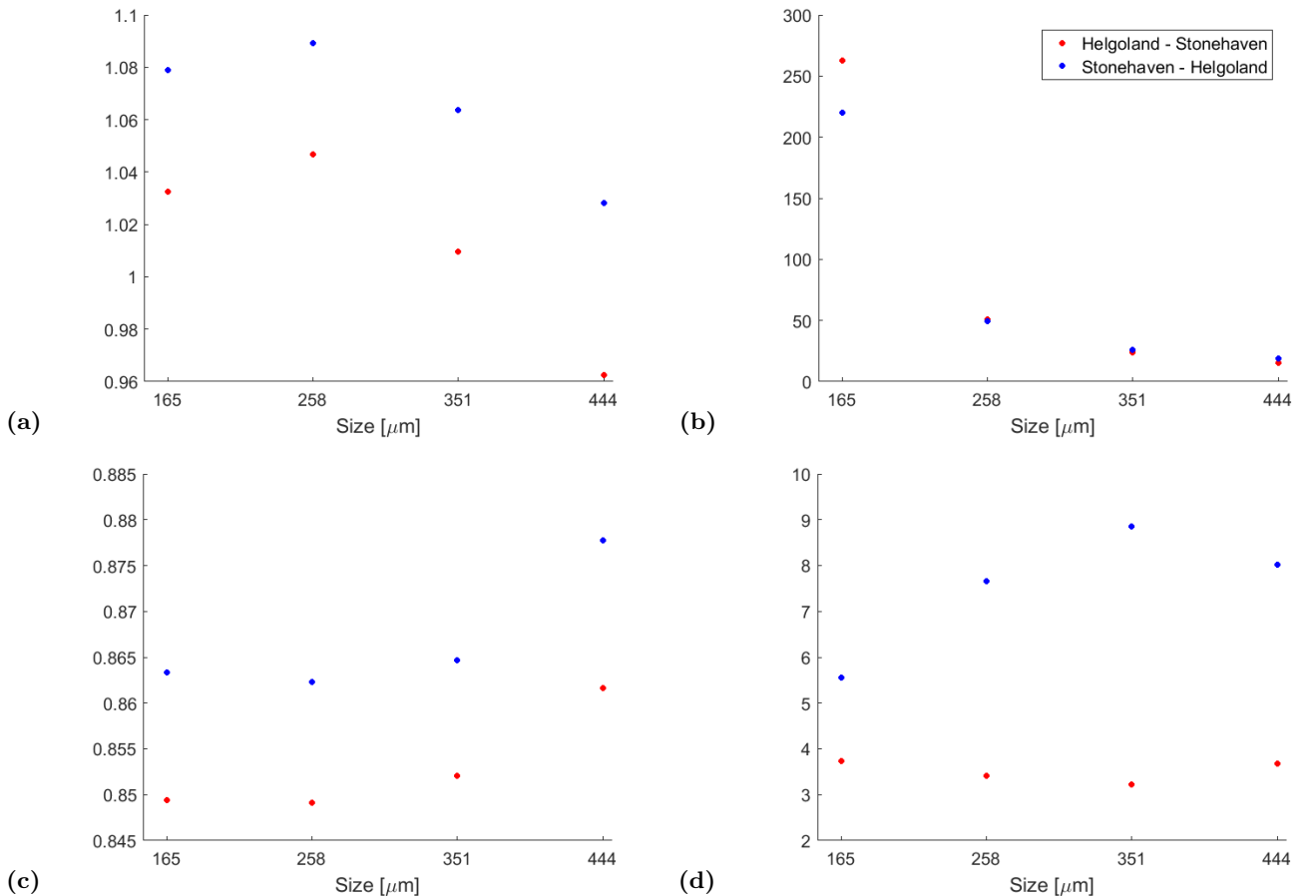


**Figure 3.1** – Cost functions for different size classes. Left: cost function A. Right: cost function B. (a) and (b) Microzooplankton (c) and (d) Mesozooplankton.

Generally, both cost functions exhibited similar patterns for the microzooplankton and mesozooplankton through the size classes of the transects H - S and S - H. Only the mesozooplankton computed

by cost function B exhibits an opposite trend between the tracks H - S and S - H (see Figure 3.1d). This is caused by differently calculated values of the standard deviation (SD) for each size class between both transects.

As can be seen in Figure 3.1b cost function B has a huge mean relative error for microzooplankton which is caused by a small derived SD. The mean relative error increases through higher size classes.

An opposite trend can be remarked by comparing the microzooplankton and mesozooplankton of the cost function A in the Figures 3.1a and 3.1c. It indicates that the mean of the normalised difference of anomaly between simulated and observed data decreased for higher size classes of microzooplankton whereas for mesozooplankton it increased. But the discrepancies in anomalies for both microzooplankton and mesozooplankton are small.

The lowest mean difference anomaly exhibited the mesozooplankton size class 258  $\mu m$  in the cost function A for both transects and a small mean relative error shows the cost function B from the transect H - S. Hence, it has been decided the threshold at the size class 258  $\mu m$ .

## 3.2 Comparison between the observed and simulated expedition transects

In the following subsections, the transects from Helgoland - Stonehaven (left) and Stonehaven - Helgoland (right) are illustrated for all six parameters. For each parameter, the upper are the observed images and the lower are the simulated images. To better structure the setup, the following sections of the transect have been defined to simplify the comparison between the simulation and observation, as follows:

- Northern part: ECOHAM index 41 - 58
- Northernly DB: ECOHAM index 57 - 58
- Dogger Bank (DB): ECOHAM index 59
- Southern part: ECOHAM index 59 - 69
- Southern DB: ECOHAM index 60 - 61
- Oyster Ground (OG): ECOHAM index 62 - 63

### 3.2.1 Temperature

The simulated and the observed temperature transect from H - S and S - H in Figures 3.2 (a) - (d) reflected the summer situation in the North Sea from northwest (NW) to southeast (SE). The water columns in northern part and the region from the southern Dogger Bank (DB) to Oyster Grounds (OG) are stratified, whereas towards Helgoland they are well mixed from the surface to the bottom. However, in the observed transects a weak thermocline can be identified which hinders an entire stirring of the water column unlike for the simulated transects, where a well-mixed column can be seen from ECOHAM index 64 - 69 in Figures 3.2a and 3.2b. A pool of cold water can be observed in the interior of the transects.

Generally, the temperature of the simulated transects is in good agreement with the observed data for both transects. Particularly, the interior of the transects depicted similarities. The observed thermocline is mostly formed around 10 m deeper than the simulated thermocline in the northern part of both transects (compare for example Figures 3.2a and 3.2c, respectively, Figures A.5a and B.4a in the appendix). The simulated surface layer temperatures revealed slightly higher values (mostly 1°C) in contrast to the observed temperatures.

Additionally, a spatial temperature gradient from NW to SE can be identified in the observed transects whereas in the simulated transects such a gradient cannot be detected. As the thermocline is situated higher in the simulated transects, the thickness of the mixed layer in the water columns is mostly between 10 - 15 m. The observed transects exhibit a mixed layer depth (MLD) mostly between the 20 - 25 m in the water columns. Hence, the upper layers of the simulated transects are heated more compared to the upper layers in the observed transects due to smaller MLD. The thickness of the MLD may be the reason for the increased simulated temperatures in the surface (see above).

Towards northern part of the DB, a gradient can be observed in the simulated transects. Such gradient cannot be found in the observed transects. Warmer water from the upper layers probably intrudes into the colder lower layers and was mixed by the bottom mixed layer (BML).

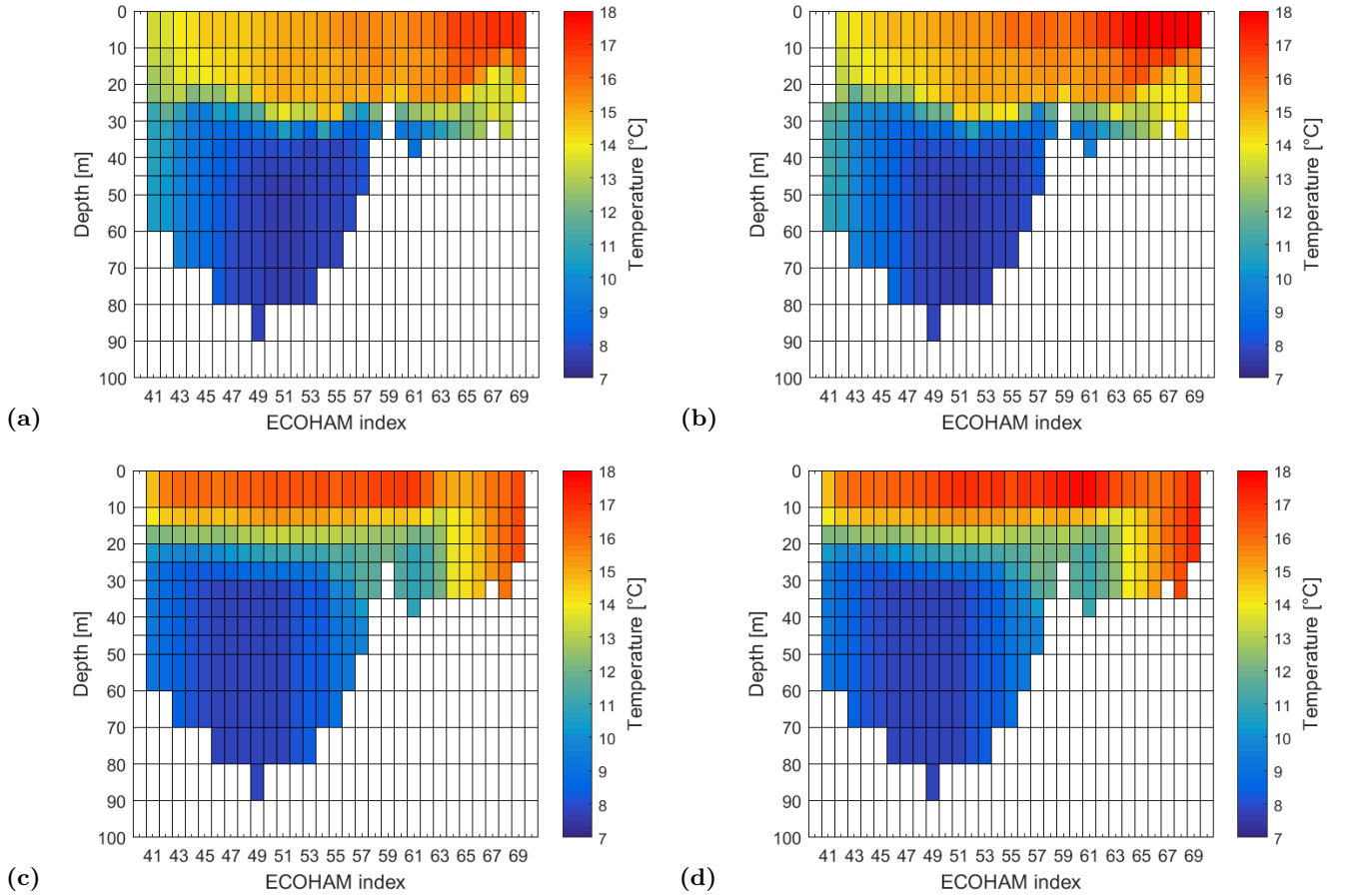


**Figure 3.2** – Temperature transects. Left: Helgoland - Stonehaven (H - S). Right: Stonehaven - Helgoland (S - H). (a) and (b) Observed. (c) and (d) simulated. Note the observed missing data in ECOHAM index 41 (0 - 25 m) in transect S - H.

As mentioned above, a thermocline can be identified in the observed transects in the shallower southern part which weakens towards Helgoland. In contrary, a thermocline is only developed between the DB and OG in the simulated transects. Towards Helgoland, the water columns are well-mixed from the surface to the bottom (compare for example Figures 3.2a and 3.2c, respectively, Figures A.5a and B.4a in the appendix). A cold water pool shows the region of ECOHAM index 60 - 62 at the bottom layer in the observed transects. It is less distinctive in the simulated transects and, additionally, the upper layers are affected due to higher situated thermocline.

### 3.2.2 Salinity

The simulated and the observed salinity transect from H - S and S - H Figures 3.3 (a) - (d) depicted the summer situation in the North Sea from NW to SE. Caused by the riverine input, a less saline region towards Helgoland was observed as well as towards the Scottish coast (Stonehaven). Higher concentrations in salinity exhibited the interior of the transects. A remarkable tongue of less saltier water revealed the simulated transects at the surface layer around the north of the DB.

As well as the parameter temperature, the simulated salinity transects are in good agreement compared with the observed transects from H - S and S - H. Especially, the interior of the transects revealed similarities. Slightly increased concentrations between 0.2 - 0.3 were found in the core of the simulated transects towards DB (see ECOHAM index 49 - 58 in Figures 3.3c and 3.3d).

As indicated above, the surface layer of the northern part showed disparity between observed and modelled transects. The Baltic inflow (see ECOHAM index 54 - 58 in Figures 3.3c and 3.3d) can be observed in the simulated transects. Such an inflow is not detectable in the observed transects. It should be mentioned that the structure from ECOHAM index 54 - 58 at the simulated surface layer in Figures 3.3c and 3.3d is not caused by the 2-Delta-L problem. This can occur e.g. by using for example a stepped transect in the model as it is used in the present work (personal communication with Dr. Thomas Pohlmann) (see red dots in Figure A.9 in the appendix). An examination revealed

that the part of ECOHAM index 54 - 58 for both transects are located at the edge of the simulated Baltic inflow (Figure not shown).

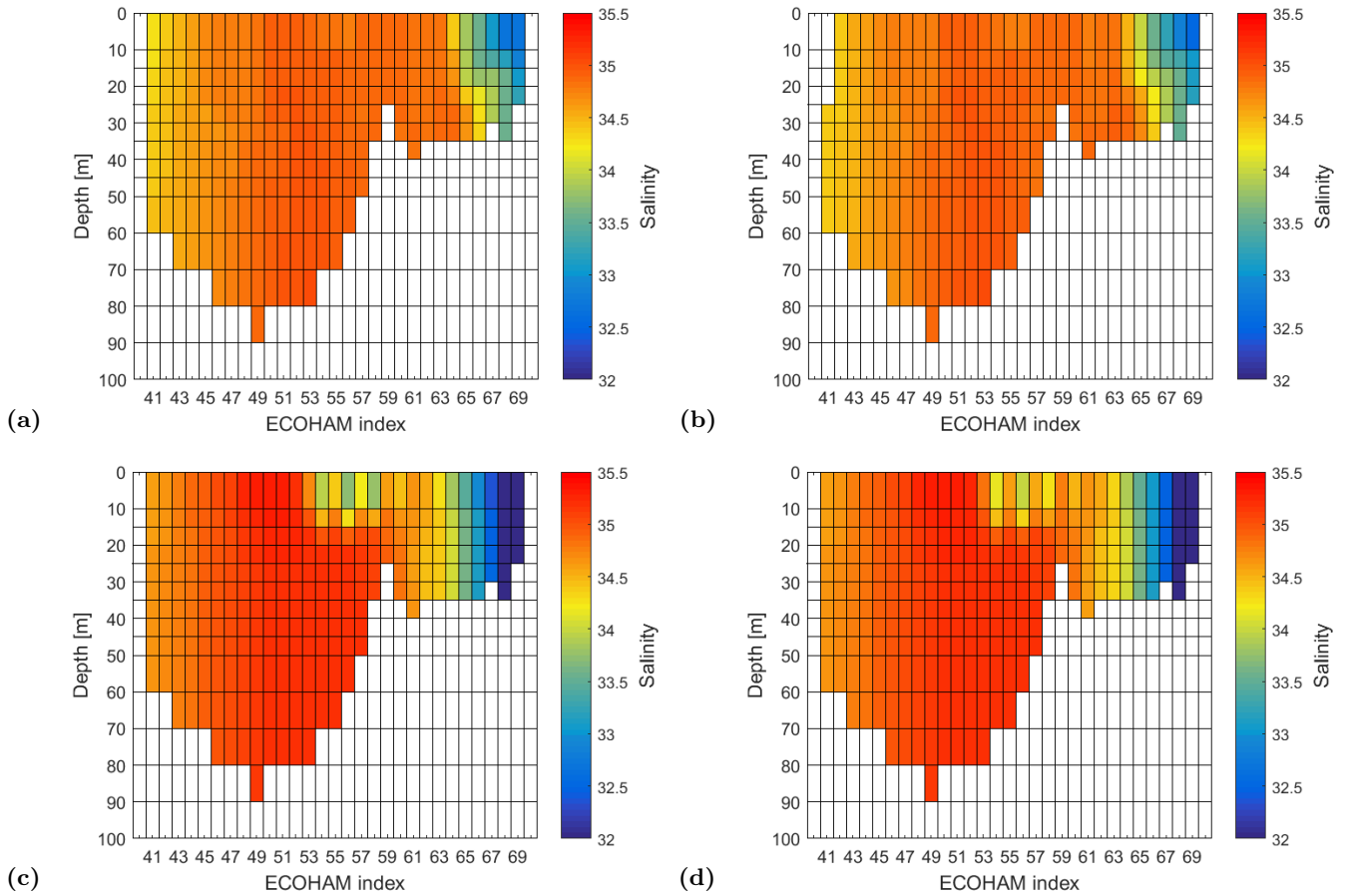


**Figure 3.3** – Salinity transects. Left: Helgoland - Stonehaven (H - S). Right: Stonehaven - Helgoland (S - H). (a) and (b) Observed. (c) and (d) simulated. Note the observed missing data in ECOHAM index 41 (0 - 25 m) from S - H.

In the shallower southern part, the model reproduced the influenced riverine freshwater input well which is detectable by a spatial salinity gradient (see ECOHAM index 61 - 69 in Figures 3.3c and 3.3d). Remarkable differences can be identified onshore between the simulated and observational transects. Due to the overestimated influence of freshwater input, the simulated gradient is steeper and larger in space with respect to the observed gradient. A vertical gradient depicts in the observed transects from the surface to the bottom (see ECOHAM index 66 - 69 in Figures 3.3a and 3.3b). Such a vertical gradient cannot be identified in the simulated transects. The relatively homogeneous simulated concentration in the affected water columns is caused by vertical mixing. A higher vertical grid-resolution in the model is most likely to improve the resolution of a vertical gradient. However, all simulated parameters are affected by the problem in the southern part of the transects towards Helgoland.

Some water masses can be identified in the transects. The interior of the transects revealed salinities of  $>35$  for the simulated transects and of approximately 35 for the observed transects. It can be considered that it originates from the Atlantic water which is transported by the Dooley Current (DC) into the central North Sea. Towards Stonehaven, the concentration decreases in the observed as well in the simulated transects (see ECOHAM index 41 - 46 in the Figures 3.3 (a) - (d)). It indicates that water masses were admixed with freshwater from the Scottish coast which is transported by the Scottish Coastal Current (SCC). In the southern part water masses cannot be clearly identified in the observed and simulated transects.

### 3.2.3 Oxygen

The observed oxygen transect from H - S and S - H in Figures 3.4a and 3.4b revealed 4 remarkable regions: (1) High oxygen concentrations (mostly  $>280 \text{ mmol/m}^3$ ) can be identified around the

thermocline (see ECOHAM index 51 - 57 in Figures 3.4a and 3.4b) which indicates a deep chlorophyll maximum (DCM). (2) In the interior, the oxygen concentrations decrease towards the bottom due to remineralisation and nitrification by bacteria. (3) Below the weak thermocline a huge oxygen consumption (partially  $<180 \text{ mmol/m}^3$ ) occurs so that an oxygen deficiency can be detected (see ECOHAM index 64 - 69 in Figures 3.4a and 3.4b). High concentrations of microzooplankton and mesozooplankton indicate ongoing grazing in this region which results in oxygen deficiency (see for example Figures 3.6b and 3.7b). (4) Both adjacents of the DB reveal a large oxygen consumption (see ECOHAM index 57 - 58 and ECOHAM index 60 - 61 in Figures 3.4a and 3.4b). At the northerly DB even a depth of 45 - 50 m it can be identified.

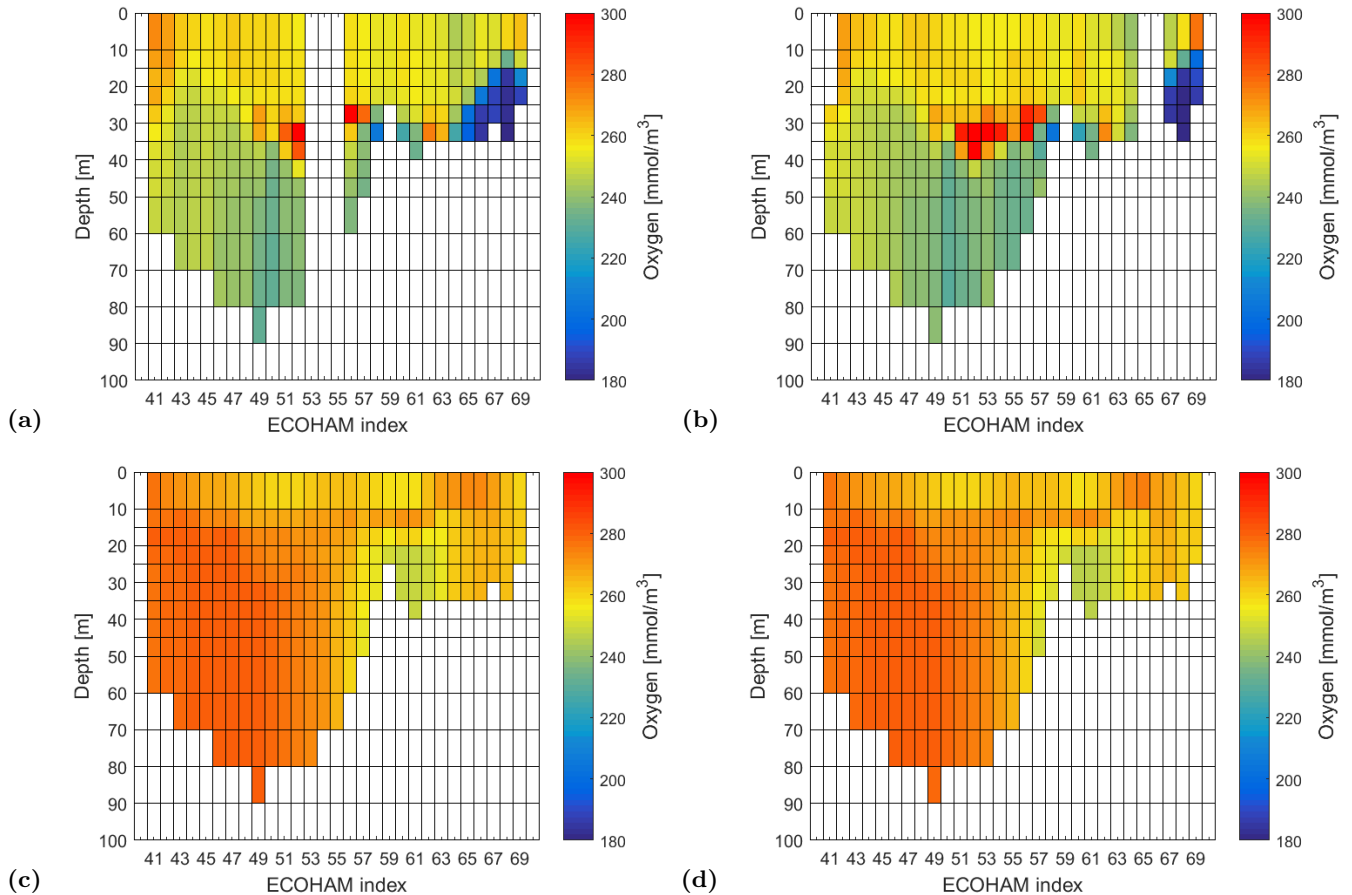


**Figure 3.4** – Oxygen transects. Left: Helgoland - Stonehaven (H - S). Right: Stonehaven - Helgoland (S - H). (a) and (b) Observed. (c) and (d) simulated. Note the observed missing data in ECOHAM index 53 - 55 from H - S, respectively, ECOHAM index 41 (0 - 25 m) and ECOHAM index 65 - 66 from S - H.

Generally, there exist no considerably similar regions between the observed and simulated oxygen transects from H - S and S - H (see Figures 3.4 (a) - (d)). An exception depicted both adjacents of the DB. Lower oxygen concentrations in this region indicates that biological processes which consume oxygen are involved (see the AOU in Figures A.10a and A.10b, B.6a and B.6b in the appendix). The oxygen consumption at the Southern DB has different origins for the observed and simulated transects. The oxygen consumption in the observed transects is due to uptake of phytoplankton (or detritus) by microzooplankton to mesozooplankton (see for example Figures 3.5a and 3.5c, 3.6a and 3.6b, 3.7a and 3.7b). In contrary, the oxygen consumption in the simulated transects at the southern adjacent and partially of the OG is predominantly caused by remineralisation and nitrification processes. Elevated ammonium and nitrate concentration in the region of ECOHAM index 60 - 62 of the simulated transects of ammonium and nitrate indicate such processes (see Figures B.3a and B.3b, B.3c and B.3d in the appendix).

In the interior of the transects an opposite trend can be observed. Meanwhile the oxygen concentrations of the simulated transects slightly augment below the thermocline towards the bottom, the observed oxygen concentrations decrease mainly caused by biological activity. The opposite trend in the simulated oxygen transects is probably caused by the solubility of oxygen which depends by tem-

perature and salinity in sea water. The temperature is the significant variable. Oxygen concentration will increase by decreasing temperature. As the interior of the simulated temperature transects exhibit a cold pool, the oxygen concentrations are augmented (see Figures 3.2c and 3.2d) in the simulated oxygen transects. The oxygen required processes remineralisation and nitrification are probably small in the interior of the simulated transects so that a larger oxygen consumption can be detected towards the bottom.

Due to the absence of a stratification from ECOHAM index 64 - 69 in the southern part of the simulated temperature transects (see Figures 3.2c and 3.2d), the simulated oxygen transects cannot reflect the large oxygen consumption which is shown in the observed oxygen transects.

### 3.2.4 Phytoplankton

The simulated and observed phytoplankton transects in Figures 3.5 (a) - (d) reflect the summer situation in the North Sea from NW to SE. The northern part reveals low observed and simulated chlorophyll-a concentrations and is located around the thermocline. Meanwhile the southern part shows high observed and simulated chlorophyll-a concentrations towards Helgoland. A remarkable difference of the observed chlorophyll-a concentrations can be found between the transect from H - S and S - H in the regions across the DB and in the southern part towards Helgoland (see ECOHAM index 64 - 69 in Figures 3.5a and 3.5b). Elevated discrepancies of chlorophyll-a concentrations revealed only the southern part towards Helgoland in the simulated transects (see ECOHAM index 64 - 69 in Figures 3.5c and 3.5d). The interior depicts the lowest chlorophyll-a concentration for the simulated phytoplankton and observed phytoplankton transects.

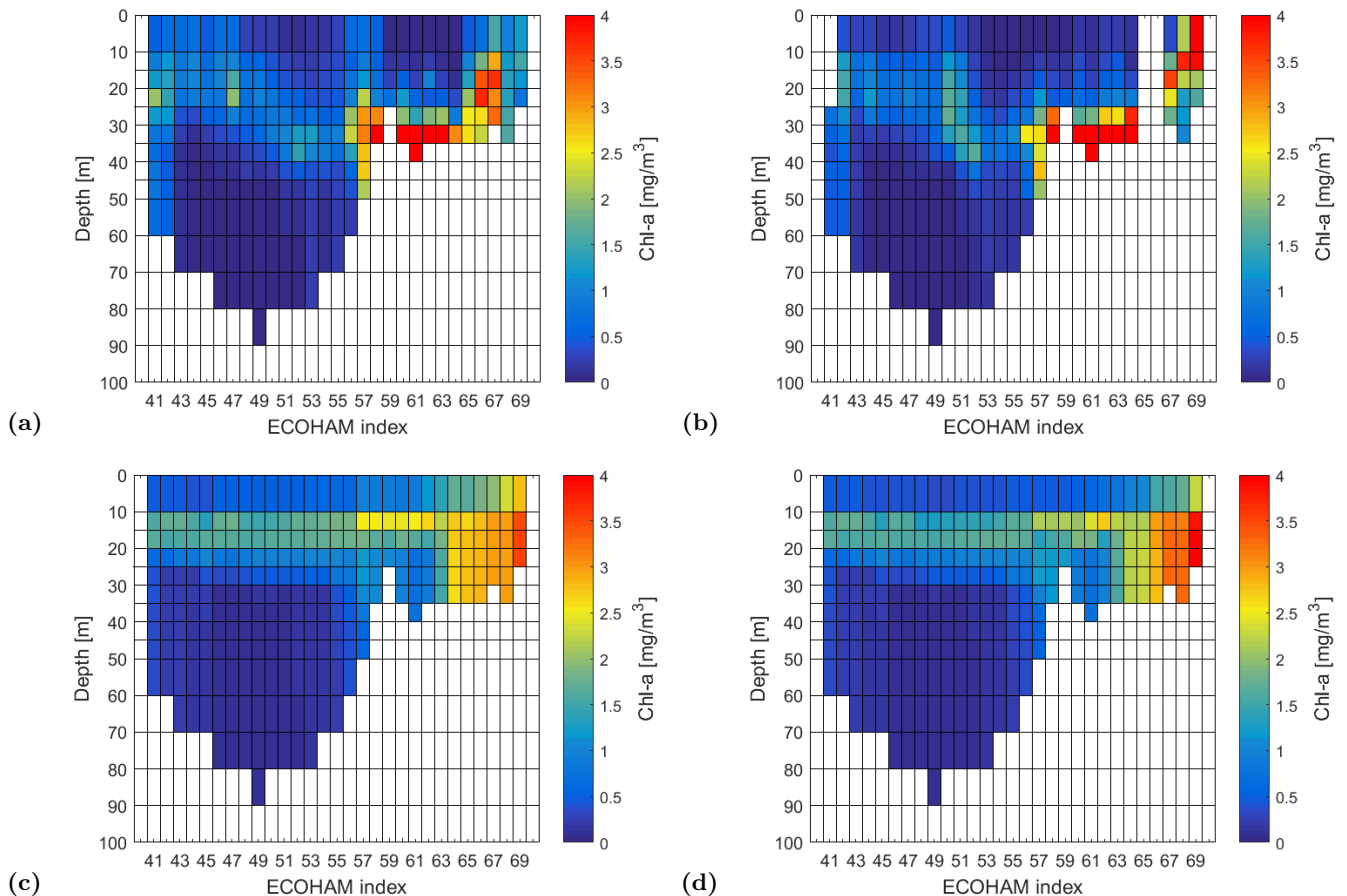


**Figure 3.5** – Phytoplankton transects. Left: Helgoland - Stonehaven (H - S). Right: Stonehaven - Helgoland (S - H). (a) and (b) Observed. (c) and (d) simulated. Note the observed missing data in ECOHAM index 41 (0 - 25 m) and ECOHAM index 65 - 66 from S - H, respectively.

In the northern part, a high concentration can be identified in the simulated transects at around of 10 - 20 m depth. But the observed concentrations is lower and mostly located in the deeper layers of the transects due to a deeper situated thermocline (see Figures in section 3.2.1). Towards the northern part of DB, the observed concentration increases and reveals the highest value at the northerly DB ( $>6$

$mg/m^3$ ). The increased chlorophyll-a concentration indicates that at the northerly DB an upwelling is occurs, which transports cold nutrient-rich water into the upper layers. Even at a depth of 45 - 50 m it is still recognisable (see ECOHAM index 57 in Figures 3.5a and 3.5b). Although with a lower chlorophyll-a concentration, a similar trend can be identified at the northerly DB in the simulated transects.

A possible marine food web from the phytoplankton (trophic level 1) to microzooplankton (trophic level 2) to mesozooplankton (trophic level 3) can be identified at the northerly DB in the observed and simulated transects due to a similar pattern (compare Figures in section 3.2.5 and 3.2.6).

Regarding the southern part, some phytoplankton distributions are not reproduced by the model such as the DCM around the weakly thermocline (see ECOHAM index 64 - 69 in Figures 3.5a and 3.5b), the areas of the southerly adjacent of DB and the OG. Largest observed chlorophyll-a concentrations were revealed at the OG where the values exceeded  $5 mg/m^3$ . A possible marine food web from the trophic levels 1 - 3 (see above) can be identified in observed transects from ECOHAM index 64 - 69 (see Figures 3.5a and 3.5b) due to similarly distributed concentrations of the observed microzooplankton and mesozooplankton transects (compare Figures in section 3.2.5 and 3.2.6).

### 3.2.5 Microzooplankton

Mostly, the microzooplankton concentration of the simulated transect from H - S and S - H in Figures 3.6c and 3.6d is distributed within the mixed layer. In contrary, most of the observed microzooplankton concentration from the transect H - S and S - H is located around or below of the thermocline. Elevated observed concentrations can be identified in the deep (40 - 60 m) towards Stonehaven (see Figures 3.6a and 3.6b). The lowest concentration exhibits the interior of the transects for the simulated and observed microzooplankton.

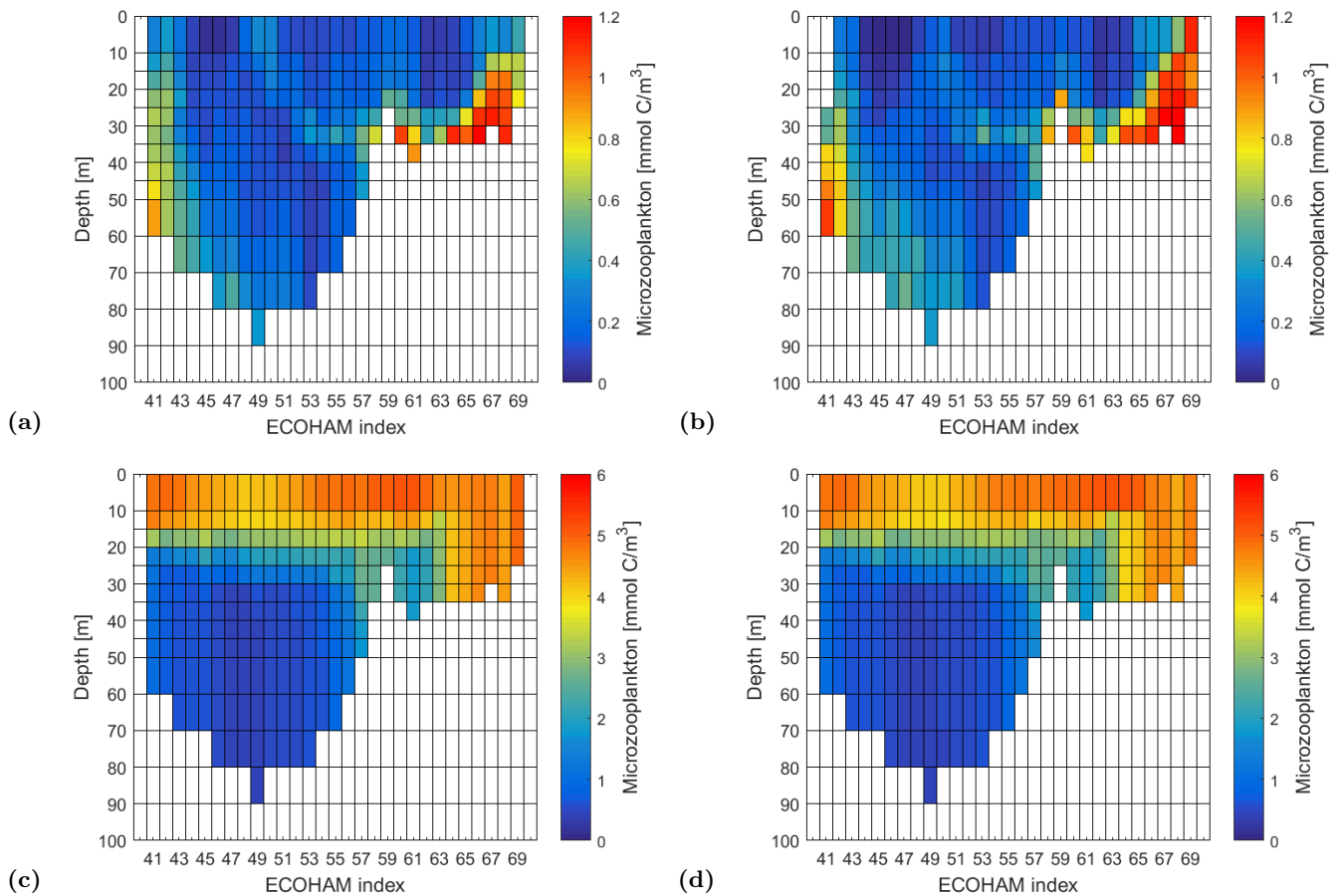


**Figure 3.6** – Microzooplankton transects. Left: Helgoland - Stonehaven (H - S). Right: Stonehaven - Helgoland (S - H). (a) and (b) Observed (threshold: size class  $258 \mu m$ ). (c) and (d) simulated. Note the different scale between observed and simulated data and the observed missing data in ECOHAM index 41 (0 - 25 m) from S - H.

In general, no considerable similar distribution between the observed and modelled transects can

be identified. An exception is depicted by the adjacents of the DB and the interior of the transects. Regarding the observed concentration, the simulated concentrations of microzooplankton are predominantly overestimated (compare the scale of the color bar in Figures 3.6 (a) - (d)). Particularly, the surface mixed layer (SML) revealed a huge discrepancy with respect to the observed concentrations. However, the scarcely matching pattern of the simulated transects is caused for two reasons:

The first is referred to the simulated detritus. As the microzooplankton take up detritus, the distribution of the microzooplankton concentration is similar to the distributed concentration of detritus in the transects. High concentrations ( $>5 \text{ mmol C/m}^3$ ) for the parametrised slow sinking detritus can be found in the stratified region and in the well mixed zone of the southern part (see Figures B.5c and B.5d in the appendix). With respect to the parametrised fast sinking detritus, lower concentrations ( $\sim 0.3 \text{ mmol C/m}^3$ ) can be found below the thermocline and higher concentrations ( $>0.6 \text{ mmol C/m}^3$ ) in the well mixed zone of the southern part (see Figures B.5a and B.5b in the appendix). Hence, the slow sinking detritus has an effect on the microzooplankton distribution in the mixed layer as well in the southern well mixed part in the transects. In contrary, the fast sinking detritus has an effect on the microzooplankton distribution below the thermocline in the transects. Due to the parametrised slow sinking velocity of detritus, the simulated transects show weakly agreement with the observed transects. A sensitivity analysis should be performed to obtain a closer agreement between the simulated data and observed data.

The second is related to the simulated phytoplankton. Due to the uptake of phytoplankton by microzooplankton, the phytoplankton distribution influences the distribution of the microzooplankton in the transects and shows therefore a similar pattern in the transects.

A remarkable difference of observed microzooplankton concentrations can be found between the transect from H - S and S - H in the regions across the DB and in the southern part towards Helgoland (see ECOHAM index 64 - 69 in Figures 3.6a and 3.6b). Weak differences of observed concentration are shown in the region around the thermocline in the central North Sea (see ECOHAM index 53 - 56 in Figures 3.6a and 3.6b). Regarding the simulated microzooplankton concentration between both transects revealed low discrepancies.

Some areas in the observed transects should be emphasised. As mentioned in section 3.2.3, below the weak thermocline a huge oxygen consumption appears in the southern part (see Figures A.10a and b in the appendix) which leads at some places to an oxygen deficiency (see ECOHAM index 64 - 69 in Figures 3.4a and 3.4b). The presence of large observed microzooplankton and mesozooplankton concentrations (see Figures 3.7a and 3.7b) and, additionally, low or absence of phytoplankton at this region indicate that the oxygen consumption has not been compensated by newly generated oxygen from the primary production. A similar trend appears at the adjacent of DB and partially at OG. A larger chlorophyll-a concentration indicates that the primary production may be able to compensate the oxygen consumption which can be observed at higher AOU concentration compared to the AOU concentration in the region of ECOHAM index 64 - 69 (see Figures 3.5c and 3.5d, and Figures A.10a and A.10b in the appendix).

An augmented observed microzooplankton concentration exhibits the deeper part (20 - 70 m) of the transects towards Stonehaven (see ECOHAM index 41 - 43 in Figures 3.6a and 3.6b). Examining of the observed parameters of AOU, oxygen, phytoplankton and zooplankton revealed not a clear relationship between oxygen consumption, regenerated oxygen or uptake by zooplankton.

### 3.2.6 Mesozooplankton

Generally, the concentration of the simulated mesozooplankton transect from H - S and S - H in Figures 3.7c and 3.7d is distributed within the mixed layer. Only in the southern part the simulated concentration reaches the bottom. In the transect from H - S and S - H, most of the observed mesozooplankton concentration is located in the southern part, at the northerly DB and around the thermocline. High observed concentrations can be identified in the deep (40 - 60 m) towards Stonehaven (see Figures 3.7a and 3.7b). Lowest concentration show the interior of the transects for the simulated and observed mesozooplankton.

In contrast to the simulated microzooplankton, some considerably similar patterns between the observed and modelled transects from H - S and S - H can be identified. Especially in the southern part of the transects. Regarding the observed mesozooplankton concentration, the model values are closer to the observed values comparing to the values into the simulated and observed microzooplank-

ton transects. In contrary to the microzooplankton transects, the values of the mesozooplankton are underestimated by the model with respect to observed values.

The lower difference of mesozooplankton concentration between the observed and simulated transects as well as the augmented similarity of mesozooplankton distribution in the southern part of the transects at the size class  $258 \mu\text{m}$  explain the best fit for the cost functions (see Figures 3.1c and 3.1c) compared to the other size classes (see Figures of the other size classes in section A.16.1 in the appendix).

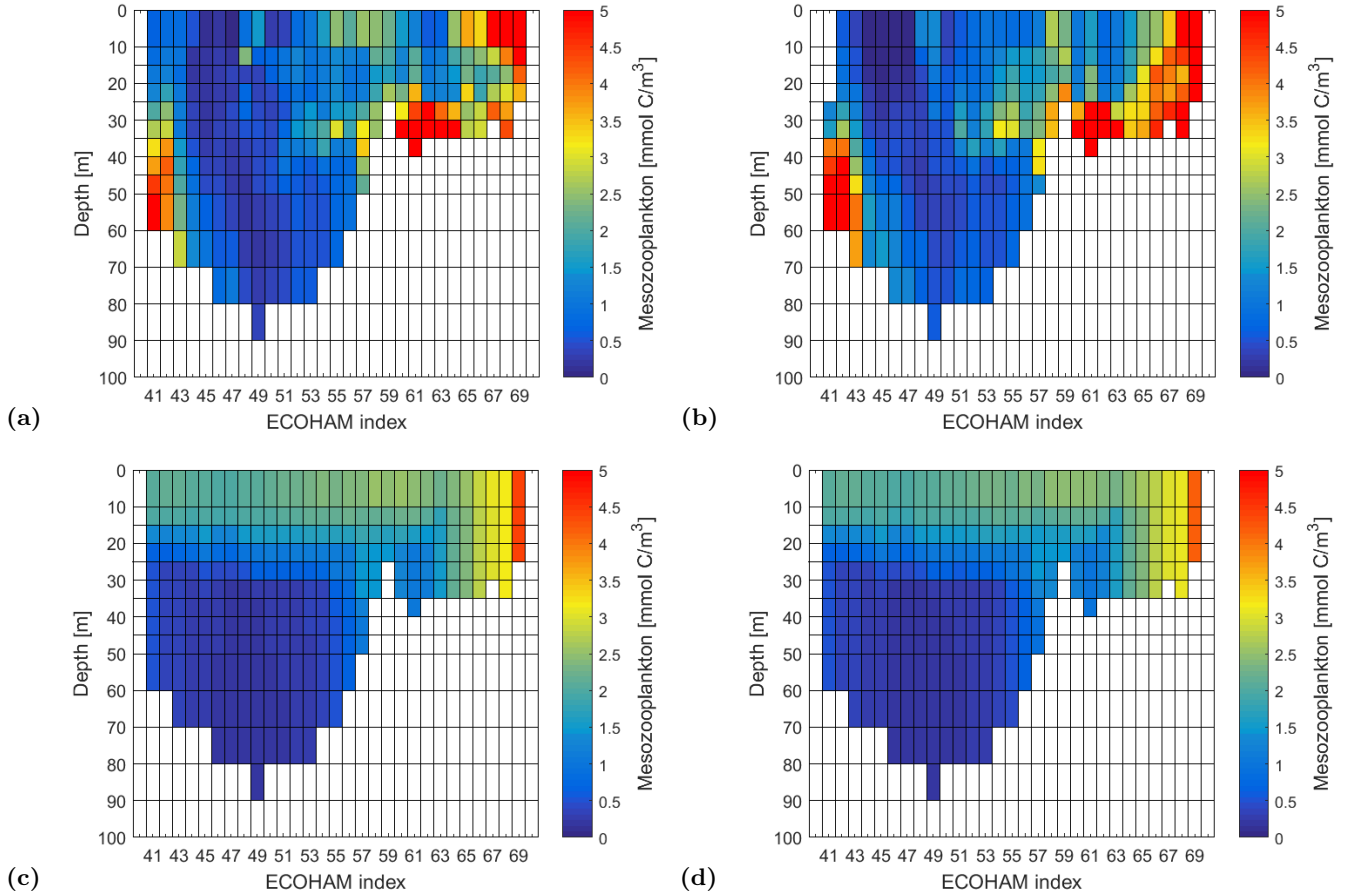


**Figure 3.7** – Mesozooplankton transects. Left: Helgoland - Stonehaven (H - S). Right: Stonehaven - Helgoland (S - H). (a) and (b) Observed (threshold: size class  $258 \mu\text{m}$ ). (c) and (d) simulated. Note the observed missing data in ECOHAM index 41 (0 - 25 m) from S - H.

A difference in observed mesozooplankton concentration can be determined between both tracks around the thermocline in the central North Sea (see ECOHAM index 53 - 56 in Figures 3.7a and 3.7b) as well as the regions across the DB and in the southern part towards Helgoland (see ECOHAM index 64 - 69 in Figures 3.7a and 3.7b). It is noticed most in the southern part. In contrary, marginal discrepancies revealed the simulated transect between H - S and S - H. A possible marine food web from the trophic levels 1 - 3 (see section 3.2.4) can be identified around the thermocline in the central North Sea from the observed transects due to existing of DCM (see Figures 3.6a and 3.6b as well as 3.7a and 3.7b).

### 3.3 Representativeness of the simulated expedition transects

Variability is a measure of how significantly a parameter varies between its minimum and maximum value. When the transect shows a weak variability for a parameter, the parameter can be considered representative throughout the transect. In contrary, a high variability through the transect cannot be considered representative for the parameter. Hence, the simulated expedition transect (stated as red line) is considered representative in case of low variability or the expedition values are situated around the center in case of larger variability across the transect.

In the following subsections, the variability for transects from Helgoland - Stonehaven (left) and Stonehaven - Helgoland (right) are illustrated for all six parameters. If possible, images of the transect

H - S were used which shows a small variability for each parameter, whereas images of the transect S - H were used which shows a large variability for each parameter.

### 3.3.1 Temperature

Examinations of the short time series (1 - 2 weeks before and after the expedition, respectively, see Table B.2 in the appendix) and long time series (2001 - 2014) as well as the displaced transects (displacing the expedition transects 60 and 120 km towards SW and NE, respectively) for all three depth layers (0 - 10 m, 30 - 35 m and 60 - 70 m) revealed marginal differences between both tracks for the temperature variability and for the modelled expedition values.

Figure 3.8a shows the modelled temperature variability of the short time series from depth layer 30 - 35 m in the transect from H - S. Lowest variability can be observed in the deeper central North Sea and towards Scottish coast (Stonehaven) with  $\sim 0.1 - 0.5^\circ\text{C}$  and  $\sim 0.5 - 0.7^\circ\text{C}$ , respectively (see ECOHAM index 41 - 54). Towards the northern Dogger Bank (DB) the variability increases ( $\sim 0.7 - 1.5^\circ\text{C}$ ). Higher variability exhibits in the shallower southern part of the North Sea. The southerly DB exhibits  $1.2 - 1.7^\circ\text{C}$ , whereas the strongest variability depicts the region of Oyster Grounds (OG) towards Helgoland ( $\sim 2.3 - 2.5^\circ\text{C}$ ). The higher variability at the northerly DB is probably caused by an upwelling or from the intruding warmer water of the upper layers into colder lower layers and is mixed by the bottom mixed layer (BML). In the shallower southern part of the North Sea, larger variability is probably caused by stronger mixing from tides.

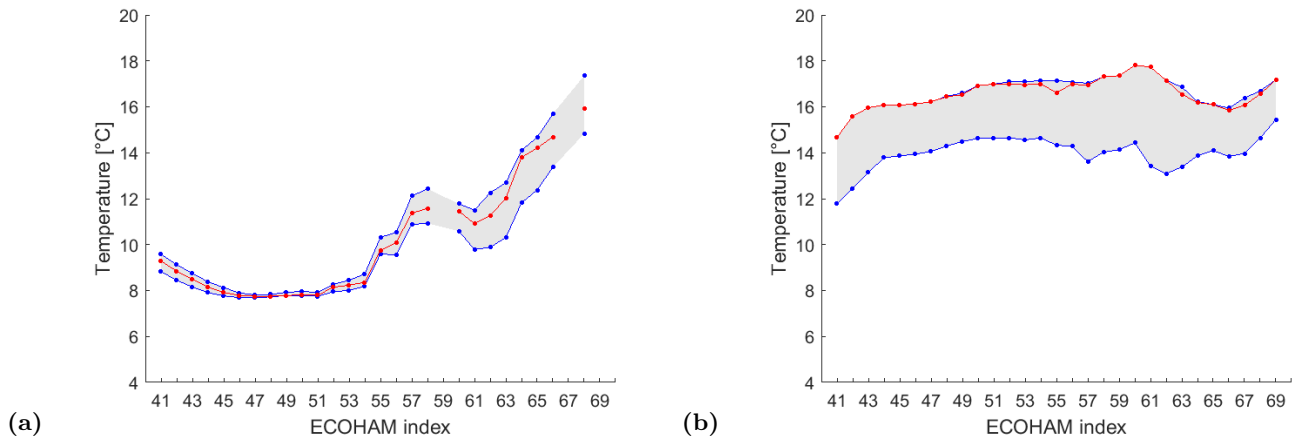


**Figure 3.8** – Simulated temperature variability transect. (a) Short time series (see Table B.2 in the appendix): Helgoland - Stonehaven (30 - 35 m). Missing ECOHAM indexes are caused by bottom topography. (b) Long time series (2001 - 2014): Stonehaven - Helgoland (0 - 10 m). Blue line: minimum and maximum values. Red line: expedition transect.

Figure 3.8b shows the modelled temperature variability of the long time series from the surface layer (0 - 10 m) in the transect from S - H. The temperature variability within the transect exhibits mostly  $2 - 3^\circ\text{C}$ . Elevated values can be observed within the region from the DB to the OG (see ECOHAM index 57 - 63) with  $\sim 3.3 - 4^\circ\text{C}$ . This region with an increased variability most likely is a result of tidal mixing which also influences the upper layers. A further explanation can be found in variability being caused by winds.

The modelled expedition transect (see red line in Figure 3.8a) is predominantly situated in the center of the minimum and maximum values. A similar trend revealed the expedition transects from depth layer 60 - 70 m for the short time series and for the shifted transects (Figures not shown). Accordingly, the simulated temperature values of the expedition can be regarded within the deeper part of the transects as representative with respect to the short time series and, especially, the interior of the transect from H - S and S - H with respect to the short time series and space.

In contrary, the expedition transect from the surface layer cannot be considered as representative for the transect S - H in Figure 3.8b, where the temperature values are mostly located at the maximum. The surface layer of both the short time series and the displaced transects as well as the depth layer 30 - 35 m for the long time series and (partially) displaced transects cannot be considered as representative due to a large variability (Figures not shown). Accordingly, a representativeness of the transects from H - S and S - H cannot be identified neither within the long term in all three depth

layers and short term in the surface layer nor within space in the surface layer and (partially) in the depth layer 30 - 35 m.

A spatial temperature gradient across the transect can be observed in Figure 3.8a. In the region of the DB, a remarkable increase in temperature can be identified. Whereas towards the northern DB a gradient of approximately  $1^{\circ}\text{C}/\text{km}$  (see ECOHAM index 54 - 57) can be found, the southerly DB exhibits approximately  $0.5^{\circ}\text{C}/\text{km}$ . The temperature increase towards the northern DB is probably caused by the intrusion of warmer water from the upper layers. The bottom mixed layer (BML) admixes the warmer water with the colder water from the lower layers. A gradual spatial increases can be observed towards Stonehaven with  $\sim 0.5^{\circ}\text{C}/\text{km}$  (see ECOHAM index 41 - 44), meanwhile from the OG towards Helgoland it augments to  $1 - 1.5^{\circ}\text{C}/\text{km}$  (see ECOHAM index 62 - 69). The temperature increase towards the continental coast indicates that tidal mixing acts stronger in the shallower southern part of the North Sea.

A spatial temperature gradient from NW to SE can be identified in Figure 3.8b. The temperature difference between NW and SE in the transect is probably caused by two cases: (1) The solar radiation becomes weaker due to the decreasing inclination of the sun at higher latitudes. (2) The influence of riverine input from the Scottish coast becomes increasingly important.

### 3.3.2 Salinity

As well as the simulated temperatures, the modelled salinity transects for the three depth layers in space and time revealed slight differences between both tracks for the variability of salinity and for the modelled expedition values.

Figure 3.9a shows the modelled variability of salinity for the short time series in the transect from H - S (30 - 35 m). The variability through the transect is marginal. Similar behaviour in variability exhibited the deeper part of the transects (60 - 70 m) in the short time series (Figures not shown). An onshore-offshore gradient can be identified. Especially the southern part of the transect shows a remarkable gradient which is mainly caused by the riverine input from the continental coast.

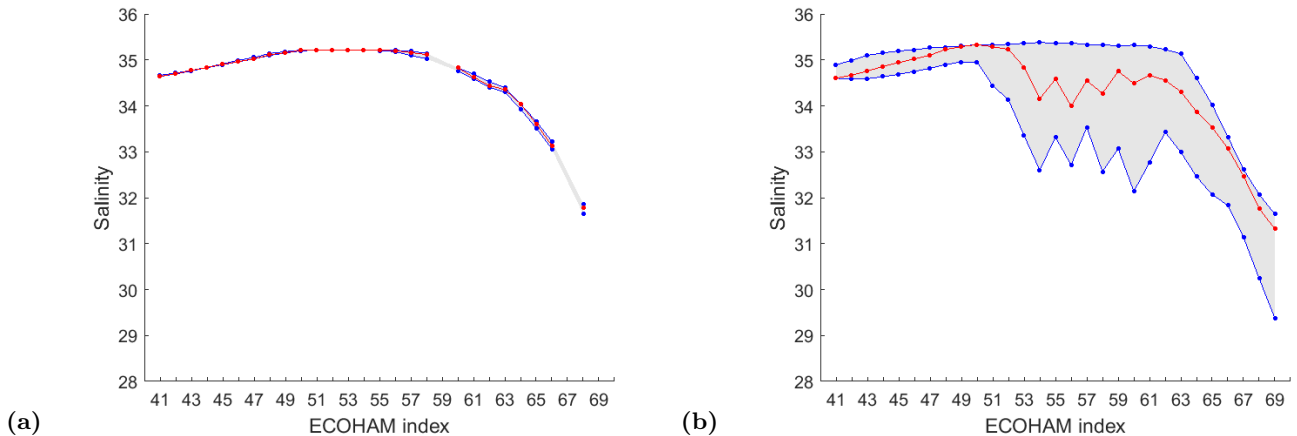


**Figure 3.9** – Simulated salinity variability transect. (a) Short time series (see Table B.2 in the appendix): Helgoland - Stonehaven (30 - 35 m). Missing ECOHAM indexes are caused by bottom topography. (b) Long time series (2001 - 2014): Stonehaven - Helgoland (0 - 10 m). Blue line: minimum and maximum values. Red line: expedition transect.

Figure 3.9b shows the modelled variability of salinity for the long time series from the surface layer in the transect from S - H. The highest variability was revealed in the central and the most southern part of the transect with 1.5 - 2.3. A variation in water masses inflow via the English Channel (EC) and a varying amount of river run-off throughout the years probably explain the high variability. Larger values exhibit the regions across the DB (see ECOHAM index 52 - 61). Here, the variability usually exceeded more than 2.5. It is mainly lead back to the influence of the Baltic Sea inflow. But, the intrusion of the Baltic Sea inflow towards central North Sea is overestimated by the model. Lowest variability can be found in the northern part of the transect (see ECOHAM index 41 - 51) with 0.3 - 0.5. A spatial gradient can be observed from NW to SE. It is strong in the southern part.

As the short time series show slight variability in Figure 3.9a, the simulated values from the expedition can be considered as representative for the deeper part and interior of the transects (Figures

not shown). Otherwise, the modelled expedition transects are not representative in space and time due to large variabilities (see Figure 3.9b, other Figures not shown).

### 3.3.3 Oxygen

The modelled oxygen transects from the three depth layers showed marginal discrepancies between both tracks in space and time for the oxygen variability and for the modelled expedition values. Larger differences between both H - S and S - H can only be recognised for the surface layer (Figures not shown). In general, each depth layer revealed considerable distances between the minimum and maximum value across the transects.

Figure 3.10a shows the modelled oxygen variability for the short time series of the transect from H - S (30 - 35 m). Lowest variability can be identified in the central North Sea with 6.5 - 8  $mmol O_2/m^3$  (see ECOHAM index 46 - 51). Towards the Scottish coast, the variability increases to approximately 11  $mmol O_2/m^3$  (see ECOHAM index 41 - 45). Similar variability exhibits the transect towards the northern DB (see ECOHAM index 55 - 58). Strongest variability can be observed in the southern part of the transect ( $\sim 13 - 20 mmol O_2/m^3$ ). A stronger variability indicates that higher biological activities occurs in the southern part in contrast to the northern part. Physical causes could also be the reason for stroger variability.

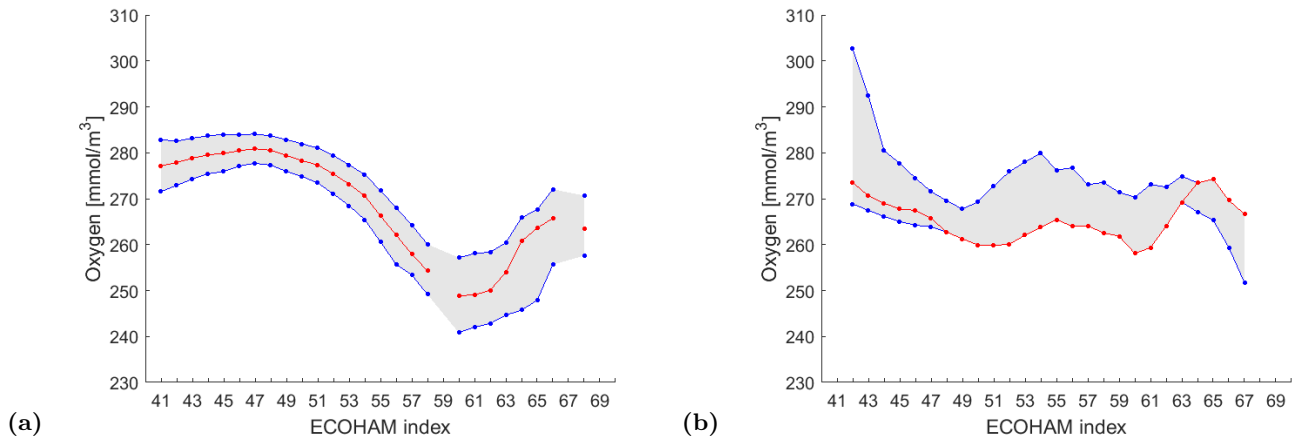


**Figure 3.10** – Simulated oxygen variability transect. (a) Short time series (see Table B.2 in the appendix): Helgoland - Stonehaven (30 - 35 m). Missing ECOHAM indexes are caused by bottom topography. (b) Shifted transects from Stonehaven - Helgoland (0 - 10 m). Blue line: minimum and maximum values. Red line: expedition transect.

Figure 3.10b shows the modelled surface oxygen variability for the transect S - H in space. Generally, a spatial gradual decrease of oxygen can be observed across the transect from  $\sim 280 mmol O_2/m^3$  to  $\sim 260 mmol O_2/m^3$ . Towards the coast an augmented variability can be observed with  $\sim 10 mmol O_2/m^3$  to  $\sim 33 mmol O_2/m^3$  (Stonehaven, see ECOHAM index 42 - 46) and  $\sim 9 mmol O_2/m^3$  to  $\sim 15 mmol O_2/m^3$  (Helgoland, see ECOHAM index 65 - 69), respectively. The elevated variability towards the coast as well as the negative gradient within the transect is probably influenced by two origins: temperature and biology. The solubility of oxygen changes in sea water by a change in temperature and salinity. But the temperature is the significant variable. The oxygen concentration will decrease by increasing temperature. Towards Stonehaven, the surface temperature decreases whereas in the direction of Helgoland it augments (see Figure B.7c in the appendix). In addition, the southern part of the transect towards Helgoland is more affected by the biological activities (see Figure B.7d in the appendix, other Figures not shown). Some processes can influence the concentrations of oxygen additionally. Especially the exchange with the atmosphere at the surface can be considered as source or sink. The advection is a further source or sink for oxygen concentration.

Mostly, the modelled expedition transect is located in the center of the minimum and maximum values (see red line in Figure 3.10a). A similar trend in the expedition's transects was revealed at depth layer 60 - 70 m for the short time series (see Figure B.7b in the appendix). Accordingly, the simulated oxygen values of the expedition can be regarded within the deeper part and interior of the transects as representative with respect to the short time series. Otherwise, the expedition values are

located at the minimum or maximum values. Additionally, most of the expedition values traverse across the transects in space and time from the maximum to minimum value or vice versa (see Figure 3.10b, other Figures not shown).

### 3.3.4 Phytoplankton

The simulated chlorophyll-a concentrations revealed different behaviour within the transects between H - S and S - H for the variability and the modelled expedition values in space and time. Highest discrepancy depicted the surface layer, whereas for the deeper layer (30 - 35 m) most differences can be found in the southern part of the transect. In the interior (60 - 70 m), both tracks are almost identical (Figures not shown). That the simulated values between H - S and S - H converge towards the deeper layers is mainly led back to the lower activity of primary production and grazing by zooplankton.

Figure 3.11a shows the modelled phytoplankton variability from the short time series in the transect from H - S (30 - 35 m). Low variability exhibits the central North Sea and towards the Scottish coast with  $\sim 0.03 - 0.1 \text{ mg/m}^3$  (see ECOHAM index 41 - 54). Augmented variability revealed the adjacents of the DB. The northern edge of the DB shows a variability of  $0.2 - 0.4 \text{ mg/m}^3$ , whereas the southern edge shows a variability of  $0.15 - 0.3 \text{ mg/m}^3$ . Highest variability can be observed towards Helgoland with a maximum of  $\sim 1.2 \text{ mg/m}^3$  (see ECOHAM index 64 - 65).

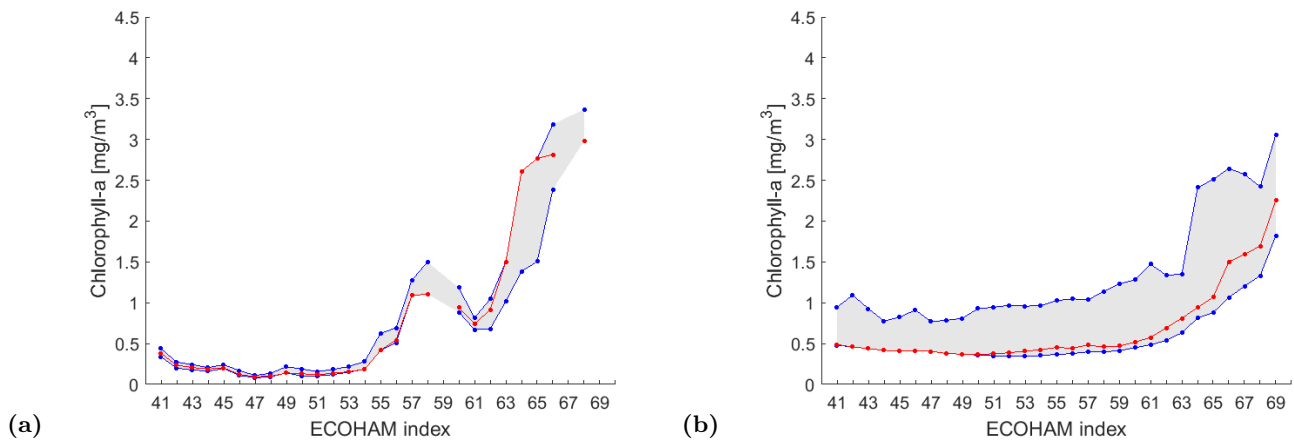


**Figure 3.11** – Simulated phytoplankton variability transects. (a) Short time series (see Table B.2 in the appendix): Helgoland - Stonehaven (30 - 35 m). Missing ECOHAM indexes are caused by bottom topography. (b) Long time series (2001 - 2014): Stonehaven - Helgoland (0 - 10 m). Blue line: minimum and maximum values. Red line: expedition transect.

Figure 3.11b shows the modelled phytoplankton variability at the surface from the long time series in the transect from S - H. The variability is similar in the central North Sea and towards Stonehaven with  $\sim 0.4 - 0.6 \text{ mg/m}^3$  (see ECOHAM index 41 - 54) and elevates within the DB ( $0.6 - 1.0 \text{ mg/m}^3$ , see ECOHAM index 56 - 62). Towards Helgoland the variability increases. The highest variability is located between ECOHAM index 64 - 66 with  $\sim 1.6 \text{ mg/m}^3$ .

The expedition transects from Stonehaven to the central North Sea in deeper layers of the transects for the short time series can only be considered as partially representative (see red line from ECOHAM index 41 - 55 in Figure 3.11a, other Figures not shown) due to low variability. In general, the expedition values are mostly located along the minimum or maximum value within the transects (see red line in Figures 3.11b and B.7d in the appendix, other Figures not shown). Additionally, an opposite trend can be observed in the surface layer for the expedition values between both transects H - S and S - H in time (Figures not shown).

The transect from Figure 3.11a shows a remarkable spatial gradient from NW to SE. An elevated gradient can be observed at the adjacents of the DB. It is more distinctive on the northern DB with  $\sim 0.5 \text{ (mg/m}^3\text{)/km}$  (see ECOHAM index 56 - 57) as on the southern DB with  $\sim 0.3 \text{ (mg/m}^3\text{)/km}$ . An augmented gradient shows the southern part with its strongest increase around the OG with  $\sim 1.5 \text{ (mg/m}^3\text{)/km}$  (see ECOHAM index 62 - 64). A considerable spatial gradient can be identified in the surface layer of the southern part from the transect S- H in Figure 3.11b with its strongest increase being  $\sim 0.5 \text{ (mg/m}^3\text{)/km}$ , located at ECOHAM index 65 - 65 and 68 - 69, respectively. Meanwhile in the northern part the gradient is marginally.

### 3.3.5 Microzooplankton

As well as the simulated chlorophyll-a concentrations, the modelled microzooplankton transects (threshold: size class  $258 \mu\text{m}$ ) revealed different behaviour between the transects from H - S and S - H for the variability and the modelled expedition values in space and time. Especially the surface layer exhibited large differences, meanwhile in the interior of the transects the discrepancies converge to identical tracks. The converging towards identical tracks in the interior is mainly caused by low activities of grazing by microzooplankton due to weak primary production.

Similarities in the variability and expedition values between microzooplankton and phytoplankton can be identified within the deeper part of the transects in space and time. Mainly, the microzooplankton concentration exhibited larger variabilities at the surface layer and into the deeper layers across the northern part of the transects as well as in the region of the DB.

Figure 3.12a shows the modelled variability of microzooplankton for the short time series in the transect from H - S (30 - 35 m). Low variability exhibits the central North Sea and the direction towards Stonehaven with  $\sim 0.05 - 0.2 \text{ mmol C/m}^3$  (see ECOHAM index 41 - 54). Elevated variability depicted the adjacents of the DB. The northern edge of the DB shows a variability of  $0.6 - 1.0 \text{ mmol C/m}^3$ , whereas the southern edge shows a variability of  $0.2 - 0.8 \text{ mmol C/m}^3$ . Strongest variability can be identified towards Helgoland with a maximum of  $\sim 1.2 \text{ mmol C/m}^3$  (see ECOHAM index 64 - 65).

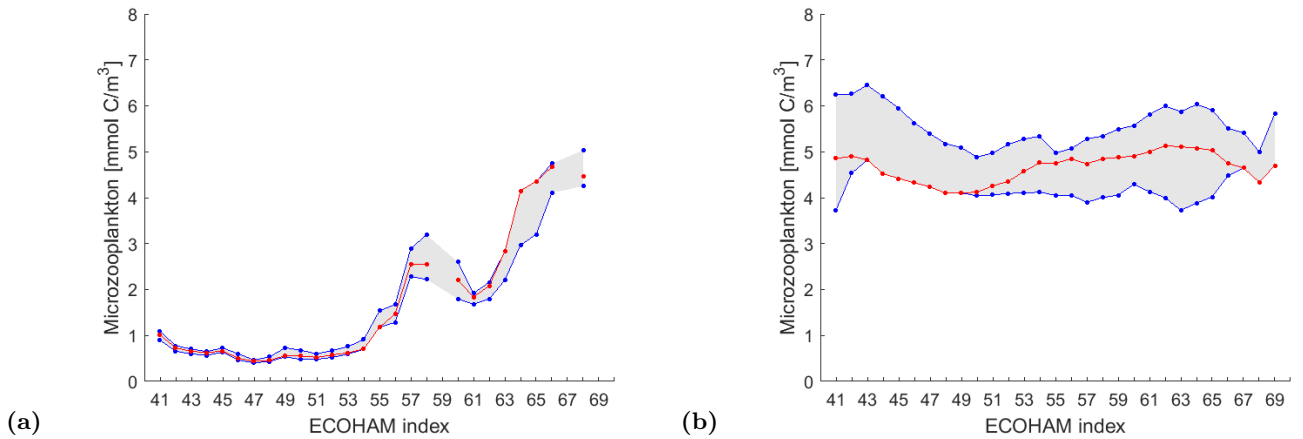


**Figure 3.12** – Simulated microzooplankton variability transect (threshold: size class  $258 \mu\text{m}$ ). (a) Short time series (see Table B.2 in the appendix): Helgoland - Stonehaven (30 - 35 m). Missing ECOHAM indexes are caused by bottom topography. (b) Long time series (2001 - 2014): Stonehaven - Helgoland (0 - 10 m). Blue line: minimum and maximum values. Red line: expedition transect.

Figure 3.12b shows the modelled variability of the microzooplankton for the long time series of the surface layer in the transect from S - H. The variability across the transect is extensive. Lowest variability exhibits the central North Sea with  $\sim 1 \text{ mmol C/m}^3$  (see ECOHAM index 48 - 52). Higher variability can be observed near the OG which exceeds  $2 \text{ mmol C/m}^3$  (see ECOHAM index 62 - 64) and towards Stonehaven with a variability mainly between  $1.3 - 1.7 \text{ mmol C/m}^3$  (see ECOHAM index 41 - 47).

Similar to the simulated expedition values of phytoplankton, the modelled expedition transects can only be regarded as partially representative to the deeper layers of the transects from Stonehaven to the central North Sea for the short time series due to slight variability (see red line of ECOHAM index 41 - 55 in Figure 3.12a, other Figures not shown). Otherwise, the expedition values are located at the extremum or the variability is large within the transects and therefore the expedition transects cannot be considered as representative (see red line in Figure 3.12b, other Figures not shown).

In contrast to the surface layer, the transect of the depth layer 30 - 35 m (see Figure 3.12a) reveals a remarkable spatial gradient from NW to SE. Elevated gradients can be found in the north of the DB and in the southern part. Whereas the northerly DB shows a gradient of  $\sim 1 (\text{mmol C/m}^3)/\text{km}$  (see ECOHAM index 56 - 57), the southerly DB exhibits a gradient of  $\sim 0.4 (\text{mmol C/m}^3)/\text{km}$ . The strongest gradient can be observed within the OG with  $\sim 1 (\text{mmol C/m}^3)/\text{km}$  (see ECOHAM index 62 - 64). Compared to the phytoplankton gradient in Figure 3.11a, the microzooplankton gradient at the northerly DB is steeper and slightly steeper at the southerly DB, respectively. In contrary, a

steeper gradient shows the phytoplankton within the OG.

### 3.3.6 Mesozooplankton

The modelled mesozooplankton transects of the three depth layers reveals mainly marginal differences for the variability and for the modelled expedition values between both tracks in space and time.

Figure 3.13a shows the modelled variability of mesozooplankton for the short time series in the transect from H - S (30 - 35 m). Low variability can be observed in the central North Sea and towards Stonehaven with  $\sim 0.02 - 0.1 \text{ mmol C/m}^3$  (see ECOHAM index 41 - 54). Augmented variability depicted the adjacents of the DB. A variability of  $\sim 0.3 - 0.45 \text{ mmol C/m}^3$  can be identified at the northern edge of the DB and a variability of  $\sim 0.15 - 0.4 \text{ mmol C/m}^3$  at the southern edge of the DB. In the southeast of the OG, the variability increases towards Helgoland to  $\sim 0.4 \text{ mmol C/m}^3$  in the southeast of OG (see ECOHAM index 64 - 65) and shows its maximum nearby Helgoland ( $\sim 0.45 \text{ mmol C/m}^3$ , see ECOHAM index 69).

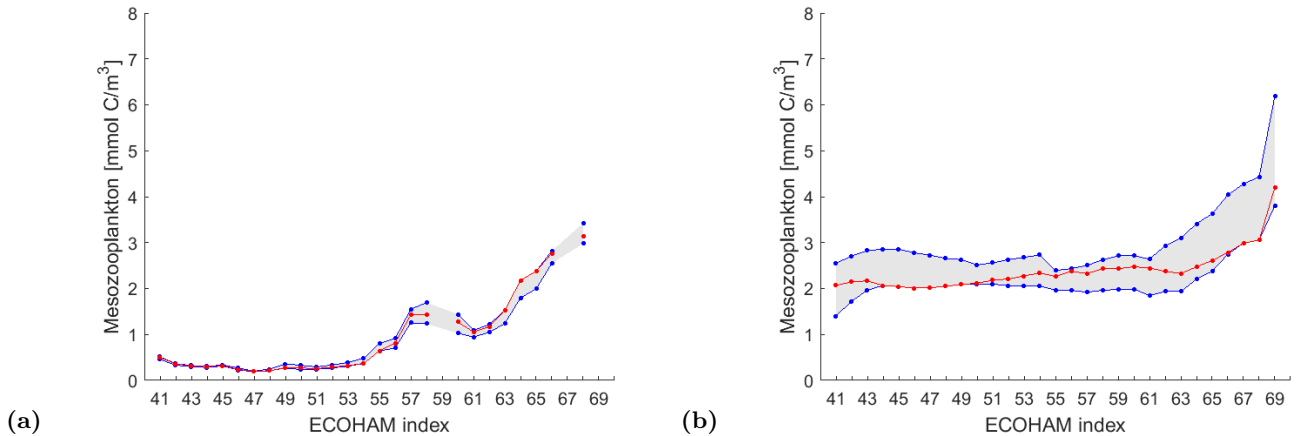


**Figure 3.13** – Simulated mesozooplankton variability transect (threshold: size class  $258 \mu\text{m}$ ). (a) Short time series (see Table B.2 in the appendix): Helgoland - Stonehaven (30 - 35 m). Missing ECOHAM indexes are caused by bottom topography. (b) Long time series (2001 - 2014): Stonehaven - Helgoland (0 - 10 m). Blue line: minimum and maximum values. Red line: expedition transect.

Figure 3.13b shows the modelled variability of the mesozooplankton for the long time series of the surface layer in the transect from S - H. The variability within the transect is large. Lowest variability can be found in the central North Sea with  $\sim 0.4 - 0.6 \text{ mmol C/m}^3$  (see ECOHAM index 48 - 52). Higher variability shows the transect towards Stonehaven ( $0.7 - 1.15 \text{ mmol C/m}^3$ , see ECOHAM index 41 - 47). The strongest variability can be identified in the southern part of the OG towards Helgoland with  $\sim 1 - 2.4 \text{ mmol C/m}^3$  (see ECOHAM index 62 - 69).

The modelled expedition transects can only be considered as partially representative in the transects from Stonehaven to the central North Sea with respect to the short time series due to slight variability (see red line from ECOHAM index 41 - 55 in Figure 3.13a) or due to the values being located at the midpoint between the minimum and maximum (Figures not shown). Otherwise, the expedition values are mostly located at the extremum or the variability is large across the transects, that the expedition transect cannot be considered as representative (see Figure 3.13b, other Figures not shown).

In contrast to the microzooplankton transect of depth layer 30 - 35 m (see Figure 3.12a), the spatial gradient of the mesozooplankton is less distinctive from NW to SE in the depth layer 30 - 35 m (see Figure 3.13a). Augmented gradients can be identified at the region of the DB and towards Helgoland. The northerly DB shows a gradient of  $\sim 0.6 (\text{mmol C/m}^3)/\text{km}$  (see ECOHAM index 56 - 57), whereas the southerly DB shows a gradient of  $\sim 0.2 (\text{mmol C/m}^3)/\text{km}$ . The strongest gradient can be found within the OG ( $\sim 0.4 (\text{mmol C/m}^3)/\text{km}$ , see ECOHAM index 62 - 64). Regarding the microzooplankton gradient at the DB and in the southern part, the mesozooplankton gradient is smooth from NW to SE (see Figures 3.12a and 3.13a).

With respect to the surface layer microzooplankton transect in Figure 3.12b, a considerable spatial gradient can be observed from NW to SE (see Figure 3.13b). Especially the southern part shows an elevated gradient towards Helgoland with  $\sim 0.3 (\text{mmol C/m}^3)/\text{km}$  (see ECOHAM index 63 - 68). The

steepest gradient can be identified nearby Helgoland ( $\sim 0.8$  ( $mmol\ C/m^3$ )/ $km$ , see ECOHAM index 68 - 69).

### 3.4 Statistic analysis of the transects in space and time

Graphical comparison of both transects with all six parameters in space and time is extensive. Hence, two cost functions have been applied: (1) The cost function A describes the mean normalised difference of anomaly between the modelled and observed transects. (2) The cost function B describes the mean relative error between the modelled and observed transects. Both cost functions show the calculated "distance" between the simulated and observational data. Smaller distances of the expedition transect in space and time reveal better agreement between the simulated and observed data. As possible, images were selected where a trend through space or time can be identified of the expedition transects for the physical and biological parameters.

#### 3.4.1 Cost functions of physical parameters

The cost function A (see left hand side in Figure 3.14) and cost function B (see right hand side in Figure 3.14) show a similar trend between the transects from Helgoland - Stonehaven (H - S) and Stonehaven - Helgoland (S - H) for all physical parameters. Due to splitting the expedition of HE428 chronologically into two transects, each transect has a different amount of measurements (see Table A.2) as well as each cell among each other. Therefore, the appearing of larger discrepancy between H - S and S - H in cost function B is caused by differently calculated standard deviations (SD) from the observed transect (see for example Figure 3.14b). Additionally, both cost functions revealed a relatively similar trend among each other with exception of the cost function A for oxygen on short term. It shows at the beginning an opposite trend in contrast to the cost function B (see Figures 3.14e and 3.14f).

The values in cost function A reveal slight discrepancies between all physical parameters. Only the salinity reveals a larger discrepancy by displacing the transects (see Figure 3.14c). The increasing values in cost function A towards NE is mainly caused by the Baltic inflow and, additionally, the southern part of the expedition transects moves closer to the less saltier continental coast (Figures not shown). A huge error shows the displaced transects of salinity which can be led back to the mentioned causes in section 3.3.2 (see Figure 3.14d).

As expected, towards the warmest month of the year (August), the temperature anomalies as well the relative error with respect to the short time series increase. The displaced temperature transect of both tracks revealed an increase in difference anomalies towards NE in cost function A. Whereas no specific behaviour can be detected from the displaced transects in cost function B (Figures not shown).

As mentioned above, the relative error in cost function B and the difference anomalies in cost function A augment towards NE for the salinity. With respect to the short time series, the error and the anomalies are small (Figures not shown).

Regarding the short time series of oxygen, the difference anomalies and the relative error decrease. The decreasing of the simulated oxygen concentrations in some regions of the transect (surface layer, interior and southern part) is an indicator for the modelled transects to improve after the expedition (Figures not shown). In the displaced transects, the relative error of oxygen augments from SW to NE. Less biological activities probably explain such behaviour (Figures not shown). Additionally, the temperatures can play as an important role which change the solubility of oxygen concentrations. With respect to the long time series, a trend cannot be remarked in transects H - S and S - H for both cost functions in all physical parameters (Figures not shown).

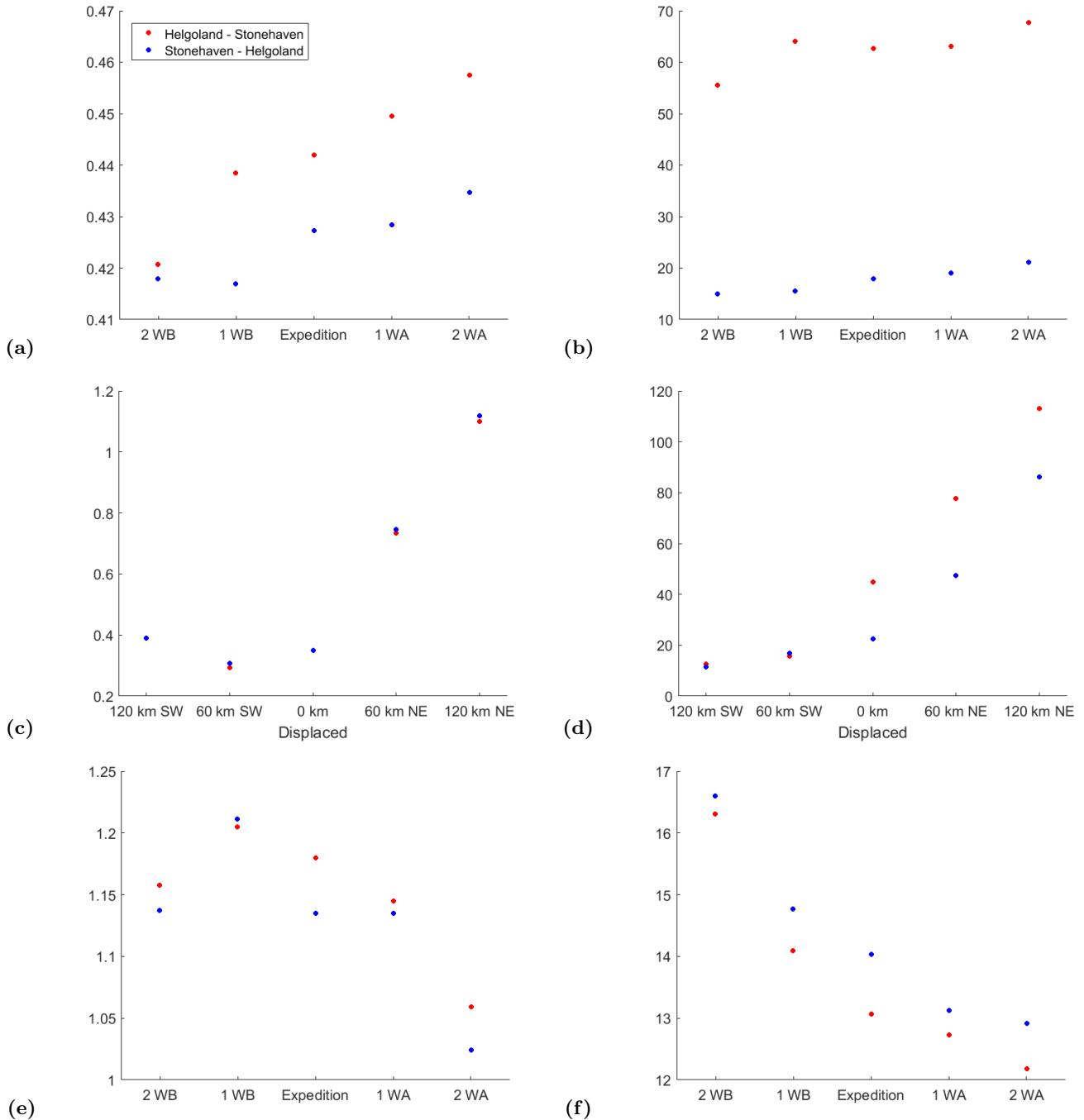


**Figure 3.14** – Cost functions of the physical parameters. Left: cost function A. Right: cost function B. WB: week before the expedition. WA: week after the expedition (see Table B.2 in the appendix). (a) and (b) temperature of the short time series. (c) and (d) salinity of the displaced transects. (e) and (f) oxygen of the short time series. Note the different scale in the y-axis.

### 3.4.2 Cost functions biological parameters

In general, cost function A (see left hand side in Figure 3.15) and cost function B (see right hand side in Figure 3.15) show a similar trend between the transects from H - S and S - H for biological parameters. As mentioned above, due to differently calculated SD from the observed transects, cost function B reveals larger discrepancies between the transects H - S and S - H (see for example Figure 3.15f). Both cost functions show a relatively similar trend among each other in the displaced transects with exception of phytoplankton towards NE (see Figures 3.15a and 3.15b) and from the parameter mesozooplankton in the displaced transects of 60 km towards NE (see Figures 3.15e).

Mostly, the values augment in both functions by displacing the transects towards SW as well as towards NE for all biological parameters which is led back to a different regime of biological productivities. The shallower southwestern part of the North Sea exhibits a higher biological productivity in contrast to the deeper northeastern part where the productivity mostly occurs onshore. The higher biological productiv-

ity across the DB in the simulated shifted transects towards SW (Figures not shown) probably explains the improved matching with the observed expedition transects in cost function A. Such trend cannot be identified in cost function B. Yet, an opposite trend can be observed towards NE in the phytoplankton (see Figure 3.15b). The improved matching between the observed expedition transects and the displaced simulated transects of phytoplankton is probably caused by lower simulated concentrations due to a lower productivity of phytoplankton (Figures not shown). An improved match between the shifted transects and the observed expedition transects can also be induced by the omission of water columns (ECOHAM index) at the beginning or end of the transect (see Figures B.2 (a) - (d) in the appendix). However, the values in cost function A show low discrepancies between the biological parameters in space. Analogue behaviour reveals also cost function B. Only the microzooplankton shows augmented error values in space (see Figure 3.15d).

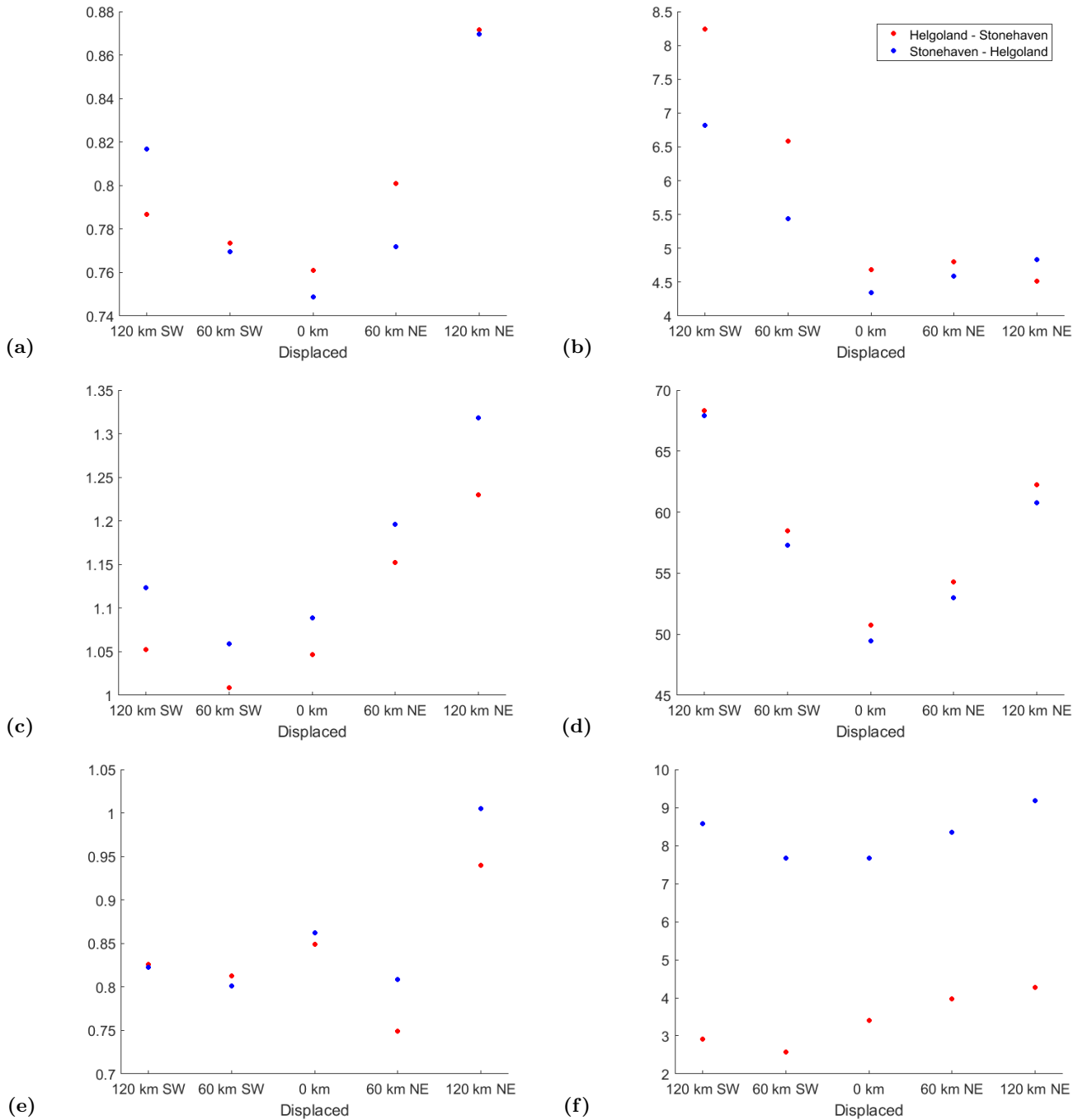


**Figure 3.15** – Cost functions of the biological parameters. Left: cost function A. Right: cost function B. WB: week before the expedition. WA: week after the expedition (see Table B.2 in the appendix). (a) and (b) phytoplankton of the displaced transects. (c) and (d) microzooplankton of the displaced transects. (e) and (f) mesozooplankton of the displaced transects. Threshold of zooplankton: size class  $258 \mu m$ . Note the different scale in the y-axis.

Regarding the short time series, a trend cannot be identified in transects H - S and S - H for both cost

functions for the parameter phytoplankton and for the parameters mircozooplankton and mesozooplankton in cost function A. In contrary, the cost function B reveals a trend for mircozooplankton and mesozooplankton: Both parameters show a decrease of the mean relative error throughout the short time series which is less for mesozooplankton (see Figure 3.15f). The decreasing in cost function B is led back to the simulated concentrations of mircozooplankton and mesozooplankton that continuously decreases throughout the short time series (Figures not shown). With respect to the long time series, a trend cannot be found in transects H - S and S - H for both cost functions in all biological parameters (Figures not shown).

### 3.4.3 Correlation coefficient and significance levels of the transects in space and time

Two correlation coefficients have been calculated to examine the physical and biological parameters in space and time for the transects H - S and S - H. The correlation coefficient  $r_1$  shows the statistical representativeness of the modelled expedition data. On the other hand, the correlation coefficient  $r_2$  quantifies the agreement between the simulated and observed data.

Tables 3.1 and 3.2 show both computed correlations coefficients and, additionally, a two sided significance level  $\alpha_{5\%}$  and  $\alpha_{1\%}$  in space and time for the physical and biological parameters for both tracks. The significance levels were only performed for  $r_2$ . A check mark in significant level  $\alpha$  for all parameters points out significance for  $r_2$ .

The evaluated correlation coefficient  $r_1$  showed mostly high values (0.85 - 1.0) for all parameters and both transects in space and time. An exception depicted oxygen which revealed lower values for the long time series. For oxygen the years 2005 and 2010 are remarkable with values of  $r_1 = 0.56$  for the transect H - S. Similar behaviour showed the transect S - H. Generally, the statistical representativeness in both tracks of the modelled expedition data for all parameters is in good agreement in space and time. Only oxygen is in less agreement with the modelled expedition data for long time series in both transects.

With respect to  $r_2$ , a high positive correlation can be seen for the temperature and salinity for both transects in space and time. An exception revealed the salinity by displacing the transects towards NE: The value of  $r_2$  decreased continuously. It is led back to the simulated Baltic inflow which becomes a predominant role towards NE in the upper layers of the transects. Additionally, the southern part of the expedition transect moves closer to the less saltier continental coast (see Figure A.9 in the appendix, Figures not shown). Such trend can be seen also for  $r_1$  in both transects. Regarding the biological parameters, low to moderate positive correlation is shown for phytoplankton ( $r_2 = 0.3 - 0.5$ ) and mesozooplankton ( $r_2 = 0.25 - 0.45$ ) for both tracks in space and time. Microzooplankton (threshold: 258  $\mu m$ ) showed negligible correlation for both transects in space and time.

In general, a significance in both levels  $\alpha$  of  $r_2$  of the data between simulated and observed parameters depicted temperature, salinity, phytoplankton and mesozooplankton in space and time for the transects H - S and S - H. In contrary, most of the oxygen and microzooplankton data showed no significance in both levels  $\alpha$  for both transects in space and time.

Hence, a good agreement between the simulated and observed data can be considered for temperature and salinity for the transects H - S and S - H in space and time. Meanwhile, for oxygen and microzooplankton a poor agreement exists between the simulated and observed data for both transects in space and time. On the other hand, a moderate agreement can be considered between the simulated and observed data for phytoplankton and mesozooplankton for both tracks in space and time.

**Table 3.1** – Correlation coefficients and t-test significance level  $\alpha$  of the physical and biological parameters for the transect Helgoland - Stonehaven.  $r_1$ : correlation coefficient calculated only with simulated data itself.  $r_2$ : correlation coefficient calculated with observational and simulated data.  $\alpha_{5\%}$ : significance level of 5%.  $\alpha_{1\%}$ : significance level of 1%. Blank: not significant. Note that the significance levels have been tested on  $r_2$ . WB: Week before the expedition. WA: Week after the expedition. Distance 60 and 120 are in km. Threshold of zooplankton: size class  $258 \mu m$  (see section 2.10.1).

	Helgoland - Stonehaven																							
	physical parameter												biological parameter											
	Temperature				Salinity				Oxygen				Phytoplankton				Microzooplankton				Mesozooplankton			
	$r_1$	$r_2$	$\alpha_{5\%}$	$\alpha_{1\%}$	$r_1$	$r_2$	$\alpha_{5\%}$	$\alpha_{1\%}$	$r_1$	$r_2$	$\alpha_{5\%}$	$\alpha_{1\%}$	$r_1$	$r_2$	$\alpha_{5\%}$	$\alpha_{1\%}$	$r_1$	$r_2$	$\alpha_{5\%}$	$\alpha_{1\%}$	$r_1$	$r_2$	$\alpha_{5\%}$	$\alpha_{1\%}$
2014	1.0	0.88	✓	✓	1.0	0.89	✓	✓	1.0	0.01			1.0	0.40	✓	✓	1.0	0.10			1.0	0.35	✓	✓
2013	0.98	0.87	✓	✓	0.95	0.85	✓	✓	0.65	-0.07			0.93	0.53	✓	✓	0.97	0.12	✓		0.98	0.43	✓	✓
2012	0.98	0.86	✓	✓	0.95	0.91	✓	✓	0.74	0.16	✓	✓	0.95	0.52	✓	✓	0.97	0.13	✓		0.97	0.42	✓	✓
2011	0.99	0.88	✓	✓	0.96	0.90	✓	✓	0.80	0.08			0.97	0.48	✓	✓	0.98	0.12	✓		0.98	0.41	✓	✓
2010	0.96	0.91	✓	✓	0.92	0.75	✓	✓	0.56	-0.23	✓	✓	0.95	0.44	✓	✓	0.97	0.07			0.95	0.39	✓	✓
2009	0.99	0.91	✓	✓	0.95	0.91	✓	✓	0.88	-0.22	✓	✓	0.98	0.43	✓	✓	0.98	0.14	✓	✓	0.98	0.37	✓	✓
2008	0.98	0.88	✓	✓	0.96	0.91	✓	✓	0.86	0.12	✓		0.95	0.52	✓	✓	0.97	0.13	✓		0.98	0.42	✓	✓
2007	0.98	0.89	✓	✓	0.94	0.92	✓	✓	0.86	0.08			0.92	0.54	✓	✓	0.98	0.16	✓	✓	0.98	0.40	✓	✓
2006	0.99	0.87	✓	✓	0.93	0.92	✓	✓	0.86	-0.11			0.96	0.50	✓	✓	0.99	0.10			0.99	0.35	✓	✓
2005	0.99	0.86	✓	✓	0.95	0.92	✓	✓	0.56	0.08			0.94	0.44	✓	✓	0.98	0.11			0.98	0.35	✓	✓
2004	0.98	0.89	✓	✓	0.97	0.90	✓	✓	0.82	0.07			0.95	0.53	✓	✓	0.97	0.17	✓	✓	0.97	0.43	✓	✓
2003	0.99	0.88	✓	✓	0.96	0.89	✓	✓	0.84	-0.08			0.96	0.51	✓	✓	0.98	0.14	✓		0.98	0.43	✓	✓
2002	0.97	0.89	✓	✓	0.95	0.91	✓	✓	0.71	0.26	✓	✓	0.94	0.55	✓	✓	0.96	0.14	✓		0.95	0.43	✓	✓
2001	0.98	0.87	✓	✓	0.95	0.80	✓	✓	0.86	-0.12	✓		0.95	0.47	✓	✓	0.97	0.08			0.98	0.42	✓	✓
2 WB	0.99	0.89	✓	✓	0.98	0.91	✓	✓	0.94	0.06			0.95	0.43	✓	✓	0.98	0.07			0.99	0.33	✓	✓
1 WB	0.99	0.87	✓	✓	0.99	0.86	✓	✓	0.96	-0.05			0.96	0.47	✓	✓	0.99	0.08			0.99	0.35	✓	✓
1 WA	1.0	0.88	✓	✓	1.0	0.90	✓	✓	0.95	0.0			0.97	0.44	✓	✓	1.0	0.09			1.0	0.36	✓	✓
2 WA	1.0	0.87	✓	✓	0.98	0.91	✓	✓	0.93	0.14	✓		0.95	0.41	✓	✓	0.99	0.08			0.99	0.34	✓	✓
120 NE	0.97	0.87	✓	✓	0.54	0.03			0.68	-0.10			0.92	0.20	✓	✓	0.96	-0.29	✓	✓	0.97	0.18	✓	✓
60 NE	0.99	0.88	✓	✓	0.68	0.37	✓	✓	0.93	-0.10			0.98	0.31	✓	✓	0.91	-0.11			0.99	0.45	✓	✓
60 SW	0.97	0.88	✓	✓	0.94	0.92	✓	✓	0.90	0.06			0.94	0.39	✓	✓	0.96	0.21	✓	✓	0.96	0.40	✓	✓
120 SW	0.94	0.89	✓	✓	0.90	0.87	✓	✓	0.74	0.13	✓		0.84	0.41	✓	✓	0.87	0.19	✓	✓	0.93	0.43	✓	✓

**Table 3.2** – Correlation coefficients and t-test significance level  $\alpha$  of the physical and biological parameters for the transect Stonehaven - Helgoland.  $r_1$ : correlation coefficient calculated only with simulated data itself.  $r_2$ : correlation coefficient calculated with observational and simulated data.  $\alpha_{5\%}$ : significance level of 5%.  $\alpha_{1\%}$ : significance level of 1%. Blank: not significant. Note that the significance levels have been tested on  $r_2$ . WB: Week before the expedition. WA: Week after the expedition. Distance 60 and 120 are in km. Threshold of zooplankton: size class  $258 \mu m$  (see section 2.10.1).

	Stonehaven - Helgoland																							
	physical parameter												biological parameter											
	Temperature				Salinity				Oxygen				Phytoplankton				Microzooplankton				Mesozooplankton			
	$r_1$	$r_2$	$\alpha_{5\%}$	$\alpha_{1\%}$	$r_1$	$r_2$	$\alpha_{5\%}$	$\alpha_{1\%}$	$r_1$	$r_2$	$\alpha_{5\%}$	$\alpha_{1\%}$	$r_1$	$r_2$	$\alpha_{5\%}$	$\alpha_{1\%}$	$r_1$	$r_2$	$\alpha_{5\%}$	$\alpha_{1\%}$	$r_1$	$r_2$	$\alpha_{5\%}$	$\alpha_{1\%}$
2014	1.0	0.89	✓	✓	1.0	0.90	✓	✓	1.0	0.0			1.0	0.40	✓	✓	1.0	0.04			1.0	0.27	✓	✓
2013	0.99	0.88	✓	✓	0.96	0.84	✓	✓	0.78	-0.03			0.97	0.44	✓	✓	0.97	0.05			0.98	0.36	✓	✓
2012	0.98	0.87	✓	✓	0.96	0.90	✓	✓	0.81	0.14	✓		0.97	0.46	✓	✓	0.97	0.07			0.97	0.36	✓	✓
2011	0.98	0.89	✓	✓	0.97	0.90	✓	✓	0.82	0.05			0.98	0.45	✓	✓	0.98	0.06			0.98	0.32	✓	✓
2010	0.97	0.92	✓	✓	0.91	0.74	✓	✓	0.71	-0.24	✓	✓	0.96	0.36	✓	✓	0.97	0.01			0.96	0.30	✓	✓
2009	0.98	0.92	✓	✓	0.97	0.91	✓	✓	0.89	-0.20	✓	✓	0.97	0.43	✓	✓	0.98	0.09			0.98	0.31	✓	✓
2008	0.97	0.89	✓	✓	0.97	0.91	✓	✓	0.88	0.07			0.95	0.47	✓	✓	0.97	0.07			0.98	0.36	✓	✓
2007	0.97	0.90	✓	✓	0.96	0.92	✓	✓	0.84	0.05			0.92	0.53	✓	✓	0.97	0.10			0.98	0.35	✓	✓
2006	0.99	0.89	✓	✓	0.95	0.93	✓	✓	0.88	-0.12	✓		0.99	0.39	✓	✓	0.99	0.06			0.99	0.28	✓	✓
2005	0.99	0.88	✓	✓	0.96	0.92	✓	✓	0.61	0.06			0.98	0.38	✓	✓	0.98	0.05			0.98	0.26	✓	✓
2004	0.96	0.91	✓	✓	0.98	0.89	✓	✓	0.87	0.01			0.93	0.49	✓	✓	0.96	0.11	✓		0.97	0.38	✓	✓
2003	0.99	0.90	✓	✓	0.97	0.89	✓	✓	0.89	-0.07			0.98	0.46	✓	✓	0.98	0.08			0.97	0.36	✓	✓
2002	0.98	0.90	✓	✓	0.97	0.91	✓	✓	0.73	0.21	✓	✓	0.95	0.52	✓	✓	0.97	0.06			0.96	0.38	✓	✓
2001	0.96	0.89	✓	✓	0.96	0.80	✓	✓	0.92	-0.03			0.91	0.46	✓	✓	0.95	0.10			0.97	0.38	✓	✓
2 WB	0.99	0.89	✓	✓	0.99	0.90	✓	✓	0.97	0.01			0.98	0.38	✓	✓	0.99	0.01			0.99	0.25	✓	✓
1 WB	1.0	0.90	✓	✓	1.0	0.90	✓	✓	0.96	-0.05			0.98	0.39	✓	✓	0.99	0.04			1.0	0.27	✓	✓
1 WA	1.0	0.89	✓	✓	0.99	0.91	✓	✓	0.97	-0.02			0.97	0.37	✓	✓	1.0	0.03			1.0	0.27	✓	✓
2 WA	1.0	0.87	✓	✓	0.99	0.91	✓	✓	0.95	0.10			0.98	0.37	✓	✓	0.99	0.0			0.99	0.25	✓	✓
120 NE	0.97	0.88	✓	✓	0.49	0.02			0.63	-0.01			0.94	0.19	✓	✓	0.98	-0.42	✓	✓	0.96	0.04		
60 NE	0.99	0.89	✓	✓	0.65	0.39	✓	✓	0.91	-0.05			0.98	0.34	✓	✓	0.99	-0.16	✓	✓	0.90	0.27	✓	✓
60 SW	0.98	0.89	✓	✓	0.96	0.92	✓	✓	0.90	0.0			0.94	0.37	✓	✓	0.97	0.14	✓		0.96	0.37	✓	✓
120 SW	0.94	0.90	✓	✓	0.92	0.87	✓	✓	0.71	0.08			0.89	0.33	✓	✓	0.94	0.10			0.94	0.38	✓	✓

## Second part

### 3.5 Mixed layer depth in the selected water columns

A temperature criterion of  $0.4\text{ K}$  (see equation 2.11) has been selected to calculate the depth of the mixed layer ( $D_{ML}$ ) in the water columns. The onset of a persistent stratification occurred in April for all suggested water columns ECOHAM index 47 - 54 in the specified area of the transects (see Table B.6 in the appendix).

Figure 3.16a shows the simulated temperatures throughout the year 2014 for the water column of ECOHAM index 48. The water column exhibits a seasonal temperature cycle. The stratification period starts on 19 April and ends on 23 November (see dashed line in Figure 3.16a). During summer, the mixed layer depth (MLD) is mostly stable at 15 m depth. At the end of the summer it deepens and is located at 25 m depth.

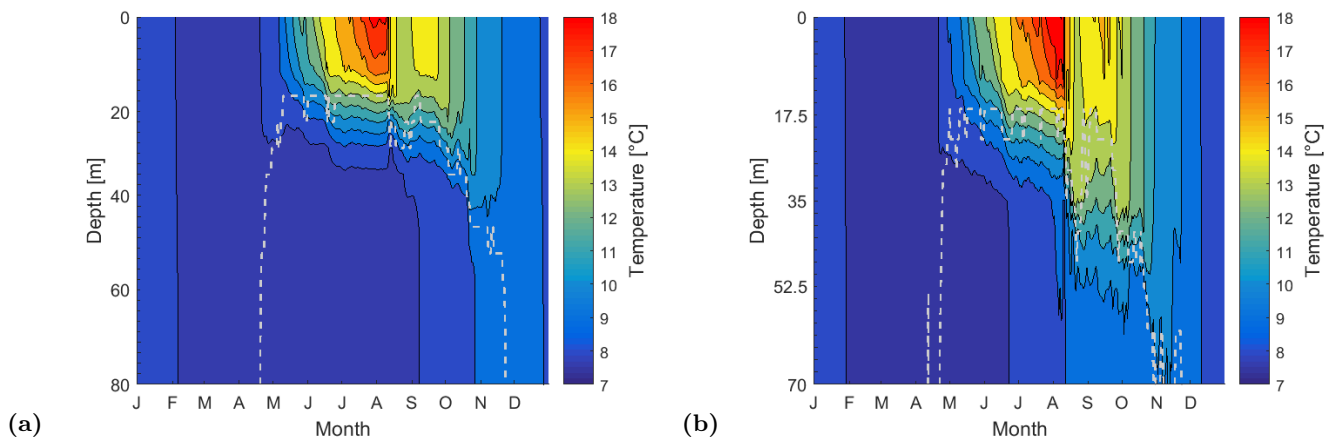


**Figure 3.16** – Simulated temperature of a water column throughout the year 2014. Dashed line: mixed layer depth (MLD). Criterion:  $0.4\text{ K}$  (see equation (2.11)). (a) ECOHAM index 48. (b) ECOHAM index 54. Note the different depth of the water columns.

Figure 3.16b illustrates the simulated temperatures throughout the year of 2014 for the water column of ECOHAM index 54. A seasonal temperature cycle can be observed which is more distinctive compared to the water column of ECOHAM index 48. Additionally, warmer temperatures penetrate into the deeper layers during summer-autumn. Probably, the bottom mixed layer (BML) becomes a predominant factor towards the Dogger Bank (DB) which admixes the intruding warmer water from the upper layers into the colder water of the lower layers. A stratification builds up on 11 April but breaks down rapidly (see dashed line in Figure 3.16b). Such behaviour can be identified as well in the water columns of ECOHAM index 51 - 53 (see Figures B.8 (d) - (f) in the appendix). However, the stratification period starts on 21 April and ends on 10 November. After a couple of days, a stratification builds up again and breaks down after a few days. During summer, the MLD is usually situated at 15 m depth. In contrast to the water column of ECOHAM index 48, the water column of ECOHAM index 54 revealed periods where the MLD is situated at 20 m, before it deepens at the end of the summer. The alternating of the MLD between 15 m and 20 m indicates that the stratification during summer is weaker in ECOHAM index 54 than in ECOHAM 48. Steeper temperature gradients through the thermocline in ECOHAM index 48 probably explain the stronger stratification.

### 3.6 Regenerated component

#### 3.6.1 Remineralisation and nitrification using the AOU in a selected cell

Obtaining the quantity of the produced concentrations ammonium and nitrate from the simulation with respect to the model ratio, the cell ECOHAM index 48 (40 - 45 m) from H - S has been selected to illustrate details of calculation by using the remineralisation value of  $R_0 = 151.5$  ( $d = 16$ ) (details for the remineralisation value  $R_0$  see section 2.14.6). Additionally, the produced amounts with  $R_0 = 140$  ( $d = 18$ ) and  $R_0 = 138$  ( $d = 16$ ) are given only as results. The derived AOU value of the selected cell is  $52.0203\text{ mmol O}_2/\text{m}^3$  (see Table A.5 in the appendix) and the simulated mass budget from the

remineralsation and nitrification are  $0.9 \text{ mmol N/m}^3$  and  $0.84 \text{ mmol N/m}^3$ , respectively (see Table B.5 in the appendix).

The maximum produced amount of ammonium ( $x_{remi,max}$ ) through remineralisation can be obtained by using the equation (2.17) as follows:

$$52.0203 \text{ mmol O}_2/\text{m}^3 = x_{remi,max} \text{ mmol N/m}^3 \frac{R_0}{d} q, \text{ with } q = \frac{\text{mmol O}_2/\text{m}^3}{\text{mmol N/m}^3} \quad (3.1)$$

$$\Rightarrow x_{remi,max} = \frac{52.0203 \text{ mmol O}_2/\text{m}^3}{9.4688 q} = \underline{\underline{5.4939 \text{ mmol N/m}^3}},$$

and for  $R_0 = 140$  shows  $x_{remi,max} = 6.6883 \text{ mmol N/m}^3$  and for  $R_0 = 138$  shows  $x_{remi,max} = 6.0313 \text{ mmol N/m}^3$ .

In contrast to the produced ammonium concentration, the maximum produced quantity of nitrate ( $x_{nitri,max}$ ) through nitrification is valid for all  $R_0$  values and can be evaluated by applying the equation (2.17) as follows:

$$52.0203 \text{ mmol O}_2/\text{m}^3 = 2y_{nitri,max} \text{ mmol N/m}^3 q \quad (3.2)$$

$$\Rightarrow y_{nitri,max} = \frac{52.0203 \text{ mmol O}_2/\text{m}^3}{2 q} = \underline{\underline{26.0102 \text{ mmol N/m}^3}}.$$

According to step two in section 2.14.6, the model ratio from the simulated mass budget can be written as

$$\frac{x_{mass \text{ budget},remi}}{y_{mass \text{ budget},nitri}} = \frac{0.9}{0.84}, \quad (3.3)$$

and modifying the model ratio as remineralisation ratio with respect to equation (2.17) gives

$$x_{ECOHAM\bullet,remi} = \frac{0.9}{0.84} y_{ECOHAM\bullet,nitri} \text{ mmol N/m}^3, \quad (3.4)$$

and as nitrification ratio

$$y_{ECOHAM\bullet,nitri} = \frac{0.84}{0.9} x_{ECOHAM\bullet,remi} \text{ mmol N/m}^3, \quad (3.5)$$

where  $x_{ECOHAM\bullet,remi}$  and  $y_{ECOHAM\bullet,nitri}$  is the produced ammonium and nitrate concentration by AOU with respect to the model ratio from equation (3.3), respectively.

Inserting the remineralisation ratio from equation (3.4) into equation (2.17) yields a produced nitrate concentration of

$$52.0203 \text{ mmol O}_2/\text{m}^3 = 1.0714 y_{ECOHAM\bullet,nitri} \text{ mmol N/m}^3 \frac{R_0}{d} q + 2y_{ECOHAM\bullet,nitri} \text{ mmol N/m}^3 q$$

$$= y_{ECOHAM\bullet,nitri} \text{ mmol N/m}^3 q \left( 1.0714 \frac{R_0}{d} + 2 \right) \quad (3.6)$$

$$\Rightarrow y_{ECOHAM\bullet,nitri} = \frac{52.0203 \text{ mmol O}_2/\text{m}^3}{\left( 1.0714 \frac{R_0}{d} + 2 \right) q} = \underline{\underline{4.2832 \text{ mmol N/m}^3}}.$$

The produced nitrate concentration with respect to the model ratio for  $R_0 = 140$  and  $R_0 = 138$  are  $5.0342 \text{ mmol N/m}^3$  and  $4.6277 \text{ mmol N/m}^3$ , respectively.

Reciprocal, inserting the nitrification ratio from equation (3.5) into equation (2.17) yields a produced ammonium concentration of

$$\begin{aligned}
52.0203 \text{ mmol } O_2/m^3 &= x_{ECOHAM^\bullet,remi} \text{ mmol } N/m^3 \frac{R_0}{d} q \\
&\quad + 2 \cdot 0.93334 x_{ECOHAM^\bullet,remi} \text{ mmol } N/m^3 q \\
&= x_{ECOHAM^\bullet,remi} \text{ mmol } N/m^3 q \left( \frac{R_0}{d} + 1.8667 \right) \tag{3.7} \\
\Rightarrow x_{ECOHAM^\bullet,remi} &= \frac{52.0203 \text{ mmol } O_2/m^3}{\left( \frac{R_0}{d} + 1.8667 \right) q} = \underline{\underline{4.5892 \text{ mmol } N/m^3}}.
\end{aligned}$$

The produced ammonium concentrations with respect to the model ratio for  $R_0 = 140$  and  $R_0 = 138$  are  $5.3938 \text{ mmol } N/m^3$  and  $4.9582 \text{ mmol } N/m^3$ , respectively. A graphical result of ECOHAM<sup>•</sup> of the cell ECOHAM index 48, depth layer 40 - 45 m, is illustrated in Figures 3.17a for  $R_0 = 151.5$  and for  $R_0 = 140$  and for  $R_0 = 138$  in Figures 3.17d and 3.17b, respectively.

The proceedings on how to retrieve the produced ammonium and nitrate with respect to the modelled ratio for the variable ECOHAM<sup>•</sup> with  $R_0 = 151.5$  were shown exemplary and in detail above. This procedure is necessary to obtain the factor  $m$  and  $(1 - m)$  with the determined produced concentration of introduced variable ECOHAM<sup>•</sup>.

### 3.6.2 Range of remineralisation and nitrification over the AOU in the selected cells

A range of observational data from the grid configuration ND130 (minimum, maximum and mean) has been introduced to obtain the possible produced amount of nitrate and ammonium concentrations over the slope of the AOU (see section 2.14.7) and has been applied for the remineralisation values  $R_0 = 151.5$ ,  $R_0 = 140$  and  $R_0 = 138$  (see section 2.14.6).

Figures 3.17 (a) - (c) illustrate the range of the produced ammonium and nitrate concentrations as well as the produced simulated concentrations ECOHAM<sup>•</sup> with respect to the model ratio over the slope of the AOU for the cells of ECOHAM index 47 - 49, depth layer 40 - 45 m, of the transect H - S for the three remineralisation values (see above). Meanwhile, Figures 3.17 (d) - (f) depict the range of the produced ammonium and nitrate concentrations as well as the produced simulated concentrations of ECOHAM<sup>•</sup> over the slope of the AOU from the cells of ECOHAM index 53 - 54, depth layer 40 - 45, of the transect S - H, again for all three remineralisation values.

The produced ammonium and nitrate concentrations of ECOHAM<sup>•</sup> are situated outside the range of ND130 in ECOHAM index 47 - 49 for both transects and all three remineralisation values (see black dots in Figures 3.17 (a) - (c) and Figures A.11a, A.12a and A.13a in the appendix). A calculated ECOHAM<sup>•</sup> which is located outside the range of ND130 leads predominantly to an overestimation of the produced ammonium concentration or nitrate concentration. In contrary, it is situated inside the range in ECOHAM index 50 - 54 for both transects and all three remineralisation values (see black dots in Figures 3.17 (d) - (f) and Figures A.11 (b) and (c), A.12 (b) and (c), and A.13 (b) and (c) in the appendix).

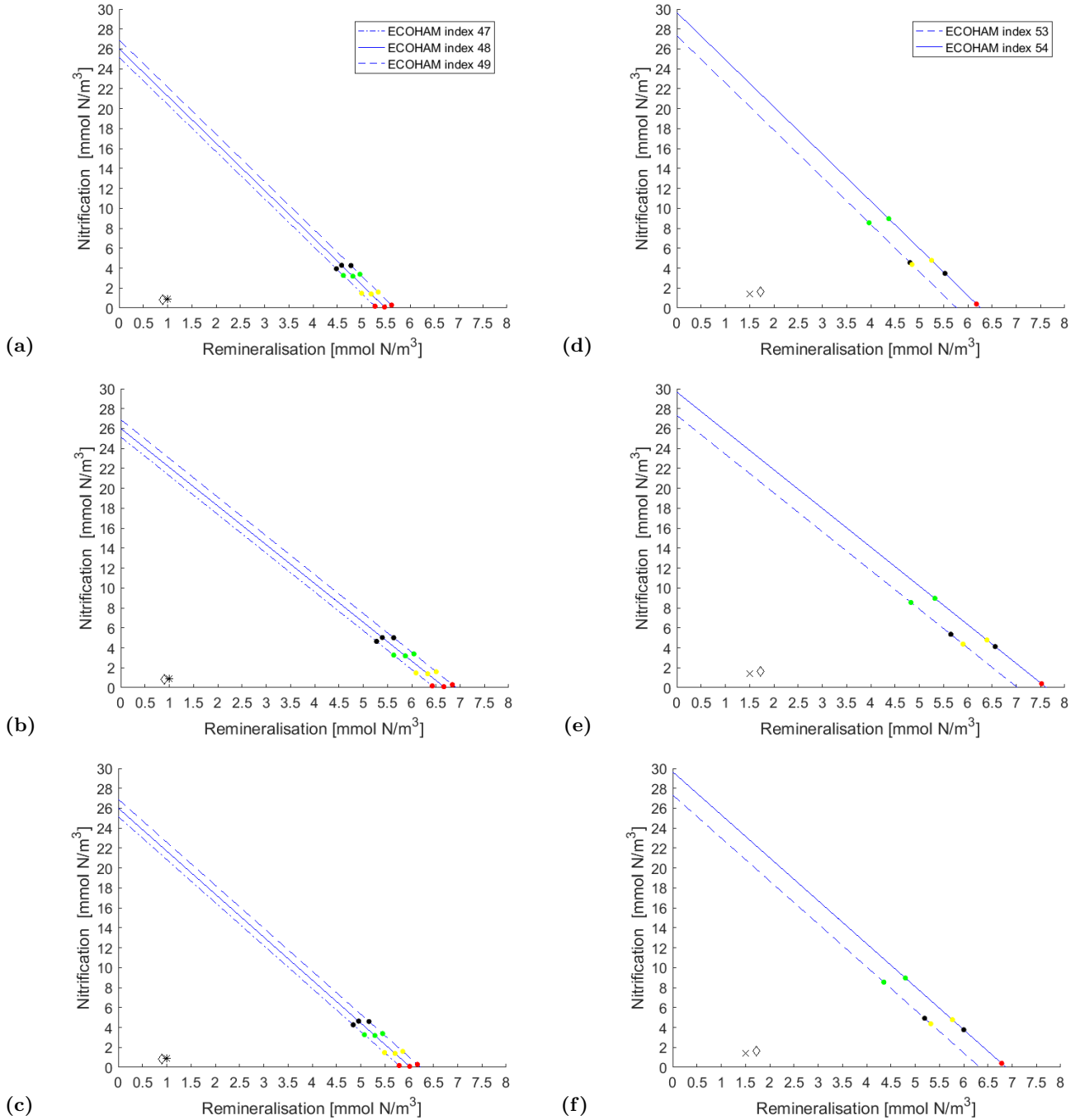


**Figure 3.17** – Range of remineralisation and nitrification over the slope of AOU in the selected cells of the top layer (40 - 45 m) for the defined areas (see Fig. A.10a and (b) in the appendix). Maximum: green dots. Mean: yellow dots. Minimum: red dots. ECOHAM<sup>•</sup>: black dots. Crosses (ECOHAM index 47 and 53), diamonds (ECOHAM index 48 and 54) and asterisks (ECOHAM index 49) are from the simulated  $NH_3$  and  $HNO_3$  concentrations (see Tables B.5 and B.6 in the appendix). Left: ECOHAM index 47 - 49 from the transect Helgoland - Stonehaven. Right: ECOHAM index 53 - 54 from the transect Stonehaven - Helgoland.  $R_0$ : remineralisation value (see Table 2.1). (a) and (d)  $R_0 = 151.5$ . (b) and (e)  $R_0 = 140$ . (c) and (f)  $R_0 = 138$ .

### 3.7 Physical component

The evaluated simulated physical mass budgets of the cells of ECOHAM index 47 - 52, depth layer 40 - 45 m for H - S and of the cells of ECOHAM index 47 - 54 for S - H show opposite values for ammonium and nitrate concentration. Whereas the simulated advection and vertical mixing reveal positive values for ammonium, the values of the advection and vertical mixing are negative for nitrate in both tracks (see Tables B.5 and B.6 in the appendix). With respect to the advection and vertical mixing, ammonium was entered into the cells of both transects while nitrate was discharged during the period from the day of the onset of the persistent stratification until the expedition day.

A remarkable trend can be observed for the vertical mixing of ammonium. The concentration

increases towards the DB in both specified areas of the transect. An indication that the bottom mixed layer (BML) towards the DB is playing an increasingly important role. But an increasing concentration towards DB is not detectable for vertical mixing of nitrate. Additionally, a trend cannot be identified for the advection of ammonium and nitrate concentration. However, adding the advection and vertical mixing concentration of ammonium and nitrate which were compiled by the model, to the "physics" component plays an essential role for the estimation of the nutrients.

### 3.8 Estimation of nitrate and ammonium concentrations in the specified area

Estimation of nitrate and ammonium concentrations with the parameter  $Nutrient_{ECOHAM}^*$  by using  $R_0 = 138$  exhibited the best agreement with the observation in the transect S - H. Figure 3.18a shows the estimated concentration of nitrate with the parameter  $Nutrient_{ECOHAM}^*$  ( $R_0 = 138$ ), whereas Figure 3.18b shows the estimated concentration of ammonium with the parameter  $Nutrient_{ECOHAM}^*$  ( $R_0 = 138$ ).

The overestimation of both nutrient concentrations is clearly illustrated (see ECOHAM index 47 - 49 in the Figures 3.18a and 3.18b). Regarding the remineralisation values of  $R_0 = 151.5$  and  $R_0 = 140$ , the estimation of nitrate and ammonium concentrations with  $Nutrient_{ECOHAM}^*$  were in agreement with the observation in both transects, but ECOHAM index 53 - 54 of transect S - H revealed an underestimation for ammonium concentrations (see Table B.11 in the appendix).

In general, the estimation of nutrient concentrations in both specified areas of the transects H - S and S - H revealed two different behaviours for all three remineralisation values of  $R_0$  for the parameter  $Nutrient_{ECOHAM}^*$  and for the ND130 parameter  $Nutrient_{mean}^*$  (see equation (2.20)). (1) Towards the DB, the estimation of nitrate and ammonium becomes more accurate with concentrations of  $\sim 2 - 3 \text{ mmol/m}^3$  for ammonium and  $\sim 5 - 8 \text{ mmol/m}^3$  for nitrate which is in agreement with the observation in Table C.1 in the appendix. (2) In contrary, towards the deeper part of the central North Sea both nutrient concentrations tend to be overestimated. Here, observed concentrations of  $\sim 1 - 2 \text{ mmol/m}^3$  for ammonium and  $\sim 4.5 - 6 \text{ mmol/m}^3$  for nitrate have to be expected (see Table C.1 in the appendix).

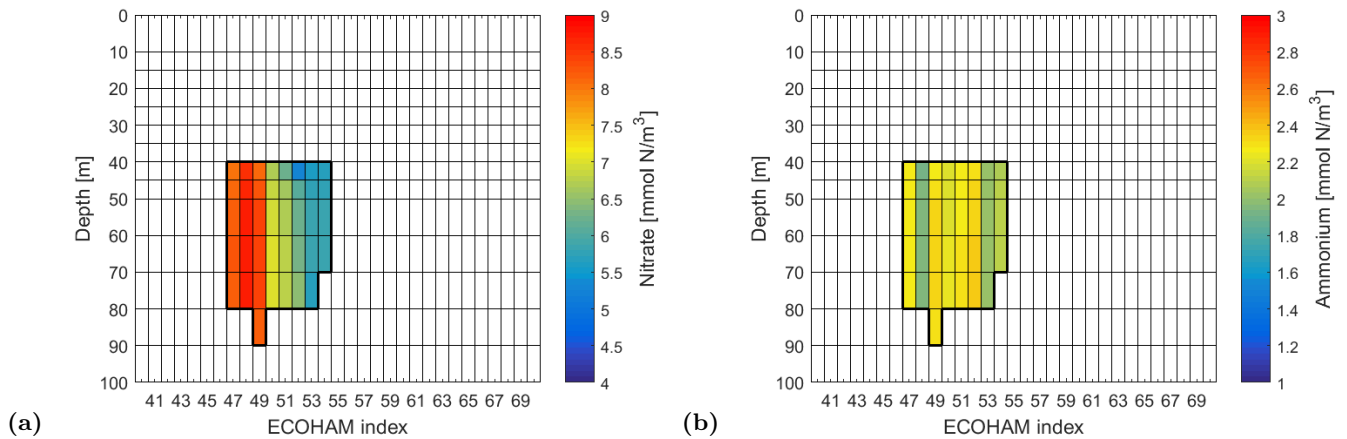


**Figure 3.18** – Estimated nutrient concentrations of ECOHAM\* with remineralisation value  $R_0 = 138$  for the specified area in the transect Stonehaven - Helgoland. (a) Nitrate. (b) Ammonium.

## 4 Discussion

### First part

#### 4.1 Spatial displacement of the transects towards SW and NE

In section 2.11 a method to displace the expedition transect by  $45^\circ$  in the direction of NE and SW was introduced. After having chosen a distance, equations (2.6) and (2.7) compute the towards NE and SW displaced coordinates from the expedition. Due to geodesics which are the great circles on the sphere, the distance between two points is an arc and no more a straight line. Consequently, selecting longer a distance leads to higher deviation (see Table B.1 in the appendix). However, with

respect to the grid resolution of ECOHAM and HAMSOM (approximately 20 km in both directions), the transects can be displaced by around 670 km towards SW and NE.

## 4.2 Determined threshold between microzooplankton and mesozooplankton

Two cost functions have been utilised to identify the threshold of size class between the microzooplankton and mesozooplankton. The best size class revealed on 258  $\mu\text{m}$ . Using the static method of pearson's correlation coefficient and confidence intervals of 5% and 1% the best threshold of size class is shown at 444  $\mu\text{m}$  for microzooplankton and mesozooplankton (see correlation coefficient  $r_2$  as well as significance level  $\alpha_{5\%}$  and  $\alpha_{1\%}$  in Tables 3.1 and 3.2 for the size class 258  $\mu\text{m}$  and Tables A.13 and A.14 for the size class 444  $\mu\text{m}$  in the appendix).

## 4.3 Southern Dogger Bank and Oyster Grounds

A large chlorophyll-a concentration for phytoplankton is seen in the observed transects from H - S and S - H at the southerly DB and Oyster Grounds (OG). The phytoplankton is probably trapped in this region due to stratification. Low turbidity (Figures not shown) indicates that the mixing in this regions is weakly. Since the southerly DB and the OG are still in the euphotic zone, the phytoplankton can perform photosynthesis and could explain the large concentration. The meted high chlorophyll-a values can have a different origin. Dead phytoplankton (detritus) sinking towards the bottom may still have living fluorescent cells. The Turner C6 multisensor used on the expedition detects these cells and registers them as concentration. As mentioned in section 2.10.2, the Laser Optical Plankton Counter (LOPC) device cannot distinct between living and dead particles such as detritus and marine snow. As the southerly DB and OG show large concentration for zooplankton, it could be possible that the LOPC device measured a larger amount of dead particles.

## 4.4 Simulated oxygen data from 2010 and 2005

A correlation coefficient  $r_1$  has been calculated to determine the statistical representativeness of the simulated expedition data from H - S and S - H in space and time. Less agreement revealed the simulated oxygen from years 2005 and 2010 in the long time series by computing  $r_1$  in both transects (see Tables 3.1 and 3.2). Accordingly, an investigation has been performed to examine the occurring statistical anomalies of oxygen from 2005 and 2010 for the transect H - S. The simulated oxygen expedition transects of 2005 and 2010 from the transect H - S are illustrated in Figures B.9a and B.9b in the appendix. Oxygen mass budgets throughout the year of 2005 and 2010 have been compiled for the cell ECOHAM index 55, depth layer 10 - 15 m. The compiled oxygen mass budgets in both cells revealed a change in oxygen concentration during summer is predominately caused by the vertical mixing (Figures not shown). It indicates that the vertical mixing played an important role for the summer distribution of the simulated oxygen concentrations in the transects of 2005 and 2010 from H - S.

# Second part

## 4.5 Temperature criterion for the mixed layer depth

As mentioned in section 2.14.3, the calculation of the mixed layer depth (MLD) is a common method to determine the day of onset of persistent stratification. A temperature criterion of  $\Delta T = 0.4 \text{ K}$  (see equation 2.11) has been selected to calculate the depth of the mixed layer ( $D_{ML}$ ) in the water columns of ECOHAM index 47 - 54 (see dashed line in Figures 3.16 (a) and (b) as well as in Figures B.8 (a) - (f) in the appendix). All water columns revealed an onset of persistent stratification in April by applying  $\Delta T = 0.4 \text{ K}$  (see Table B.6 in the appendix).

According to Kara et al. (2000), the values of  $\Delta T$  exhibit a range from 0.1 - 1.0  $\text{K}$ . Accordingly, calculations with the values  $\Delta T = 0.1 \text{ K}$  and  $\Delta T = 1.0 \text{ K}$  have been conducted to obtain the monthly range for which the onset of persistent stratification occurs for each water column. The results are given in Table B.3 in the appendix. Using the criterion of  $\Delta T = 1.0 \text{ K}$ , all water columns revealed the onset of a persistent stratification in April with exception of the water column ECOHAM index 47 which occurs in May. Applying the criterion of  $\Delta T = 0.1 \text{ K}$  the specified region in the transect

is divided into two parts. The onset of the persistent stratification occurs for the water columns ECOHAM index 47 - 50 in April, whereas for the water columns ECOHAM index 51 - 54 the onset of the persistent stratification occurs in March.

With respect to the value of April for the "preformed" component, the estimation of nitrate concentration tends to overestimation for the water columns ECOHAM index 51 - 54 when using the criterion of  $\Delta T = 0.1 K$ . On the other hand, the estimation of ammonium concentration tends to underestimate for the water columns ECOHAM index 51 - 54 when using the criterion of  $\Delta T = 0.1 K$ . Utilising the nitrate and ammonium values from March (see Table C.1 in the appendix) for the "preformed" component cannot improve the estimation of nitrate and ammonium concentration in the water columns of ECOHAM index 51 - 54. One possibility would be to use more recently observed data for ammonium and nitrate in April. The deployed observed data from ND130 covers the time series from 1960 - 1994.

## 4.6 Regenerated component

The "regenerated" component is the part which influences the estimation of nutrients the most. The concept is based on some assumptions which were utilised to simplify the estimation of nitrate and ammonium. However, the determined slope of AOU in the cells have to be moved (in best case parallel) closer to the origin of the Cartesian coordinates that an enhanced estimation of nitrate and ammonium concentrations of the "regenerated" component can be obtained (see Figures 3.17 (a) - (f)). Possible sources for improving the regenerated concentrations for nitrate and ammonium are for example the determined remineralisation value  $R_0$ , the factor  $m$ , simulation of oxygen mass budgets, True Oxygen Utilisation (TOU) and processes which have not been considered in this concept.

### 4.6.1 Remineralisation value $R_0$

In the underlying concept, the remineralisation values  $R_0 = 151.5$ ,  $R_0 = 140$  and  $R_0 = 138$  have been selected to determine the slope of the observed AOU between the remineralisation and nitrification processes (see step one in section 2.14.6). The remineralisation value  $R_0$  is the required molar amount of dissolved oxygen by remineralisation and depends on the stoichiometric values of a, b, c and d which can be obtained from Table 2.1.  $R_0$  scales together with d the produced ammonium concentration over the observed AOU (see equation (2.17)).

The variable ECOHAM<sup>•</sup> (details see sections 2.14.6 and 2.14.8) is situated outside the range over the slope of the AOU for the cells of ECOHAM index 47 - 49, depth layer 40 - 45 m, of the transects H - S and S - H for all three  $R_0$  (see black dots for example Figures 3.17 (a) - (c)). An location outside the range leads to an overestimation of produced ammonium and nitrate concentration. Using a larger value of  $R_0$  and  $d = 16$ , the slope of the observed AOU is getting steeper between the remineralisation and nitrification. The degree of overestimation is reduced for high remineralisation values. The maximum possible remineralisation is  $R_0 = 151.5$  obtained from the Table 2.1. Consequently, the produced ammonium or nitrate concentration in the cells of ECOHAM index 47 - 49 is always overestimated for ECOHAM<sup>•</sup>. Shifting the AOU slope towards the origin is most likely the best option to move ECOHAM<sup>•</sup> into the range.

### 4.6.2 Factor $m$ for each cell of the selected area

Factor  $m$  and  $(1 - m)$  have been evaluated for the cells of the top layer in the specified area (40 - 45 m) from ECOHAM index 47 - 52 of transect H - S and from ECOHAM index 47 - 54 of transect S - H (see Tables B.7 and B.8 in the appendix). Factor  $m$  scales the quantity of produced ammonium over the observed AOU, whereas factor  $(1 - m)$  scales the quantity of produced nitrate over the observed AOU (see equation (2.8)). Both determined factors have been regarded as constant for its deeper layers (see Figures A.10a and A.10b in the appendix).

Obtaining an improved calculation of the "regenerated" component for ammonium and nitrate concentration, both factors have to be determined for each cell of the water column in the specified areas of the transect. A simulated mass budget (advection, vertical mixing, remineralisation and nitrification) for each deeper layer was calculated for the cell ECOHAM index 48, depth layer 40 - 45 m, from H - S to determine the remineralisation and nitrification towards the bottom. The nitrification value decreases marginally ( $0.01 \text{ mmolN/m}^3$ ) as well as the remineralisation value ( $0.04 \text{ mmolN/m}^3$ )

from the top layer to the bottom. Consequently, the values of both factors will not change significantly and show similar values which was derived by the parameter ECOHAM<sup>•</sup> (details see sections 2.14.6 and 2.14.8). On the other hand, an augmented change of values towards the bottom can be identified for ammonium and nitrate from the simulated advection and vertical mixing. The advection revealed a decrease of  $0.05 \text{ mmolN/m}^3$  for ammonium and  $0.08 \text{ mmolN/m}^3$  for nitrate. The decrease of values towards the bottom in the simulated advection is probably caused by the bottom friction. Regarding the simulated vertical mixing, the ammonium values increase ( $0.08 \text{ mmolN/m}^3$ ) as well as nitrate ( $0.1 \text{ mmolN/m}^3$ ) from the top layer to the bottom. The increase of values towards the bottom in the simulated vertical mixing indicates that the bottom mixed layer (BML) takes a predominant role.

Generally, it is recommended to compile simulated mass budgets for each cell in the specified area of the transects for three reasons: (1) The performed mass budgets for only one water column does not represent the whole specified area. Each water column can have different properties for physical and biological activity. Especially in the direction of the DB, when the water column is getting smaller and the BML is playing an increasingly important role. (2) The value changes in the mass balance from the advection and vertical mixing from the top layer towards the bottom. It is an important finding to apply a more accurate determination of the introduced "physics" component in equation (2.10). (3) The observed AOU concentration mostly augments from the top layer (40 - 45 m) of the specified area towards the bottom in the transects (see Tables A.5 and A.6 in the appendix). Since all three all three aspects would extent the scope of the this thesis it have not been considered.

### 4.6.3 Simulation of oxygen mass budget

Identically to the introduced physical component in the equation (2.10), the calculation of AOU can be enhanced with an oxygen "physics" component:

$$AOU^* = O_{2,saturation}(T,S) - O_{2,observed} + O_{2,physics}, \quad (4.1)$$

where  $O_{2,saturation}(T,S)$  is the oxygen saturation concentration obtained from a function of salinity and temperature by using *in situ* data,  $O_{2,observed}$  is the observed oxygen concentration and term  $O_{2,physics}$  is the sum of the advected and vertically mixed oxygen concentration.  $AOU^*$  is modified by applying the physical component. Due to the derivation of the onset of persistent stratification ( $t_{stratification}$ ) for the "preformed" component, the concentration of  $O_{2,physics}$  can be obtained by the model output. Mass budgets are compiled for oxygen values of ECOHAM index 47 - 54, depth layer 40 - 45 m, for transect H - S and of ECOHAM index 47 - 54, depth layer 40 - 45 m, for transect S - H. Oxygen concentration for the advection and vertical mixing of the cells for both tracks is given in Tables B.5 and B.6 in the appendix.

Generally, both concentrations in the cells (see above) decrease towards DB. Towards the deeper part a trend cannot be identified. Hence, obtaining the regenerated concentration of ammonium and nitrate by applying the modified AOU improves the results retrieved from ECOHAM index 50 - 54. In contrary, the improvement by using the modified AOU in the cells of ECOHAM index 47 - 49 is marginal. As mentioned in section 4.6.2, simulated mass budgets of  $O_{2,physics}$  should be compiled for each cell in the specified area of the transects.

### 4.6.4 True Oxygen Utilisation

In this concept, the Apparent Oxygen Utilisation (AOU) from a specified area in transects H - S and S - H have been derived by the calculated oxygen saturation and oxygen from the observed data (see section 2.14.5). The determined AOU in the transects could contain errors caused by processes such as non-linearity in the solubility of oxygen and respiration involving denitrification (Ito et al., 2004). According to Ito et al. (2004), an enhanced approach can be obtained by using the True Oxygen Utilisation (TOU):

$$TOU = O_{2,preformed} - O_{2,observed}, \quad (4.2)$$

where  $O_{2,preformed}$  is the concentration which was transported and subducted into the interior of the ocean by physical circulation. Its concentration corresponds to the concentration from the previous day of the onset of a persistent stratification ( $t_{stratification}$ ). The term  $O_{2,observed}$  is the observed oxygen concentration. As the days  $t_{stratification}$  have been evaluated for the "preformed" component

(see Table B.6 in the appendix), the concentration of  $O_{2,preformed}$  can be obtained from the model output or from a compiled observational dataset.

#### 4.6.5 Not considered processes

Some processes have been neglected in the methodology which could shift the slope of the AOU towards its origin: loss of ammonium concentrations during nitrification for nitric oxide ( $NO$ ), nitrous oxide ( $N_2O$ ) and nitrogen ( $N_2$ ) as well as assimilation processes of ammonium, nitrite and nitrate to organic matter (OM) (see Figure 2.10).

Determining both the amount of nitrogen [ $mmol/m^3$ ] being lost during nitrification in form of  $NO$ ,  $N_2O$ , as well as  $N_2$  and the amount of nitrite being lost during assimilation to OM, allows to subtract these values from the produced quantity of nitrate ( $y_{nitri}$ ).  $y_{nitri}$  is determined from the AOU by using equation (2.17). On the other hand, determining the amount of nitrogen being lost during the assimilation of ammonium to OM, allows to subtract this value from the produced quantity of ammonium ( $x_{remi}$ ).  $x_{remi}$  can be retrieved analogue to  $y_{nitri}$ .

## 5 Outlook

### 5.1 Threshold between microzooplankton and mesozooplankton

In the present work, the threshold has been selected at the size class of  $258 \mu m$  due to best agreement derived by the cost functions. In a further step, size classes around the value of  $258 \mu m$  can be selected to identify an improved threshold between the microzooplankton and mesozooplankton by applying the cost functions.

### 5.2 Estimations of nitrate and ammonium concentrations

Some points are listed in the second part of the discussion which can also be regarded as an outlook such as TOU and not considered processes. If a more accurate estimation of the nutrients ammonium and nitrate in a selected area is possible in the ocean, the next step could be to evaluate the ratio of DIN/DIP in this area. The dissolved inorganic Nitrogen (DIN) is mainly composed of the nutrients nitrate and ammonium, while the dissolved inorganic phosphate (DIP) is mainly composed of phosphate. The phosphate concentration can be obtained by using the derived Apparent Oxygen Utilisation from observed data divided by the remineralisation value  $R_0$  (see Table 2.1).

## 6 Appendix

### A Observed transect

#### A.1 TRIAXUS samples

Eleven different spatial and temporal samples were conducted with the Remote Operated Towed Vehicle (ROTV) TRIAXUS during the expedition. Table A.1 illustrates the conducted samples.

**Table A.1** – TRIAXUS samples with the corresponding coordinates and time during the research of HE428.

TRIAXUS	Latitude [°]		Longitude [°]		Day		Time [hh:mm:ss]	
	Start	End	Start	End	Start	End	Start	End
sample 1	54.16833	54.96426	7.6722253	5.842419	09. July	10. July	20:10:57	06:10:42
sample 2	54.95760	55.65059	5.8552030	3.876344	10. July	10. July	08:18:33	18:42:22
sample 3	55.65551	56.15800	3.8586460	1.952590	10. July	11. July	20:26:08	06:30:06
sample 4	56.15770	56.31655	1.9633150	1.306737	11. July	11. July	08:38:24	11:39:23
sample 5	56.32093	56.60754	1.3152510	-0.152657	11. July	11. July	13:27:46	18:46:49
sample 6	56.60707	56.89205	-0.1581540	-1.652172	11. July	12. July	21:17:03	05:03:02
sample 7	56.91674	56.56713	-1.6655150	-0.491344	12. July	12. July	08:20:13	17:26:05
sample 8	56.58355	56.02462	-0.3796550	2.539077	12. July	13. July	20:27:51	06:27:12
sample 9	56.02014	55.51540	2.5648660	4.291928	13. July	13. July	08:21:41	16:39:12
sample 10	55.51505	54.89494	4.2968160	6.016809	13. July	14. July	22:04:20	06:48:16
sample 11	54.90961	54.15646	5.9768780	7.677481	14. July	14. July	08:18:28	18:11:23

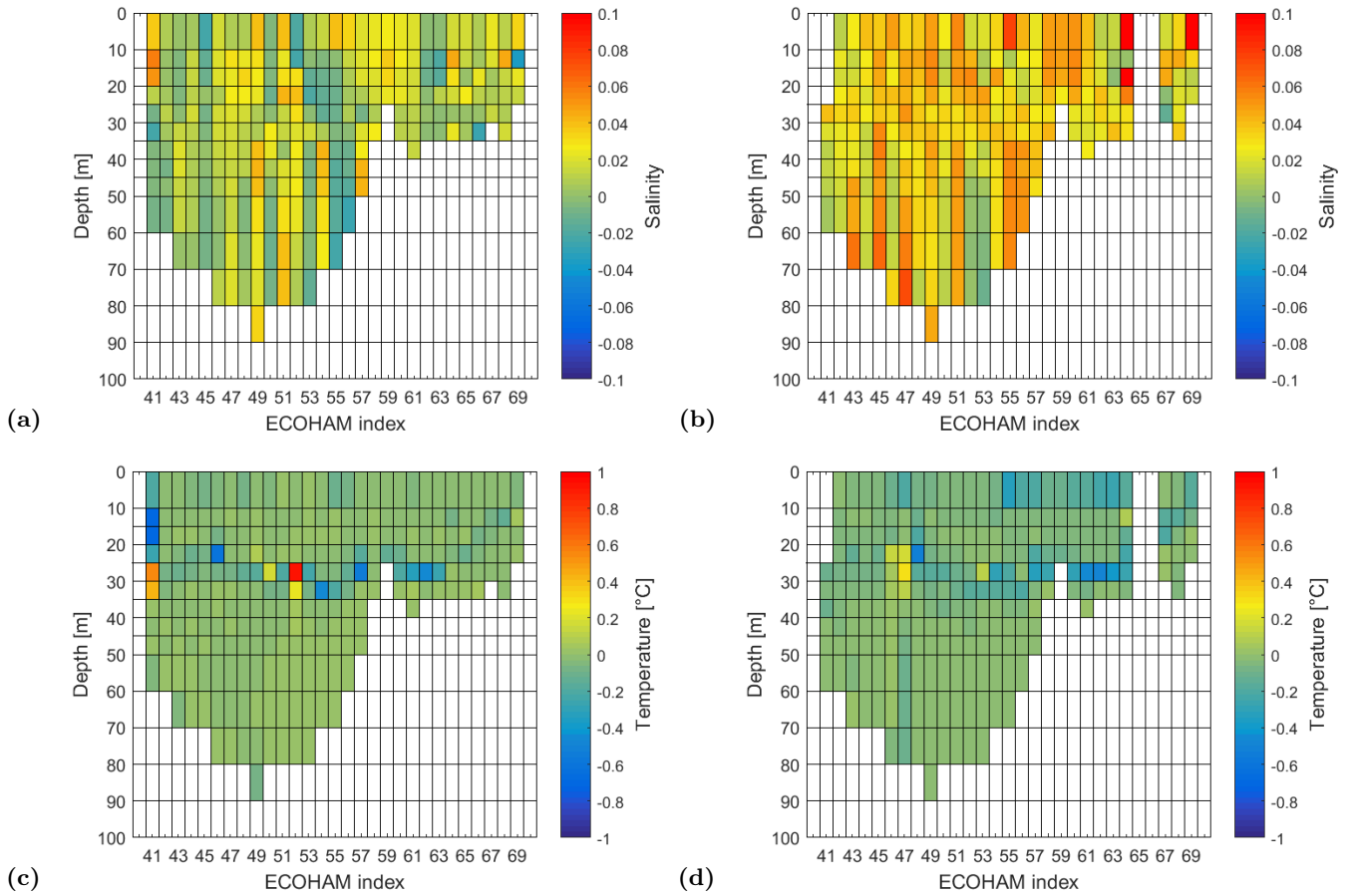
#### A.2 Amount of measurements from the expedition of HE428

**Table A.2** – Counts of *in situ* measurements from the LOPC device and other devices (Turner C6, Aanderaa Oxygen Optopode 4330F and CDT<sub>TRIAXUS</sub>). H - S: transect from Helgoland - Stonehaven. S - H: transect from Stonehaven - Helgoland. Note the different amount of *in situ* measurements between H - S and S - H.

	Total (9.-14. July)	H - S (9.-12. July)	S - H (12.-14. July)
LOPC device	321815	161418	160397
Other devices	332561	167259	165302

#### A.3 Difference of salinity and temperature between LOPC device and TRIAXUS

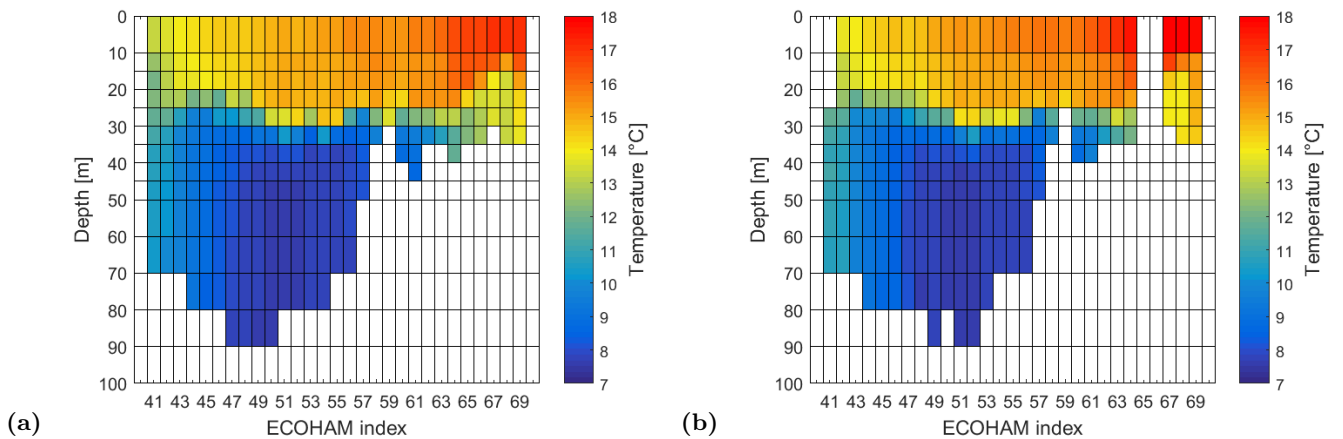
Figures A.1 (a) - (d) show the difference between the salinity and temperature of the LOPC device and Triaxus from Helgoland - Stonehaven (H - S) and Stonehaven - Helgoland (S - H), respectively.



**Figure A.1** – Difference between the LOPC device and TRIAXUS. Left: transect from Helgoland - Stonehaven (H - S). Right: transect from Stonehaven - Helgoland (S - H). (a) and (b) Observed salinity. (c) and (d) Observed temperature. Note the missing data in ECOHAM index 41 (0 - 25 m) and in ECOHAM index 65 - 66 from S - H.

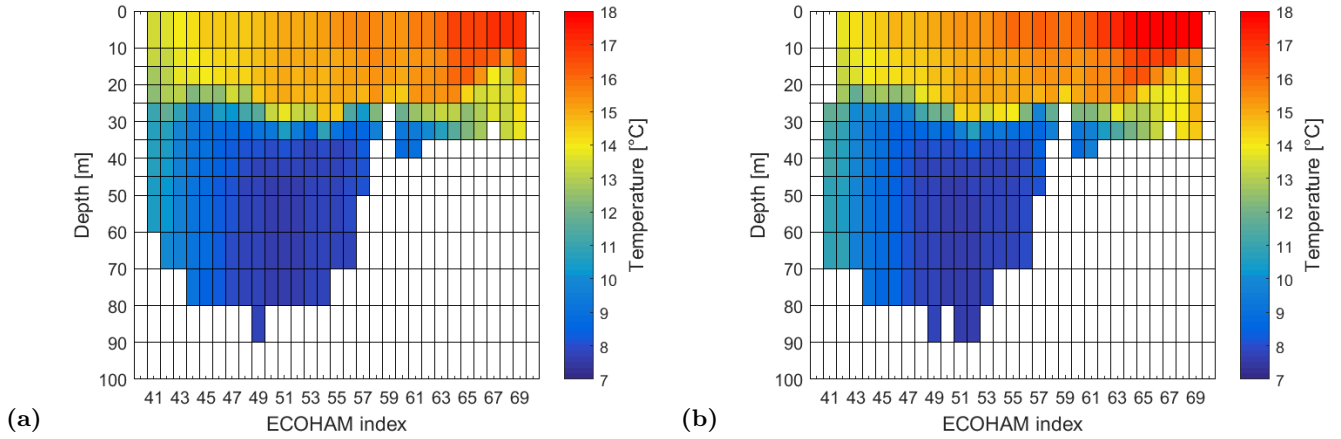
## A.4 Original depth measurements

### A.4.1 TRIAXUS



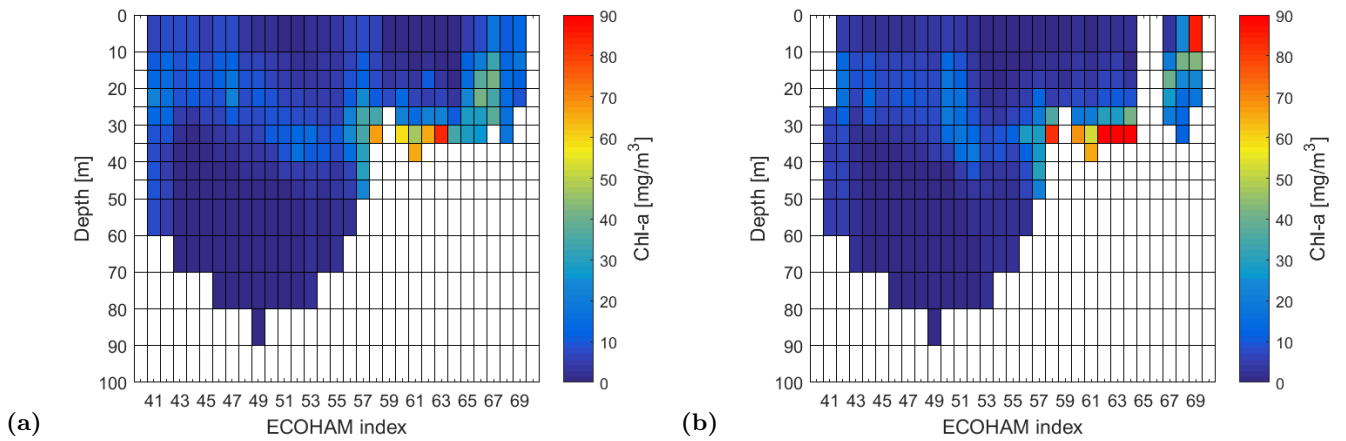
**Figure A.2** – Observed original depth of measurements (temperature) from the TRIAXUS. (a) transect from Helgoland - Stonehaven (H - S). (b) transect from Stonehaven - Helgoland (S - H). Note the missing data in ECOHAM index 41 (0 - 25 m) and ECOHAM index 65 - 66 from S - H.

### A.4.2 LOPC device



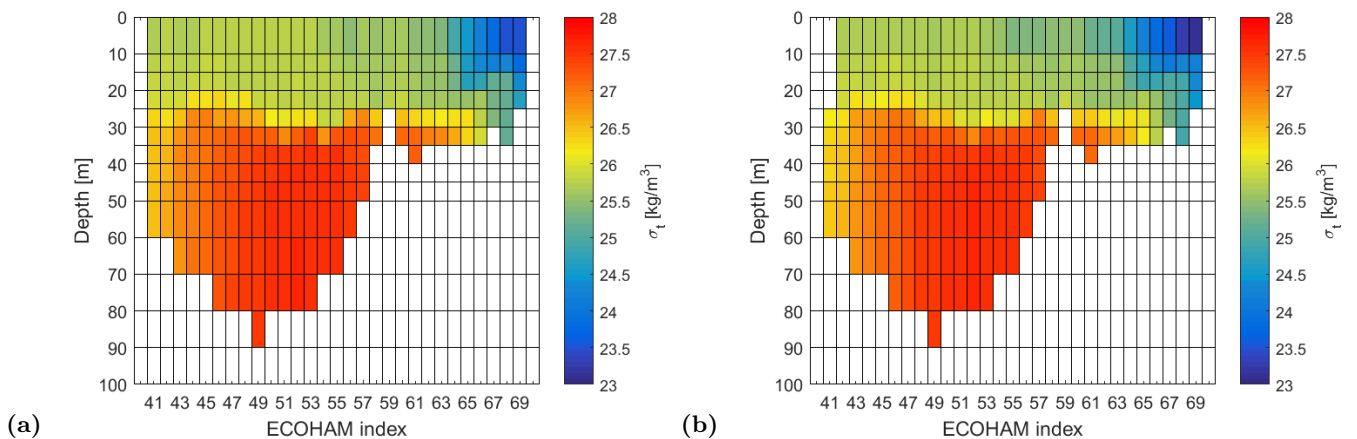
**Figure A.3** – Observed original depth of measurements (temperature) from the LOPC device. (a) transect from Helgoland - Stonehaven (H - S). (b) transect from Stonehaven - Helgoland (S - H). Note the missing data in ECOHAM index 41 (0 - 25 m) from S - H.

### A.5 Original chlorophyll-a measurements of the TRIAXUS



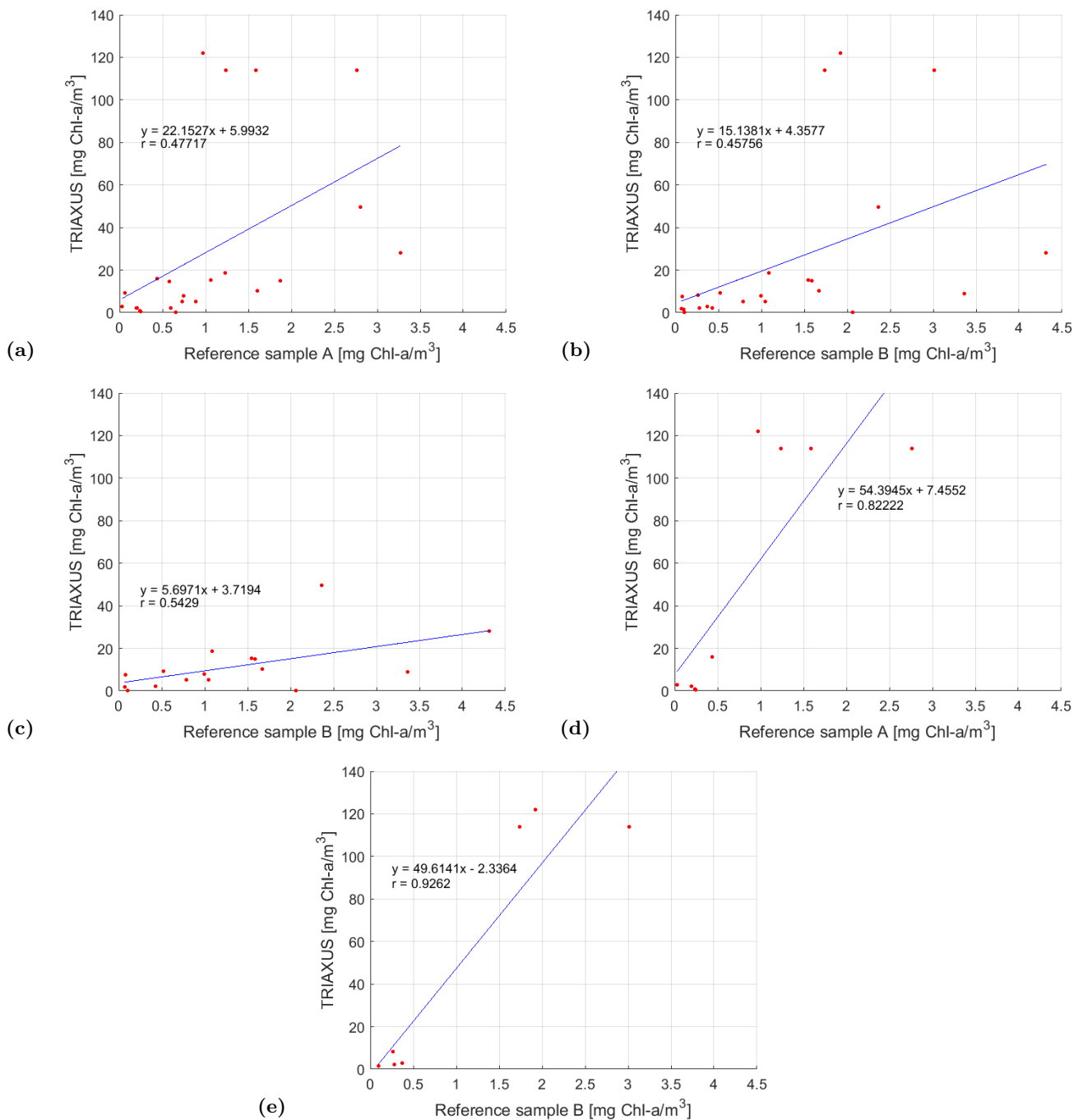
**Figure A.4** – Original measurements of observed chlorophyll-a. (a) transect from Helgoland - Stonehaven (H - S). (b) transect from Stonehaven - Helgoland (S - H). Note the missing data in ECOHAM index 41 (0 - 25 m) and ECOHAM index 65 - 66 from S - H.

### A.6 Potential density anomalies



**Figure A.5** – Observed potential density anomalies. (a) transect from Helgoland - Stonehaven (H - S). (b) transect from Stonehaven - Helgoland (S - H). Note the missing data in ECOHAM index 41 (0 - 25 m).

## A.7 Linear regression of chlorophyll-a of reference samples and TRIAXUS samples



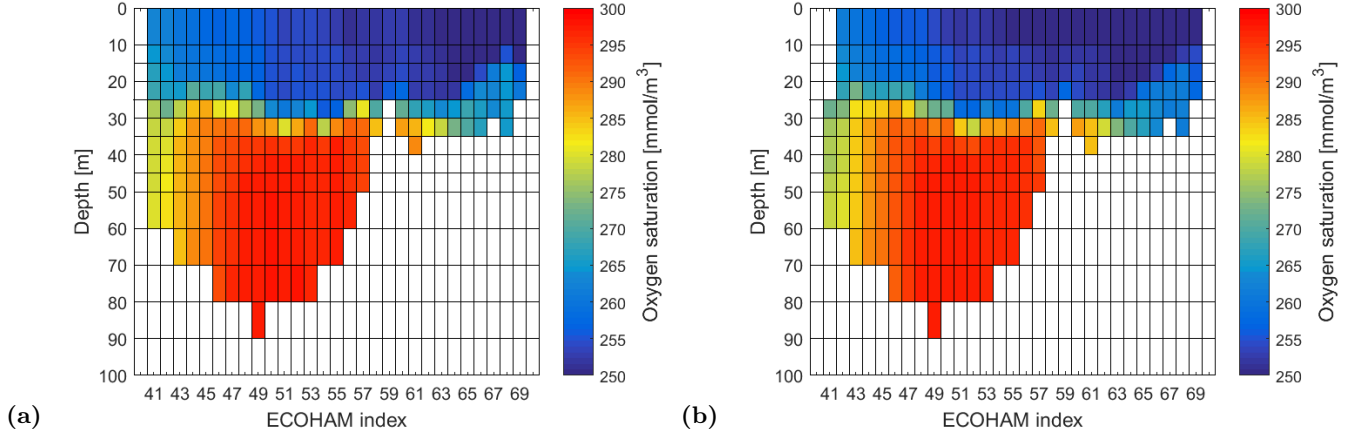
**Figure A.6** – Linear regressions of chlorophyll-a from the reference samples A and B and the suggested corresponding TRIAXUS samples (see Table A.3 in the appendix). 9.7 - 14.7: transect H - S and S - H merged. y: best-fit line r: correlation coefficient. (a) Reference sample A from 9.7 - 14.7. (b) Reference sample B from 9.7 - 14.7. (c) Reference sample B from the transect Helgoland - Stonehaven (H - S). (d) Reference sample A from the transect Stonehaven - Helgoland (S - H). (e) Reference sample B from S - H.

Table A.3 shows the reference samples A and B of chlorophyll-a and their corresponding TRIAXUS samples. Additionally, the deviation between TRIAXUS samples and reference samples has been calculated.

**Table A.3** – Chlorophyll-a concentrations of the reference samples during the cruise of HE428 with their suggested TRIAXUS chlorophyll-a concentrations in space and time. Chl-a A: reference sample A. Chl-a B: reference sample B. Units of chlorophyll-a:  $[mg\ Chl-a/m^3]$ . Units of time: hh:mm:ss. Blank: no value exists or the reference samples were odd. Deviation: discrepancy in space and time between the reference sample and suggested TRIAXUS sample.

Date		Reference samples					TRIAXUS samples					Deviation	
2014	Time	Depth [m]	Latitude [°]	Longitude [°]	Chl-a A	Chl-a B	Time	Depth [m]	Latitude [°]	Longitude [°]	Chl-a	Offset	Depth [m]
09.07.	18:03:00	35	54.17000000	7.66300000	1.227	1.089	21:07:12	34	54.25054900	7.48708100	18.6	3h 04min 12s	1
09.07.	18:06:00	17	54.17166667	7.66266667	1.063	1.545	20:38:24	17	54.19511200	7.60487000	15.4	2h 32min 24s	0
09.07.	18:14:59	5	54.17050000	7.66200000	1.87	1.589	20:53:49	5	54.19678300	7.60113600	14.9	2h 38min 50s	0
10.07.	06:21:00	37	54.96900000	5.83966667		3.362	05:02:00	35	54.88265300	6.05999200	8.88	1h 19min 00s	2
10.07.	06:24:00	27	54.96900000	5.83950000	0.581		05:54:46	27	54.95415800	5.86732400	14.5	29min 14s	0
10.07.	06:34:59	5	54.96883333	5.83933333		0.102	05:53:02	5	54.94858700	5.88223400	0.16	41min 57s	0
10.07.	18:52:00	34	55.65316667	3.87200000	3.27	4.313	21:07:12	33	55.694563	3.738945	28.1	2h 15min 12s	1
10.07.	18:56:00	28	55.65350000	3.87166667	2.802	2.363	18:29:47	28	55.63982600	3.90498700	49.6	26min 13s	0
10.07.	19:03:59	5	55.65383333	3.87116667	0.203		18:28:16	5	55.63561500	3.91793700	2.26	35min 43s	0
11.07.	06:40:00	29	56.15966667	1.94883333	0.891	1.046	08:52:48	29	56.16762300	1.906678	5.23	2h 12min 40s	0
11.07.	11:50:00	81	56.32033333	1.29933333	0.654	2.062	13:55:12	75	56.34247100	1.23909000	0	2h 05min 12s	6
11.07.	11:56:00	29	56.31983333	1.29850000		0.079	11:16:48	29	56.28380600	1.39893100	7.57	39min 12s	0
11.07.	12:05:59	5	56.31916666	1.29733333		0.07	11:02:24	5	56.27985100	1.41290800	1.7	1h 03min 35s	0
11.07.	18:54:00	5	56.60950000	0.14833333	0.743	0.992	18:28:48	5	56.60228400	0.20148300	7.81	25min 12s	0
11.07.	18:59:00	25	56.61133333	0.14816667	0.066	0.519	18:25:02	25	56.60195200	0.20584300	9.25	33min 58s	0
12.07.	05:59:00	63	56.90766667	-1.70450000	0.596	0.427	04:36:54	61	56.89257900	-1.619085	2.28	1h 22min 06s	2
12.07.	06:03:00	16	56.90850000	-1.70433333	1.603	1.668	05:02:24	16	56.89669800	-1.64945600	10.3	1h 00min 36s	0
12.07.	06:15:59	5	56.91083333	-1.70066667	0.733	0.785	04:33:37	5	56.89037200	-1.60798300	5.13	1h 42min 22s	0
12.07.	18:27:59	5	56.58400000	0.37200000	0.031	0.372	16:33:36	5	56.58895200	0.32916200	2.99	1h 54min 23s	0
13.07.	06:37:00	72	56.02383333	2.54550000	0.198	0.28	05:02:24	72	56.09565800	2.22463400	2.09	1h 34min 36s	0
13.07.	16:48:00	5	55.51783333	4.29100000	0.244		16:28:28	5	55.51478500	4.29109400	0.47	19min 32s	0
13.07.	16:53:00	21	55.51783333	4.29000000	0.24	0.264	16:27:20	21	55.52058500	4.26770700	8.4	25min 40s	0
14.07.	06:55:00	36	54.89583333	6.01616667	0.967	1.921	05:45:36	33	54.96578600	5.83459500	122	1h 09min 24s	3
14.07.	06:59:00	27	54.89566667	6.01516667	0.441		06:33:01	27	54.90546100	6.00021300	15.9	25min 59s	0
14.07.	07:09:59	5	54.15933333	6.01366667		0.096	06:31:33	5	54.90786400	5.99388500	1.35	38min 26s	0
14.07.	18:23:00	30	54.15933333	7.66716667	1.239		17:45:36	29	54.17756400	7.64445300	6.04	37min 24s	1
14.07.	18:27:00	7	54.15966667	7.66716667	1.586	1.737	17:56:27	7	54.16923000	7.66268100	114	30min 33s	0
14.07.	18:35:59	4	54.15950000	7.66516667	2.762	3.013	17:56:37	5	54.16910000	7.66297100	114	39min 22s	1

## A.8 Oxygen saturation concentration



**Figure A.7** – Observed oxygen saturation concentration. (a) transect from Helgoland - Stonehaven (H - S). (b) transect from Stonehaven - Helgoland (S - H). Note the missing data in ECOHAM index 41 (0 - 25 m) from S - H.

## A.9 Oxygen saturation in percentage

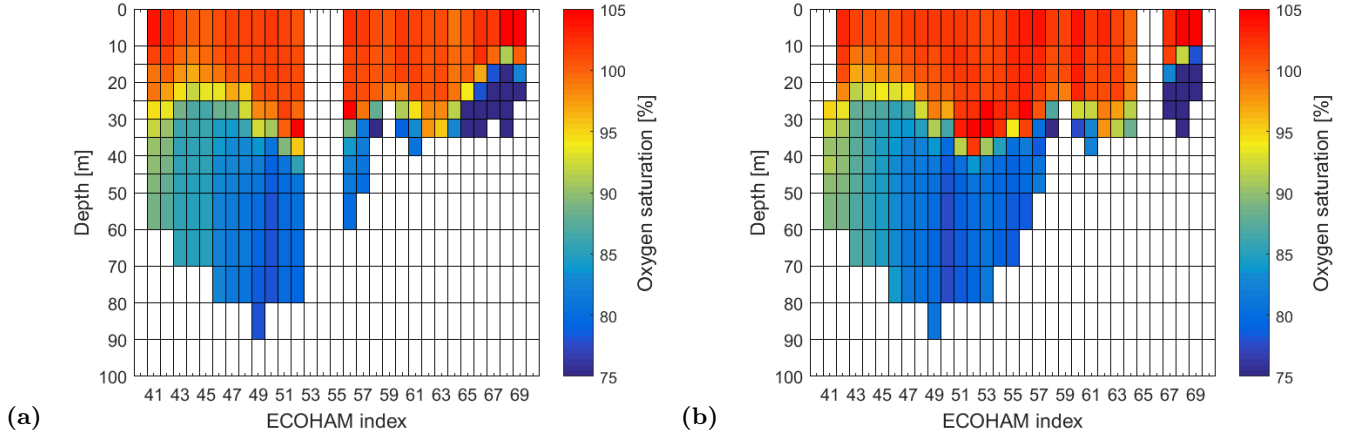


**Figure A.8** – Observed oxygen saturation in percentage. (a) transect from Helgoland - Stonehaven (H - S). Note the missing data in ECOHAM index 53 - 55. (b) transect from Stonehaven - Helgoland (S - H). Note the missing data in ECOHAM index 41 (0 - 25 m) and ECOHAM index 66 - 67.

## A.10 Expedition transect through ECOHAM-grid

Each ECOHAM-cell with their corresponding ECOHAM-coordinates has its assigned index number in longitude (x-direction) from 1 to 88 and in latitude (y-direction) from 1 to 82. The model exhibits a matrix resolution of 82 x 88 (see Figure A.9 in the appendix).

Using the coordinates of the observed transect through the ECOHAM-grid, the corresponding ECOHAM index can be obtained as follows:

$$ECOHAM\ index_{lon} = \left( \frac{Obs_{lon} - x_{first}}{x_{inc}} \right) + 1, \quad (A.1)$$

$$ECOHAM\ index_{lat} = \left( \frac{Obs_{lat} - y_{first}}{y_{inc}} \right) + 1,$$

with the starting coordinates of the model

$$\begin{aligned}
x_{first} &= -15.08333333 \\
x_{inc} &= 0.33333333 \\
y_{first} &= 47.68333333 \\
y_{inc} &= 0.2,
\end{aligned}
\tag{A.2}$$

where  $ECOHAM\ index_{lon}$  and  $ECOHAM\ index_{lat}$  are the index number in the model resolution. Whereas  $Obs_{lon}$  and  $Obs_{lat}$  are the coordinates of the observed transect, the  $x_{first}$  and  $y_{first}$  are the starting coordinates located in the northern hemisphere. The  $x_{inc}$  and  $y_{inc}$  are the increments in x-coordinate and in y-coordinate, respectively. All ECOHAM index with their corresponding indices of the expedition and moved transects are given in Table A.4 in the appendix.

Once the ECOHAM index is determined in the model resolution, the corresponding ECOHAM-coordinates can be easily computed by rearranging the equation (A.1) in the appendix and using the evaluated ECOHAM index yields

$$\begin{aligned}
ECOHAM_{lon} &= (ECOHAM\ index_{lon} - 1) x_{inc} + x_{first}, \\
ECOHAM_{lat} &= (ECOHAM\ index_{lat} - 1) y_{inc} + y_{first}.
\end{aligned}
\tag{A.3}$$

The calculated ECOHAM coordinates of the corresponding ECOHAM index is given in Table B.1 in the appendix. Note that negative (positive) values correspond to coordinates in the west (east).

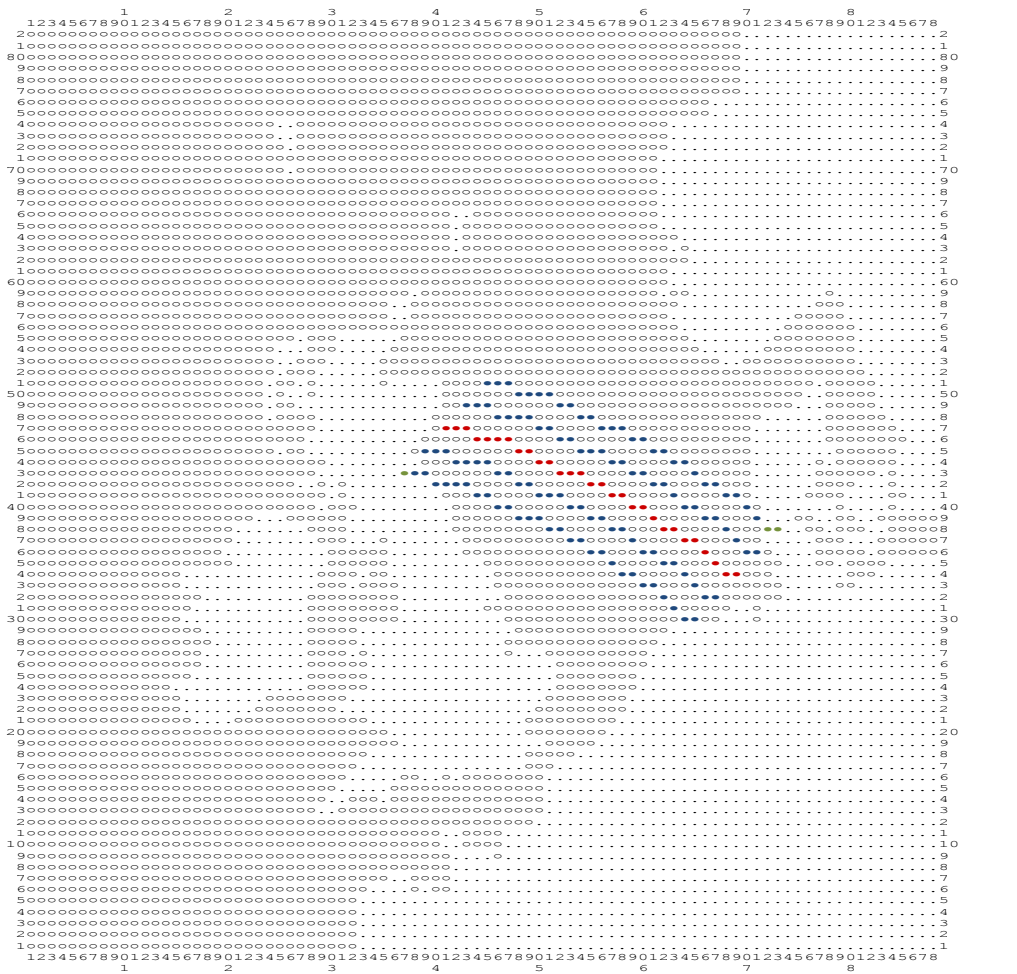


**Figure A.9** – ECOHAM-HAMSOM index map. X-axis:  $ECOHAM\ index_{lon}$ . Y-axis:  $ECOHAM\ index_{lat}$ . Red line: observed transect. Blue lines: shifted (60 and 120 km) transects towards NE and SW, respectively. Green dots: land mass. All ECOHAM index with their corresponding indices of the expedition and moved transects are given in the Table A.4 in the appendix.

**Table A.4** – ECOHAM index and their corresponding indices of the expedition and shifted transects in the model. The  $i$  index denotes the number in  $x$ -direction and  $j$  index in  $y$ -direction, respectively (see Fig. A.9 in the appendix). The ECOHAM coordinates of the correspondig ECOHAM index is given in Table B.1 in the appendix.

ECOHAM index	120 km SW $i,j$	60 km SW $i,j$	Expedition $i,j$	60 km NE $i,j$	120 km NE $i,j$
37	37,43				
38	38,43				
39	39,43	39,45			
40	40,42	40,45			
41	41,42	41,45	41,47		
42	42,42	42,44	42,47		
43	43,42	43,44	43,47	43,49	
44	44,41	44,44	44,46	44,49	
45	45,41	45,44	45,46	45,49	45,51
46	46,40	46,43	46,46	46,48	46,51
47	47,40	47,43	47,46	47,48	47,51
48	48,39	48,42	48,45	48,48	48,50
49	49,39	49,42	49,45	49,48	49,50
50	50,39	50,41	50,44	50,47	50,50
51	51,38	51,41	51,44	51,47	51,50
52	52,38	52,41	52,43	52,46	52,49
53	53,37	53,40	53,43	53,46	53,49
54	54,37	54,40	54,43	54,45	54,48
55	55,36	55,39	55,42	55,45	55,48
56	56,36	56,39	56,42	56,45	56,47
57	57,35	57,38	57,41	57,44	57,47
58	58,35	58,38	58,41	58,44	58,47
59	59,34	59,37	59,40	59,43	59,46
60	60,33	60,37	60,40	60,43	60,46
61	61,33	61,36	61,39	61,42	61,45
62	62,32	62,35	62,39	62,42	62,45
63	63,31	63,35	63,38	63,41	63,44
64	64,30	64,34	64,37	64,40	64,44
65	65,30	65,33	65,37	65,40	65,43
66		66,32	66,36	66,39	66,42
67		67,32	67,35	67,39	67,42
68			68,34	68,38	68,41
69			69,34	69,37	69,41
70				70,36	70,40
71				71,36	71,39
72					72,38
73					73,38

## A.11 Apparent Oxygen Utilisation

### A.11.1 Values of the AOU of the selected area in the transects

**Table A.5** – Calculated observed AOU concentration of the specified area from the transects Helgoland - Stonehaven and Stonehaven - Helgoland (see black thick line in Figures A.10a and b in the appendix) in the equation (2.12). Note that AOU values of ECOHAM index 53 - 54 does not exist from the transect Helgoland - Stonehaven due to absence of the meted oxygen (see Figure 3.4a). Blank: bottom topography.

Depth [m]	AOU [ $mmol\ O_2/m^3$ ]													
	Helgoland - Stonehaven						Stonehaven - Helgoland							
	ECOHAM index						ECOHAM index							
	47	48	49	50	51	52	47	48	49	50	51	52	53	54
40 - 45	50.3163	52.0203	53.7970	62.5705	56.5072	43.1586	53.7719	55.6009	55.8737	63.3629	57.7508	49.0333	54.6485	59.3089
45 - 50	52.6095	56.0146	56.3090	63.9527	59.1760	57.2616	54.5669	56.7119	58.3188	65.4837	61.9063	57.1783	56.1742	60.8706
50 - 60	54.2227	56.4810	59.2251	65.0704	59.3373	57.9171	55.5068	57.3158	59.7587	66.3920	62.8151	59.1978	56.5831	61.4449
60 - 70	55.2934	56.0576	61.3733	65.6403	59.6251	59.3362	56.1001	57.8227	60.4042	66.8563	63.4477	59.9161	56.5697	61.7014
70 - 80	55.7051	57.1734	63.4927	65.9367	60.3748	61.2462	55.2980	58.0160	60.1251	67.1443	63.5834	61.3671	55.2610	
80 - 90			65.5323						57.4517					

**Table A.6** – Deviation of the observed AOU concentration from the top layer (40 - 45 m) to the deepest layer in the specified area from the transects Helgoland - Stonehaven and Stonehaven - Helgoland (see black thick line in Figures A.10a and b in the appendix). AOU values of the top layer have been selected as the reference value (AOU values see Table A.5 in the appendix). Note that AOU values of ECOHAM index 53 - 54 does not exist from the transect Helgoland - Stonehaven due to the absence of the meted oxygen (see Figure 3.4a). Blank: bottom topography.

Depth [m]	Deviation [%]													
	Helgoland - Stonehaven						Stonehaven - Helgoland							
	ECOHAM index						ECOHAM index							
	47	48	49	50	51	52	47	48	49	50	51	52	53	54
40 - 45	0	0	0	0	0	0	0	0	0	0	0	0	0	0
45 - 50	4.56	7.68	4.67	2.21	4.72	32.68	1.48	2.01	4.38	3.35	7.2	16.61	2.79	2.63
50 - 60	7.76	8.57	10.09	3.91	5.01	34.2	3.23	3.08	6.95	4.78	8.77	20.73	3.54	3.6
60 - 70	9.89	7.76	14.08	4.91	5.52	37.48	4.33	4.0	8.11	5.51	9.86	22.19	3.52	4.03
70 - 80	10.71	9.91	18.02	5.38	6.84	41.91	2.84	4.34	7.61	5.97	10.1	25.19	1.12	
80 - 90			21.81						2.82					

### A.11.2 AOU concentrations in the observed transects

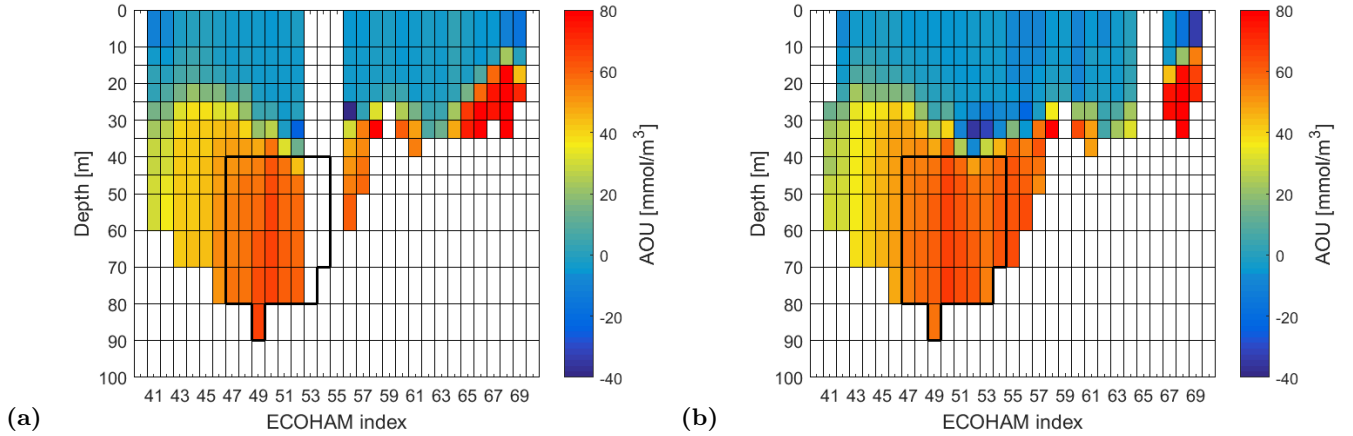


**Figure A.10** – Transects of the observed apparent oxygen utilization (AOU). (a) Helgoland - Stonehaven (H - S). (b) Stonehaven - Helgoland (S - H). Black thick line: defined area of the estimated nutrients. Note the missing data in ECOHAM index 53 - 55 from H - S and ECOHAM index 65 - 66 from S - H, respectively.

### A.12 Range of remineralisation and nitrification over the AOU in the selected cells

#### A.12.1 Remineralisation value: $R_0 = 151.5$

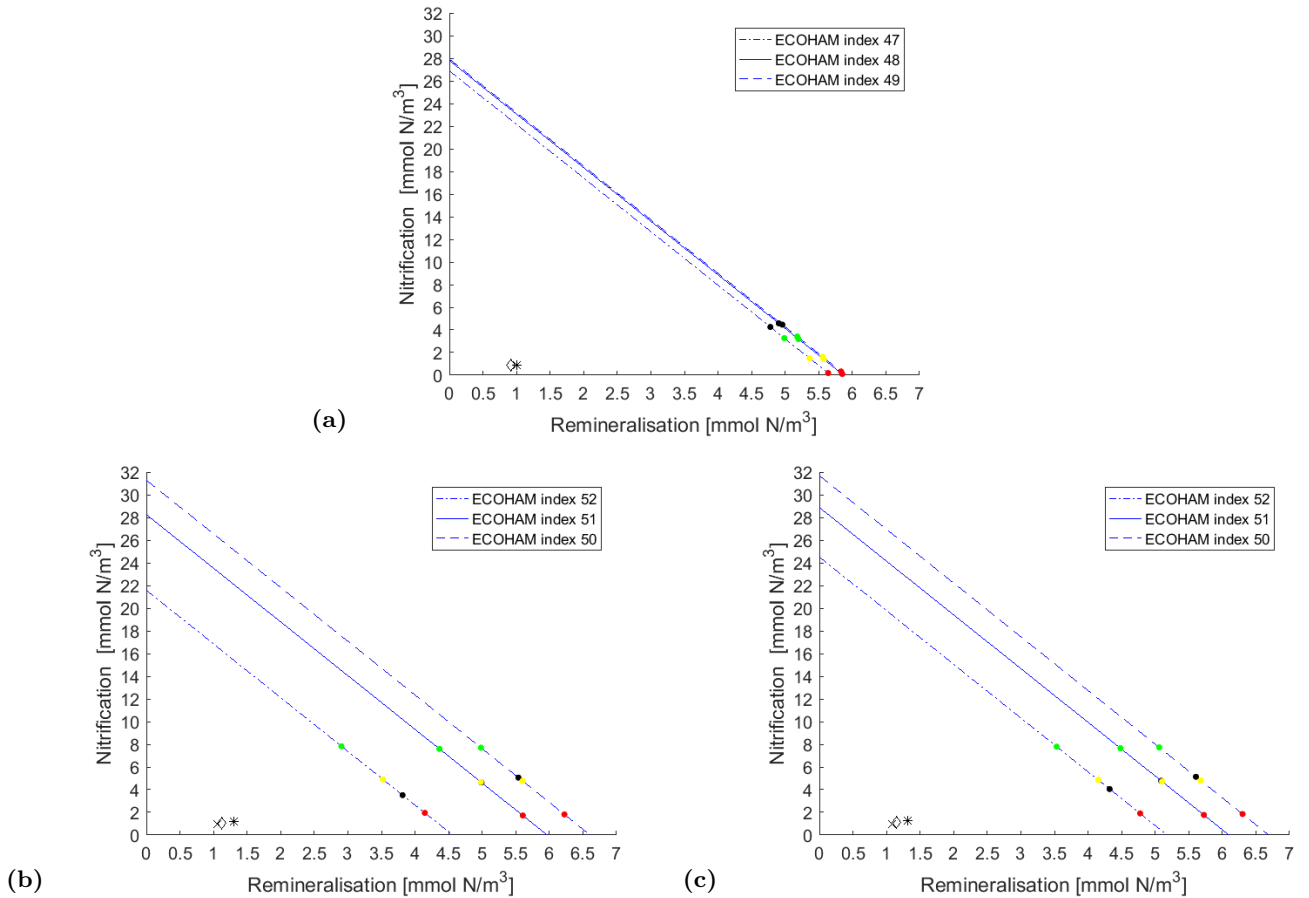


**Figure A.11** – Range of remineralisation and nitrification over the slope of the AOU in the selected cells of the top layer (40 - 45 m) from the specified areas (see Fig. A.10a and b in the appendix) with  $R_0 = 151.5$ . Maximum: green dots. Mean: yellow dots. Minimum: red dots. ECOHAM\*: black dots. Crosses (ECOHAM index 47 and 50), diamonds (ECOHAM index 48 and 51) and asterisks (ECOHAM index 49 and 52) are the simulated  $NH_3$  and  $HNO_3$  concentrations from the mass budget (see Table B.5 and B.6 in the appendix).  $R_0$ : remineralisation value (see the equation (2.13)). H - S: transect from Helgoland - Stonehaven. S - H: transect from Stonehaven - Helgoland. (a) ECOHAM index 47 - 49 from S - H. (b) ECOHAM index 50 - 52 from H - S. (c) ECOHAM index 50 - 52 from S - H. Note that ECOHAM index 53 - 54 from H - S does not exist due to missing AOU values.

### A.12.2 Remineralisation value: $R_0 = 140$

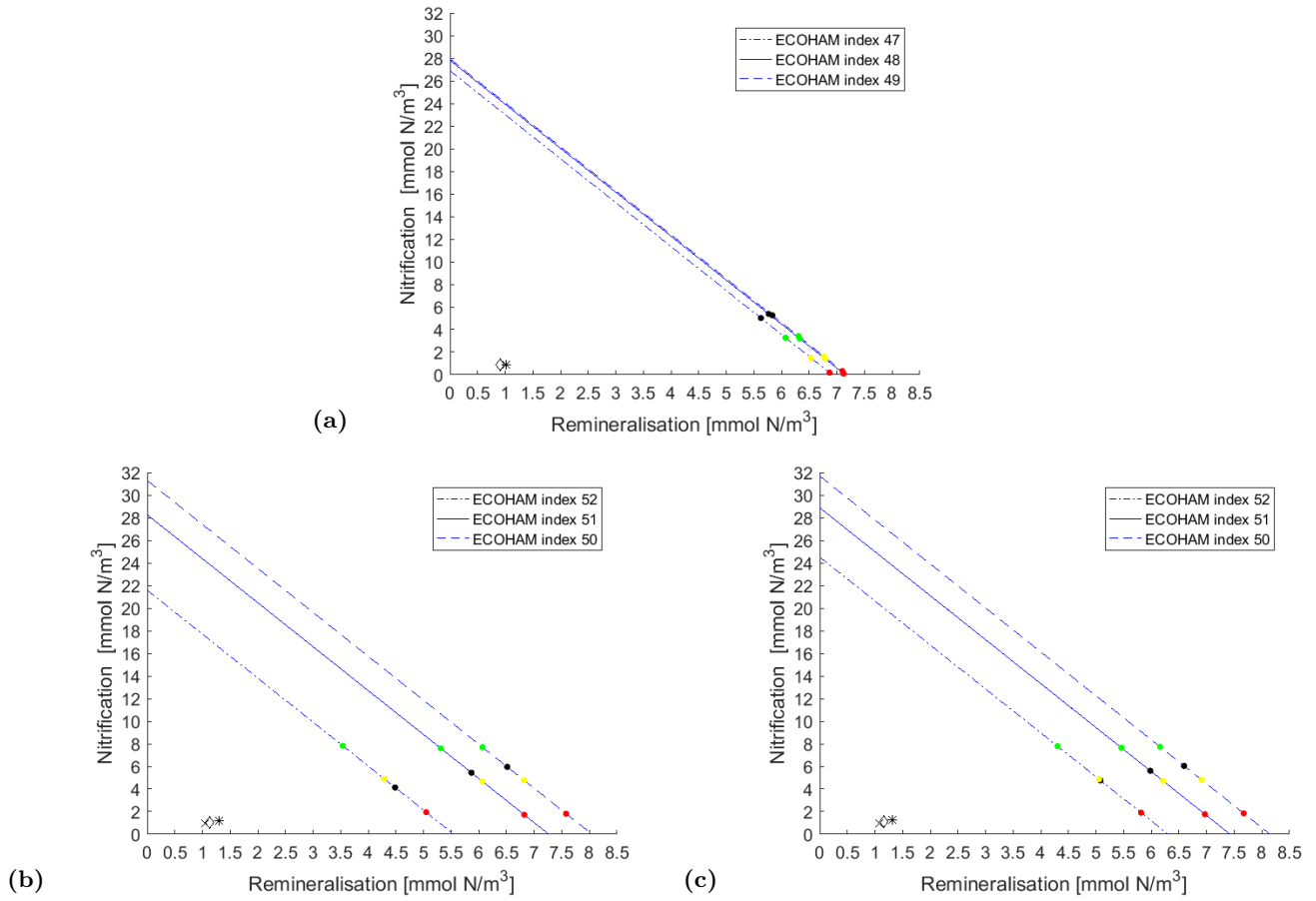


**Figure A.12** – Range of remineralisation and nitrification over the slope of the AOU in the selected cells of the top layer (40 - 45 m) from the specified areas (see Fig. A.10a and b in the appendix) with  $R_0 = 140$ . Maximum: green dots. Mean: yellow dots. Minimum: red dots. ECOHAM\*: black dots. Crosses (ECOHAM index 47 and 50), diamonds (ECOHAM index 48 and 51) and asterisks (ECOHAM index 49 and 52) are the simulated  $NH_3$  and  $HNO_3$  concentrations from the mass budget (see Table B.5 and B.6 in the appendix).  $R_0$ : remineralisation value (see the equation (2.13)). H - S: transect from Helgoland - Stonehaven. S - H: transect from Stonehaven - Helgoland. (a) ECOHAM index 47 - 49 from S - H. (b) ECOHAM index 50 - 52 from H - S. (c) ECOHAM index 50 - 52 from S - H. Note that ECOHAM index 53 - 54 from H - S does not exist due to missing AOU values.

### A.12.3 Remineralisation value: $R_0 = 138$

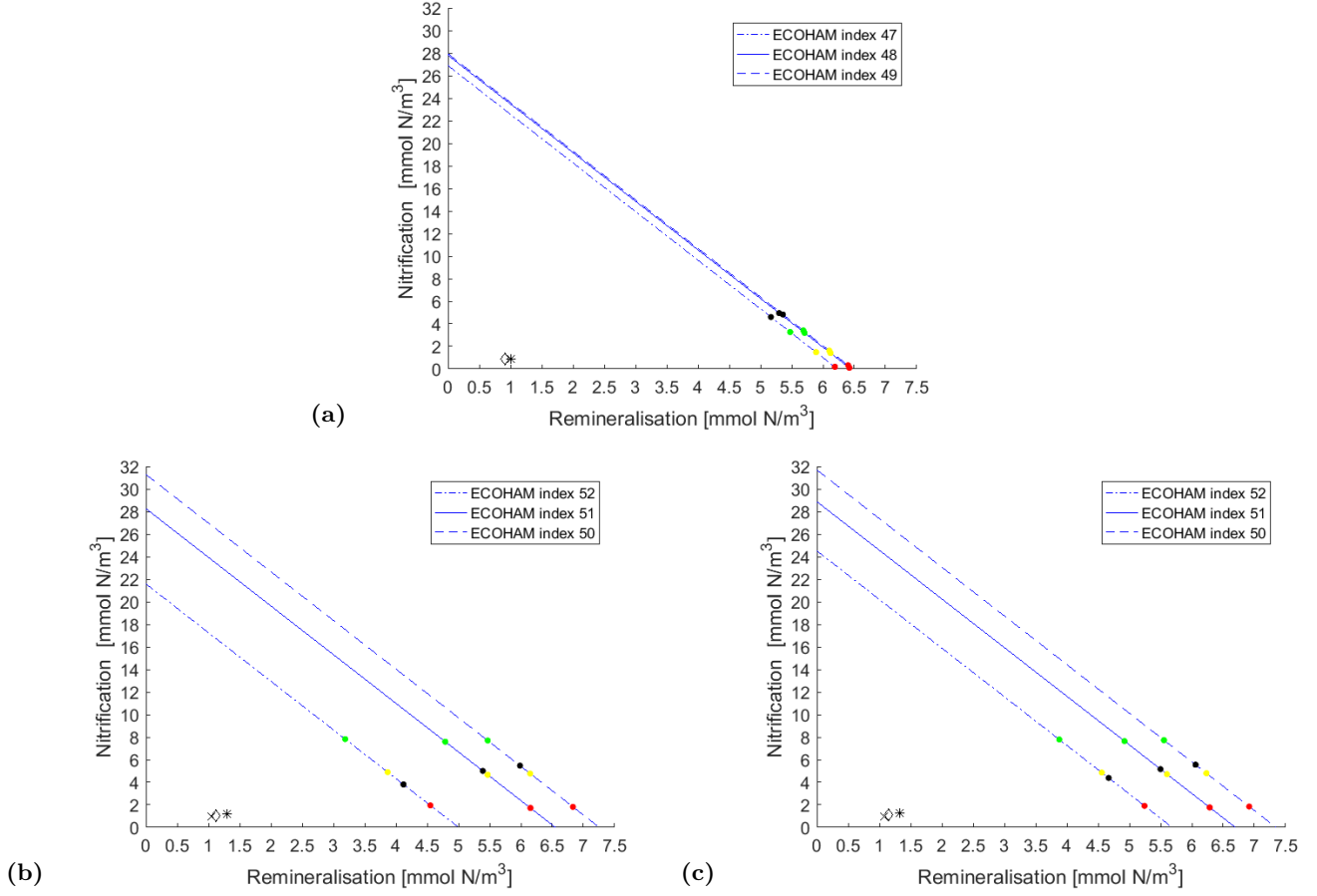


**Figure A.13** – Range of remineralisation and nitrification over the slope of the AOU in the selected cells of the top layer (40 - 45 m) from the specified areas (see Fig. A.10a and b in the appendix) with  $R_0 = 138$ . Maximum: green dots. Mean: yellow dots. Minimum: red dots. ECOHAM\*: black dots. Crosses (ECOHAM index 47 and 50), diamonds (ECOHAM index 48 and 51) and asterisks (ECOHAM index 49 and 52) are the simulated  $NH_3$  and  $HNO_3$  concentrations from the mass budget (see Table B.5 and B.6 in the appendix).  $R_0$ : remineralisation value (see the equation (2.13)). H - S: transect from Helgoland - Stonehaven. S - H: transect from Stonehaven - Helgoland. (a) ECOHAM index 47 - 49 from S - H. (b) ECOHAM index 50 - 52 from H - S. (c) ECOHAM index 50 - 52 from S - H. Note that ECOHAM index 53 - 54 from H - S does not exist due to missing AOU values.

### A.13 Conversion from particle into concentration units

During the expedition of HE 428 the LOPC device stored the counted particles into two different variables: particle counts per liter (cpl) determined as the unit [*individuals/l*] and number of particles per bin (npb). The bin size is determined by the size class of  $15 \mu m$ . Note that the LOPC device recorded in each sample 128 bins covers a size spectrum from  $15 \mu m$  -  $1920 \mu m$ .

Due to diverse of units between the simulated data,  $mmol C/m^3$ , and observed data (see above) from the parameter zooplankton, a conversion of the observed data is necessary to perform.

The abundance of the zooplankton for each bin can be derived as follows:

$$Abundance_{zoo,per\ bin} = \frac{cpl [individuals/l] npb}{\sum_{i=1}^{128} npb}, \quad (A.4)$$

where cpl is the counted individuals per liter and npb is the counted particles.

Utilising the factor 1000 with the units [ $l/m^3$ ] yields

$$Abundance_{zoo,per\ bin} = cpl [individuals/m^3] 1000. \quad (A.5)$$

The equivalent spherical diameter (ESD) for a bin is determined on a size class of  $15 \mu m$ . Considering that the shape of the zooplankton is approximately a spheroid and using the ratio of  $0.03 mg C/mm^3$  from Zhou et al. (2010), the weight of the zooplankton for a bin can be obtained as

$$\begin{aligned}
Weight_{zoo,per\ bin} &= \frac{4}{3} \pi \left( \frac{ESD}{2} \right)^3 0.03\ mg\ C/mm^3 \\
&= \frac{4}{3} \pi \left( \frac{15\ \mu m}{2} \right)^3 0.03\ mg\ C/mm^3 \\
&= \frac{4}{3} \pi \left( \frac{15\ 10^{-3}\ mm}{2} \right)^3 0.03\ mg\ C/mm^3 \tag{A.6} \\
&= \frac{4}{3} \pi \frac{15^3\ mm^3}{8\ 10^9} 0.03\ mg\ C/mm^3 \\
&= \frac{15^3}{6\ 10^9} \pi\ 0.03\ mg\ C.
\end{aligned}$$

Combining and multiplying the equations (A.5) and (A.6), the biomass of zooplankton per bin yields

$$\begin{aligned}
Biomass_{zoo,per\ bin} &= cpl\ [individuals/m^3]\ 1000\ \frac{15^3}{6\ 10^9} \pi\ 0.03\ mg\ C \\
&= cpl\ [individuals/m^3]\ \frac{15^3}{6\ 10^9} \pi\ 30\ mg\ C \tag{A.7} \\
&= cpl\ [individuals\ mg\ C/m^3]\ \frac{15^3}{2\ 10^8} \pi.
\end{aligned}$$

According to the first and second steps from section 2.10, a new size spectra (150  $\mu m$  - 1920  $\mu m$ ) has been divided into 20 classes and 4 of it (165  $\mu m$ , 258  $\mu m$ , 351  $\mu m$  and 444  $\mu m$ ) have been tested to identify the threshold between the parameters (microzooplankton and mesozooplankton).

Hence, the concentration of the microzooplankton and mesozooplankton can be derived as follows:

$$\begin{aligned}
Microzoo_{threshold} &= \frac{\sum_{i=1}^n Biomass_{zoo,per\ bin_i}\ mmol\ C/m^3}{12}, \tag{A.8} \\
Mesozoo_{threshold} &= \frac{\sum_{i=1}^n Biomass_{zoo,per\ bin_i}\ mmol\ C/m^3}{12},
\end{aligned}$$

where the factor 12 is the coefficient of the molar mass of carbon (12  $mg/mmol$ ) that converses the biomass into the carbon concentration unit. The  $Microzoo_{threshold}$  is the concentration of the microzooplankton which includes the bins in the size spectra from 150  $\mu m$  to the threshold, and the  $Mesozoo_{threshold}$  is the concentration of the mesozooplankton which includes the bins from the threshold to the end of the size spectra (1920  $\mu m$ ).

#### A.14 Confidence interval for Pearson's Correlation

Assuming a bivariate normal population, then the calculated correlation coefficient  $r$  from a sample is an estimation of the correlation coefficient  $\rho$  of the appertaining population.

According to Kreyszig (1970, 2011) and Storch and Zwiers (1999), the transformation from the correlation coefficient  $r$  to a z-value of the standard normal distribution is based on Fisher's z-transform,

$$z_r = \frac{1}{2} \ln \left( \frac{1+r}{1-r} \right), \tag{A.9}$$

which converges rapidly to the standard normal distribution when  $r$  is non zero. In case of  $r = 0$ , a null hypothesis t-test has to be applied (see below).

Using the variance  $1/(n - 3)$  (Fisher, 1921), the lower and upper confidence limits for  $\rho$  are performed by computing:

$$\begin{aligned} z_U &= z_r + Z_{1-\alpha/2} \sqrt{\frac{1}{n-3}} \\ z_L &= z_r - Z_{1-\alpha/2} \sqrt{\frac{1}{n-3}}, \end{aligned} \tag{A.10}$$

where  $z_U$  and  $z_L$  are the upper and lower confidence limits,  $n$  is the size of the sample and  $Z_{1-\alpha/2}$  is  $1 - \alpha/2$ -quantile of the standard normal distribution.

Two sided confidence interval of 95% and 99% has been selected from the standard normal distribution. The corresponding numerical  $Z_{1-\alpha/2}$  value for the two sided confidence interval of 95% and 99% are  $\pm 1.96$  and  $\pm 2.58$ , respectively, obtained from the Table in Appendix D of Storch and Zwiers (1999).

After that, the values of the confidence limit  $z_U$  and  $z_L$  have to be transformed back to the correlation scale by applying the inverse transformations:

$$\begin{aligned} r_U &= \tanh(z_U), \\ r_L &= \tanh(z_L), \end{aligned} \tag{A.11}$$

where  $r_U$  and  $r_L$  encompass the limits of the evaluated correlation coefficient  $r$  and in this way the confidence interval can be obtained as

$$r_L \leq r \leq r_U. \tag{A.12}$$

Tables A.7 and A.8 in the appendix show the upper and lower limits of the confidence interval of 95% and 99% for the physical and biological parameters from transects Helgoland to Stonehaven (H - S) and Stonehaven - Helgoland (S - H), whereas Tables A.11 and A.12 in the appendix show the upper and lower limits of the confidence interval of 95% and 99% for the other size classes of microzooplankton and mesozooplankton (see sections 2.10.1 and 3.1) from tracks H - S and S - H.

As mentioned above, a null hypothesis t-test ( $H_0: r = 0$ ) has to be performed against the alternative hypothesis of  $r > 0$  or  $r < 0$  for all parameters in space and time.

Following Kreyszig (1970, 2011) and Storch and Zwiers (1999), the null hypothesis test can be derived by computing

$$z_0 = r \sqrt{\frac{n-2}{1-r^2}}, \tag{A.13}$$

where  $z_0$  corresponds to a random value from the t distribution with  $n - 2$  degrees of freedom and  $r$  is the correlation coefficient. Due to the fact that the size of the sample from the transects include more than  $n = 30$ , the t distribution converges to the z-values of the standard normal distribution (Storch and Zwiers, 1999). As a consequence of the converge, the critical z-value ( $z_{crit}$ ) for the two sided significant level of  $\alpha = 5\%$  is  $\pm 1.96$  and for  $\alpha = 1\%$  is  $\pm 2.58$ , respectively, which are identical to the z-values of the two sided  $1 - \alpha/2$ -quantile from the standard normal distribution.

The null hypothesis will be rejected if  $z_0 \leq -z_{crit}$  or  $z_0 \geq z_{crit}$  ( $r$  is significant), and accepted if  $-z_{crit} < z_0 < z_{crit}$  ( $r$  is not significant). Tables A.9 and A.10 in the appendix show the calculated  $z_0$  values and, additionally, the p-values for the physical and the biological parameters, whereas Table A.15 and A.16 in the appendix show the calculated  $z_0$  values and p-values for the other size classes of microzooplankton and mesozooplankton from the transects H - S and S - H. Note that the p-values have been evaluated between  $z_0 = 0$  to  $z_0 = \pm 3.5$  from the standard normal distribution (Table downloaded from <http://www.analysis-schmeisser.uni-jena.de/matia2media/Baaske/Schaden/tabelle.pdf>).

## A.15 Statistic of the transects in space and time

**Table A.7** – Confidence interval of 95% and 99% from the standard normal distribution of the physical and biological parameters from the transect Helgoland - Stonehaven. WB: Week before the expedition. WA: Week after the expedition. Distance 60 and 120 are in km.  $r_U$ : upper range.  $r_L$ : lower range. Note that the threshold of the class size 258  $\mu\text{m}$  has been taken between the parameters microzooplankton and mesozooplankton (see sections 2.10.1 and 3.1).

	Helgoland - Stonehaven																							
	physical parameter												biological parameter											
	Temperature				Salinity				Oxygen				Phytoplankton				Microzooplankton				Mesozooplankton			
	95%		99%		95%		99%		95%		99%		95%		99%		95%		99%		95%		99%	
$r_U$	$r_L$	$r_U$	$r_L$	$r_U$	$r_L$	$r_U$	$r_L$	$r_U$	$r_L$	$r_U$	$r_L$	$r_U$	$r_L$	$r_U$	$r_L$	$r_U$	$r_L$	$r_U$	$r_L$	$r_U$	$r_L$	$r_U$	$r_L$	
2014	0.90	0.85	0.91	0.84	0.91	0.86	0.92	0.86	0.12	-0.11	0.16	-0.15	0.49	0.30	0.51	0.27	0.21	0.0	0.24	-0.04	0.44	0.25	0.47	0.22
2013	0.89	0.84	0.90	0.83	0.88	0.82	0.89	0.81	0.04	-0.19	0.08	-0.22	0.60	0.45	0.63	0.42	0.23	0.01	0.26	-0.02	0.51	0.33	0.54	0.30
2012	0.89	0.83	0.90	0.82	0.92	0.88	0.93	0.88	0.28	0.05	0.31	0.01	0.59	0.43	0.62	0.41	0.23	0.02	0.26	-0.02	0.51	0.33	0.53	0.30
2011	0.90	0.85	0.91	0.84	0.92	0.88	0.93	0.87	0.20	-0.03	0.23	-0.07	0.56	0.39	0.58	0.37	0.23	0.01	0.26	-0.02	0.49	0.31	0.52	0.28
2010	0.92	0.88	0.93	0.88	0.79	0.69	0.80	0.68	-0.12	-0.34	-0.08	-0.37	0.52	0.34	0.55	0.31	0.18	-0.04	0.21	-0.07	0.48	0.30	0.51	0.27
2009	0.93	0.89	0.93	0.88	0.92	0.88	0.93	0.88	-0.10	-0.33	-0.07	-0.36	0.51	0.34	0.54	0.30	0.25	0.03	0.28	0.0	0.46	0.28	0.49	0.24
2008	0.90	0.86	0.91	0.85	0.93	0.89	0.93	0.88	0.24	0.01	0.27	-0.03	0.60	0.44	0.62	0.41	0.24	0.02	0.27	-0.01	0.50	0.33	0.53	0.29
2007	0.91	0.87	0.92	0.86	0.94	0.90	0.94	0.90	0.20	-0.04	0.23	-0.07	0.61	0.45	0.63	0.43	0.27	0.05	0.30	0.02	0.48	0.30	0.51	0.27
2006	0.89	0.84	0.90	0.83	0.94	0.90	0.94	0.90	0.01	-0.22	0.05	-0.26	0.53	0.36	0.56	0.33	0.21	-0.01	0.24	-0.04	0.44	0.25	0.47	0.22
2005	0.89	0.83	0.89	0.82	0.94	0.91	0.94	0.90	0.19	-0.04	0.23	-0.08	0.52	0.35	0.55	0.32	0.21	0.0	0.25	-0.03	0.44	0.25	0.47	0.22
2004	0.91	0.87	0.92	0.86	0.92	0.88	0.92	0.87	0.19	-0.04	0.23	-0.08	0.60	0.41	0.61	0.44	0.27	0.06	0.30	0.03	0.51	0.34	0.54	0.31
2003	0.91	0.86	0.91	0.85	0.91	0.88	0.92	0.86	0.03	-0.20	0.07	-0.24	0.59	0.43	0.61	0.40	0.25	0.03	0.28	0.0	0.52	0.34	0.54	0.31
2002	0.91	0.86	0.91	0.85	0.93	0.89	0.93	0.89	0.37	0.15	0.40	0.12	0.62	0.47	0.64	0.44	0.24	0.03	0.28	0.0	0.52	0.34	0.54	0.31
2001	0.90	0.85	0.90	0.84	0.83	0.76	0.84	0.74	-0.01	-0.24	0.03	-0.27	0.55	0.38	0.57	0.35	0.19	-0.02	0.22	-0.06	0.50	0.32	0.53	0.29
2 WB	0.91	0.87	0.92	0.86	0.92	0.89	0.93	0.88	0.18	-0.06	0.21	-0.09	0.52	0.34	0.54	0.31	0.18	-0.04	0.21	-0.07	0.43	0.23	0.45	0.20
1 WB	0.91	0.86	0.91	0.85	0.89	0.83	0.90	0.82	0.07	-0.16	0.11	-0.20	0.55	0.38	0.57	0.35	0.18	-0.03	0.22	-0.07	0.44	0.25	0.47	0.22
1 WA	0.90	0.85	0.91	0.84	0.92	0.87	0.92	0.87	0.12	-0.12	0.15	-0.15	0.53	0.35	0.55	0.32	0.20	-0.02	0.23	-0.05	0.45	0.26	0.47	0.23
2 WA	0.90	0.84	0.90	0.83	0.93	0.89	0.93	0.89	0.25	0.02	0.29	-0.01	0.50	0.32	0.52	0.29	0.17	-0.04	0.21	-0.08	0.44	0.26	0.46	0.21
120 NE	0.89	0.84	0.90	0.83	0.14	-0.09	0.18	-0.12	0.02	-0.22	0.06	-0.26	0.31	0.09	0.34	0.05	-0.18	-0.39	-0.14	-0.42	0.29	0.07	0.32	0.03
60 NE	0.90	0.85	0.91	0.84	0.46	0.27	0.49	0.24	0.02	-0.22	0.06	-0.26	0.41	0.20	0.44	0.17	0.0	-0.22	0.04	-0.25	0.53	0.35	0.55	0.32
60 SW	0.91	0.86	0.91	0.85	0.94	0.90	0.94	0.89	0.19	-0.06	0.22	-0.08	0.48	0.29	0.51	0.25	0.31	0.09	0.35	0.06	0.50	0.30	0.52	0.27
120 SW	0.91	0.86	0.92	0.85	0.90	0.85	0.91	0.83	0.26	0.0	0.30	-0.04	0.51	0.31	0.54	0.27	0.30	0.07	0.34	0.03	0.52	0.33	0.55	0.29

**Table A.8** – Confidence interval of 95% and 99% from the standard normal distribution of the physical and biological parameters from the transect Stonehaven - Helgoland. WB: Week before the expedition. WA: Week after the expedition. Distance 60 and 120 are in km.  $r_U$ : upper range.  $r_L$ : lower range. Note that the threshold of the class size 258  $\mu m$  has been taken between the parameters microzooplankton and mesozooplankton (see sections 2.10.1 and 3.1).

	Stonehaven - Helgoland																							
	physical parameter												biological parameter											
	Temperature				Salinity				Oxygen				Phytoplankton				Microzooplankton				Mesozooplankton			
	95%		99%		95%		99%		95%		99%		95%		99%		95%		99%		95%		99%	
$r_U$	$r_L$	$r_U$	$r_L$	$r_U$	$r_L$	$r_U$	$r_L$	$r_U$	$r_L$	$r_U$	$r_L$	$r_U$	$r_L$	$r_U$	$r_L$	$r_U$	$r_L$	$r_U$	$r_L$	$r_U$	$r_L$	$r_U$	$r_L$	
2014	0.91	0.87	0.92	0.86	0.92	0.87	0.92	0.87	0.11	-0.11	0.15	-0.15	0.49	0.30	0.52	0.27	0.15	-0.07	0.18	-0.10	0.37	0.16	0.40	0.13
2013	0.91	0.86	0.91	0.85	0.87	0.81	0.88	0.80	0.09	-0.14	0.12	-0.17	0.53	0.35	0.55	0.32	0.16	-0.07	0.19	-0.09	0.45	0.26	0.48	0.23
2012	0.90	0.84	0.90	0.83	0.92	0.88	0.92	0.87	0.28	0.03	0.28	-0.01	0.54	0.36	0.56	0.33	0.18	-0.04	0.21	-0.07	0.45	0.26	0.48	0.23
2011	0.91	0.87	0.92	0.86	0.92	0.88	0.93	0.87	0.16	-0.06	0.19	-0.10	0.53	0.35	0.56	0.32	0.17	-0.05	0.21	-0.08	0.42	0.22	0.44	0.19
2010	0.93	0.90	0.94	0.89	0.79	0.69	0.80	0.67	-0.13	-0.34	-0.10	-0.37	0.46	0.26	0.48	0.23	0.12	-0.10	0.15	-0.13	0.40	0.20	0.43	0.17
2009	0.94	0.90	0.94	0.89	0.92	0.88	0.93	0.88	-0.09	-0.31	-0.07	-0.34	0.52	0.33	0.54	0.30	0.20	-0.02	0.23	-0.05	0.41	0.21	0.43	0.17
2008	0.91	0.86	0.92	0.85	0.92	0.88	0.93	0.88	0.18	-0.05	0.21	-0.08	0.57	0.40	0.59	0.37	0.18	-0.04	0.21	-0.08	0.45	0.26	0.48	0.22
2007	0.92	0.87	0.92	0.87	0.93	0.90	0.94	0.89	0.16	-0.06	0.20	-0.10	0.61	0.44	0.63	0.42	0.21	-0.01	0.24	-0.04	0.44	0.25	0.47	0.21
2006	0.91	0.86	0.91	0.85	0.95	0.92	0.95	0.91	-0.01	-0.23	0.03	-0.26	0.48	0.29	0.51	0.26	0.17	-0.05	0.20	-0.09	0.38	0.18	0.41	0.14
2005	0.90	0.85	0.91	0.84	0.94	0.91	0.94	0.90	0.17	-0.05	0.20	-0.09	0.47	0.28	0.50	0.25	0.16	-0.06	0.19	-0.09	0.36	0.16	0.39	0.12
2004	0.92	0.88	0.93	0.88	0.91	0.86	0.91	0.85	0.12	-0.10	0.15	-0.14	0.57	0.41	0.60	0.38	0.22	0.0	0.25	-0.03	0.47	0.28	0.49	0.25
2003	0.92	0.87	0.92	0.86	0.91	0.87	0.92	0.86	0.05	-0.18	0.08	-0.21	0.54	0.37	0.57	0.34	0.19	-0.03	0.23	-0.06	0.45	0.26	0.48	0.23
2002	0.92	0.87	0.92	0.86	0.93	0.89	0.93	0.88	0.31	0.08	0.34	0.06	0.60	0.43	0.62	0.40	0.17	-0.05	0.20	-0.09	0.47	0.28	0.49	0.25
2001	0.91	0.86	0.91	0.85	0.83	0.75	0.84	0.74	0.08	-0.14	0.12	-0.17	0.54	0.36	0.57	0.33	0.21	-0.01	0.24	-0.04	0.47	0.29	0.50	0.26
2 WB	0.91	0.87	0.92	0.86	0.92	0.87	0.92	0.87	0.12	-0.10	0.15	-0.14	0.47	0.27	0.49	0.27	0.12	-0.10	0.15	-0.14	0.35	0.14	0.38	0.11
1 WB	0.92	0.87	0.92	0.86	0.92	0.88	0.93	0.87	0.06	-0.16	0.10	-0.19	0.48	0.29	0.51	0.26	0.15	-0.07	0.19	-0.10	0.37	0.17	0.40	0.13
1 WA	0.91	0.87	0.92	0.86	0.93	0.89	0.93	0.88	0.09	-0.13	0.13	-0.17	0.46	0.27	0.49	0.23	0.14	-0.08	0.18	-0.11	0.36	0.16	0.39	0.13
2 WA	0.91	0.86	0.91	0.85	0.93	0.89	0.93	0.88	0.21	-0.01	0.24	-0.05	0.46	0.27	0.49	0.23	0.11	-0.11	0.14	-0.14	0.35	0.15	0.38	0.11
120 NE	0.91	0.86	0.91	0.85	0.14	-0.10	0.17	-0.13	0.11	-0.13	0.14	-0.17	0.30	0.08	0.34	0.04	-0.32	-0.51	-0.29	-0.54	0.15	-0.08	0.19	-0.11
60 NE	0.91	0.86	0.92	0.86	0.48	0.29	0.51	0.26	0.06	-0.16	0.10	-0.20	0.44	0.23	0.47	0.20	-0.05	-0.27	-0.01	-0.30	0.37	0.16	0.40	0.12
60 SW	0.91	0.87	0.92	0.86	0.93	0.90	0.94	0.89	0.12	-0.12	0.15	-0.16	0.45	0.26	0.49	0.23	0.25	0.03	0.29	-0.01	0.46	0.26	0.49	0.23
120 SW	0.92	0.87	0.92	0.86	0.90	0.84	0.91	0.83	0.21	-0.04	0.24	-0.09	0.44	0.22	0.47	0.18	0.22	-0.02	0.25	-0.06	0.48	0.27	0.50	0.23

**Table A.9** – Slope, intercept, z-values and probability values of the physical and biological parameters from the transect Helgoland - Stonehaven. a: slope. b: intercept.  $z_0$ : calculated z-value from the equation (A.13) with the correlation coefficient from  $r_2$  (see Table 3.1). Critical z-value of the two sided significant level  $\alpha$  for 5% and 1% from the t distribution is  $z_{crit,5\%} = \pm 1.96$  and  $z_{crit,1\%} = \pm 2.58$ , respectively. p: probability value is in [%]. Note that the z-values between  $z_0=0$  to  $z_0 = \pm 3.5$  have been selected to obtain the p-values. <: p-value is less than 0.04% ( $z_0 > 3.5$  or  $z_0 < -3.5$ ). WB: Week before the expedition. WA: Week after the expedition. Distance 60 and 120 are in km. Note that the threshold of the class size  $258 \mu m$  has been taken between the parameters microzooplankton and mesozooplankton (see sections 2.10.1 and 3.1).

	Helgoland - Stonehaven																							
	physical parameter												biological parameter											
	Temperature				Salinity				Oxygen				Phytoplankton				Microzooplankton				Mesozooplankton			
	a	b	$z_0$	p	a	b	$z_0$	p	a	b	$z_0$	p	a	b	$z_0$	p	a	b	$z_0$	p	a	b	$z_0$	p
2014	0.86	1.97	33.44	<	0.46	18.75	35.02	<	0.01	244.91	0.09	92.82	0.46	0.33	7.85	<	0.01	0.25	1.89	5.88	0.88	0.63	6.78	<
2013	0.90	2.87	31.87	<	0.30	24.39	29.29	<	-0.23	313.59	-1.20	23.03	0.58	0.18	11.26	<	0.01	0.24	2.19	2.86	0.91	0.35	8.50	<
2012	1.01	0.92	30.90	<	0.52	16.49	38.42	<	0.55	98.44	2.79	0.52	0.59	0.21	10.91	<	0.02	0.23	2.31	2.14	1.06	0.35	8.38	<
2011	0.86	2.41	33.20	<	0.40	20.78	37.51	<	0.17	202.30	1.40	16.16	0.47	0.29	9.78	<	0.01	0.24	2.21	2.72	0.85	0.51	7.99	<
2010	0.92	1.96	38.55	<	0.25	26.08	20.23	<	-0.61	414.87	-3.97	<	0.44	0.30	8.74	<	0.01	0.25	1.32	18.68	0.80	0.61	7.74	<
2009	0.87	2.00	39.23	<	0.42	20.13	38.44	<	-0.43	362.21	-3.73	<	0.45	0.31	8.53	<	0.02	0.23	2.58	0.98	0.91	0.68	7.26	<
2008	0.90	1.75	33.77	<	0.45	19.05	39.86	<	0.29	167.71	2.06	3.94	0.56	0.23	11	<	0.02	0.24	2.38	1.74	0.99	0.42	8.30	<
2007	0.90	1.26	35.77	<	0.46	18.64	42.52	<	0.21	191.26	1.35	17.7	0.50	0.23	11.44	<	0.02	0.23	2.94	0.32	0.96	0.48	7.79	<
2006	0.84	2.79	31.68	<	0.50	17.16	42.46	<	-0.20	302.98	-1.81	7.02	0.51	0.31	9.05	<	0.01	0.25	1.83	6.72	0.91	0.59	6.71	<
2005	0.88	2.35	30.42	<	0.51	17.04	43.75	<	0.16	204.12	1.32	18.68	0.54	0.30	8.76	<	0.01	0.24	1.95	5.12	0.84	0.59	6.71	<
2004	1.02	0.51	35.54	<	0.47	18.45	37.26	<	0.23	185.42	1.26	20.76	0.54	0.24	11.10	<	0.02	0.22	3.08	0.20	0.98	0.39	8.57	<
2003	0.82	2.35	33.97	<	0.36	22.31	35.87	<	-0.20	301.02	-1.44	14.98	0.50	0.26	10.72	<	0.02	0.23	2.57	1.02	0.87	0.45	8.63	<
2002	0.94	1.36	34.35	<	0.37	21.96	40.14	<	0.70	57.94	4.58	<	0.51	0.22	11.83	<	0.02	0.24	2.51	1.20	0.94	0.42	8.70	<
2001	0.86	2.67	32.41	<	0.33	23.36	23.36	<	-0.29	328.42	-2.08	3.76	0.47	0.28	9.48	<	0.01	0.25	1.52	12.86	0.73	0.50	8.24	<
2 WB	0.98	1.16	35.73	<	0.44	19.52	36.53	<	0.02	243.76	0.14	88.86	0.67	0.24	7.07	<	0.0	0.31	0.13	89.66	0.56	1.09	4.64	<
1 WB	0.94	1.34	36.07	<	0.45	18.92	37.30	<	-0.10	274.93	-0.86	38.44	0.62	0.22	7.36	<	0.01	0.30	0.78	43.54	0.64	1.01	5.01	<
1 WA	0.82	2.22	35.31	<	0.47	18.38	39.53	<	-0.03	257.51	-0.36	71.88	0.57	0.27	6.91	<	0.01	0.30	0.60	54.86	0.68	1.03	4.92	<
2 WA	0.75	2.83	34.23	<	0.47	18.36	38.91	<	0.16	205.28	1.76	7.84	0.56	0.30	6.87	<	0.0	0.31	0.02	98.40	0.66	1.08	4.62	<
120 NE	0.83	2.50	31.62	<	0.0	34.65	0.37	71.14	-0.01	254.78	-0.18	85.72	0.29	0.38	3.24	0.12	-0.04	0.36	-7.76	<	0.08	1.44	0.65	51.56
60 NE	0.83	2.49	33.61	<	0.11	30.88	7.34	<	-0.08	271.71	-0.86	38.98	0.55	0.30	6.14	<	-0.02	0.33	-2.80	0.52	0.44	1.14	4.85	<
60 SW	0.92	1.22	33.61	<	0.50	17.21	38.99	<	-0.01	251.14	-0.05	96.02	0.59	0.20	6.54	<	0.02	0.23	2.45	1.42	0.89	0.49	6.69	<
120 SW	0.89	1.46	32.67	<	0.52	16.93	29.15	<	0.15	209.81	1.33	18.36	0.54	0.17	5.59	<	0.01	0.23	1.61	10.74	0.91	0.26	6.57	<

**Table A.10** – Slope, intercept, z-values and probability values of the physical and biological parameters from the transect Stonehaven - Helgoland. a: slope. b: intercept.  $z_0$ : calculated z-value from the equation (A.13) with the correlation coefficient from  $r_2$  (see Table 3.1). Critical z-value of the two sided significant level  $\alpha$  for 5% and 1% from the t distribution is  $z_{crit,5\%} = \pm 1.96$  and  $z_{crit,1\%} = \pm 2.58$ , respectively. p: probability value is in [%]. Note that the z-values between  $z_0=0$  to  $z_0 = \pm 3.5$  have been selected to obtain the p-values. <: p-value is less than 0.04% ( $z_0 > 3.5$  or  $z_0 < -3.5$ ). WB: Week before the expedition. WA: Week after the expedition. Distance 60 and 120 are in km. Note that the threshold of the class size  $258 \mu m$  has been taken between the parameters microzooplankton and mesozooplankton (see sections 2.10.1 and 3.1).

	Stonehaven - Helgoland																							
	physical parameter												biological parameter											
	Temperature				Salinity				Oxygen				Phytoplankton				Microzooplankton				Mesozooplankton			
	a	b	$z_0$	p	a	b	$z_0$	p	a	b	$z_0$	p	a	b	$z_0$	p	a	b	$z_0$	p	a	b	$z_0$	p
2014	0.87	1.88	35.19	<	0.45	19.05	36.51	<	0.0	248.78	-0.02	98.40	0.66	0.24	7.65	<	0.01	0.30	0.71	47.78	0.65	1.03	4.94	<
2013	0.92	2.69	33.66	<	0.28	25.17	28.12	<	-0.08	270.79	-0.46	64.56	0.70	0.15	8.66	<	0.01	0.29	0.95	34.22	0.72	0.75	6.91	<
2012	1.04	0.73	31.91	<	0.48	17.85	36.93	<	0.42	133.62	2.48	1.32	0.71	0.16	8.94	<	0.01	0.29	1.26	20.76	0.87	0.72	6.87	<
2011	0.90	2.06	35.54	<	0.38	21.52	37.85	<	0.09	224.93	0.83	40.66	0.65	0.18	8.71	<	0.01	0.29	1.15	25.02	0.65	0.91	6.05	<
2010	0.95	1.69	40.59	<	0.24	26.41	16.67	<	-0.70	440.96	-4.29	<	0.51	0.28	6.79	<	0.0	0.31	0.21	83.36	0.62	0.99	5.72	<
2009	0.90	1.65	41.87	<	0.39	21.11	38.14	<	-0.44	365.74	-3.64	<	0.60	0.20	8.33	<	0.02	0.28	1.66	9.70	0.74	0.88	5.81	<
2008	0.93	1.59	34.53	<	0.42	19.99	38.29	<	0.15	208.49	1.14	25.42	0.72	0.15	9.73	<	0.01	0.29	1.23	21.86	0.82	0.77	6.81	<
2007	0.93	0.99	36.51	<	0.44	19.49	41.29	<	0.14	212.19	0.91	36.28	0.67	0.12	10.91	<	0.01	0.28	1.80	7.18	0.79	0.79	6.57	<
2006	0.87	2.53	34.16	<	0.48	18.08	46.16	<	-0.22	309.43	-2.14	3.24	0.62	0.27	7.40	<	0.01	0.29	1.05	29.38	0.68	0.97	5.24	<
2005	0.89	2.21	32.91	<	0.48	17.86	43.20	<	0.12	215.05	1.01	31.24	0.61	0.29	7.17	<	0.01	0.29	0.89	37.34	0.61	1.03	4.86	<
2004	1.07	-0.15	38.22	<	0.43	19.87	34.44	<	0.02	242.01	0.13	89.66	0.68	0.13	9.94	<	0.02	0.27	1.98	4.78	0.81	0.71	7.27	<
2003	0.85	2.05	35.89	<	0.34	22.80	35.51	<	-0.15	288.74	-1.15	25.02	0.62	0.20	9.03	<	0.01	0.28	1.51	13.10	0.68	0.83	6.94	<
2002	0.96	1.18	36.05	<	0.35	22.37	39.75	<	0.54	101.47	3.69	<	0.69	0.11	10.62	<	0.01	0.29	1.05	29.38	0.78	0.76	7.24	<
2001	0.95	1.97	34.03	<	0.30	24.20	23.50	<	-0.07	268.18	-0.50	61.70	0.54	0.17	8.97	<	0.01	0.28	1.79	7.34	0.69	0.72	7.45	<
2 WB	0.96	1.25	35.35	<	0.45	18.90	38.80	<	0.14	209.95	1.04	29.84	0.52	0.30	8.59	<	0.01	0.26	1.27	20.40	0.77	0.70	6.36	<
1 WB	0.90	1.68	34.51	<	0.43	19.67	30.96	<	0.09	272.14	-0.78	43.54	0.57	0.25	9.54	<	0.01	0.25	1.39	16.46	0.82	0.65	6.66	<
1 WA	0.78	2.59	32.87	<	0.47	18.42	36.58	<	0.0	248.13	-0.02	97.20	0.50	0.31	8.88	<	0.01	0.60	1.69	9.10	0.92	0.61	6.86	<
2 WA	0.72	3.07	32.16	<	0.49	17.69	40.29	<	0.22	189.76	2.37	1.78	0.49	0.34	8.15	<	0.01	0.26	1.21	22.62	0.92	0.66	6.61	<
120 NE	0.82	2.62	29.57	<	0.01	34.61	0.47	63.84	0.13	287.44	-1.60	10.96	0.25	0.44	3.50	0.04	-0.03	0.30	-5.07	<	0.35	0.99	3.13	0.18
60 NE	0.81	2.61	31.77	<	0.11	31.02	7.0	<	-0.15	290.97	-1.65	9.90	0.35	0.40	5.56	<	-0.01	0.28	-1.89	5.88	0.77	0.62	8.76	<
60 SW	0.91	1.24	32.43	<	0.53	16.29	40.44	<	0.12	215.54	1.03	30.30	0.39	0.28	7.2	<	0.03	0.19	3.62	<	1.06	0.21	7.55	<
120 SW	0.88	1.55	31.07	<	0.54	16.03	29.49	<	0.25	182.26	2.04	4.14	0.41	0.19	7.36	<	0.02	0.17	3.16	0.16	1.15	-0.12	7.73	<

## A.16 Microzooplankton and Mesozooplankton of other size classes

### A.16.1 Expedition transects

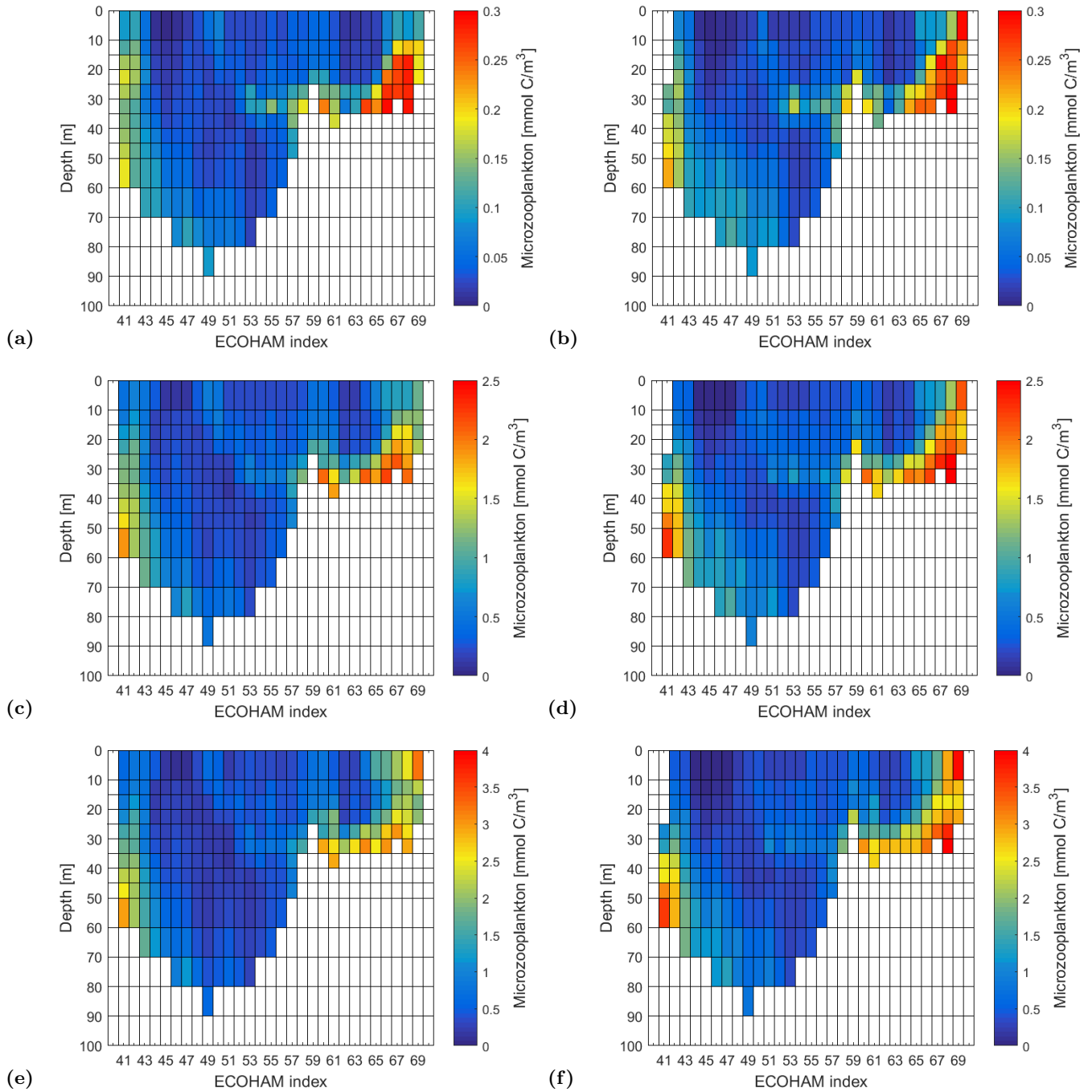


**Figure A.14** – Transects of the other size classes from the observed microzooplankton. Left: Helgoland - Stonehaven. Right: Stonehaven - Helgoland. (a) and (b) 165  $\mu\text{m}$ . (c) and (d) 351  $\mu\text{m}$ . (e) and (f) 444  $\mu\text{m}$ . Note the different scale between observed and simulated data and the observed missing data in ECOHAM index 41 (0 - 25 m) from Stonehaven - Helgoland.

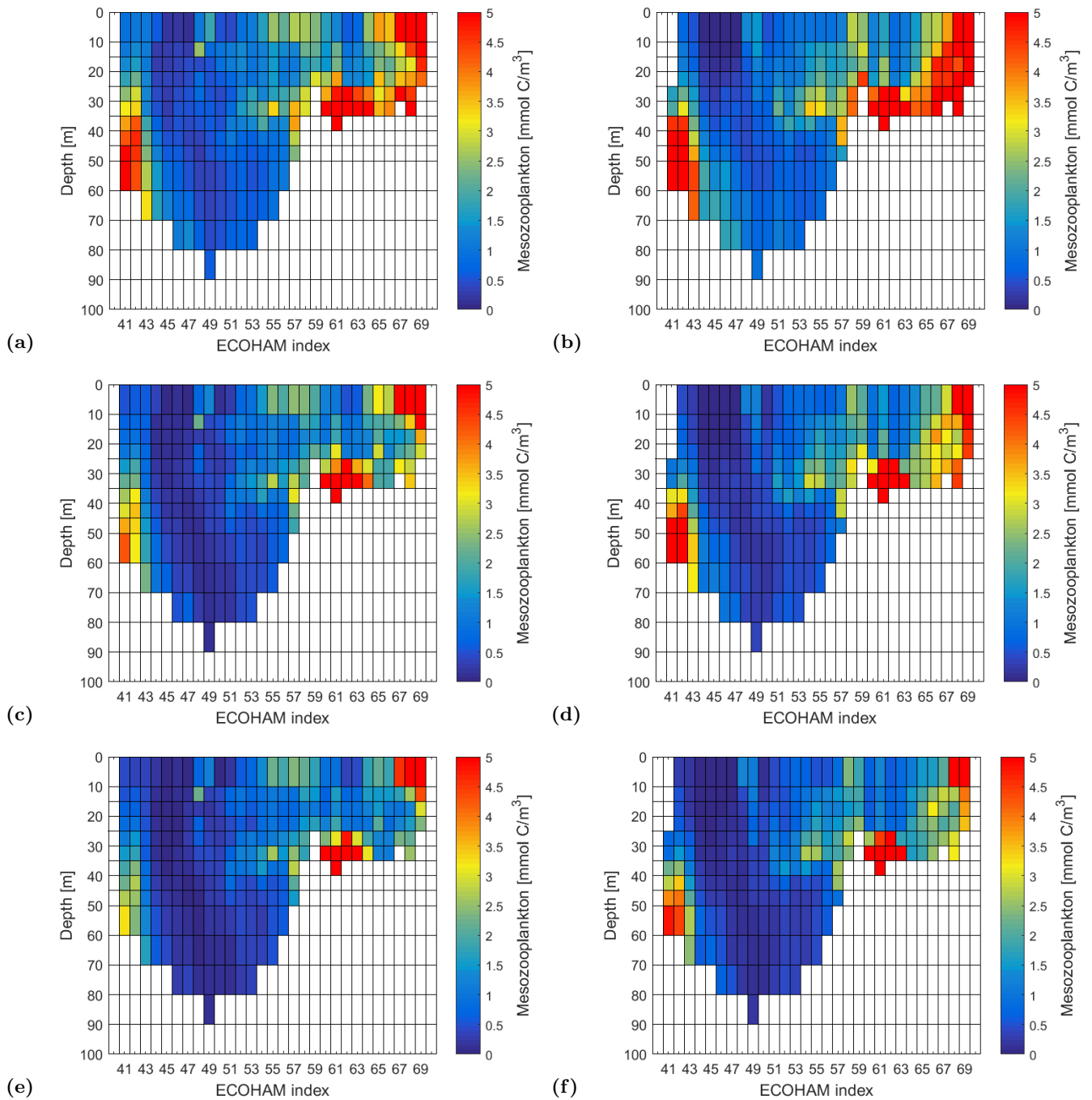


**Figure A.15** – Transects of the other size classes from the observed mesozooplankton. Left: Helgoland - Stonehaven. Right: Stonehaven - Helgoland. (a) and (b) 165  $\mu\text{m}$ . (c) and (d) 351  $\mu\text{m}$ . (e) and (f) 444  $\mu\text{m}$ . Note the missing data in ECOHAM index 41 (0 - 25 m) from Stonehaven - Helgoland.

## A.16.2 Statistic in space and time

**Table A.11** – Confidence interval of 95% and 99% from the standard normal distribution of the microzooplankton and mesozooplankton size classes 165  $\mu m$ , 351  $\mu m$  and 444  $\mu m$  (see sections 2.10.1 and 3.1) from the transect Helgoland - Stonehaven. WB: Week before the expedition. WA: Week after the expedition. Distance 60 and 120 are in km.  $r_U$ : upper range.  $r_L$ : lower range.

	Helgoland - Stonehaven																							
	Microzooplankton												Mesozooplankton											
	165 $\mu m$				351 $\mu m$				444 $\mu m$				165 $\mu m$				351 $\mu m$				444 $\mu m$			
	95%		99%		95%		99%		95%		99%		95%		99%		95%		99%		95%		99%	
$r_U$	$r_L$	$r_U$	$r_L$	$r_U$	$r_L$	$r_U$	$r_L$	$r_U$	$r_L$	$r_U$	$r_L$	$r_U$	$r_L$	$r_U$	$r_L$	$r_U$	$r_L$	$r_U$	$r_L$	$r_U$	$r_L$	$r_U$	$r_L$	
2014	0.26	0.05	0.29	0.02	0.24	0.03	0.28	0.0	0.31	0.11	0.35	0.07	0.45	0.26	0.47	0.22	0.44	0.25	0.47	0.21	0.41	0.22	0.44	0.19
2013	0.27	0.06	0.03	0.03	0.26	0.05	0.29	0.02	0.34	0.13	0.37	0.10	0.51	0.34	0.54	0.31	0.50	0.33	0.53	0.29	0.48	0.30	0.51	0.26
2012	0.27	0.06	0.30	0.03	0.27	0.06	0.30	0.03	0.35	0.14	0.37	0.11	0.51	0.33	0.53	0.30	0.50	0.32	0.53	0.29	0.48	0.29	0.50	0.26
2011	0.27	0.06	0.30	0.03	0.26	0.05	0.29	0.02	0.34	0.13	0.37	0.10	0.50	0.31	0.52	0.28	0.48	0.30	0.51	0.27	0.46	0.27	0.48	0.24
2010	0.23	0.02	0.26	-0.02	0.21	-0.01	0.24	-0.04	0.27	0.06	0.30	0.03	0.49	0.30	0.51	0.27	0.47	0.29	0.50	0.26	0.45	0.26	0.47	0.22
2009	0.30	0.10	0.33	0.06	0.27	0.06	0.30	0.03	0.34	0.13	0.37	0.10	0.47	0.28	0.49	0.25	0.46	0.27	0.48	0.24	0.43	0.24	0.46	0.21
2008	0.28	0.07	0.31	0.03	0.27	0.06	0.30	0.03	0.34	0.14	0.37	0.10	0.51	0.33	0.53	0.30	0.50	0.32	0.52	0.28	0.47	0.28	0.50	0.25
2007	0.31	0.10	0.34	0.07	0.30	0.09	0.33	0.06	0.37	0.17	0.40	0.14	0.49	0.31	0.51	0.27	0.48	0.29	0.50	0.26	0.45	0.26	0.48	0.23
2006	0.26	0.05	0.29	0.01	0.24	0.02	0.27	-0.01	0.30	0.10	0.34	0.06	0.44	0.25	0.47	0.22	0.44	0.24	0.46	0.21	0.41	0.22	0.44	0.19
2005	0.27	0.05	0.30	0.02	0.25	0.03	0.29	0.0	0.32	0.11	0.35	0.08	0.44	0.25	0.47	0.22	0.44	0.24	0.46	0.21	0.41	0.22	0.44	0.19
2004	0.32	0.11	0.35	0.07	0.31	0.10	0.34	0.07	0.35	0.08	0.41	0.15	0.52	0.34	0.54	0.31	0.50	0.32	0.53	0.29	0.48	0.29	0.50	0.26
2003	0.29	0.08	0.33	0.05	0.28	0.07	0.31	0.04	0.35	0.15	0.38	0.12	0.52	0.34	0.55	0.31	0.51	0.33	0.53	0.30	0.48	0.29	0.50	0.26
2002	0.28	0.07	0.31	0.04	0.28	0.07	0.31	0.04	0.35	0.15	0.38	0.11	0.52	0.35	0.55	0.32	0.51	0.33	0.53	0.30	0.48	0.30	0.51	0.27
2001	0.24	0.02	0.27	-0.01	0.23	0.02	0.26	-0.02	0.31	0.10	0.34	0.06	0.50	0.32	0.53	0.29	0.50	0.31	0.52	0.28	0.47	0.28	0.50	0.25
2 WB	0.23	0.02	0.26	-0.02	0.21	-0.01	0.24	-0.04	0.28	0.07	0.31	0.03	0.43	0.23	0.45	0.20	0.42	0.23	0.45	0.19	0.40	0.20	0.43	0.17
1 WB	0.24	0.02	0.27	-0.01	0.22	0.0	0.25	-0.03	0.29	0.08	0.32	0.04	0.44	0.25	0.47	0.22	0.43	0.24	0.46	0.21	0.41	0.22	0.44	0.18
1 WA	0.25	0.04	0.28	0.0	0.24	0.02	0.27	-0.01	0.31	0.10	0.34	0.07	0.45	0.26	0.48	0.23	0.44	0.25	0.47	0.22	0.42	0.22	0.44	0.19
2 WA	0.25	0.01	0.26	-0.02	0.21	-0.01	0.24	-0.04	0.29	0.08	0.32	0.04	0.44	0.25	0.46	0.21	0.43	0.24	0.46	0.21	0.41	0.21	0.43	0.18
120 NE	-0.36	-0.14	-0.39	-0.11	-0.10	-0.32	-0.07	-0.35	0.02	-0.21	0.05	-0.25	0.27	0.04	0.30	0.01	0.31	0.09	0.34	0.05	0.30	0.08	0.33	0.04
60 NE	0.06	-0.16	0.10	-0.19	0.07	-0.16	0.10	-0.19	0.19	-0.03	0.22	-0.07	0.52	0.34	0.55	0.31	0.54	0.36	0.56	0.33	0.51	0.33	0.54	0.30
60 SW	0.36	0.14	0.37	0.11	0.36	0.15	0.39	0.11	0.44	0.24	0.47	0.20	0.50	0.31	0.53	0.28	0.48	0.29	0.51	0.25	0.45	0.25	0.48	0.22
120 SW	0.34	0.11	0.37	0.07	0.36	0.14	0.40	0.10	0.45	0.23	0.48	0.20	0.53	0.33	0.57	0.30	0.51	0.31	0.54	0.28	0.48	0.28	0.51	0.24

**Table A.12** – Confidence interval of 95% and 99% from the standard normal distribution of the microzooplankton and mesozooplankton size classes 165  $\mu m$ , 351  $\mu m$  and 444  $\mu m$  (see sections 2.10.1 and 3.1) from the transect Stonehaven - Helgoland. WB: Week before the expedition. WA: Week after the expedition. Distance 60 and 120 are in km.  $r_U$ : upper range.  $r_L$ : lower range.

	Stonehaven - Helgoland																							
	Microzooplankton												Mesozooplankton											
	165 $\mu m$				351 $\mu m$				444 $\mu m$				165 $\mu m$				351 $\mu m$				444 $\mu m$			
	95%		99%		95%		99%		95%		99%		95%		99%		95%		99%		95%		99%	
$r_U$	$r_L$	$r_U$	$r_L$	$r_U$	$r_L$	$r_U$	$r_L$	$r_U$	$r_L$	$r_U$	$r_L$	$r_U$	$r_L$	$r_U$	$r_L$	$r_U$	$r_L$	$r_U$	$r_L$	$r_U$	$r_L$	$r_U$	$r_L$	
2014	0.19	-0.03	0.22	-0.06	0.17	-0.05	0.20	-0.08	0.22	0.0	0.25	-0.03	0.37	0.16	0.40	0.13	0.36	0.16	0.39	0.12	0.34	0.13	0.37	0.09
2013	0.20	-0.02	0.23	-0.05	0.18	-0.04	0.22	-0.07	0.23	0.02	0.26	-0.02	0.45	0.26	0.48	0.23	0.45	0.26	0.47	0.22	0.42	0.23	0.45	0.19
2012	0.21	-0.01	0.24	-0.04	0.20	-0.01	0.24	-0.05	0.26	0.04	0.29	0.01	0.45	0.26	0.48	0.23	0.45	0.25	0.47	0.22	0.42	0.23	0.45	0.19
2011	0.21	-0.01	0.24	-0.04	0.19	-0.02	0.23	-0.06	0.24	0.03	0.28	-0.01	0.42	0.22	0.45	0.19	0.41	0.21	0.44	0.18	0.38	0.18	0.41	0.14
2010	0.16	-0.06	0.20	-0.09	0.14	-0.08	0.17	-0.12	0.18	-0.04	0.21	-0.08	0.41	0.21	0.44	0.18	0.39	0.19	0.42	0.16	0.36	0.15	0.39	0.12
2009	0.24	0.03	0.27	-0.01	0.22	0.0	0.25	-0.03	0.27	0.05	0.30	0.02	0.41	0.21	0.44	0.18	0.40	0.20	0.43	0.17	0.38	0.17	0.40	0.14
2008	0.21	0.03	0.24	-0.04	0.20	-0.02	0.23	-0.05	0.25	0.04	0.28	0.0	0.45	0.26	0.48	0.23	0.44	0.25	0.47	0.22	0.42	0.22	0.45	0.19
2007	0.24	0.02	0.27	-0.01	0.23	0.02	0.27	-0.02	0.29	0.07	0.32	0.04	0.44	0.25	0.47	0.22	0.43	0.24	0.46	0.21	0.41	0.21	0.44	0.18
2006	0.21	0.0	0.25	-0.04	0.18	-0.03	0.22	-0.07	0.23	0.01	0.26	-0.02	0.38	0.18	0.41	0.14	0.38	0.17	0.40	0.14	0.35	0.15	0.38	0.11
2005	0.20	-0.01	0.24	-0.05	0.18	-0.04	0.21	-0.08	0.22	0.01	0.25	-0.03	0.36	0.16	0.39	0.13	0.36	0.15	0.39	0.12	0.33	0.13	0.36	0.09
2004	0.25	0.03	0.28	0.0	0.24	0.03	0.27	-0.01	0.30	0.08	0.33	0.05	0.47	0.28	0.50	0.25	0.46	0.27	0.49	0.24	0.43	0.23	0.46	0.20
2003	0.25	0.02	0.27	-0.02	0.21	-0.01	0.23	-0.06	0.26	0.04	0.29	0.01	0.46	0.27	0.49	0.24	0.44	0.25	0.47	0.22	0.41	0.21	0.44	0.18
2002	0.20	-0.02	0.23	-0.05	0.19	-0.03	0.22	-0.06	0.24	0.03	0.28	-0.01	0.47	0.28	0.49	0.25	0.46	0.27	0.49	0.24	0.44	0.24	0.46	0.21
2001	0.24	0.02	0.27	-0.01	0.23	0.02	0.26	-0.02	0.28	0.07	0.31	0.04	0.48	0.29	0.50	0.26	0.47	0.28	0.49	0.25	0.44	0.25	0.47	0.22
2 WB	0.16	-0.06	0.19	-0.10	0.14	-0.08	0.17	-0.12	0.18	-0.03	0.22	-0.07	0.35	0.15	0.38	0.11	0.35	0.14	0.38	0.11	0.32	0.12	0.35	0.09
1 WB	0.19	-0.02	0.23	-0.06	0.17	-0.05	0.20	-0.08	0.22	0.0	0.25	-0.03	0.37	0.17	0.40	0.13	0.36	0.16	0.39	0.13	0.34	0.13	0.37	0.10
1 WA	0.19	-0.03	0.22	-0.07	0.16	-0.06	0.20	-0.09	0.21	-0.01	0.24	-0.04	0.37	0.16	0.40	0.13	0.36	0.15	0.39	0.12	0.33	0.13	0.37	0.09
2 WA	0.15	-0.07	0.19	-0.10	0.13	-0.09	0.16	-0.12	0.17	-0.04	0.21	-0.07	0.35	0.15	0.38	0.11	0.35	0.14	0.38	0.11	0.32	0.11	0.35	0.08
120 NE	-0.30	-0.50	-0.27	-0.52	-0.25	-0.45	-0.21	-0.48	-0.16	-0.37	-0.12	-0.41	0.13	-0.11	0.16	-0.14	0.18	-0.05	0.22	-0.09	0.19	-0.04	0.23	-0.08
60 NE	0.01	-0.21	0.05	-0.25	-0.01	-0.23	0.03	-0.27	0.07	-0.15	0.11	-0.19	0.37	0.16	0.40	0.12	0.37	0.16	0.40	0.13	0.34	0.12	0.37	0.09
60 SW	0.30	0.07	0.33	0.04	0.28	0.06	0.32	0.02	0.34	0.12	0.37	0.08	0.47	0.27	0.50	0.24	0.45	0.25	0.48	0.21	0.42	0.21	0.45	0.17
120 SW	0.26	0.02	0.29	-0.02	0.26	0.02	0.29	-0.02	0.32	0.09	0.35	0.05	0.48	0.27	0.51	0.23	0.47	0.26	0.50	0.22	0.44	0.22	0.47	0.19

**Table A.13** – Correlation coefficients and t-test significance level  $\alpha$  of the microzooplankton and mesozooplankton size classes 165  $\mu\text{m}$ , 351  $\mu\text{m}$  and 444  $\mu\text{m}$  (see sections 2.10.1 and 3.1) from the transect Helgoland - Stonehaven.  $r_1$ : correlation coefficient calculated only with simulated data itself.  $r_2$ : correlation coefficient calculated with observational data and simulated data.  $\alpha_{5\%}$ : significance level of 5%.  $\alpha_{1\%}$ : significance level of 1%. Blank: not significant. Note that the significance levels have been tested on  $r_2$ . WB: Week before the expedition. WA: Week after the expedition. Distance 60 and 120 are in km.

	Helgoland - Stonehaven																							
	Microzooplankton												Mesozooplankton											
	165 $\mu\text{m}$				351 $\mu\text{m}$				444 $\mu\text{m}$				165 $\mu\text{m}$				351 $\mu\text{m}$				444 $\mu\text{m}$			
	$r_1$	$r_2$	$\alpha_{5\%}$	$\alpha_{1\%}$	$r_1$	$r_2$	$\alpha_{5\%}$	$\alpha_{1\%}$	$r_1$	$r_2$	$\alpha_{5\%}$	$\alpha_{1\%}$	$r_1$	$r_2$	$\alpha_{5\%}$	$\alpha_{1\%}$	$r_1$	$r_2$	$\alpha_{5\%}$	$\alpha_{1\%}$	$r_1$	$r_2$	$\alpha_{5\%}$	$\alpha_{1\%}$
2014	1.0	0.16	✓	✓	1.0	0.14	✓		1.0	0.21	✓	✓	1.0	0.35	✓	✓	1.0	0.35	✓	✓	1.0	0.32	✓	✓
2013	0.97	0.17	✓	✓	0.97	0.16	✓	✓	0.97	0.24	✓	✓	0.98	0.43	✓	✓	0.98	0.42	✓	✓	0.98	0.39	✓	✓
2012	0.97	0.17	✓	✓	0.97	0.17	✓	✓	0.97	0.25	✓	✓	0.97	0.42	✓	✓	0.97	0.41	✓	✓	0.97	0.39	✓	✓
2011	0.98	0.17	✓	✓	0.98	0.16	✓	✓	0.98	0.24	✓	✓	0.98	0.41	✓	✓	0.98	0.40	✓	✓	0.98	0.37	✓	✓
2010	0.97	0.12	✓		0.97	0.10			0.97	0.17	✓	✓	0.95	0.40	✓	✓	0.95	0.39	✓	✓	0.95	0.35	✓	✓
2009	0.98	0.20	✓	✓	0.98	0.17	✓	✓	0.98	0.24	✓	✓	0.98	0.38	✓	✓	0.98	0.37	✓	✓	0.98	0.34	✓	✓
2008	0.97	0.17	✓	✓	0.97	0.17	✓	✓	0.97	0.24	✓	✓	0.98	0.42	✓	✓	0.98	0.41	✓	✓	0.98	0.38	✓	✓
2007	0.98	0.21	✓	✓	0.98	0.20	✓	✓	0.98	0.28	✓	✓	0.98	0.40	✓	✓	0.98	0.39	✓	✓	0.98	0.36	✓	✓
2006	0.99	0.15	✓	✓	0.99	0.13	✓		0.99	0.20	✓	✓	0.99	0.35	✓	✓	0.99	0.34	✓	✓	0.99	0.32	✓	✓
2005	0.98	0.16	✓	✓	0.98	0.14	✓		0.98	0.22	✓	✓	0.98	0.35	✓	✓	0.98	0.34	✓	✓	0.98	0.32	✓	✓
2004	0.97	0.21	✓	✓	0.97	0.21	✓	✓	0.97	0.28	✓	✓	0.97	0.44	✓	✓	0.97	0.42	✓	✓	0.97	0.39	✓	✓
2003	0.98	0.19	✓	✓	0.98	0.18	✓	✓	0.98	0.26	✓	✓	0.98	0.44	✓	✓	0.98	0.42	✓	✓	0.98	0.39	✓	✓
2002	0.96	0.18	✓	✓	0.96	0.18	✓	✓	0.96	0.25	✓	✓	0.95	0.44	✓	✓	0.95	0.42	✓	✓	0.95	0.39	✓	✓
2001	0.97	0.13	✓		0.97	0.12	✓		0.97	0.20	✓	✓	0.98	0.42	✓	✓	0.98	0.41	✓	✓	0.98	0.38	✓	✓
2 WB	0.98	0.13	✓		0.98	0.10			0.98	0.18	✓	✓	0.99	0.33	✓	✓	0.99	0.33	✓	✓	0.99	0.30	✓	✓
1 WB	0.99	0.13	✓		0.99	0.11	✓		0.99	0.19	✓	✓	0.99	0.35	✓	✓	0.99	0.34	✓	✓	0.99	0.32	✓	✓
1 WA	1.0	0.15	✓	✓	1.0	0.13	✓		1.0	0.21	✓	✓	1.0	0.36	✓	✓	1.0	0.35	✓	✓	1.0	0.32	✓	✓
2 WA	0.99	0.12	✓		0.99	0.10			0.99	0.18	✓	✓	0.99	0.35	✓	✓	0.99	0.34	✓	✓	0.99	0.31	✓	✓
120 NE	0.96	-0.26	✓	✓	0.96	-0.21	✓	✓	0.96	-0.10			0.97	0.16	✓	✓	0.97	0.20	✓	✓	0.97	0.19	✓	✓
60 NE	0.91	-0.05			0.91	-0.05			0.91	0.08			0.99	0.44	✓	✓	0.99	0.45	✓	✓	0.99	0.42	✓	✓
60 SW	0.96	0.25	✓	✓	0.96	0.26	✓	✓	0.96	0.34	✓	✓	0.96	0.41	✓	✓	0.96	0.39	✓	✓	0.96	0.35	✓	✓
120 SW	0.94	0.23	✓	✓	0.94	0.25	✓	✓	0.94	0.34	✓	✓	0.93	0.44	✓	✓	0.93	0.42	✓	✓	0.93	0.38	✓	✓

**Table A.14** – Correlation coefficients and t-test significance level  $\alpha$  of the microzooplankton and mesozooplankton size classes 165  $\mu m$ , 351  $\mu m$  and 444  $\mu m$  (see sections 2.10.1 and 3.1) from the transect Stonehaven - Helgoland.  $r_1$ : correlation coefficient calculated only with simulated data itself.  $r_2$ : correlation coefficient calculated with observational data and simulated data.  $\alpha_{5\%}$ : significance level of 5%.  $\alpha_{1\%}$ : significance level of 1%. Blank: not significant. Note that the significance levels have been tested on  $r_2$ . WB: Week before the expedition. WA: Week after the expedition. Distance 60 and 120 are in km.

	Stonehaven - Helgoland																							
	Microzooplankton												Mesozooplankton											
	165 $\mu m$				351 $\mu m$				444 $\mu m$				165 $\mu m$				351 $\mu m$				444 $\mu m$			
	$r_1$	$r_2$	$\alpha_{5\%}$	$\alpha_{1\%}$	$r_1$	$r_2$	$\alpha_{5\%}$	$\alpha_{1\%}$	$r_1$	$r_2$	$\alpha_{5\%}$	$\alpha_{1\%}$	$r_1$	$r_2$	$\alpha_{5\%}$	$\alpha_{1\%}$	$r_1$	$r_2$	$\alpha_{5\%}$	$\alpha_{1\%}$	$r_1$	$r_2$	$\alpha_{5\%}$	$\alpha_{1\%}$
2014	1.0	0.08			1.0	0.06			1.0	0.11	✓		1.0	0.27	✓	✓	1.0	0.26	✓	✓	1.0	0.23	✓	✓
2013	0.97	0.09			0.97	0.07			0.97	0.13	✓		0.98	0.36	✓	✓	0.98	0.36	✓	✓	0.98	0.33	✓	✓
2012	0.97	0.10			0.97	0.10			0.97	0.15	✓	✓	0.97	0.36	✓	✓	0.97	0.35	✓	✓	0.97	0.33	✓	✓
2011	0.98	0.10			0.98	0.07			0.98	0.14	✓		0.98	0.33	✓	✓	0.98	0.31	✓	✓	0.98	0.28	✓	✓
2010	0.97	0.05			0.97	0.03			0.97	0.07			0.96	0.31	✓	✓	0.96	0.29	✓	✓	0.96	0.26	✓	✓
2009	0.98	0.14	✓		0.98	0.11	✓		0.98	0.16	✓	✓	0.98	0.31	✓	✓	0.98	0.30	✓	✓	0.98	0.28	✓	✓
2008	0.97	0.10			0.97	0.09			0.97	0.15	✓	✓	0.98	0.36	✓	✓	0.98	0.35	✓	✓	0.98	0.32	✓	✓
2007	0.97	0.13	✓		0.97	0.13	✓		0.97	0.18	✓	✓	0.98	0.35	✓	✓	0.98	0.34	✓	✓	0.98	0.31	✓	✓
2006	0.99	0.11			0.99	0.08			0.99	0.12	✓		0.99	0.28	✓	✓	0.99	0.28	✓	✓	0.99	0.25	✓	✓
2005	0.98	0.09			0.98	0.07			0.98	0.12	✓		0.98	0.26	✓	✓	0.98	0.26	✓	✓	0.98	0.23	✓	✓
2004	0.96	0.14	✓	✓	0.96	0.14	✓		0.96	0.19	✓	✓	0.97	0.38	✓	✓	0.97	0.37	✓	✓	0.97	0.34	✓	✓
2003	0.98	0.13	✓		0.98	0.10			0.98	0.15	✓	✓	0.97	0.37	✓	✓	0.97	0.35	✓	✓	0.97	0.32	✓	✓
2002	0.97	0.09			0.97	0.08			0.97	0.14	✓		0.96	0.38	✓	✓	0.96	0.37	✓	✓	0.96	0.34	✓	✓
2001	0.95	0.13	✓		0.95	0.13	✓		0.95	0.18	✓	✓	0.97	0.39	✓	✓	0.97	0.38	✓	✓	0.97	0.35	✓	✓
2 WB	0.99	0.05			0.99	0.03			0.99	0.08			0.99	0.25	✓	✓	0.99	0.25	✓	✓	0.99	0.22	✓	✓
1 WB	0.99	0.09			0.99	0.06			0.99	0.11	✓		1.0	0.27	✓	✓	1.0	0.26	✓	✓	1.0	0.24	✓	✓
1 WA	1.0	0.08			1.0	0.05			1.0	0.10			1.0	0.27	✓	✓	1.0	0.26	✓	✓	1.0	0.23	✓	✓
2 WA	0.99	0.04			0.99	0.02			0.99	0.07			0.99	0.25	✓	✓	0.99	0.25	✓	✓	0.99	0.22	✓	✓
120 NE	0.98	-0.40	✓	✓	0.98	-0.36	✓	✓	0.98	-0.27	✓	✓	0.96	0.01			0.96	0.06			0.96	0.08		
60 NE	0.99	-0.10			0.99	-0.12	✓		0.99	-0.04			0.90	0.27	✓	✓	0.90	0.27	✓	✓	0.90	0.23	✓	✓
60 SW	0.97	0.19	✓	✓	0.97	0.17	✓	✓	0.97	0.23	✓	✓	0.96	0.37	✓	✓	0.96	0.35	✓	✓	0.96	0.32	✓	✓
120 SW	0.94	0.14	✓		0.94	0.14	✓		0.94	0.21	✓	✓	0.94	0.38	✓	✓	0.94	0.37	✓	✓	0.94	0.33	✓	✓

**Table A.15** – Slope, intercept, z-values and probability values of the microzooplankton and mesozooplankton size classes 165  $\mu m$ , 351  $\mu m$  and 444  $\mu m$  (see sections 2.10.1 and 3.1) from the transect Helgoland - Stonehaven. a: slope. b: intercept.  $z_0$ : calculated z-value from the equation (A.13) with the correlation coefficient from  $r_2$  (see Table A.13 in appendix). Critical z-value of the two sided significant level  $\alpha$  for 5% and 1% from the t distribution is  $z_{crit,5\%} = \pm 1.96$  and  $z_{crit,1\%} = \pm 2.58$ , respectively. p: probability value is in [%]. Note that z-values between  $z_0 = 0$  to  $z_0 = \pm 3.5$  have been selected to calculate the p-values. <: p-value is less than 0.04% ( $z_0 > 3.5$  or  $z_0 < -3.5$ ). WB: Week before the expedition. WA: Week after the expedition. Distance 60 and 120 are in km.

	Helgoland - Stonehaven																							
	Microzooplankton												Mesozooplankton											
	165 $\mu m$				351 $\mu m$				444 $\mu m$				165 $\mu m$				351 $\mu m$				444 $\mu m$			
	a	b	$z_0$	p	a	b	$z_0$	p	a	b	$z_0$	p	a	b	$z_0$	p	a	b	$z_0$	p	a	b	$z_0$	p
2014	0.01	0.05	2.88	0.4	0.01	0.45	2.52	1.18	0.09	0.59	3.95	<	0.91	0.80	6.81	<	0.81	0.46	6.65	<	0.67	0.36	6.07	<
2013	0.01	0.05	3.07	0.22	0.04	0.43	3.0	0.27	0.09	0.56	3.95	<	0.95	0.51	8.56	<	0.85	0.20	8.31	<	0.71	0.14	7.65	<
2012	0.01	0.05	3.08	0.2	0.04	0.43	3.07	0.22	0.09	0.57	4.56	<	1.11	0.51	8.44	<	0.98	0.20	8.18	<	0.82	0.14	7.55	<
2011	0.01	0.05	3.08	0.2	0.04	0.44	2.89	0.38	0.09	0.57	4.38	<	0.89	0.67	8.07	<	0.79	0.35	7.79	<	0.65	0.27	7.10	<
2010	0.0	0.06	2.25	2.44	0.03	0.47	1.86	6.28	0.07	0.63	3.06	0.22	0.84	0.77	7.84	<	0.74	0.45	7.53	<	0.61	0.36	6.81	<
2009	0.01	0.05	3.71	<	0.04	0.42	3.10	0.20	0.10	0.56	4.43	<	0.95	0.68	7.31	<	0.84	0.35	7.12	<	0.70	0.27	6.55	<
2008	0.01	0.05	3.17	0.16	0.04	0.43	3.09	0.20	0.09	0.57	4.47	<	1.04	0.57	8.39	<	0.92	0.27	8.08	<	0.77	0.20	7.43	<
2007	0.01	0.05	3.79	<	0.05	0.41	3.68		0.11	0.53	5.17	<	1.01	0.63	7.89	<	0.89	0.32	7.56	<	0.73	0.25	6.92	<
2006	0.0	0.05	2.82	0.48	0.03	0.45	2.41	1.60	0.08	0.61	3.73	<	0.94	0.76	6.73	<	0.84	0.42	6.59	<	0.71	0.32	6.09	<
2005	0.01	0.05	2.95	0.32	0.03	0.44	2.57	1.02	0.09	0.59	3.98	<	0.87	0.76	6.72	<	0.78	0.42	6.60	<	0.65	0.33	6.07	<
2004	0.01	0.05	3.95	<	0.05	0.41	3.81	<	0.11	0.52	5.31	<	1.03	0.54	8.70	<	0.91	0.24	8.30	<	0.75	0.18	7.55	<
2003	0.01	0.05	3.51	0.04	0.04	0.42	3.27	0.10	0.09	0.55	4.77	<	0.91	0.61	8.74	<	0.80	0.30	8.37	<	0.66	0.23	7.60	<
2002	0.01	0.05	3.26	0.12	0.04	0.43	3.25	0.12	0.09	0.56	4.67	<	0.98	0.57	8.81	<	0.86	0.27	8.43	<	0.72	0.21	7.71	<
2001	0.0	0.07	2.41	1.60	0.03	0.46	2.26	2.38	0.07	0.61	3.77	<	0.76	0.66	8.28	<	0.68	0.34	8.05	<	0.57	0.25	7.38	<
2 WB	0.0	0.07	2.29	2.20	0.02	0.47	1.84	6.58	0.06	0.63	3.23	0.12	0.80	0.87	6.37	<	0.72	0.51	6.25	<	0.60	0.41	5.73	<
1 WB	0.0	0.06	2.38	1.74	0.03	0.46	2.0	4.56	0.07	0.62	3.41	0.06	0.85	0.82	6.67	<	0.76	0.47	6.56	<	0.63	0.37	6.03	<
1 WA	0.01	0.05	2.66	0.78	0.03	0.45	2.37	1.78	0.09	0.60	3.83	<	0.96	0.78	6.89	<	0.85	0.44	6.71	<	0.70	0.35	6.12	<
2 WA	0.0	0.06	2.21	2.72	0.03	0.47	1.87	6.14	0.08	0.63	3.34	0.08	0.96	0.83	6.63	<	0.86	0.48	6.48	<	0.71	0.39	5.90	<
120 NE	-0.01	0.07	-4.48	<	-0.04	0.54	-3.07	0.22	-0.03	0.73	-1.69	9.10	0.32	1.21	2.72	0.66	0.37	0.76	3.44	0.06	0.32	0.60	3.31	0.10
60 NE	0.0	0.06	-0.83	40.66	-0.01	0.50	-0.82	41.22	0.03	0.67	1.39	16.46	0.77	0.81	8.50	<	0.74	0.43	8.90	<	0.62	0.34	8.17	<
60 SW	0.01	0.04	4.43	<	0.06	0.33	4.59	<	0.13	0.40	6.21	<	1.12	0.0	7.71	<	0.97	0.09	7.22	<	0.80	0.08	6.46	<
120 SW	0.01	0.04	3.83	<	0.06	0.30	4.27	<	0.13	0.34	5.91	<	1.20	0.0	7.85	<	1.07	-0.21	7.45	<	0.88	-0.18	6.72	<

**Table A.16** – Slope, intercept, z-values and probability values of the microzooplankton and mesozooplankton size classes 165  $\mu\text{m}$ , 351  $\mu\text{m}$  and 444  $\mu\text{m}$  (see sections 2.10.1 and 3.1) from the transect Stonehaven - Helgoland. a: slope. b: intercept.  $z_0$ : calculated z-value from the equation (A.13) with the correlation coefficient from  $r_2$  (see Table A.13 in appendix). Critical z-value of the two sided significant level  $\alpha$  for 5% and 1% from the t distribution is  $z_{crit,5\%} = \pm 1.96$  and  $z_{crit,1\%} = \pm 2.58$ , respectively. p: probability value is in [%]. Note that z-values between  $z_0 = 0$  to  $z_0 = \pm 3.5$  have been selected to calculate the p-values. <: p-value is less than 0.04% ( $z_0 > 3.5$  or  $z_0 < -3.5$ ). WB: Week before the expedition. WA: Week after the expedition. Distance 60 and 120 are in km.

	Stonehaven - Helgoland																							
	Microzooplankton												Mesozooplankton											
	165 $\mu\text{m}$				351 $\mu\text{m}$				444 $\mu\text{m}$				165 $\mu\text{m}$				351 $\mu\text{m}$				444 $\mu\text{m}$			
	a	b	$z_0$	p	a	b	$z_0$	p	a	b	$z_0$	p	a	b	$z_0$	p	a	b	$z_0$	p	a	b	$z_0$	p
2014	0.0	0.06	1.48	13.88	0.02	0.56	1.09	27.58	0.05	0.77	1.97	4.88	0.69	1.22	4.97	<	0.58	0.82	4.82	<	0.47	0.67	4.31	<
2013	0.0	0.06	1.64	10.10	0.02	0.55	1.33	18.36	0.05	0.75	2.26	2.38	0.76	0.92	6.95	<	0.65	0.56	6.79	<	0.53	0.44	6.22	<
2012	0.0	0.06	1.82	6.88	0.03	0.53	1.75	8.02	0.07	0.73	2.73	0.64	0.92	0.89	6.88	<	0.79	0.54	6.76	<	0.65	0.42	6.22	<
2011	0.0	0.06	1.82	6.88	0.02	0.54	1.15	12.12	0.06	0.74	2.47	1.36	0.70	1.08	6.14	<	0.58	0.72	5.86	<	0.47	0.59	5.24	<
2010	0.0	0.07	0.97	33.20	0.01	0.58	0.49	62.42	0.03	0.82	1.23	21.86	0.67	1.15	5.88	<	0.54	0.80	5.46	<	0.42	0.66	4.75	<
2009	0.01	0.06	2.45	1.42	0.04	0.52	2.0	4.56	0.08	0.71	2.91	0.36	0.79	1.05	5.86	<	0.66	0.68	5.69	<	0.54	0.55	5.16	<
2008	0.0	0.06	1.81	7.02	0.03	0.54	1.69	9.1	0.06	0.73	2.64	0.82	0.87	0.94	6.86	<	0.74	0.59	6.66	<	0.60	0.46	6.08	<
2007	0.0	0.06	2.36	1.82	0.04	0.51	2.29	2.2	0.08	0.69	3.31	0.1	0.85	0.96	6.62	<	0.71	0.60	6.43	<	0.58	0.48	5.86	<
2006	0.0	0.06	1.89	5.88	0.02	0.55	1.35	17.70	0.06	0.76	2.18	2.92	0.73	1.16	5.26	<	0.62	0.77	5.15	<	0.50	0.62	4.68	<
2005	0.0	0.06	1.70	8.92	0.02	0.55	1.21	22.62	0.05	0.77	2.07	3.84	0.65	1.22	4.88	<	0.55	0.82	4.76	<	0.44	0.66	4.28	<
2004	0.0	0.06	2.58	0.98	0.04	0.50	2.46	1.38	0.09	0.67	3.49	0.04	0.87	0.87	7.38	<	0.73	0.53	7.06	<	0.59	0.43	6.36	<
2003	0.0	0.06	2.28	2.26	0.03	0.53	1.86	6.28	0.07	0.72	2.78	0.54	0.73	1.0	7.08	<	0.60	0.65	6.69	<	0.48	0.51	5.95	<
2002	0.0	0.06	1.62	10.52	0.02	0.54	1.51	13.10	0.06	0.75	2.47	1.36	0.83	0.93	7.29	<	0.70	0.57	7.09	<	0.58	0.45	6.50	<
2001	0.0	0.06	2.37	1.78	0.03	0.51	2.27	2.32	0.08	0.69	3.26	0.12	0.74	0.89	7.50	<	0.62	0.54	7.29	<	0.51	0.43	6.67	<
2 WB	0.0	0.07	0.87	38.44	0.01	0.58	0.49	62.42	0.03	0.81	1.36	17.38	0.60	1.28	4.66	<	0.51	0.87	4.55	<	0.41	0.71	4.07	<
1 WB	0.0	0.06	1.55	12.12	0.02	0.56	1.12	26.28	0.05	0.77	1.97	4.88	0.68	1.20	5.04	<	0.57	0.80	4.91	<	0.46	0.65	4.41	<
1 WA	0.0	0.07	1.39	16.46	0.02	0.56	0.96	33.70	0.05	0.78	1.83	6.72	0.72	1.22	4.96	<	0.61	0.82	4.81	<	0.49	0.67	4.29	<
2 WA	0.0	0.07	0.80	42.38	0.01	0.59	0.39	69.66	0.04	0.82	1.26	20.76	0.70	1.28	4.64	<	0.59	0.87	4.53	<	0.47	0.71	4.04	<
120 NE	-0.01	0.08	-7.40	<	-0.07	0.67	-6.36	<	-0.09	0.94	-4.69	<	0.02	1.71	0.19	84.94	0.12	1.15	1.08	28.02	0.13	0.90	1.27	20.40
60 NE	0.0	0.07	-1.76	7.84	-0.03	0.61	-2.14	3.24	-0.02	0.85	-0.73	46.54	0.46	1.33	4.81	<	0.40	0.92	4.83	<	0.31	0.77	4.17	<
60 SW	0.01	0.05	3.22	0.12	0.05	0.43	2.98	0.28	0.10	0.56	4.02	<	0.95	0.62	6.84	<	0.79	0.35	6.39	<	0.64	0.29	5.65	<
120 SW	0.0	0.05	2.35	1.82	0.04	0.42	2.26	2.38	0.08	0.53	3.42	0.06	0.96	0.39	6.63	<	0.83	0.13	6.37	<	0.68	0.10	5.73	<

## B ECOHAM transect

### B.1 Topography

#### B.1.1 Original

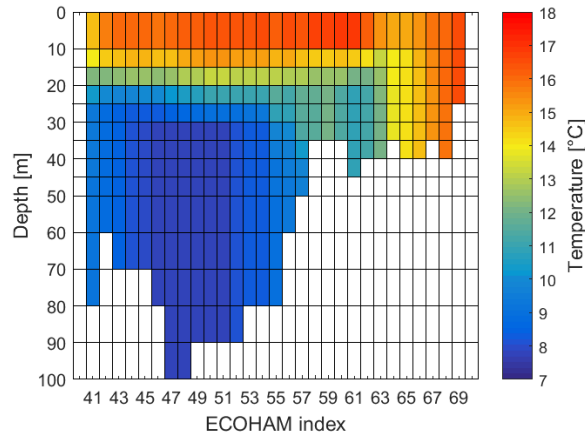


**Figure B.1** – Bottom topography of the modelled expedition transect from the transect Helgoland - Stonehaven (simulated temperature).

#### B.1.2 Shifted

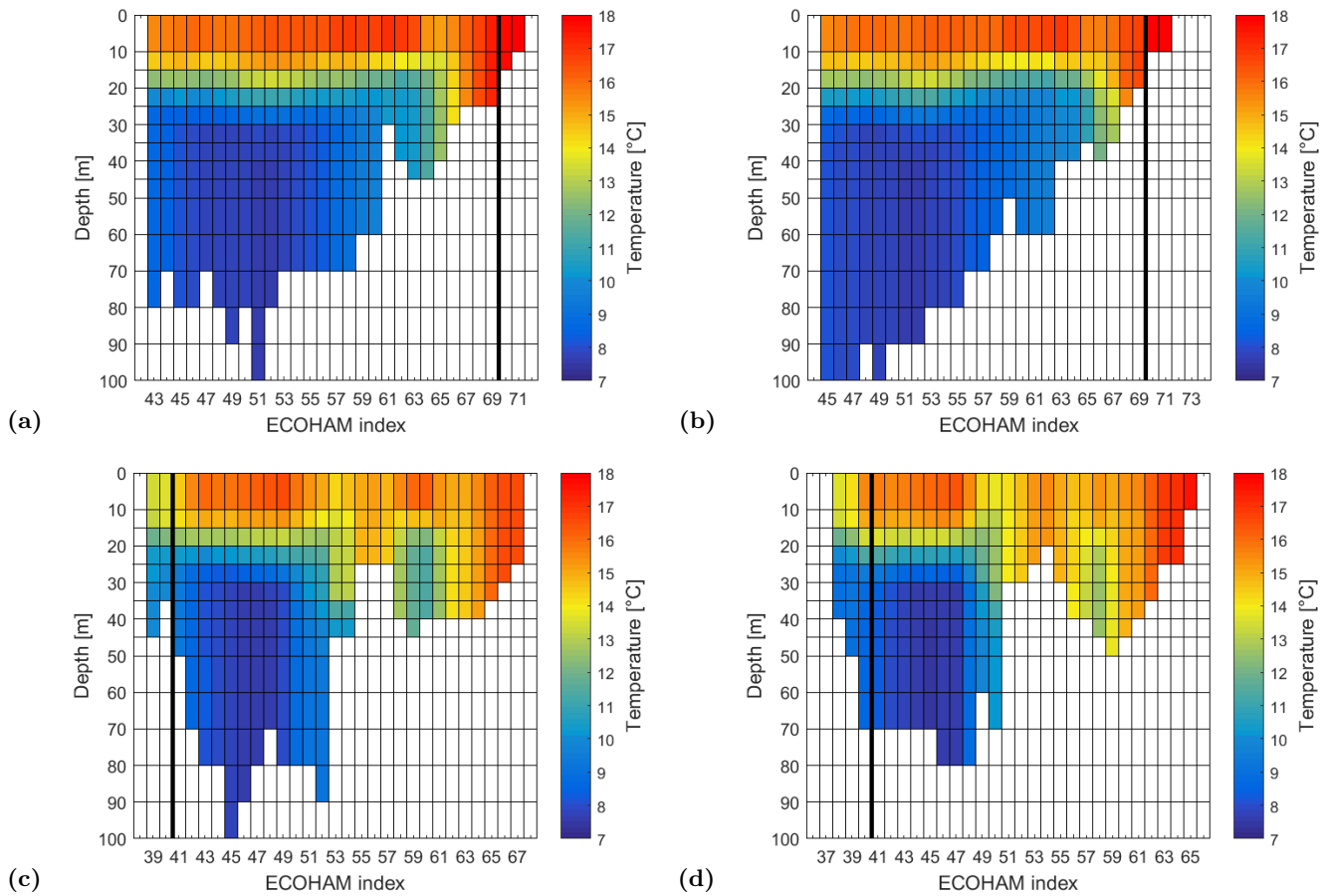


**Figure B.2** – Bottom topography of the shifted modelled transects from the transect Helgoland - Stonehaven (simulated temperature). (a) 60 km NE. (b) 120 km NE. (c) 60 km SE. (d) 120 km SE. Black thick line shows the end and the beginning of the expedition transect, respectively.

## B.2 Transect shifting towards NE and SW

In most cases two points of coordinates are given and the distance is the desired parameter. In the present case, for each shifted transect the distances and the coordinates of the expedition transect are well-known but the respective coordinates of the moved transects are unidentified.

According to the Pythagorean theorem, the equation is defined as follows:

$$d^2 = l_{cath,A}^2 + l_{cath,B}^2, \quad (B.1)$$

where  $d$  is the distance between two coordinates, and  $l_{cath,A}$  is the length of the adjacent side from the gradient triangle, and  $l_{cath,B}$  is the length of the opposite leg from the gradient triangle. Due to the fact that the gradient triangle of  $45^\circ$  has a value of one, the length of both cathetus are identical.

Keeping a gradient triangle of  $45^\circ$  and rearranging the equation (B.1), the length of the cathetus can be written as

$$l_{cath} = \frac{d}{\sqrt{2}}. \quad (B.2)$$

Remaining an identical latitude and rearranging the equation (2.5) with respect to a gradient triangle of  $45^\circ$  yields

$$\cos\left(\frac{l_{cath}}{R}\right) = \sin(lat_1) \sin(lat_1) + \cos(lat_1) \cos(lat_1) \cos(lon_1 - lon_2). \quad (B.3)$$

Where  $R$  is the earth radius in km with multiplying by  $\pi/180$ ,  $l_{cath}$  is the length of the cathetus from the gradient triangle,  $lat_1$  is the coordinate of latitude and  $lon_1$  and  $lon_2$  are the coordinates of longitude, respectively.

Rearranging the equation (B.3) for  $lon_2$  becomes

$$lon_2 = \arccos\left[\frac{\cos\left(\frac{l_{cath}}{R}\right) - \sin^2(lat_1)}{\cos^2(lat_1)}\right] + lon_1 \text{ for NE}, \quad (B.4)$$

$$lon_2 = lon_1 - \arccos\left[\frac{\cos\left(\frac{l_{cath}}{R}\right) - \sin^2(lat_1)}{\cos^2(lat_1)}\right] \text{ for SW}.$$

Keeping an equal longitude, the equation (2.5) can be simplified as

$$\cos\left(\frac{l_{cath}}{R}\right) = \sin(lat_1) \sin(lat_2) + \cos(lat_1) \cos(lat_2), \quad (B.5)$$

and applying the trigonometric addition theorem  $\cos(x \pm y) = \cos(x) \cos(y) \mp \sin(x) \sin(y)$ , the equation (B.5) can be eased to

$$\cos\left(\frac{l_{cath}}{R}\right) = \cos(lat_1 \pm lat_2). \quad (B.6)$$

Rearranging the equation (B.6) for  $lat_2$  yields

$$lat_2 = lat_1 + \frac{l_{cath}}{R} \text{ for NE}, \quad (B.7)$$

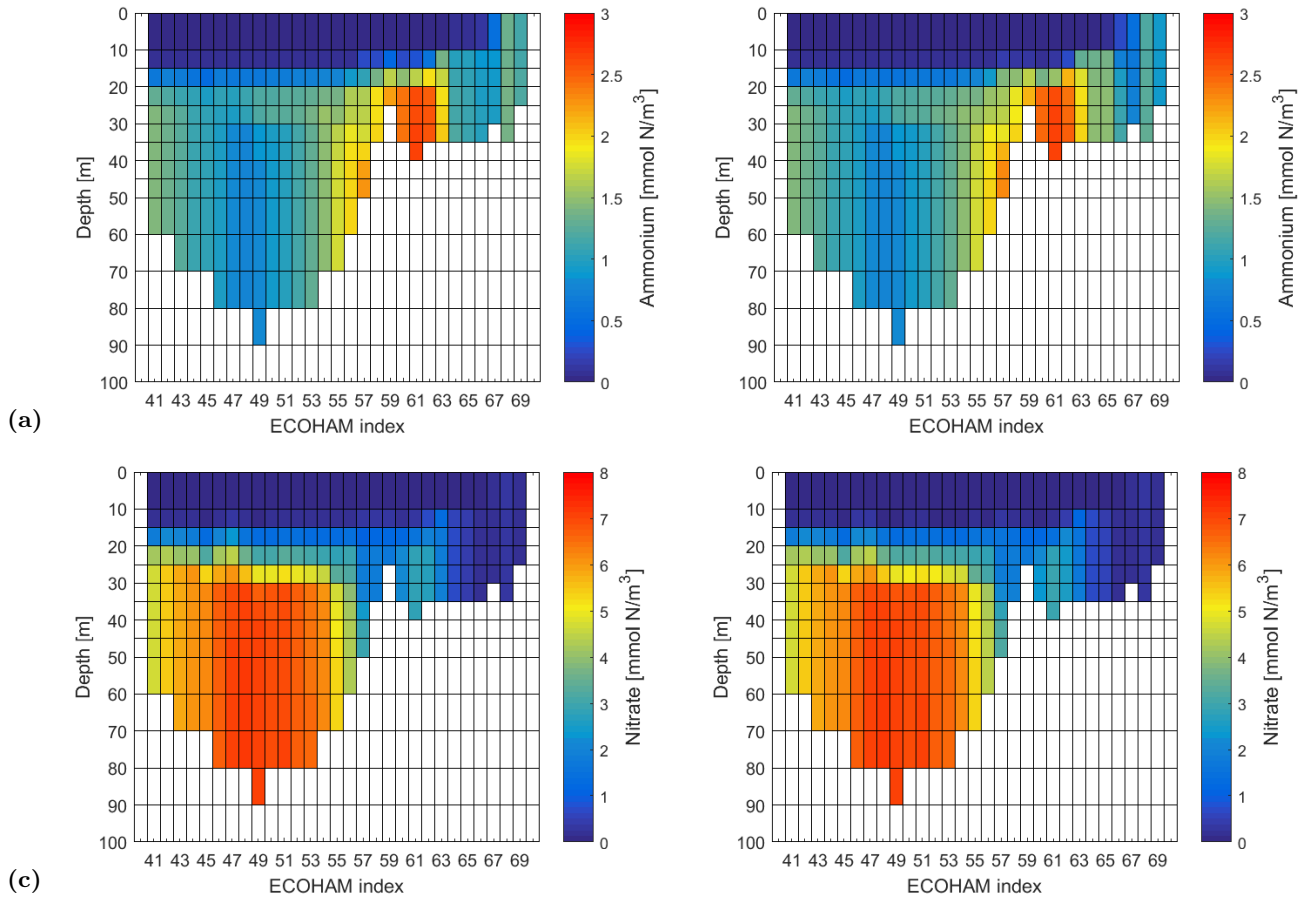
$$lat_2 = lat_1 - \frac{l_{cath}}{R} \text{ for SW}.$$

Table B.1 in the appendix shows the calculated ECOHAM-coordinates of the shifted transects from 60 km and 120 km, respectively, towards NE and SW by using the equations (B.7) and (B.4). The zero km marks the non-shifted transect.

**Table B.1** – ECOHAM index with the corresponding ECOHAM-coordinates [°]. Shifted transects are obtained by the equations (B.4) and (B.7). Expedition transect is derived by the equation (A.1). Distance [km] is calculated by the equation (2.5). Deviation [%] is the discrepancy with 60 and 120 km.

ECOHAM Index	120 km SW	Distance	Deviation	60 km SW	Distance	Deviation	Expedition	60 km NE	Distance	Deviation	120 km NE	Distance	Deviation
37	56.121,-3.145	120.61	0.51										
38	56.121,-2.812	120.61	0.51										
39	56.060,-2.476	120.61	0.51	56.502,-2.448	60.15	0.25							
40	55.921,-2.138	120.60	0.50	56.502,-2.114	60.15	0.25							
41	55.921,-1.804	120.60	0.50	56.442,-1.780	60.15	0.25	56.883,-1.750						
42	55.921,-1.471	120.60	0.50	56.302,-1.444	60.15	0.25	56.883,-1.417						
43	55.892,-1.137	120.60	0.50	56.302,-1.111	60.15	0.25	56.823,-1.083	57.264,-1.052	59.85	0.26			
44	55.721,-0.797	120.60	0.50	56.302,-0.777	60.15	0.25	56.683,-0.750	57.264,-0.719	59.85	0.26			
45	55.721,-0.464	120.60	0.50	56.273,-0.443	60.15	0.25	56.683,-0.417	57.204,-0.387	59.85	0.26	57.646,-0.355	119.38	0.51
46	55.545,-0.124	120.60	0.50	56.102,-0.107	60.15	0.25	56.683,-0.083	57.064,-0.056	59.85	0.25	57.646,-0.022	119.38	0.51
47	55.521, 0.210	120.59	0.50	56.102, 0.227	60.15	0.25	56.654, 0.250	57.064, 0.277	59.85	0.25	57.585, 0.310	119.39	0.51
48	55.369, 0.549	120.59	0.49	55.926, 0.563	60.15	0.25	56.483, 0.583	57.064, 0.611	59.85	0.25	57.446, 0.638	119.39	0.51
49	55.321, 0.884	120.59	0.49	55.902, 0.897	60.15	0.25	56.483, 0.917	57.035, 0.943	59.85	0.25	57.446, 0.971	119.39	0.51
50	55.300, 1.218	120.59	0.49	55.751, 1.233	60.15	0.25	56.307, 1.250	56.864, 1.274	59.85	0.25	57.446, 1.304	119.39	0.51
51	55.121, 1.558	120.59	0.49	55.702, 1.567	60.15	0.25	56.283, 1.583	56.864, 1.607	59.85	0.25	57.416, 1.637	119.39	0.51
52	55.121, 1.891	120.59	0.49	55.681, 1.901	60.15	0.25	56.132, 1.917	56.688, 1.937	59.85	0.25	57.246, 1.964	119.39	0.50
53	54.952, 2.230	120.58	0.49	55.502, 2.237	60.15	0.24	56.083, 2.250	56.664, 2.270	59.85	0.25	57.246, 2.297	119.39	0.50
54	54.918, 2.565	120.58	0.48	55.502, 2.571	60.15	0.24	56.062, 2.583	56.513, 2.601	59.85	0.25	57.069, 2.624	119.40	0.50
55	54.721, 2.905	120.58	0.48	55.334, 2.907	60.15	0.24	55.883, 2.917	56.464, 2.933	59.85	0.25	57.046, 2.957	119.40	0.50
56	54.680, 3.240	120.58	0.48	55.300, 3.241	60.15	0.24	55.883, 3.250	56.444, 3.266	59.85	0.25	56.894, 3.284	119.40	0.50
57	54.521, 3.578	120.57	0.48	55.102, 3.577	60.14	0.24	55.715, 3.583	56.264, 3.596	59.85	0.25	56.846, 3.616	119.40	0.50
58	54.416, 3.915	120.57	0.48	55.061, 3.912	60.14	0.24	55.681, 3.917	56.264, 3.930	59.85	0.25	56.825, 3.949	119.40	0.50
59	54.321, 4.252	120.57	0.47	54.902, 4.248	60.14	0.24	55.483, 4.250	56.096, 4.260	59.85	0.24	56.646, 4.276	119.41	0.49
60	54.140, 4.591	120.56	0.47	54.800, 4.583	60.14	0.24	55.442, 4.583	56.062, 4.593	59.85	0.24	56.646, 4.609	119.41	0.49
61	54.069, 4.927	120.56	0.47	54.702, 4.918	60.14	0.24	55.283, 4.917	55.864, 4.923	59.85	0.24	56.477, 4.936	119.41	0.49
62	53.921, 5.265	120.56	0.47	54.521, 5.254	60.14	0.24	55.178, 5.250	55.823, 5.255	59.85	0.24	56.443, 5.269	119.41	0.49
63	53.738, 5.604	120.56	0.46	54.500, 5.588	60.14	0.24	55.083, 5.583	55.664, 5.586	59.86	0.24	56.246, 5.595	119.42	0.49
64	53.591, 5.942	120.55	0.46	54.302, 5.924	60.14	0.23	54.903, 5.917	55.559, 5.917	59.86	0.24	56.204, 5.927	119.42	0.49
65	53.479, 6.279	120.55	0.46	54.119, 6.260	60.14	0.23	54.831, 6.250	55.464, 6.249	59.86	0.24	56.046, 6.255	119.42	0.48
66				53.972, 6.596	60.14	0.23	54.683, 6.583	55.284, 6.580	59.86	0.24	55.940, 6.585	119.42	0.48
67				53.860, 6.931	60.14	0.23	54.500, 6.917	55.212, 6.912	59.86	0.24	55.846, 6.915	119.43	0.48
68							54.353, 7.250	55.064, 7.243	59.86	0.24	55.665, 7.242	119.43	0.48
69							54.241, 7.583	54.881, 7.573	59.86	0.23	55.593, 7.573	119.43	0.47
70								54.734, 7.904	59.86	0.23	55.446, 7.902	119.43	0.47
71								54.622, 8.235	59.86	0.23	55.262, 8.229	119.44	0.47
72											55.115, 8.558	119.44	0.47
73											55.003, 8.888	119.44	0.46

### B.3 Ammonium and nitrate concentration



**Figure B.3** – Transects of the simulated nutrients. Left: Helgoland - Stonehaven. Right: Stonehaven - Helgoland. (a) and (b) Ammonium. (c) and (d) Nitrate.

### B.4 Potential density anomalies

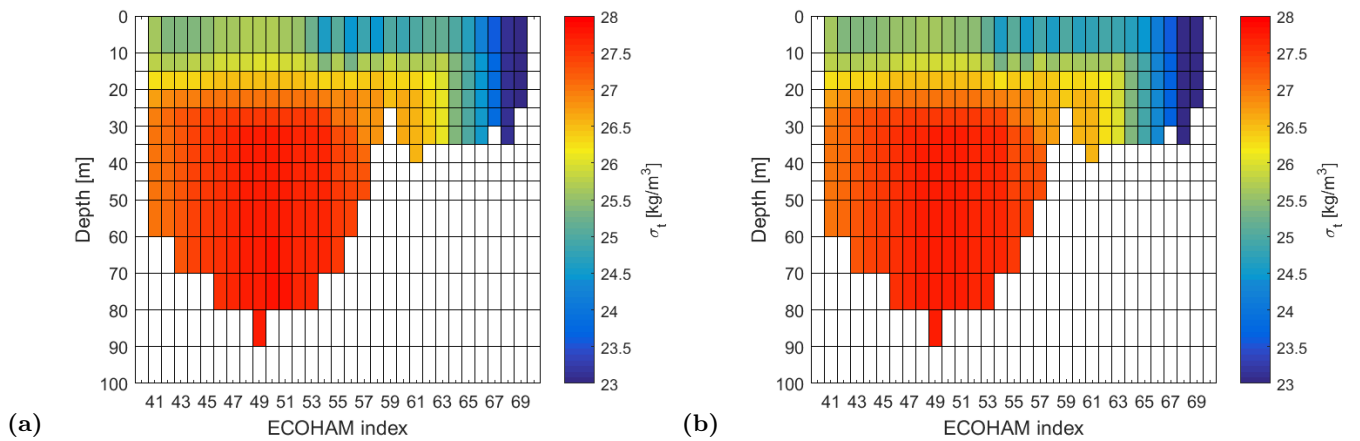


**Figure B.4** – Transects of the simulated potential density anomalies. (a) Helgoland - Stonehaven. (b) Stonehaven - Helgoland.

## B.5 Fast and slow sinking detritus concentration

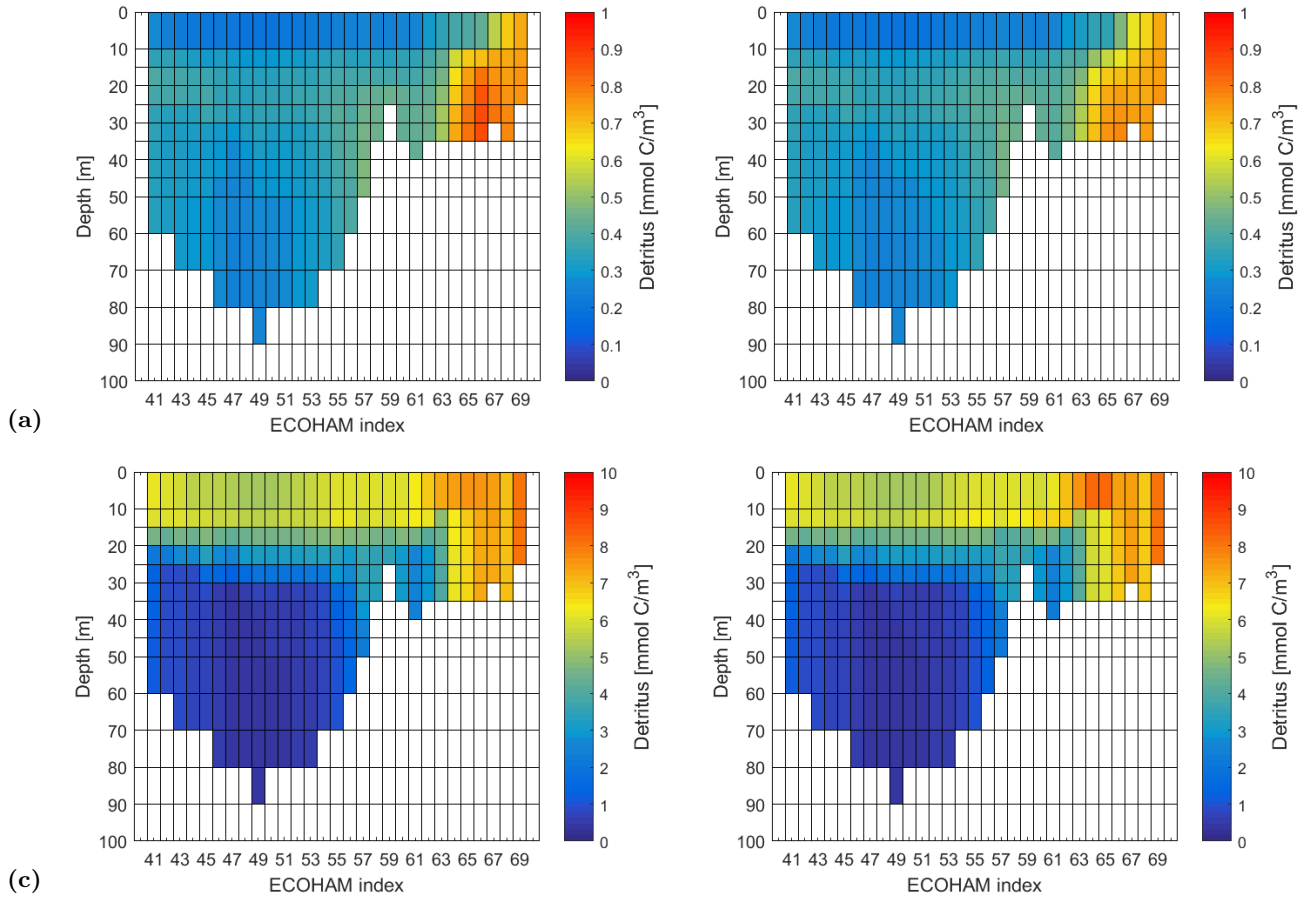


**Figure B.5** – Transects of the simulated detritus with differently sinking velocity. Left: Helgoland - Stonehaven. Right: Stonehaven - Helgoland. (a) and (b) Fast sinking. (c) and (d) Slow sinking.

## B.6 Apparent Oxygen Utilisation

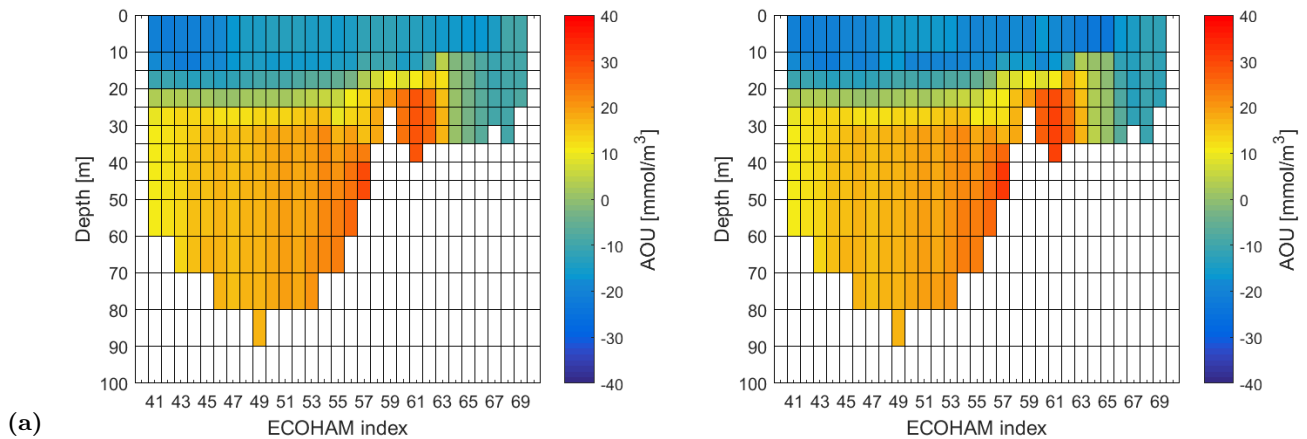


**Figure B.6** – Transects of the simulated apparent oxygen utilisation. (a) Helgoland - Stonehaven. (b) Stonehaven - Helgoland.

## B.7 Representativeness of the modelled expedition transects

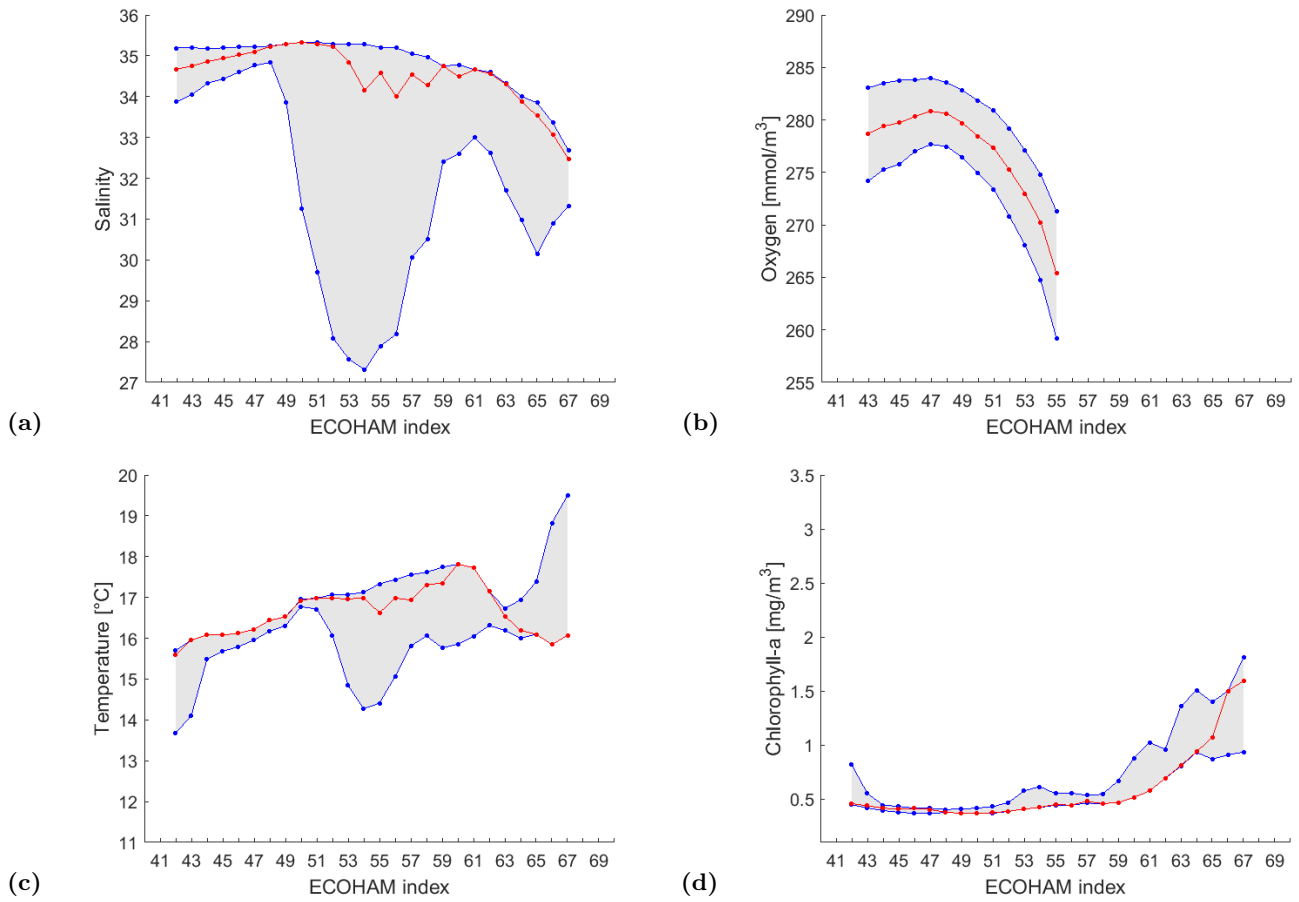


**Figure B.7** – Simulated variability of the transects. H - S: transect from Helgoland - Stonehaven. S - H: transect from Stonehaven - Helgoland. Blue line: minimum and maximum values. Red line: expedition transect. (a) Salinity of the surface layer (0 - 10 m) of the shifted transects from S - H. (b) Oxygen of the depth layer 60 - 70 m of the short time series from H - S. (c) Temperature of the surface layer of the shifted transects from S - H. (d) Phytoplankton of the surface layer of the shifted transects from S - H.

## B.8 Short time series

**Table B.2** – Short time series. H - S: transect from Helgoland - Stonehaven. S - H: transect from Stonehaven - Helgoland.

	H - S	S - H
two weeks before	25.-28.6.	28.-30.6.
one week before	2.-5.7.	5.-7.7.
expedition week	9.-12.7.	12.-14.7.
one week after	16.-19.7.	19.-21.7.
two weeks after	23.-26.7.	26.-28.7.

## B.9 Mixed layer depth of ECOHAM water columns from the selected area

Temperature of water column throughout the year 2014 from the model of the selected area (see black thick line in Figure A.10a and b in the appendix).

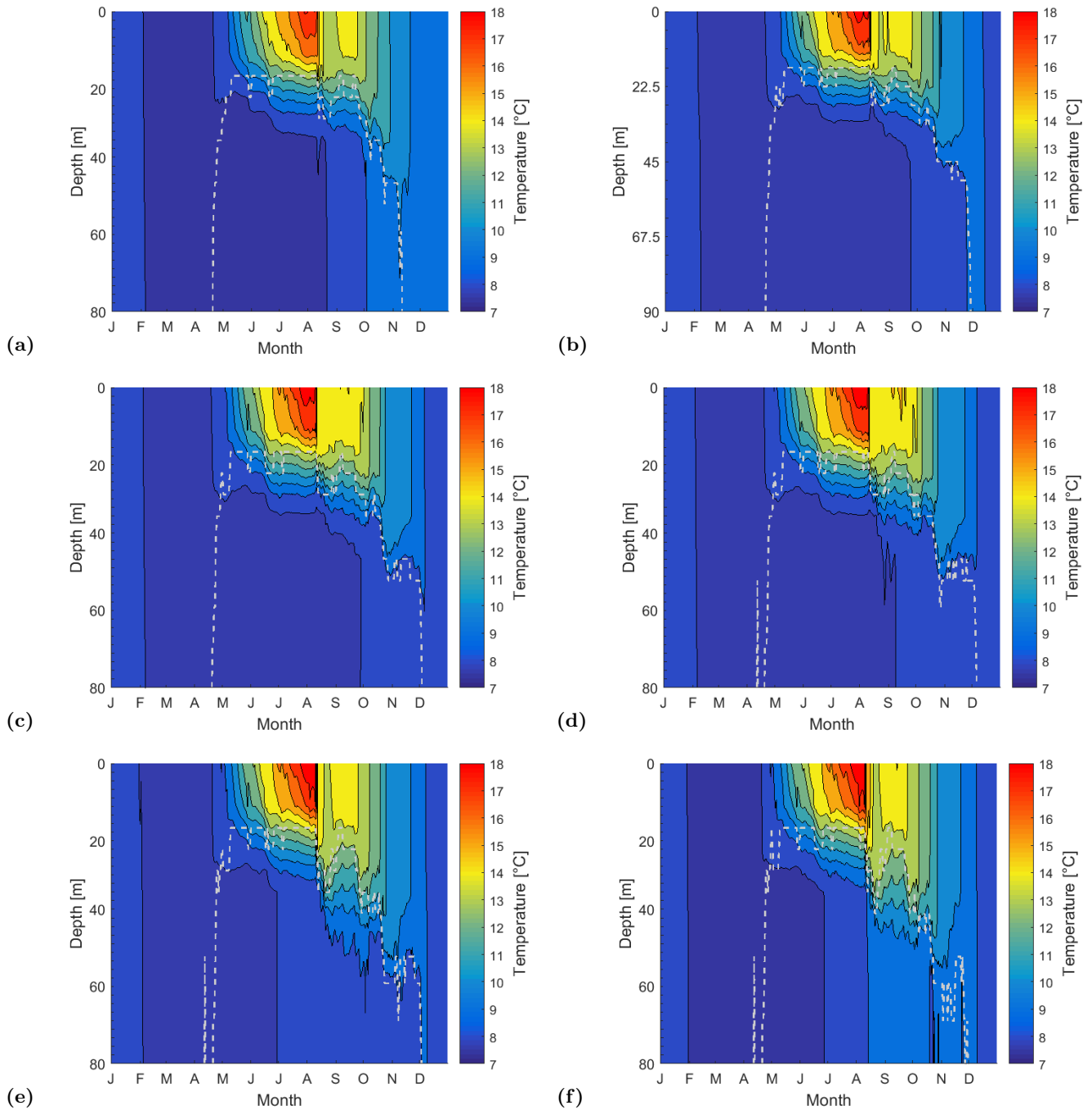


**Figure B.8** – Simulated temperature of a Water column throughout the year 2014. Dashed line: mixed layer depth (MLD). Criterion: 0.4 K (see the equation (2.11)). (a) ECOHAM index 47. (b) ECOHAM index 49. (c) ECOHAM index 50. (d) ECOHAM index 51. (e) ECOHAM index 52. (f) ECOHAM index 53. Note the differently depth of the water columns.

**Table B.3** – Day of the onset of persistent stratification ( $t_{stratification}$ ) for each water column in the selected area of the transect.  $\Delta T = 0.1 K$  and  $\Delta T = 1.0 K$  are the minimum and maximum values of the MLD criterion (see the equation (2.11)) within the range of literature values from Kara et al. (2000).

ECOHAM index	$\Delta T = 0.1 K$	$\Delta T = 1.0 K$
47	5. April	1. May
48	4. April	28. April
49	4. April	28. April
50	4. April	27. April
51	29. March	27. April
52	29. March	27. April
53	29. March	27. April
54	28. March	26. April

## B.10 State variables of the reduced ECOHAM dataset

**Table B.4** – State variables of the reduced dataset from ECOHAM and their corresponding units. Note that the state variables Diatom and Flagellate are stored as different units.

Physical	Nutrients	Biological	Other
Temperature [ $^{\circ}C$ ]	Ammonium [ $mmol N/m^3$ ]	Diatom [ $mg Chl-a/m^3$ ] or [ $mmol C/m^3$ ]	Detritus (slow sinking) [ $mmol C/m^3$ ]
Salinity	Phosphate [ $mmol P/m^3$ ]	Flagellate [ $mg Chl-a/m^3$ ] or [ $mmol C/m^3$ ]	Detritus (fast sinking) [ $mmol C/m^3$ ]
Oxygen [ $mmol /m^3$ ]	Nitrate [ $mmol N/m^3$ ] Silicate [ $mmol Si/m^3$ ]	Microzooplankton [ $mmol C/m^3$ ] Mesozooplankton [ $mmol C/m^3$ ]	Cell area [ $m^2$ ] Volume of water in grid cell [ $m^3$ ]

## B.11 Simulated oxygen expedition transect 2005 and 2010 from Helgoland - Stonehaven

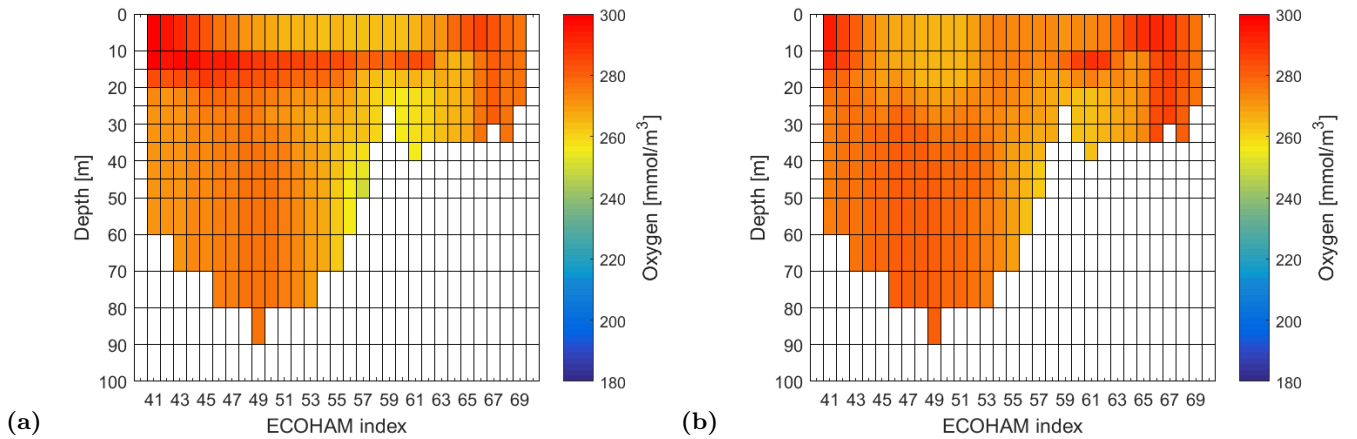


**Figure B.9** – Simulated oxygen transects from Helgoland - Stonehaven. (a) 2005. (b) 2010.

## B.12 Simulated mass budgets of the selcted cells

**Table B.5** – Physical and biological simulated mass budgets of the cells of ECOHAM index 47 - 52, depth layer 40 - 45 m, from Helgoland - Stonehaven. Start: previous day of  $t_{stratification}$ . End: day of the expedition.  $NH_3$ : ammonium.  $HNO_3$ : nitrate. Note that biological mass budgets for  $O_2$  were not listed.

Helgoland - Stonehaven										
ECOHAM index	Start 2014	End 2014	$NH_3$ [ $mmol\ N/m^3$ ]			$HNO_3$ [ $mmol\ N/m^3$ ]			$O_2$ [ $mmol/m^3$ ]	
			Physical		Biological	Physical		Biological	Physical	
			advection	vert. mixing	reminalisation	advection	vert. mixing	nitrification	advection	vert. mixing
47	18. April	11. July	0.19	0.03	1.0	-0.69	-0.32	0.88	0.39	-1.04
48	18. April	11. July	0.14	0.09	0.90	-0.39	-0.54	0.84	0.10	-0.67
49	18. April	11. July	-0.01	0.24	1.0	-0.48	-0.65	0.89	2.28	-2.76
50	18. April	11. July	0.08	0.23	1.05	-0.38	-0.75	0.96	0.73	-2.33
51	18. April	11. July	0.11	0.26	1.12	-0.26	-0.77	1.04	-0.38	-2.45
52	19. April	11. July	0.19	0.25	1.30	-0.76	-0.50	1.20	0.20	-3.62

**Table B.6** – Physical and biological simulated mass budgets of the cells of ECOHAM index 47 - 54, depth layer 40 - 45 m, from Stonehaven - Helgoland. Start: previous day of  $t_{stratification}$ . End: day of the expedition.  $NH_3$ : ammonium.  $HNO_3$ : nitrate. Note that biological mass budgets for  $O_2$  were not listed.

Stonehaven - Helgoland										
ECOHAM index	Start 2014	End 2014	$NH_3$ [ $mmol\ N/m^3$ ]			$HNO_3$ [ $mmol\ N/m^3$ ]			$O_2$ [ $mmol/m^3$ ]	
			Physical		Biological	Physical		Biological	Physical	
			advection	vert. mixing	reminalisation	advection	vert. mixing	nitrification	advection	vert. mixing
47	18. April	12. July	0.2	0.03	1.01	-0.71	-0.31	0.90	0.33	-1.06
48	18. April	12. July	0.14	0.09	0.91	-0.39	-0.55	0.85	0.09	-0.71
49	18. April	12. July	0.0	0.23	1.01	-0.49	-0.67	0.91	2.36	-2.66
50	18. April	13. July	0.09	0.22	1.08	-0.4	-0.76	0.99	0.61	-2.47
51	18. April	13. July	0.13	0.26	1.15	-0.29	-0.79	1.08	-0.57	-2.61
52	19. April	13. July	0.2	0.27	1.32	-0.8	-0.42	1.24	-0.04	-4.09
53	19. April	13. July	0.2	0.33	1.51	-0.89	-0.6	1.43	-0.07	-4.89
54	20. April	13. July	0.29	0.30	1.72	-1.24	-0.65	1.65	-0.49	-5.23

## B.13 The factor $m$

**Table B.7** – The factor  $m$  and  $(1 - m)$  of the "regenerated" component from the cells ECOHAM index 47 - 52, depth layer 40 - 45 m, in the transect of Helgoland - Stonehaven. Parameter minimum, mean, maximum are from ND130.  $R_0$ : remineralisation value (see the equation (2.13)).  $R_0 = 151.5$ : maximum amount.  $R_0 = 140$ : proposed amount.  $R_0 = 138$ : Redfield. ECOHAM $\bullet$ : produced concentration over the slope of AOU with respect to the model ratio. Model ratio have been evaluated from the Table B.5 in the appendix.

Helgoland - Stonehaven												
ECOHAM	$m$						$(1 - m)$					
	ND130			ECOHAM $\bullet$			ND130			ECOHAM $\bullet$		
	index	minimum	mean	maximum	$R_0 = 151.5$	$R_0 = 140$	$R_0 = 138$	minimum	mean	maximum	$R_0 = 151.5$	$R_0 = 151.5$
47	0.99	0.94	0.87	0.84	0.82	0.83	0.01	0.06	0.13	0.16	0.18	0.17
48	0.99	0.95	0.88	0.84	0.81	0.82	0.01	0.05	0.12	0.16	0.19	0.18
49	0.99	0.94	0.87	0.84	0.81	0.83	0.01	0.06	0.13	0.16	0.19	0.17
50	0.94	0.85	0.75	0.84	0.81	0.83	0.06	0.15	0.25	0.16	0.19	0.17
51	0.94	0.83	0.73	0.84	0.81	0.82	0.06	0.17	0.27	0.16	0.19	0.18
52	0.91	0.77	0.64	0.84	0.81	0.82	0.09	0.23	0.36	0.16	0.19	0.18

**Table B.8** – The factor  $m$  and  $(1 - m)$  of the "regenerated" component from the cells ECOHAM index 47 - 54, depth layer 40 - 45 m, in the transect of Stonehaven - Helgoland. Parameter minimum, mean, maximum are from ND130.  $R_0$ : remineralisation value (see the equation (2.13)).  $R_0 = 151.5$ : maximum amount.  $R_0 = 140$ : proposed amount.  $R_0 = 138$ : Redfield. ECOHAM $\bullet$ : produced concentration over the slope of the AOU with respect to the model ratio. Model ratio have been evaluated from the Table B.6. Blank: no values exist due to the negative result of the "regenerated" component from the equation (2.18).

Stonehaven - Helgoland												
ECOHAM	$m$						$(1 - m)$					
	ND130			ECOHAM $\bullet$			ND 130			ECOHAM $\bullet$		
	index	minimum	mean	maximum	$R_0 = 151.5$	$R_0 = 140$	$R_0 = 138$	minimum	mean	maximum	$R_0 = 151.5$	$R_0 = 151.5$
47	0.99	0.94	0.88	0.84	0.81	0.83	0.01	0.06	0.12	0.16	0.19	0.17
48	1.0	0.95	0.89	0.84	0.81	0.82	0.0	0.05	0.11	0.16	0.19	0.18
49	0.99	0.94	0.88	0.84	0.81	0.83	0.01	0.06	0.12	0.16	0.19	0.17
50	0.94	0.85	0.76	0.84	0.81	0.82	0.06	0.15	0.24	0.16	0.19	0.18
51	0.94	0.84	0.74	0.83	0.81	0.82	0.06	0.16	0.26	0.17	0.19	0.18
52	0.92	0.80	0.68	0.83	0.81	0.82	0.08	0.20	0.32	0.17	0.19	0.18
53		0.84	0.69	0.83	0.80	0.82		0.16	0.31	0.17	0.20	0.18
54	0.99	0.84	0.70	0.83	0.80	0.82	0.01	0.16	0.30	0.17	0.20	0.18

## B.14 Estimation of nitrate and ammonium concentrations

**Table B.9** – Estimated nitrate concentrations ( $HNO_3^*$ ) from the selected area of the transect Helgoland - Stonehaven. Note that values from minimum to maximum is illustrated for each ECOHAM index.  $HNO_{3,minimum}^*$ ,  $HNO_{3,mean}^*$  and  $HNO_{3,maximum}^*$  evaluated from observational data ND130.  $HNO_{3,ECOHAM}^*$  evaluated from simulated data.  $R_0$ : remineralisation value (see Table 2.1).  $R_0 = 151.5$ : maximum amount.  $R_0 = 140$ : proposed amount.  $R_0 = 138$ : Redfield. Bold: inside the range of expected *in situ* measurements for nitrate and ammonium (see Table B.10 in the appendix). Note that values for ECOHAM index 53 - 54 does not exist due to absence of AOU values (see Fig. A.10a in the appendix).

Helgoland - Stonehaven												
ND130												
ECOHAM	$HNO_{3,minimum}^*$ [mmol N/m <sup>3</sup> ]			$HNO_{3,mean}^*$ [mmol N/m <sup>3</sup> ]			$HNO_{3,maximum}^*$ [mmol N/m <sup>3</sup> ]			$HNO_{3,ECOHAM}^*$ [mmol N/m <sup>3</sup> ]		
index	$R_0 = 151.5$	$R_0 = 140$	$R_0 = 138$	$R_0 = 151.5$	$R_0 = 140$	$R_0 = 138$	$R_0 = 151.5$	$R_0 = 140$	$R_0 = 138$	$R_0 = 151.5$	$R_0 = 140$	$R_0 = 138$
47	3.71 - 3.74	3.71 - 3.74	3.71 - 3.74	4.97 - 5.13	4.97 - 5.13	4.97 - 5.13	6.73 - 7.08	6.73 - 7.08	6.73 - 7.08	7.49 - 7.92	7.99 - 8.48	7.74 - 8.20
48	3.80 - 3.83	3.80 - 3.83	3.80 - 3.83	4.84 - 4.97	4.84 - 4.97	4.84 - 4.97	6.66 - 6.97	6.66 - 6.97	6.66 - 6.97	7.70 - 8.12	8.49 - 8.97	8.23 - 8.69
49	3.61 - 3.67	3.61 - 3.67	3.61 - 3.67	4.96 - 5.31	4.96 - 5.31	4.96 - 5.31	6.84 - 7.60	6.84 - 7.60	6.84 - 7.60	7.65 - 8.59	8.45 - 9.57	7.92 - 8.91
50	2.87 - 2.97	2.87 - 2.97	2.87 - 2.97	5.68 - 5.94	5.68 - 5.94	5.68 - 5.94	8.81 - 9.23	8.81 - 9.23	8.81 - 9.23	<b>6.00 - 6.26</b>	<b>6.93 - 7.25</b>	6.31 - 6.59
51	2.79 - 2.90	2.79 - 2.90	2.79 - 2.90	<b>5.89 - 6.22</b>	5.89 - 6.22	5.89 - 6.22	8.72 - 9.24	8.72 - 9.24	8.72 - 9.24	<b>5.61 - 5.92</b>	<b>6.46 - 6.83</b>	<b>6.18 - 6.52</b>
52	2.80 - 3.62	2.80 - 3.62	2.80 - 3.62	<b>5.82 - 7.90</b>	<b>5.82 - 7.90</b>	<b>5.82 - 7.90</b>	8.63 - 11.88	8.63 - 11.88	8.63 - 11.88	<b>4.31 - 5.76</b>	<b>4.96 - 6.68</b>	<b>4.74 - 6.37</b>

**Table B.10** – Estimated ammonium concentrations ( $NH_3^*$ ) from the selected area of the transect Helgoland - Stonehaven. Note that the values from minimum to maximum is illustrated for each ECOHAM index.  $NH_{3,minimum}^*$ ,  $NH_{3,mean}^*$  and  $NH_{3,maximum}^*$  evaluated from observational data ND130.  $NH_{3,ECOHAM}^*$  evaluated from simulated data.  $R_0$ : remineralisation value (see Table 2.1).  $R_0 = 151.5$ : maximum amount.  $R_0 = 140$ : proposed amount.  $R_0 = 138$ : Redfield. Bold: inside the range of expected *in situ* measurements for nitrate and ammonium (see Table B.9 in the appendix). Note that the values for ECOHAM index 53 - 54 does not exist due to absence of AOU values (see Fig. A.10a in the appendix).

Helgoland - Stonehaven												
ND130												
ECOHAM	$NH_{3,minimum}^*$ [mmol N/m <sup>3</sup> ]			$NH_{3,mean}^*$ [mmol N/m <sup>3</sup> ]			$NH_{3,maximum}^*$ [mmol N/m <sup>3</sup> ]			$NH_{3,ECOHAM}^*$ [mmol N/m <sup>3</sup> ]		
index	$R_0 = 151.5$	$R_0 = 140$	$R_0 = 138$	$R_0 = 151.5$	$R_0 = 140$	$R_0 = 138$	$R_0 = 151.5$	$R_0 = 140$	$R_0 = 138$	$R_0 = 151.5$	$R_0 = 140$	$R_0 = 138$
47	6.65 - 7.19	7.79 - 8.45	7.16 - 7.76	5.13 - 5.50	6.21 - 6.70	5.61 - 6.04	4.75 - 5.09	5.76 - 6.20	5.21 - 5.59	2.08 - 2.13	2.42 - 2.50	2.21 - 2.27
48	6.83 - 7.34	8.01 - 6.64	7.36 - 7.93	5.57 - 5.96	6.70 - 7.20	6.08 - 6.52	5.18 - 5.53	6.24 - 6.69	5.66 - 6.05	2.10 - 2.15	2.13 - 2.17	1.91 - 1.94
49	7.01 - 8.17	8.32 - 9.66	7.56 - 8.84	5.38 - 6.19	6.54 - 7.60	5.90 - 6.83	4.98 - 5.71	6.05 - 7.01	5.46 - 6.29	2.12 - 2.22	2.14 - 2.25	2.25 - 2.39
50	6.21 - 6.45	7.56 - 7.87	6.82 - 7.09	2.80 - 2.85	4.03 - 4.14	3.35 - 3.43	2.14 - 2.16	3.22 - 3.29	2.63 - 2.67	<b>2.43 - 2.45</b>	<b>2.45 - 2.48</b>	2.58 - 2.62
51	5.85 - 6.12	7.07 - 7.43	6.40 - 6.71	<b>2.09 - 2.10</b>	3.17 - 3.25	2.57 - 2.62	1.46 - 1.49	2.44 - 2.47	1.92	<b>2.43 - 2.47</b>	<b>2.46 - 2.49</b>	<b>2.23 - 2.25</b>
52	4.22 - 5.14	5.12 - 6.42	4.62 - 5.72	<b>0.0 - 0.56</b>	<b>1.03 - 1.32</b>	<b>0.43 - 0.90</b>	< 0	0.01 - 0.6	< 0	<b>2.39 - 2.54</b>	<b>2.40 - 2.57</b>	<b>2.23 - 2.32</b>

**Table B.11** – Estimated nitrate concentrations ( $HNO_3^*$ ) from the selected area of the transect Stonehaven - Helgoland. Note that the values from minimum to maximum is illustrated for each ECOHAM index.  $HNO_{3,minimum}^*$ ,  $HNO_{3,mean}^*$  and  $HNO_{3,maximum}^*$  evaluated from observational data ND 130.  $HNO_{3,ECOHAM}^*$  evaluated from simulated data.  $R_0$ : remineralisation value (see Table 2.1).  $R_0 = 151.5$ : maximum amount.  $R_0 = 140$ : proposed amount.  $R_0 = 138$ : Redfield. Bold: inside the range of expected *in situ* measurements for nitrate and ammonium (see Table B.12 in the appendix). Note that the values for  $HNO_{3,minimum}^*$  does not exist in ECOHAM index 53.

Stonehaven - Helgoland												
ND 130												
ECOHAM	$HNO_{3,minimum}^*$ [mmol N/m <sup>3</sup> ]			$HNO_{3,mean}^*$ [mmol N/m <sup>3</sup> ]			$HNO_{3,maximum}^*$ [mmol N/m <sup>3</sup> ]			$HNO_{3,ECOHAM}^*$ [mmol N/m <sup>3</sup> ]		
index	$R_0 = 151.5$	$R_0 = 140$	$R_0 = 138$	$R_0 = 151.5$	$R_0 = 140$	$R_0 = 138$	$R_0 = 151.5$	$R_0 = 140$	$R_0 = 138$	$R_0 = 151.5$	$R_0 = 140$	$R_0 = 138$
47	3.72 - 3.73	3.72 - 3.73	3.72 - 3.73	5.07 - 5.14	5.07 - 5.14	5.07 - 5.14	6.68 - 6.82	6.68 - 6.82	6.68 - 6.82	7.76 - 7.94	8.56 - 8.78	8.02 - 8.22
48	3.53	3.53	3.53	4.92 - 4.98	4.92 - 4.98	4.92 - 4.98	6.59 - 6.72	6.59 - 6.72	6.59 - 6.72	7.98 - 8.17	8.81 - 9.04	8.54 - 8.75
49	3.59 - 3.62	3.59 - 3.62	3.59 - 3.62	4.99 - 5.13	4.99 - 5.13	4.99 - 5.13	6.67 - 6.94	6.67 - 6.94	6.67 - 6.94	7.78 - 8.15	8.62 - 9.05	8.06 - 8.45
50	2.86 - 2.97	2.86 - 2.97	2.86 - 2.97	5.71 - 6.00	5.71 - 6.00	5.71 - 6.00	8.56 - 9.02	8.56 - 9.02	8.56 - 9.02	<b>6.03 - 6.33</b>	<b>6.98 - 7.34</b>	<b>6.66 - 7.00</b>
51	2.77 - 2.95	2.77 - 2.95	2.77 - 2.95	<b>5.66 - 6.13</b>	5.66 - 6.13	5.66 - 6.13	8.55 - 9.31	8.55 - 9.31	8.55 - 9.31	<b>5.95 - 6.44</b>	<b>6.53 - 7.08</b>	<b>6.24 - 6.76</b>
52	2.86 - 3.36	2.86 - 3.36	2.86 - 3.36	<b>5.80 - 7.04</b>	<b>5.80 - 7.04</b>	<b>5.80 - 7.04</b>	8.75 - 10.72	8.75 - 10.72	8.75 - 10.72	<b>5.07 - 6.12</b>	<b>5.56 - 6.73</b>	<b>5.31 - 6.42</b>
53				<b>5.09 - 5.25</b>	5.09 - 5.25	<b>5.09 - 5.25</b>	9.19 - 9.49	9.19 - 9.49	9.19 - 9.49	<b>5.37 - 5.53</b>	<b>6.18 - 6.38</b>	<b>5.64 - 5.81</b>
54	0.61 - 0.62	0.61 - 0.62	0.61 - 0.62	<b>5.05 - 5.25</b>	5.05 - 5.25	<b>5.05 - 5.25</b>	9.21 - 9.57	9.21 - 9.57	9.21 - 9.57	<b>5.35 - 5.55</b>	<b>6.24 - 6.48</b>	<b>5.65 - 5.86</b>

**Table B.12** – Estimated ammonium concentrations ( $NH_3^*$ ) from the selected area of the transect Stonehaven - Helgoland. Note that the values from minimum to maximum is illustrated for each ECOHAM index.  $NH_{3,minimum}^*$ ,  $NH_{3,mean}^*$  and  $NH_{3,maximum}^*$  evaluated from observational data ND 130.  $NH_{3,ECOHAM}^*$  evaluated from simulated data.  $R_0$ : remineralisation value (see Table 2.1).  $R_0 = 151.5$ : maximum amount.  $R_0 = 140$ : proposed amount.  $R_0 = 138$ : Redfield. Bold: inside the range of expected *in situ* measurements for nitrate and ammonium (see Table B.11 in the appendix). Note that the values for  $NH_{3,minimum}^*$  does not exist in ECOHAM index 53.

Stonehaven - Helgoland												
ND 130												
ECOHAM	$NH_{3,minimum}^*$ [mmol N/m <sup>3</sup> ]			$NH_{3,mean}^*$ [mmol N/m <sup>3</sup> ]			$NH_{3,maximum}^*$ [mmol N/m <sup>3</sup> ]			$NH_{3,ECOHAM}^*$ [mmol N/m <sup>3</sup> ]		
index	$R_0 = 151.5$	$R_0 = 140$	$R_0 = 138$	$R_0 = 151.5$	$R_0 = 140$	$R_0 = 138$	$R_0 = 151.5$	$R_0 = 140$	$R_0 = 138$	$R_0 = 151.5$	$R_0 = 140$	$R_0 = 138$
47	7.00 - 7.24	8.23 - 8.51	7.55 - 7.81	5.38 - 5.54	6.54 - 6.75	5.90 - 6.08	5.03 - 5.18	6.12 - 6.31	5.52 - 5.69	2.12 - 2.14	2.14 - 2.16	2.25 - 2.28
48	7.52 - 7.78	8.80 - 9.11	8.10 - 8.38	5.84 - 6.02	7.05 - 7.29	6.38 - 6.59	5.49 - 5.65	6.62 - 6.84	6.00 - 6.18	2.13 - 2.16	2.16 - 2.18	1.93 - 1.94
49	7.21 - 7.66	8.48 - 9.04	7.78 - 8.28	5.52 - 5.83	6.73 - 7.14	6.06 - 6.40	5.17 - 5.45	6.30 - 6.67	5.67 - 6.00	2.14 - 2.17	2.16 - 2.20	2.28 - 2.33
50	6.27 - 6.53	7.64 - 7.98	6.88 - 7.18	2.82 - 2.87	4.05 - 4.18	3.37 - 3.46	2.21 - 2.23	3.32 - 3.41	2.71 - 2.76	<b>2.43 - 2.47</b>	<b>2.46 - 2.49</b>	<b>2.20 - 2.22</b>
51	5.96 - 6.36	7.21 - 7.74	6.52 - 6.98	<b>2.46 - 2.51</b>	3.58 - 3.74	2.96 - 3.07	1.84 - 1.85	2.83 - 2.92	2.29 - 2.33	<b>2.11 - 2.13</b>	<b>2.49 - 2.54</b>	<b>2.25 - 2.28</b>
52	4.84 - 5.55	5.88 - 6.85	5.31 - 6.13	<b>1.09 - 1.23</b>	<b>2.18 - 2.22</b>	<b>1.60 - 1.68</b>	0.31 - 0.66	1.27 - 1.42	0.74 - 1.00	<b>2.17 - 2.20</b>	<b>2.49 - 2.60</b>	<b>2.28 - 2.35</b>
53				<b>2.21 - 2.22</b>	3.26 - 3.31	<b>2.68 - 2.71</b>	1.33 - 1.34	2.21 - 2.22	1.73	<b>1.88</b>	<b>1.89</b>	<b>2.01 - 2.02</b>
54	7.69 - 7.93	9.04 - 9.34	8.30 - 8.56	<b>2.31 - 2.33</b>	3.45 - 3.52	<b>2.82 - 2.86</b>	1.42 - 1.43	2.38 - 2.41	1.86	<b>1.95</b>	<b>1.96 - 1.97</b>	<b>2.09 - 2.10</b>

## C ND130 data: box number 123 - 125

**Table C.1** – Observational data from the box numbers 123 - 125 of the grid configuration ND130 (details see Radach et al. (1995a) and Radach et al. (1995b)). SD: standard deviation. Due to the missing data a simple linear interpolation has been performed. †: February - May. ‡: March - May. †‡: February - April. ‡#: May - December. Exeption: # data of August from Hinrichs et al. (2017). Blank: no data exist. Note that April represents the "preformed" component and July represents the considered *in situ* concentrations if one from the expedition of HE428 would be measuring there.

ND130 Nutrient	Parameter	BOX 123				BOX 124				BOX 125			
		March	April	May	July	March	April	May	July	March	April	May	July
Phosphate [mmol P/m <sup>3</sup> ]	mean	0.5 <sup>†</sup>	0.5 <sup>†</sup>	0.44	0.73	0.71	0.39	0.43	0.77	0.64	0.4	0.51	0.74
	SD			0.12	0.08	0.0	0.09	0.17	0.08	0.01	0.1	0.09	0.16
	min	0.4133 <sup>†</sup>	0.4133 <sup>†</sup>	0.35	0.68	0.0	0.33	0.21	0.66	0.63	0.28	0.39	0.6
	max	0.6167 <sup>†</sup>	0.6167 <sup>†</sup>	0.56	0.78	0.0	0.47	0.58	0.84	0.65	0.52	0.59	0.87
Nitrate [mmol N/m <sup>3</sup> ]	mean	4.4733 <sup>†</sup>	4.4733 <sup>†</sup>	3.12	4.94	6.11	2.12	5.54	5.76	6.55	2.2	5.15	5.09
	SD			0.38	1.01	0.0	0.87	0.8	2.14	0.07	1.12	1.13	2.9
	min	3.6433 <sup>†</sup>	3.6433 <sup>†</sup>	2.7	4.6	0.0	1.7	4.35	3.29	6.5	1.0	3.72	2.21
	max	5.4333 <sup>†</sup>	5.4333 <sup>†</sup>	3.6	5.9	0.0	2.6	6.31	8.27	6.6	3.7	6.38	8.07
Ammonium [mmol N/m <sup>3</sup> ]	mean	1.8	1.42 <sup>‡</sup>	1.84	1.42 <sup>‡</sup>	1.06 <sup>‡</sup>	1.57	2.03	2.0 – 2.5 <sup>#</sup>	0.7	1.2		2.5 – 3.0 <sup>#</sup>
	SD	0.57		0.39			0.73	0.24		0.0	0.6		
	min	0.6	1.0 <sup>‡</sup>	1.4	1.0286 <sup>‡</sup>	0.6 <sup>‡</sup>	0.8	1.7		0.7	0.0		
	max	1.4	1.85 <sup>‡</sup>	1.5 <sup>‡</sup>	2.3	1.9 <sup>#</sup>	2.3	2.2		0.7	0.0		

**Table C.2** – ND130 Boxes and their corresponding water columns (ECOHAM indexes) in the selected area from both observed transects.

ND130	Selected water columns
BOX 123	ECOHAM index 47 - 49
BOX 124	ECOHAM index 50 - 52
BOX 125	ECOHAM index 53 - 54

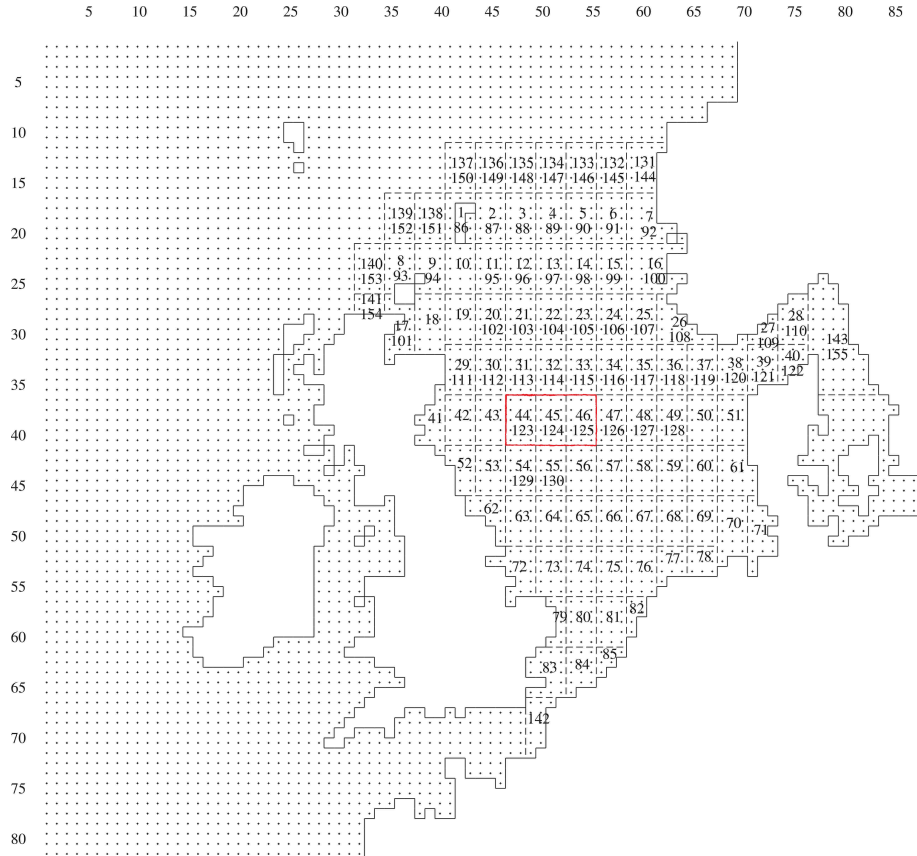


**Figure C.1** – Map of the grid configuration ND130 with 130 boxes plus 25 boundary boxes (Radach et al., 1995a). Collected data (see Table C.1 in the appendix) of the mean, standard deviation, minimum and maximum from the months April and July of the state variables ammonium, nitrate and phosphate have been extracted from the sub layer boxes 123, 124 and 125 (red framed) in the central of the North Sea. Note that the grid cell number of HAMSOM starts in north west.

## References

- Anderson, L. A. (1995). On the hydrogen and oxygen content of marine phytoplankton. *Deep Sea Research Part I: Oceanographic Research Papers*, 42(9):1675 – 1680.
- Arakawa, A. and Lamb, V. R. (1977). Computational Design of the Basic Dynamical Processes of the UCLA General Circulation Model. In CHANG, J., editor, *General Circulation Models of the Atmosphere*, volume 17 of *Methods in Computational Physics: Advances in Research and Applications*, pages 173 – 265. Elsevier.
- Azam, F., Fenchel, T., Field, J. G., Gray, J. S., Meyer-Reil, L. A., and Thingstad, F. (1983). The Ecological Role of Water-Column Microbes in the Sea. *Marine Ecology Progress Series*, 10(3):257–263.
- Backhaus, J. and Hainbucher, D. (1987). A Finite Difference General Circulation Model for Shelf Seas and Its Application to Low Frequency Variability on the North European Shelf. *Elsevier Oceanography Series*, 45:221 – 244.
- Backhaus, J. and Maier-Reimer, E. (1983). On Seasonal Circulation Patterns in the North Sea. In Sündermann, J. and Lenz, W., editors, *North Sea Dynamics*, pages 63–84. Springer Berlin Heidelberg.
- Backhaus, J. O. (1983). A semi-implicit scheme for the shallow water equations for application to shelf sea modelling. *Continental Shelf Research*, 2(4):243–254. Proceedings of a Workshop of the Joint North Sea Modelling Group on Mathematical Models of the North Sea and Surrounding Continental Shelf Seas.
- Backhaus, J. O. (1985). A three-dimensional model for the simulation of shelf sea dynamics. *Deutsche Hydrografische Zeitschrift*, 38(4):165–187.
- Boudreau, P. R. and Dickie, L. M. (1992). Biomass spectra of aquatic ecosystems in relation to fisheries yield. *Canadian Journal of Fisheries and Aquatic Sciences*, 49(8):1528–1538.
- Brockmann, U., Billen, G., and Gieskes, W. W. C. (1988). North Sea Nutrients and Eutrophication. In Salomons, W., Bayne, B. L., Duursma, E. K., and Förstner, U., editors, *Pollution of the North Sea: An Assessment*, pages 348–389. Springer Berlin Heidelberg, Berlin, Heidelberg.
- Brockmann, U., Laane, R., and Postma, J. (1990). Cycling of nutrient elements in the North Sea. *Netherlands Journal of Sea Research*, 26(2):239 – 264.
- Brockmann, U. H. and Kattner, G. (1997). Winter- to- summer changes of nutrients, dissolved and particulate organic material in the North Sea. *Deutsche Hydrografische Zeitschrift*, 49(2):229–242.
- Burson, A., Stomp, M., Akil, L., Brussaard, C. P. D., and Huisman, J. (2016). Unbalanced reduction of nutrient loads has created an offshore gradient from phosphorus to nitrogen limitation in the North Sea. *Limnology and Oceanography*, 61(3):869–888.
- Chen, X., Liu, C., O’Driscoll, K., Mayer, B., Su, J., and Pohlmann, T. (2013). On the nudging terms at open boundaries in regional ocean models. *Ocean Modelling*, 66:14–25.
- Conkright, M., Locarnini, R. A., O’Brien, H. G. T., Boyer, T., Stephens, C., and Antonov, J. (2002). 2002: World Ocean Atlas 2001: Objective Analyses, Data Statistics, and Figures, CD-ROM Documentation. *National Oceanographic Data Center, Silver Spring, MD.*, 17:1–21.
- Coulter, W. H. (1957). High speed automatic blood cell counter and cell size analyzer. *Proceedings of the National Electronics Conference*, 12:1034–1042.
- Dooley, H. D. (1974). Hypotheses concerning the circulation of the northern North Sea. *Journal du Conseil*, 36(1):54–61.
- Elton, C. S. (1927). *Animal ecology, by Charles Elton; with an introduction by Julian S. Huxley*. New York, Macmillan Co.

- Fasham, M. J. R., Ducklow, H. W., and McKelvie, S. M. (1990). A nitrogen-based model of plankton dynamics in the oceanic mixed layer. *Journal of Marine Research*, 48(3):591–639.
- Fenchel, T. (2008). The microbial loop - 25 years later. *Journal of Experimental Marine Biology and Ecology*, 366(1):99 – 103. Marine ecology: A tribute to the life and work of John S. Gray.
- Fernand, L., Weston, K., Morris, T., Greenwood, N., Brown, J., and Jickells, T. (2013). The contribution of the deep chlorophyll maximum to primary production in a seasonally stratified shelf sea, the North Sea. *Biogeochemistry*, 113(1):153–166.
- Fisher, R. A. (1921). On the probable error of a coefficient of correlation deduced from a small sample. *Metron*, 1:3–32.
- Gowen, R. J., Tett, P., Bresnan, E., Davidson, K., McKinney, A., Harrison, P. J., Milligan, S., Mills, D. K., Silke, J., and Crooks, A.-M. (2012). ANTHROPOGENIC NUTRIENT ENRICHMENT AND BLOOMS OF HARMFUL PHYTOPLANKTON. In Gibson, RN and Atkinson, RJA and Gordon, JDM and Hughes, RN, editor, *OCEANOGRAPHY AND MARINE BIOLOGY: AN ANNUAL REVIEW, VOL 50*, volume 50 of *Oceanography and Marine Biology*, pages 65–126. CRC Press.
- Greenwood, N., Parker, E. R., Fernand, L., Sivyer, D. B., Weston, K., Painting, S. J., Kröger, S., Forster, R. M., Lees, H. E., Mills, D. K., and Laane, R. W. P. M. (2010). Detection of low bottom water oxygen concentrations in the North Sea; implications for monitoring and assessment of ecosystem health. *Biogeosciences*, 7(4):1357–1373.
- Große, F., Greenwood, N., Kreuz, M., Lenhart, H.-J., Machoczek, D., Pätsch, J., Salt, L., and Thomas, H. (2016). Looking beyond stratification: a model-based analysis of the biological drivers of oxygen deficiency in the North Sea. *Biogeosciences*, 13(8):2511–2535.
- Große, F., Kreuz, M., Lenhart, H.-J., Pätsch, J., and Thomas, H. (2017). A Novel Modeling Approach to Quantify the Influence of Nitrogen Inputs on the Oxygen Dynamics of the North Sea. *Frontiers in Marine Science*, 4(383):1–21.
- Große, F., Lindemann, C., Pätsch, J., and Backhaus, J. O. (2015). The influence of winter convection on primary production: A parameterisation using a hydrostatic three-dimensional biogeochemical model. *Journal of Marine Systems*, 147:138 – 152.
- Hardy, A. C. (1939). Ecological investigations with the continuous plankton recorder: object, plan and methods. *Hull Bulletins of Marine Ecology*, 1:1–57.
- Herman, A. W. (1988). Simultaneous measurement of zooplankton and light attenuation with a new optical plankton counter. *Continental Shelf Research*, 8(2):205–221.
- Herman, A. W. (1992). Design and calibration of a new optical plankton counter capable of sizing small zooplankton. *Deep-Sea Research*, 39(3-4A):395–415.
- Herman, A. W., Beanlands, B., and Phillips, E. F. (2004). The next generation of Optical Plankton Counter: the Laser-OPC. *Journal of Plankton Research*, 26(10):1135–1145.
- Herman, A. W. and Dauphinee, T. M. (1980). Continuous and rapid profiling of zooplankton with an electric counter mounted on a batfish vehicle. *Deep-Sea Research*, 27A:79–96.
- Hill, A. E., Brown, J., Fernand, L., Holt, J., Horsburgh, K. J., Proctor, R., Raine, R., and Turrell, W. R. (2008). Thermohaline circulation of shallow tidal seas. *Geophysical Research Letters*, 35(11):n/a–n/a. L11605.
- Hinrichs, I., Gouretski, V., Pätsch, J., Emeis, K., and Stammer, D. (2017). North Sea Biogeochemical Climatology. Technical report, Center for Earth System Research and Sustainability (CEN). University of Hamburg.
- Ito, T. and Follows, M. J. (2005). Preformed phosphate, soft tissue pump and atmospheric CO<sub>2</sub>. *Journal of Marine Research*, 63(4):813–839.

- Ito, T., Follows, M. J., and Boyle, E. A. (2004). Is AOU a good measure of respiration in the oceans? *Geophysical Research Letters*, 31(17):n/a–n/a. L17305.
- Jakobsen, F. (2000). The Wind Influence on the Jutland Coastal Current Interpreted on the Basis of some Observations. *Hydrology Research*, 31(2):127–148.
- Jeffrey, S. and Humphrey, G. (1975). New spectrophotometric equations for determining chlorophylls a, b, c1 and c2 in higher plants, algae and natural phytoplankton. *Biochemie und Physiologie der Pflanzen*, 167(2):191 – 194.
- Jennings, B. R. and Parslow, K. (1988). Particle size measurement: The equivalent spherical diameter. *Proceedings of the Royal Society of London A: Mathematical, Physical and Engineering Sciences*, 419(1856):137–149.
- Kalnay, E., Kanamitsu, M., Kistler, R., Collins, W., Deaven, D., Gandin, L., Iredell, M., Saha, S., White, G., Woollen, J., Zhu, Y., Leetmaa, A., Reynolds, R., Chelliah, M., Ebisuzaki, W., Higgins, W., Janowiak, J., Mo, K. C., Ropelewski, C., Wang, J., Jenne, R., and Joseph, D. (1996). The NCEP/NCAR 40-Year Reanalysis Project. *Bulletin of the American Meteorological Society*, 77(3):437–471.
- Kara, A. B., Rochford, P. A., and Hurlburt, H. E. (2000). An optimal definition for ocean mixed layer depth. *Journal of Geophysical Research: Oceans*, 105(C7):16803–16821.
- Kistler, R., Kalnay, E., Collins, W., Saha, S., White, G., Woollen, J., Chelliah, M., Ebisuzaki, W., Kanamitsu, M., Kousky, V., van den Dool, H., Jenne, R., and Fiorino, M. (2001). The NCEP-NCAR 50-Year Reanalysis: Monthly Means CD-ROM and Documentation. *Bulletin of the American Meteorological Society*, 82(2):247–268.
- Kreyszig, E. (1970). *Introductory mathematical statistics: principles and methods*. Wiley, New York u.a.
- Kreyszig, E. (2011). Mathematical statistic. In *Advanced Engineering Mathematics. 10th Edition.*, chapter 25, pages 1063–1112. John Wiley & Sons, 111 River Street, Hoboken, NJ, USA, 10. ed., internat. student version edition.
- Kühn, W. and Radach, G. (1997). A one-dimensional physical-biological model study of the pelagic nitrogen cycling during the spring bloom in the northern North Sea (FLEX '76). *Journal of Marine Research*, 55(4):687–734.
- Longhurst, A. R., Reith, A. D., Bower, R. E., and Seibert, D. L. R. (1966). A new system for the collection of multiple serial plankton samples. *Deep-Sea Research*, 13:213–222.
- Lorenzen, C. J. (1966). A method for the continuous measurement of in vivo chlorophyll concentration. *Deep-Sea Research*, 13:223–227.
- Lorkowski, I., Pätsch, J., Moll, A., and Kähn, W. (2012). Interannual variability of carbon fluxes in the North Sea from 1970 to 2006 - Competing effects of abiotic and biotic drivers on the gas-exchange of CO<sub>2</sub>. *Estuarine, Coastal and Shelf Science*, 100:38 – 57.
- Maddux, W. S. and Kanwisher, J. W. (1965). An in situ particle counter. *Limnology and Oceanography*, 10(suppl):162–168.
- Meeus, J. (1998). *Astronomical Algorithms*. Willmann-Bell, Inc., P.O. Box 35025, Richmond, Virginia 23235, 2 edition.
- Möller, K. O., St John, M., Temming, A., Floeter, J., Sell, A. F., Herrmann, J. P., and Möllmann, C. (2012). Marine snow, zooplankton and thin layers: indications of a trophic link from small-scale sampling with the Video Plankton Recorder. *Marine Ecology Progress Series*, 468:57–69. 10.3354/meps09984.

- Müller, L. (2008). *Sauerstoffdynamik der Nordsee. Untersuchungen mit einem dreidimensionalen Ökosystemmodell*. PhD thesis, University of Hamburg. Berichte des Bundesamt für Seeschifffahrt und Hydrographie. Nr. 43/2008.
- Nielsen, T. G., L \_kkegaard, B., Richardson, K., Pedersen, F. B., and Hansen, L. (1993). Structure of Plankton Communities in the Dogger Bank Area (North Sea) during a Stratified Situation. *Marine Ecology - Progress Series*, 95:115–131.
- Otto, L., Zimmerman, J., Furnes, G., Mork, M., S \_tre, R., and Becker, G. (1990). Review of the physical oceanography of the North Sea. *Netherlands Journal of Sea Research*, 26(2):161–238.
- P \_tsch, J. and K \_hn, W. (2008). Nitrogen and carbon cycling in the North Sea and exchange with the North Atlantic-A model study. Part I. Nitrogen budget and fluxes . *Continental Shelf Research*, 28(6):767 – 787.
- P \_tsch, J., K \_hn, W., Radach, G., Casiano, J. S., Davila, M. G., Neuer, S., Freudenthal, T., and Llinas, O. (2001). Interannual variability of carbon fluxes at the North Atlantic Station ESTOC . *Deep Sea Research Part II: Topical Studies in Oceanography*, 49(1-3):253 – 288. The US JGOFS Synthesis and Modeling Project: Phase 1 .
- Paulmier, A., Kriest, I., and Oschlies, A. (2009). Stoichiometries of remineralisation and denitrification in global biogeochemical ocean models. *Biogeosciences*, 6(5):923–935.
- Pe \_a, M. A., Katsev, S., Oguz, T., and Gilbert, D. (2010). Modeling dissolved oxygen dynamics and hypoxia. *Biogeosciences*, 7(3):933–957.
- Pedersen, F. (1994). The Oceanographic and Biological Tidal Cycle Succession in Shallow Sea Fronts in the North Sea and the English Channel. *Estuarine, Coastal and Shelf Science*, 38(3):249 – 269.
- Pingree, R., Holligan, P., and Mardell, G. (1978). The effects of vertical stability on phytoplankton distributions in the summer on the northwest European Shelf. *Deep Sea Research*, 25(11):1011 – 1028.
- Pohlmann, T. (1996a). Calculating the annual cycle of the vertical eddy viscosity in the North Sea with a three-dimensional baroclinic shelf sea circulation model . *Continental Shelf Research*, 16(2):147 – 161.
- Pohlmann, T. (1996b). Predicting the thermocline in a circulation model of the North Sea - part I: model description, calibration and verification . *Continental Shelf Research*, 16(2):131 – 146.
- Pohlmann, T. (2006). A meso-scale model of the central and southern North Sea: Consequences of an improved resolution. *Continental Shelf Research*, 26(19):2367 – 2385.
- Quante, M., Colijn, F., Bakker, J. P., H \_rdtle, W., Heinrich, H., Lefebvre, C., N \_hren, I., Olesen, J. E., Pohlmann, T., Sterr, H., S \_ndermann, J., and T \_lle, M. H. (2016). Introduction to the Assessment-Characteristics of the Region. In Quante, Markus and Colijn, Franciscus, editor, *North Sea Region Climate Change Assessment*, pages 1–52. Springer International Publishing, Cham.
- Queste, B. Y., Fernand, L., Jickells, T. D., and Heywood, K. J. (2013). Spatial extent and historical context of North Sea oxygen depletion in August 2010. *Biogeochemistry*, 113(1):53–68.
- Queste, B. Y., Fernand, L., Jickells, T. D., Heywood, K. J., and Hind, A. J. (2016). Drivers of summer oxygen depletion in the central North Sea. *Biogeosciences*, 13(4):1209–1222.
- Radach, G., P \_tsch, J., Gekeler, J., and Herbig, K. (1995a). Annual Cycles of Nutrients and Chlorophyll in the North Sea. Technical report, Zentrum f \_r Meeres- und Klimaforschung der Universit \_t Hamburg. Institut f \_r Meereskunde.
- Radach, G., P \_tsch, J., Gekeler, J., and Herbig, K. (1995b). Annual Cycles of Nutrients and Chlorophyll in the North Sea. Technical report, Zentrum f \_r Meeres- und Klimaforschung der Universit \_t Hamburg. Institut f \_r Meereskunde.

- Redfield, A. (1934). On the proportions of organic derivatives in sea water and their relation to the composition of plankton. In *James Johnstone Memorial Volume*, pages 176–192. University Press of Liverpool.
- Redfield, A. C. (1958). The biological control of chemical factors in the environment. *American Scientist*, 46(3):230A–221.
- Redfield, A. C., Ketchum, B. H., and Richards, F. A. (1963). The Influence of Organisms on the Composition of Sea-Water. In Hill, M. N., editor, *The Composition of Sea-Water. Comparative and Descriptive Oceanography*, volume 2 of *The Sea*, chapter 2, pages 26–77. John Wiley & Sons, Inc.
- Rezzolla, L. (2010). Numerical Methods for the Solution of Partial Differential Equations. Lecture Notes for the COMPSTAR School on Computational Astrophysics. Caen, France. Albert Einstein Institute, Max-Planck-Institute for Gravitational Physics, Potsdam, Germany. [www.aei.mpg.de/~rezzolla](http://www.aei.mpg.de/~rezzolla).
- Rezzolla, L. and Zanotti, O. (2013). Numerical relativistic-hydrodynamics: Finite-difference methods. In *Relativistic Hydrodynamics*, chapter 8, pages 386–413. Oxford University Press.
- Richards, F. A. (1965). Anoxic Basins and Fjords. In Riley, J. P. and Skirrow, G., editors, ;, volume 1 of *Chemical Oceanography*, chapter 13, pages 611–644. Academic Press Inc, New York, USA.
- Richardson, K., Nielsen, T. G., Pedersen, F. B., Heilmann, J. P., Løkegaard, B., and Kaas, H. (1998). Spatial heterogeneity in the structure of the planktonic food web in the North Sea. *Marine Ecology Progress Series*, 168:197–211. 10.3354/meps168197.
- Richardson, K. and Pedersen, F. B. (1998). Estimation of new production in the North Sea: consequences for temporal and spatial variability of phytoplankton. *ICES Journal of Marine Science*, 55(4):574.
- Richardson, K., Visser, A., and Pedersen, F. B. (2000). Subsurface phytoplankton blooms fuel pelagic production in the North Sea. *Journal of Plankton Research*, 22(9):1663.
- Riegman, R., Colijn, F., Malschaert, J., Kloosterhuis, H., and Cadée, G. (1990). Assessment of growth rate limiting nutrients in the north sea by the use of nutrient-uptake kinetics. *Netherlands Journal of Sea Research*, 26(1):53 – 60.
- S. Brasse and A. Reimer and R. Seifert and W. Michaelis. (1999). The influence of intertidal mudflats on the dissolved inorganic carbon and total alkalinity distribution in the German Bight, southeastern North Sea. *Journal of Sea Research*, 42(2):93–103.
- Sharples, J., Tweddle, J. F., Green, J. A. M., Palmer, M. R., Kim, Y.-N., Hickman, A. E., Holligan, P. M., Moore, C. M., Rippeth, T. P., Simpson, J. H., and Krivtsov, V. (2007). Spring-Neap Modulation of Internal Tide Mixing and Vertical Nitrate Fluxes at a Shelf Edge in Summer. *Limnology and Oceanography*, 52(5):1735–1747.
- Sheldon, R. W. and Parsons, T. R. (1967). A Continuous Size Spectrum for Particulate Matter in the Sea. *Journal of the Fisheries Research Board of Canada*, 24(5):909–915.
- Sheldon, R. W., Prakash, A., and Sutcliffe, W. H. (1972). The size distribution of particles in the ocean. *Limnology and Oceanography*, XVII(3):327–340.
- Storch, H. v. and Zwiers, F. W. (1999). *Statistical Analysis in Climate Research*. Cambridge University Press.
- Sündermann, J. and Pohlmann, T. (2011). A brief analysis of the North Sea physics. *OCEANOLOGIA*, 53(3):663–689.
- Svendsen, E., Sætre, R., and Mork, M. (1991). Features of the northern North Sea circulation. *Continental Shelf Research*, 11(5):493 – 508.

- Thomas, H., Bozec, Y., de Baar, H. J. W., Elkalay, K., Frankignoulle, M., Schiettecatte, L.-S., Kattner, G., and Borges, A. V. (2005). The carbon budget of the North Sea. *Biogeosciences*, 2(1):87–96.
- Tiedje, B., Moll, A., and Kaleschke, L. (2010). Comparison of temporal and spatial structures of chlorophyll derived from MODIS satellite data and ECOHAM3 model data in the North Sea. *Journal of Sea Research*, 64(3):250 – 259.
- Turrell, W., Henderson, E., Slessor, G., Payne, R., and Adams, R. (1992). Seasonal changes in the circulation of the northern North Sea. *Continental Shelf Research*, 12(2-3):257–286.
- Turrell, W. R. (1992). New hypotheses concerning the circulation of the northern North Sea and its relation to North Sea fish stock recruitment. *ICES Journal of Marine Science: Journal du Conseil*, 49(1):107–123.
- Turrell, W. R., Slessor, G., Payne, R., Adams, R. D., and Gillibrand, P. A. (1996). Hydrography of the East Shetland Basin in relation to decadal North Sea variability. *ICES Journal of Marine Science*, 53(6):899–916.
- van Beusekom, J. E. E. and Diel-Christiansen, S. (2009). Global change and the biogeochemistry of the North Sea: the possible role of phytoplankton and phytoplankton grazing. *International Journal of Earth Sciences*, 98(2):269–280.
- van Beusekom, J. E. E. and Brockmann, U. H. and Hesse, K. -J. and Hickel, W. and Poremba, K. and Tillmann, U. (1999). The importance of sediments in the transformation and turnover of nutrients and organic matter in the Wadden Sea and German Bight. *Deutsche Hydrografische Zeitschrift*, 51(2):245–266.
- van Haren, H., Maas, L., Zimmerman, J. T. F., Ridderinkhof, H., and Malschaert, H. (1999). Strong inertial currents and marginal internal wave stability in the central North Sea. *Geophysical Research Letters*, 26(19):2993–2996.
- Vaquier-Sunyer, R. and Duarte, C. M. (2008). Thresholds of hypoxia for marine biodiversity. *Proceedings of the National Academy of Sciences*, 105(40):15452–15457.
- Villars, M., editor (1996). *Report of the ASMO Modelling Workshop on Eutrophication Issues: 5-8 November 1996, The Hague, The Netherlands / OSPAR Commission*.
- Wanninkhof, R. (1992). Relationship between wind speed and gas exchange over the ocean. *Journal of Geophysical Research: Oceans*, 97(C5):7373–7382.
- Weiss, R. (1970). The solubility of nitrogen, oxygen and argon in water and seawater. *Deep Sea Research and Oceanographic Abstracts*, 17(4):721 – 735.
- Weston, K., Fernand, L., Mills, D. K., Delahunty, R., and Brown, J. (2005). Primary production in the deep chlorophyll maximum of the central North Sea. *Journal of Plankton Research*, 27(9):909.
- Weston, K., Fernand, L., Nicholls, J., Marca-Bell, A., Mills, D., Sivyer, D., and Trimmer, M. (2008). Sedimentary and water column processes in the Oyster Grounds: A potentially hypoxic region of the North Sea . *Marine Environmental Research*, 65(3):235–249.
- Woerd, H. J. V. D. and Pasterkamp, R. (2008). HYDROPT: A fast and flexible method to retrieve chlorophyll-a from multispectral satellite observations of optically complex coastal waters. *Remote Sensing of Environment*, 112(4):1795 – 1807.
- Zhou, M., Carlotti, F., and Zhu, Y. (2010). A size-spectrum zooplankton closure model for ecosystem modelling. *Journal of Plankton Research*, 32(8):1147–1165.

## Acknowledgement

I would like to take this opportunity to thank all those who have actively supported me in the development of this work.

I would like to thank the first supervisor Dr. Thomas Pohlmann, who took care of this work and for providing the hydrodynamic data.

Furthermore, I would like to thank my second supervisor Dr. Johannes Pätsch for providing the biogeochemical data. With his ideas and experience and with many fruitful discussions he has pushed this work forward and always had an openness to questions or problems.

Additionally I would like to thank Dr. Marc Hufnagl, who provided the observed data of the expedition HE428 and for his fruitful discussions in the biological part of this work.

I would also like to thank Prof. Dr. Justus van Beusekom for providing the data from the water samples of the expedition HE428 and for his fruitful discussions in the biological part of this work.

A special thanks goes to Simon Weber, who was a great help to me to correct this work.